KINETIC, THERMODYNAMIC AND QUANTUM CHEMICAL APPROACH FOR CORROSION MITIGATION OF MILD STEEL IN AN ACID MEDIUM BY SOME NITROGEN HETEROCYCLES



Thesis submitted to

Bharathidasan University, Tiruchirappalli,
for the award of the degree of

DOCTOR OF PHILOSOPHY

IN

CHEMISTRY

Submitted by

Mrs. K. VIJAYALAKSHMI

(Ref.No:05510/Ph.D.K2/Chemistry/Part-Time/April-2018)

Under the guidance of

Dr. J. ELANGOVAN

ASSISTANT PROFESSOR OF CHEMISTRY



P. G. AND RESEARCH DEPARTMENT OF CHEMISTRY
RAJAH SERFOJI GOVERNMENT COLLEGE (AUTONOMOUS)
(NAAC "A" Grade & Affiliated to Bharathidasan University)
THANJAVUR - 613 005
TAMIL NADU, INDIA

MARCH - 2022

Dr. J. ELANGOVAN M.Sc., Ph.D.

Assistant Professor

PG & Research Department of Chemistry

Rajah Serfoji Government College (Autonomous)

Thanjavur - 613 005

Tamilnadu, India

Email: elangoorganic@gmail.com

Date:

CERTIFICATE

This is to certify that the thesis entitled, "Kinetic, Thermodynamic and Quantum chemical approach for Corrosion mitigation of Mild steel in an Acid medium by some Nitrogen Heterocycles" submitted by Mrs. K. Vijayalakshmi to Bharathidasan university for the award of the Degree of Doctor of Philosophy in Chemistry is a record of original and independent research work carried out by the candidate under my supervision during the period of 2018-2022. This work has not formed the basis for the award of any Degree, Diploma or any other similar title.

(J. ELANGOVAN)

Mrs. K. VIJAYALAKSHMI M.Sc., MPhil., B.Ed.,

Research scholar (Part-Time)

PG & Research Department of Chemistry

Rajah Serfoji Government College (Autonomous)

Thanjavur - 613 005

Tamilnadu, India

Date:

DECLARATION

I hereby declare that the thesis entitled, "Kinetic, Thermodynamic and Quantum chemical approach for Corrosion mitigation of Mild steel in an Acid medium by some Nitrogen Heterocycles" is a record of work done by me in PG & Research Department of Chemistry, Rajah Serfoji Government College (Autonomous), Thanjavur - 613 005 during the period of 2018-2022. The investigation, collection of data and the results reported in my thesis are entirely original to the best of my knowledge and have been carried out by me independently. I also declare that the work has not formed in full or part the basis for award of any previous research degree.

(K. VIJAYALAKSHMI)

CERTIFICATE OF PLAGIARISM CHECK

From

Dr. J. ELANGOVAN M.Sc., Ph.D.

Assistant professor

PG & Research Department of Chemistry

Rajah Serfoji Government College (Autonomous)

Thanjavur - 613 005

Tamilnadu, India

Email: elangoorganic@gmail.com

This is certify that the thesis is to be submitted to

Mrs. K. VIJAYALAKSHMI (Ref. No: 05510/Ph.D.K2/Chemistry/ Part-Time/

April-2018) pursued Ph.D. under my guidance is plagiarism free and the report also

has been checked for plagiarism using Urkund and found only 1% of the content from

other sources. The Librarian and Head, Department of Library and Information

Science, Bharathidasn University, Thiruchirappalli-62024, has given the certificate in

this regard which is attached here.

Place: Thanjavur

(J. ELANGOVAN)

Date:



Document Information

Analyzed document THESIS FOR PLAGIARISM MAR 22 (Vijayalakshmi K).docx (D129109368)

Submitted 2022-03-01T07:45:00.0000000

 Submitted by
 Srinivasa ragavan S

 Submitter email
 bdulib@gmail.com

Similarity 1%

Analysis address bdulib.bdu@analysis.urkund.com

Sources included in the report

W	URL: https://www.molport.com/shop/moleculelink/5-2H-1-3-benzodioxol-5-yl-1-piperidin-1-yl-penta-2-4-dien-1-one/9671559 Fetched: 2021-06-15T12:12:33.6570000	88	1
W	URL: https://patentimages.storage.googleapis.com/da/a8/7e/8362664bd54573/US9815839.pdf Fetched: 2022-03-01T07:46:19.2630000	88	7
W	URL: https://llibrary.org/document/oy8943wq-corrosion-inhibition-mild-steel-hcl-solution-using-tricholoroethelene.html Fetched: 2022-03-01T07:46:29.4370000	88	1

Dedicated To My Husband

ACKNOWLEDGEMENT

First and foremost, praises and thanks to God, the Almighty, for His showers of blessings throughout my research work to complete the research successfully.

I would like to express my sincere gratitude to my research advisor **Dr. J. Elangovan M.Sc., Ph.D.** Assistant professor, PG & Research Department of Chemistry, Rajah Serfoji Government College (Autonomous), Thanjavur - 613 005 for his continuous support, patience, motivation, enthusiasm and immense knowledge. His dynamism, vision and motivation have deeply inspired me. It was a great privilege and honor to work under his guidance. I am extremely grateful for what he has offered me. His guidance helped me in all the time of research and writing of this thesis.

I would like to thank **Prof. S. P.Elangovan M.Sc., M.Phil.,** Associate Professor and Head, PG & Research Department of Chemistry, Rajah Serfoji Government College (Autonomous), Thanjavur - 613 005 for providing me the facilities to carry out this research work.

I express my sincere thanks to our Principal **Dr. V. Senthamil Selvi M.Sc., M.Phil., Ph.D.** Rajah Serfoji Government College (Autonomous), Thanjavur - 613 005 for providing me the opportunity to carry out my work.

I express my sincere thanks to the Doctoral committee members **Dr. M. Ravi Sankar** Assistant professor, PG & Research Department of Chemistry, Rajah Serfoji Government College (Autonomous), Thanjavur - 613 005 and **Dr. S. Valarselvan**, Assistant Professor, Department of Chemistry, H. H. Rajah's College (A), Pudukkottai - 622001 for their encouragement, insightful comments and valuable suggestions of my research.

My sincere gratitude to **Prof. N. Punitha** and **Prof. M. Mangalam**, Assistant professors, PG & Research Department of Chemistry, Rajah Serfoji Government College (Autonomous), Thanjavur for their stimulating discussions throughout the research period in order to receive a deep understanding of the work.

I extend my heartfelt thanks to Mr. R. Rengasamay, Dr. J. Paulraj and Dr. D. Ganga Prasad for their esteemed assistance of my research work.

I extend my profound thanks to **all Staff Members** of the Department of chemistry Rajah Serfoji Government College (Autonomous), Thanjavur - 613 005 for their kind support and my sincere thanks to all the **lab assistants** for their timing help.

I am deeply indebted to **Dr. Helina**, **Mrs. Revathi**, **Mr. Velmurugan**, **Mr. Karthick**, **Dr. Chinnakani**, **Dr. Sharmila**, **Dr. Kasthuri**, **Dr. Sagundala** and **Ms. K. Gayathri** for their meticulous care of my research work.

I express words of indescribable gratitude to my Husband Mr. K. Raja, my daughters R. Lakshana & R. Laranya, My mother Mrs. K. Elakkiyaselvi and my sister Mrs. N. Vidhyulatha for their care, reinforcement and precious support for completing this research work and all over my life.

My heartfelt thanks to those who were directly or indirectly helped me to complete of this work successfully.

(K.VIJAYALAKSHMI)

CONTENTS

1.	INTRODUTION	
	1.1. Historical background of Corrosion	1
	1.2. Consequences of corrosion	2
	1.3. Cost of corrosion	3
	1.4. Factors that influence the rate of corrosion	3
	1.5. Prevention techniques of corrosion	4
	1.6. Iron corrosion and its inhibition mechanism	7
	1.7. Mild Steel	9
	1.8. Corrosion Inhibitors	11
	1.9. References	13
2.	REVIEW OF LITERATURE	
	2.1. Corrosion protection study by Imidazole derivatives	20
	2.2. Quinoline derivatives as corrosion inhibitors	21
	2.3. Anti - corrosive performance of Azine derivatives	23
	2.4. Corrosion mitigation performance of pyrimidine derivatives	24
	2.5. Triazole derivatives as effective corrosion protectors	25
	2.6. Inhibition characteristics of pyrazole derivatives against corrosion	31
	2.7. Corrosion-resistant behavior of piperidine derivatives	37
	2.8. References	42
3.	AIM AND SCOPE	54
4.	EXPERIMENTAL METHODS	
	4.1. Experimental methods of Corrosion inhibitors	56
	4.2. Experimental Methods of Corrosion Investigation	76
	4.3. References	82

Corrosion investigation of 4-(4-methoxy-phenyl)-1-phenethyl-1H	-
[1,2,3]triazole (MPPT) on Mild steel in 1M HCl solution	

5.	RESULTS AND DISCUSSION	
	5.1. Mass loss examination	86
	5.2. Potentiodynamic polarization investigation	87
	5.3. Impedance assessment	89
	5.4. Temperature effect on corrosion	91
	5.5. Quantum chemical study	97
	5.6. Morphological Investigation	100
	5.7. References	107
A	nti-corrosive performance of '1-benzyl-4-(naphthalen-2-yl)-1H-1,2,3-	
	iazole'(BNT) on Mild steel corrosion	
	induit (B1(1) on 1/1/14 steel corresion	
6.	RESULTS AND DISCUSSION	
	6.1. Mass loss study	110
	6.2. Polarization study	111
	6.3. Impedance study	113
	6.4. Temperature study	114
	6.5. Quantum chemical investigation	119
	6.6. Surface interpretation	122
	6.7. References	128
Co	orrosion mitigation performance of N-methyl-N-phenyl-3-	
(pl	nenylsulfonyl)-1H-pyrazole-5-carboxamide (MPSC)	
7.	RESULTS AND DISCUSSION	
	7.1. Gravimetric study	131
	7.2. Electrochemical polarization study	132
	7.3. Electrochemical impedance study	134
	7.4. Temperature analysis	135
	7.5. DFT approach	140
	11	

C	orrosion protection characteristics of 5-benzyl 3-ethyl 1H-pyrazole-3, 5
di	carboxylate (BEPD) on Mild steel corrosion
8.	RESULTS AND DISCUSSION
	8.1. Mass loss study
	8.2. Electrochemical polarization investigation
	8.3. Electrochemical impedance investigation
	8.4. Thermal study on Mild steel corrosion
	8.5. DFT investigation
	8.6. Surface investigation
	8.7. References ild steel corrosion probe of N-(4-(piperidin-1-ylsulfonyl)phenyl) etamide (PSPA) in 1M HCl solution
	ild steel corrosion probe of N-(4-(piperidin-1-ylsulfonyl)phenyl)
aco	ild steel corrosion probe of N-(4-(piperidin-1-ylsulfonyl)phenyl)
aco	ild steel corrosion probe of N-(4-(piperidin-1-ylsulfonyl)phenyl) etamide (PSPA) in 1M HCl solution
aco	ild steel corrosion probe of N-(4-(piperidin-1-ylsulfonyl)phenyl) etamide (PSPA) in 1M HCl solution RESULT AND DISCUSSION
aco	ild steel corrosion probe of N-(4-(piperidin-1-ylsulfonyl)phenyl) etamide (PSPA) in 1M HCl solution RESULT AND DISCUSSION 9.1. Mass reduction technique
aco	ild steel corrosion probe of N-(4-(piperidin-1-ylsulfonyl)phenyl) etamide (PSPA) in 1M HCl solution RESULT AND DISCUSSION 9.1. Mass reduction technique 9.2. Electrochemical polarization technique
aco	etamide (PSPA) in 1M HCl solution RESULT AND DISCUSSION 9.1. Mass reduction technique 9.2. Electrochemical polarization technique 9.3. Electrochemical impedance technique
aco	RESULT AND DISCUSSION 9.1. Mass reduction technique 9.2. Electrochemical polarization technique 9.3. Electrochemical impedance technique 9.4. Effect on temperature
aco	ild steel corrosion probe of N-(4-(piperidin-1-ylsulfonyl)phenyl) etamide (PSPA) in 1M HCl solution RESULT AND DISCUSSION 9.1. Mass reduction technique 9.2. Electrochemical polarization technique 9.3. Electrochemical impedance technique 9.4. Effect on temperature 9.5. DFT investigation
aco	ild steel corrosion probe of N-(4-(piperidin-1-ylsulfonyl)phenyl) etamide (PSPA) in 1M HCl solution RESULT AND DISCUSSION 9.1. Mass reduction technique 9.2. Electrochemical polarization technique 9.3. Electrochemical impedance technique 9.4. Effect on temperature 9.5. DFT investigation 9.6. Surface exploration

CHAPTER – I

Introduction

1.1. Historical background of Corrosion

The stint 'Corrosion' is a naturally occurring phenomenon striving by the physicochemical affinity of materials with their environment, resulting in the deterioration of their characteristics. Although the fact that various writers, philosophers and scientists have chronicled the entire history of corrosion, the Roman philosopher Pliny produced a treatise on the disintegration of iron between AD 23 and 79. Further, Faraday [1] who discovered a quantitative relationship between the chemical action and the electric current made the most significant contributions at 1791-1867. At the turn of the 19th century, notions for corrosion control began to emerge and Whitney developed a scientific basis for corrosion management premised on the electrochemical observation in 1903.

Later, Schonbein [2] discovered that iron could have been rendered inactive in 1836. U. R. Evans [3] was entrusted to offer a contemporary knowledge of the origins and prevention of corrosion based on his classical electrochemical theory and the efforts of Uhlig [4] and Fontana [5] played a pioneering role in modern knowledge of corrosion in 1923. Numerous corrosion researches have since been accomplished and it is now regarded as one of the most important research domains in this respect. As a consequence, it can be viewed as relentlessly obliterating economic conditions and our functional environment [6]. Furthermore, Corrosion is impossible to comprehend without taking into account the environmental factors such as air, humidity, acids, alkalis, soils, freshwater, distilled water, salt water, chlorine, ammonia, sulfur dioxide,

hydrogen sulfide, and fuel gases. Every environment has corrosive characteristics to a certain extent.

1.2. Consequences of corrosion

Corrosion has huge repercussions and the impacts on the safe, dependency and efficient functioning of equipment or structures are frequently more catastrophic than the loss of a quantity of metal. Even though the amount of metal lost is minimal, problems of various sorts may occur necessitating costly replacements. Thus, Corrosion has the following severe economic and societal consequences.

1.2.1. Economic consequences

Certain ostentatious economic consequences are

- > corroded equipment replacement
- > preventive measures
- > efficiency loss
- > equipment shutdown
- damage to equipment near the source of corrosion
- > corrosion-proofing by overdesigning

1.2.2. Societal consequences

Several social consequences can cause the unbearable sufferers in numerous regions such as infrastructure, highway bridges, gas transmission pipelines, waterways, railroads, ports, electrical utilities, power plants, ships, mining, drinking water systems, food processing, defense, electronics, petroleum refining, gas distribution, telecommunications, sewer systems, aircraft, automobiles, home appliances, agriculture, pharmaceutical, paper production and so on [7, 8].

1.3. Cost of corrosion

Since 1903, Corrosion has been a huge concern and a range of endeavors are accounted for. The 'International Measures of Prevention, Application and Economics of Corrosion Technology [IMPACT]' study conducted by NACE International in 2017 estimated the global cost of corrosion to be \$2.5 trillion or approximately 3.4 % of global Gross Domestic Product [GDP] and Corrosion costs of the defense division alone \$20 billion dollars. According to the report, subsequent corrosion prevention practices may save the world between 15 and 35 % of the cost of damage [\$375 to \$875 billion] [9]. The International Zinc Association [IZA] estimated India's cost of corrosion to be around 5-7 % in 2021 [10]. As a repercussion, corrosion has been perceived as an expensive and insurmountable economic crisis.

1.4. Factors that influence the rate of corrosion

Several internal and external aspects of the corrosive atmosphere such as the nature of the metals and the environment can impact the corrosion rate [11, 12].

1.4.1. Nature of the metal

The corrosion rate is influenced by metallic features such as crystal orientation, internal tension, grain size, surface conditions and metal stability factors. Furthermore, the dissolution rate is affected by the galvanic series of metals and hydrogen overvoltage [13].

1.4.2. Nature of the environment

Corrosion rates have been observed to be influenced by a variety of factors, the most important of which are pH, temperature, dissolved oxygen and concentration [14].

(i) pH of the solution

pH is one of the most essential features for speeding up corrosion in corrosive media and a drop in pH enhances hydrogen evaluation which speeds up metal

corrosion. The solubility of a protective barrier that develops on a metal surface and hence the corrosion process can be affected by changes in solution pH [15].

ii) Temperature

Raised temperatures hasten the dissolving process, accentuating the nature of the reactions by influencing the temperature dependency of both the physical and natural behavior of the reactants and products. Furthermore, the composition of the metals and their properties influenced the rate of corrosion [16, 17].

iii) Dissolved oxygen

A rise in dissolved oxygen concentration and corrosion rate control through oxygen depolarization accompanies the corrosion process. As an outcome, the rate of oxygen depolarization is determined by the rate of oxygen diffusion through the protective layer on the metal surface. As oxygen concentration rises, the rate of corrosion increases at first, but then decreases as oxygen concentration hits a critical threshold [18].

iv) Concentration

Corrosion rates can be influenced by the concentration of a solution. Corrosion does not occur linearly over a wider band. Also, concentration changes rapidly in equipment such as reactors, distillation columns and evaporators making corrosion rate prediction problematic [19].

1.5. Prevention techniques of corrosion

Corrosion can be mitigated for a limited period, but it cannot be prevented forever. Some preventative techniques are shown in (Fig.1.1).

1.5.1. Metal conditioning

It can be subdivided into two categories such as coating of metal alloys and alloying of metals [20].

(i) Metal coating

Zinc, tin, aluminum and organic compounds such as paints, polymers, resins, oils, greases, and enamels have all been used to form a corrosion-resistant barrier between the metal and the environment. Despite, protective coatings are frequently more complicated than merely acting as a barrier between the metal and the environment.

(ii) Metal alloying

By alloying normal steel with chromium and nickel to form a more corrosionresistant stainless steel is protected by a thin layer of chromium oxide that forms naturally.

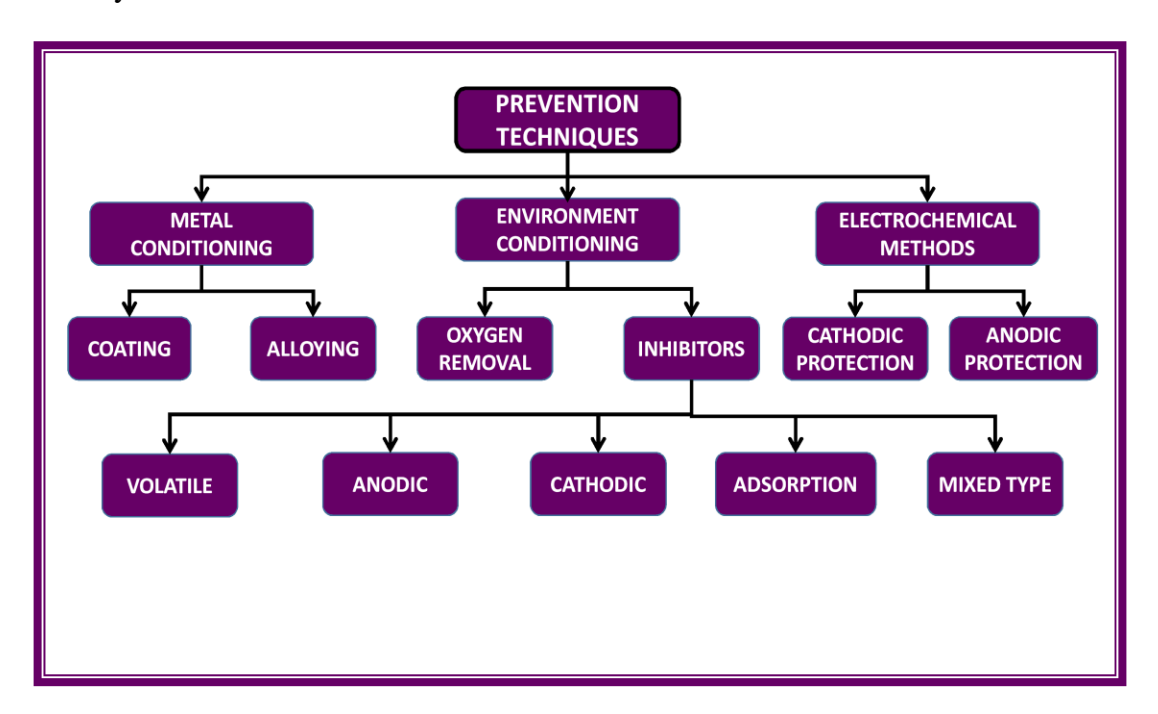


Fig.1.1. Prevention techniques of corrosion

1.5.2. Corrosive Environment conditioning

(i) Oxygen removal

To remove oxygen from a water system, sulphite can be utilized as a potent reducing agent. This corrosion prevention technique, however, is not feasible for open

evaporative cooling systems since fresh oxygen from the environment will be available at all times.

(ii) Utilization of Inhibitors

Inhibitors are categorized into several sorts based on how the environment affects corrosion such as volatile, anodic, cathodic, adsorption and mixed type inhibitors [21, 22]. Anodic inhibitors such as phosphates, arsenates, carbonates, molybdates and nitrites influence the inhibition mechanism by forming a protective layer of oxides, hydroxides and salts on the metal surface whereas cathodic inhibitors protect the metal surface by forming hydroxide inhibitive layers on the metal surface via an electrochemical reaction. Mixed inhibitors provide both of the above-mentioned types of protection [23, 24].

1.5.3. Electrochemical method

Corrosion may be explored by observing changes in metal potential overtime or employing electrical currents since it is an electrochemical process. The rate of corrosion can be influenced by passing anodic or cathodic currents through the metal. Steel corrosion is avoided in most soils and natural waterways by lowering the potential of the metal surface by 300 or 400 mV. Cathodic protection can be accomplished using a DC power source or by acquiring electrons through the anodic dissolution of a low-galvanic-series metal such as aluminum, zinc or magnesium. Anodic protection can be produced in some chemical circumstances by passing a current through the metal which releases electrons and raises its potential. This promotes anodic corrosion at first but under ideal conditions, this is followed by the development of a protective oxidized passive surface coating.

1.6. Iron corrosion and its inhibition mechanism

In the corrosive media, corrosion is caused by both anodic and cathodic electrochemical processes which result in the formation of rust on the metal surface. The loss of one or more electrons at the anode causes oxidation. The released electrons are sent to the external circuit where the hydrogen evolution occurs at the cathode. As a consequence, Mild steel rust may be prevented using inhibitors such as electrochemical processes at the anode, cathode or both. Therefore, a variety of inhibitors including anodic, cathodic and mixed type inhibitors as well as other processes have been proposed for reducing corrosion rates. Metal corrosion rates in acidic environments are influenced several ways and pinpointing a single universal mechanism for inhibition is challenging.

1.6.1. Corrosion mechanism of iron

(i) Anodic reaction

At the anode, metal is transformed into an ionic state by the loss of one or more electrons which is known as oxidation.

(ii) Cathodic reaction

At the cathode, reduction occurs by receiving an electron that has been released by the anodic processes.

1.6.2. Inhibition process

Chemisorption and physisorption are the two types of interactions that take place during the corrosion inhibition process which is presented in (Fig.1.2).

(i) Chemisorption

In this kind of adsorption, the inhibitor molecule and the metal surface share lone pair electrons, π electrons coupled to numerous bonds and weakly bonded electron pairs. There is also evidence of irreversible single layer adsorption of ions, atoms or molecules on the surface.

(ii) Physisorption

It is often attributed to weak van der Wal's interactions between charged molecules and the charged surface of the metal when exposed to a corrosive environment that includes inhibitor molecules. The charge of the metal surface, the structure and functional group of the inhibitor molecules, inhibitor synergism, polarity and the reactivity of adsorbed inhibitors in an inhibitor corrosive environment can all impact the adsorption process [25].

The number of inhibitor molecules on the metal surface as a function of concentration at a certain temperature known as isotherms determines the adsorption process. Langmuir [26–28], Dhar–Flory–Huggins and Bockris–Swinkels [29], Freundlich [30], Temkin [31, 32], Frumkin [33, 34], Flory–Huggins [35–38] and other adsorption isotherms can be used to determine the adsorption process.

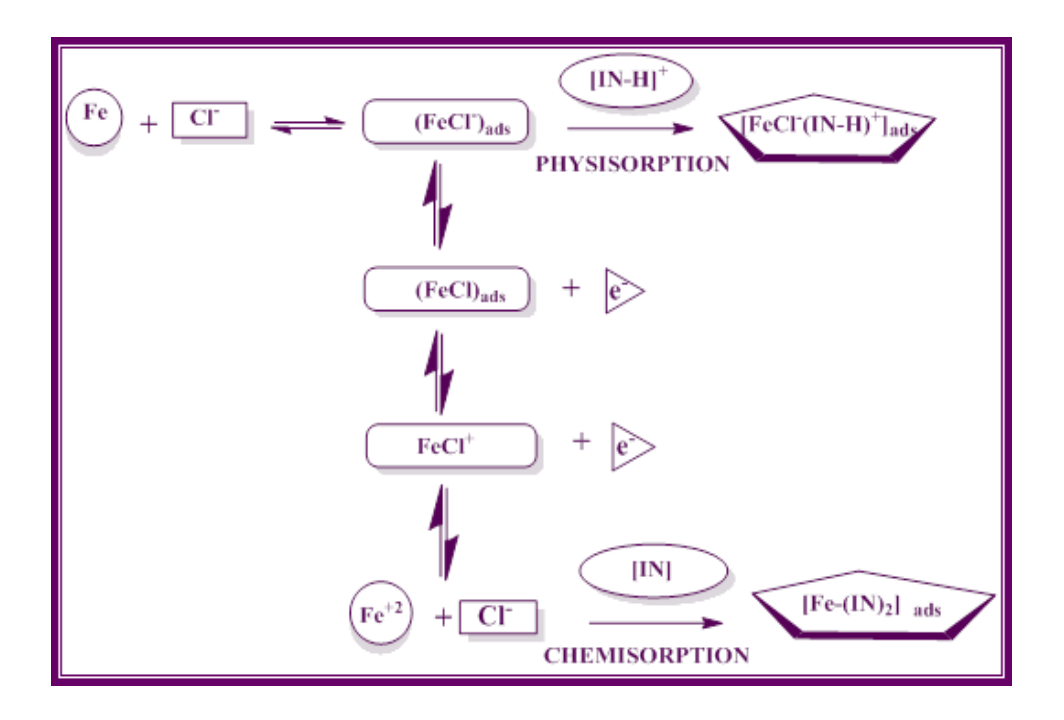


Fig.1.2. Corrosion inhibition mechanism of Iron in an acidic solution

1.7. Mild steel

Due to their low cost, ease of availability, high tensile strength and enticing diversity of properties, Mild steels and related alloys are broadly adopted materials. Mild steels are composed of iron with a carbon content ranging from 0.2 % to 2.1 % with a little amount of sulphur, silicon, phosphorous, chromium, nickel, and manganese added to expand their use range [39].

1.7.1. Physical and Chemical Properties of Mild steel

Mild steels are exceptionally durable, weldable and machinable which can be quickly manufactured from readily available natural sources. They are also fairly soft due to their enormous strength and malleability. The mechanical properties of metals are connected to the manufacturing structure and they are often used in mechanical operations such as shaping, bending and machining. The hardness and softness of Mild steel are also determined by the proportion of carbon added to the iron. Tensile strength

and hardness improve as carbon content increases but plasticity, weldability and malleability decreases [40, 41].

1.7.2. Applications of Mild steel

Mild steels are employed in a wide range of applications, including building, transportation and manufacturing [42]. They may be found in a variety of structural forms, including bars, beams, plates, and pipes for both onshore and offshore use. Furthermore, because of their high thermal and electrical conductivity as well as their corrosion resistance, they have a broad array of applications in environmental concerns. The mechanical features of Mild steels include biofouling resistance, manufacturing flexibility and joining procedures. Weldability, durability, hardness and annealing are all properties of Mild steel that allow the electric current to flow without affecting structural integrity.

On the other hand, other stainless steels with high carbon content need specialized welding procedures. High Mild steel alloys which have outstanding mechanical qualities are widely used in industries such as pickling, fabrication of a range of reaction vessels including cooling tower tanks, pipelines, submarines, bolts, engineering, bullets, nuts, chains, armor, magnets, screws, and hinges. Among the things, they were employed for petrochemicals, oil, water pipes, automobiles, ship, naval constructions and architectural disciplines [43].

1.7.3. Corrosion behavior of Mild steel

Although Mild steels have a broad range of applications, they are badly damaged when they get into contact with an acidic environment during descaling, acid cleaning, acid shipping, acid storage and other chemical processes. Conversely, nitrates, chlorates, sulphates, arsenates, phosphates and other pollutants in the environment have a detrimental influence on Mild steel quality. Because Mild steel

rusts more rapidly in acidic and humid environments, the rate of corrosion is rather high in some conditions.

The Corrosion resistance of Mild steel and its alloy is primarily determined by their composition and microstructure. Environmental conditions such as temperature and aeration level further exacerbated the rusting. Thus, corrosion prevention is a crucial solution for Mild steel that is deteriorating.

1.8. Corrosion Inhibitors

Even though numerous endeavors have been attempted to decrease metal and metal alloy disintegration in acid conditions [44 - 46], adsorption of corrosion inhibitors on Mild steel surfaces is one of the most extensively utilized methods and it has proved to be more efficient than the other proposed techniques in controlling the corrosion rates. Furthermore, chemical substances such as inorganic and organic compounds are the greatest materials for avoiding corrosion in acidic settings. A. Yurt et al. [47] provided certain criteria for choosing inhibitors to prevent metal corrosion in 2004 including having a high protective capability at low concentrations, functioning at higher temperatures and having faster protection for all exposed metal components in corrosive conditions. Additionally, they stated that the inhibitors must be long-lasting, must regulate uniform and local corrosion, must not create any undesired reaction products during heat transfer and must not be harmful or polluting.

Further, Inorganic inhibitors such as zinc chromate, phosphates, silicates, molybdates, tungstates, carbonates, arsenates and nitrates were used as corrosion inhibitors [48-50]. Nevertheless, the emancipation of these metals was not acceptable because of their destructive character which had a huge environmental impact. Due to the economic constraints, compatibility with other chemicals, greater efficiency and environmental concerns, organic inhibitors were determined to be a more effective and

appropriate method to prevent metals from corroding in corrosive environments [51-54].

The presence of polar groups, π electrons and heteroatoms in organic compounds is largely responsible for their inhibitory actions. The inhibitory features are caused by the existence of π electrons and unshared pair of electrons on the heteroatoms of the inhibitor molecules which are shared to the unoccupied d orbital of the iron to create a coordinate type bond. Heterocyclic candidates have been discovered as efficient corrosion inhibitors among all the organic compounds due to the presence of heteroatoms such as nitrogen, oxygen and sulphur [55-59].

Several substituted heterocyclic compounds have received significant attention in recent years due to their broad spectrum of agricultural, industrial and biological activities such as antimicrobial, sedative, anticonvulsant, anticancer, anti-inflammatory, diuretic, antibacterial, hypoglycemic, ant tubercular, antifungal and so on. In acidic corrosive circumstances, numerous triazole, pyrazole, piperidine, quinoline, imidazole, pyridine, etc., derivatives have also been revealed to be efficient corrosion inhibitors in that sequence [60-62].

1.9. References

- 1. Walsh F. Faraday and his laws of electrolysis. *Bulletin of Electrochem*. (1991); 7(11): 481-489.
- 2. Schonbein C. Pogg. Ann. 1936; 37: 390.
- Evans U R. An Introduction to Metallic Corrosion, 2nd ed. London: Arnold.
 1972; 7: 120- 187.
- 4. Uhlig H H. Corrosion and Corrosion Control, 3rd Ed. New York: *John Wiley and Son*; 1985.
- 5. Fontana M G. Corrosion Engineering. 3rd Ed. New York: *McGraw-Hill Book Company*; 1986.
- 6. Banerjee S N. An introduction to Science of Corrosion and Its Inhibition.

 Oxanian Press New Delhi: 1985; 286.
- 7. Bhaskaran R, Bhalla L, Rahman A, Juneja S, Sonik U, Kaur S, Kaur J, Rengaswamy N. An Analysis of the Updated Cost of Corrosion in India.

 Materials performance. 2014; 53: 56-65.
- 8. Whitney W R. The corrosion of Iron. *Journal of the American Chemical Society*. 1903; 25(4): 394-406.
- 9. https://www.jm.com.
- 10. https://www.business-standard.com/.
- 11. Akimov G V. Factors influencing Corrosion. Corrosion. 1959; 15(9): 23-36.
- 12. Roberge P. Corrosion Engineering. New York: McGraw-Hill; 2008.
- 13. Bentiss F, Fouad L, Mounim V, Herve L, Michel, Experimental and theoretical study of 3-pyridyl-substituted 1,2,4-thiadiazole and 1,3,4-thiadiazole as corrosion inhibitors of Mild steel in acidic media. *Materials Chemistry and Physics*. 2004; 87:18-23.

- Evans U R. Metallic corrosion, Passivity and protection, Edward Arnold and Co: London; 1946.
- 15. Copson H R. Effects of Velocity on Corrosion by Water. *Industrial & Engineering Chemistry*. 1952; 44 (8): 1745-1752.
- Kenworthy L, Driscoll W G O. Dezincification of Brasses. Anti-Corrosion Methods and Materials. 1955; 2(8): 247-249.
- 17. Speller F N. Corrosion Causes and Prevention. 3rd ed., MeGraw-Hill: New York; 1951.
- Antropov L I, Makushin E M, Panasenko V F. Inhibitors of Metal Corrosion.
 Metallurgia. Moscow; 1976.
- 19. Cohen M. The formation and properties of passive films on Iron. *Can J Chem*. 1959; 37(1): 286-291.
- Hoare T P. Report of the Committee on Corrosion and Protection. London: HMSO; 1971.
- James K, Rice P E. Drew Principles of industrial Water Treatment. Olney: Maryland; 1977.
- 22. F. N. Speller, Corrosion Causes and Prevention, 3rd ed., MeGraw-Hill: New York; 1951.
- Stone P J. Corrosion Inhibitors for Oil and Gas Production. Corrosion. ASM Handbook. ASM International. 1987; 13.
- 24. Rosenfeld I L. Corrosion Inhibitors. McGraw-Hill: New York; 1977.
- 25. Bailey J C, Porter F C, Pearson A W, Jarman R A. Aluminum and Aluminum Alloys in Corrosion: Metal /Environment Reactions. 3th ed., Springer: London; 1994.

- 26. Bentiss F, Traisnel M, Lagrenee M. The substituted 1,3,4-oxadiazoles: a new class of corrosion inhibitors of Mild steel in acidic media, *Corros. Sci.* 2000; 42(1): 127-146.
- 27. Sharma S, Chaudhary R S. Inhibitive action of methyl red towards corrosion of Mild steel in acids. *Bull. Electrochem.* 2000; 16 (6): 267-271.
- 28. Bentiss F, Lagrenee M, Traisnel M, Hornez J C. Corrosion inhibition of Mild steel in 1M hydrochloric acid by 2,5-bis(2-aminophenyl)-1,3,4-oxadiazole. *Corrosion*. 1999b; 55(10): 968-976.
- 29. Madkour L H, Ghoneim M M. Inhibition of the corrosion of 16/14 austenitic stainless steel by oxygen and nitrogen containing compound. *Bulletin of Electrochemistry*.1997; 13 (1): 1-7.
- 30. Ita B I, Offiong O E. Adsorption Studies on the Corrosion Inhibition Properties of 2-acetylpyrole and 2-acetylpyrole-(2-acetylthiosemicarbazone) on Mild steel in Hydrochloric Acid Medium. *Pure J. Appl. Sci.* 1999; 5(4): 497-501.
- 31. Muralidharan S, Iyer S. Pyrrole and its Derivatives as Inhibitors for the Corrosion of Mild steel in Acidic Solutions. *J. Electrochem. Soc.* 1999; 48(2): 113-120.
- 32. Hariharaputhran R, Subramaniam A, Antony AA, Sankar P M, Gopalan A, Vasudevan T, Iyer S V. Influence of substituent groups on performance of N-Benzylidine Phenyl amine-N-Oxide as corrosion inhibitor of Mild steel in acidic solutions. *British Corrosion Journal*.1998; 33(3): 214–218.
- 33. Al-Mayouf A M, Al-Suhybani A A, Al-Ameery A K. Corrosion inhibition of 304SS in sulfuric acid solutions by 2-methyl benzoazole derivatives.

 *Desalination. 1998; 116 (1): 25-33.

- 34. Touham F, Aouniti A, Abed Y, Hammouti B, Kertit S, Ramdani A. New pyrazolic compounds as corrosion inhibitors for Iron Armco in HCI media. *Bull. Electrochem.* 2000; 16: 245-249.
- 35. El-Rehim S S, Ibrahim A M, Khaled K F. 4-Aminoantipyrine as an inhibitor of Mild steel corrosion in HCl solution. *J. Appl. Electrochem.* 1999; 29: 593–599.
- 36. Bastidas J M, Polo J L, Cano E, Torres C. L. Trybutylamine as corrosion inhibitor for Mild steel in hydrochloric acid. *J. Mater. Sci.* 2000; 36: 2637-2642.
- 37. Rehim S S A E, Khaled I K F. Corrosion Report-Corrosion inhibition and adsorption behaviour of 4-aminoantipyrine on Mild steel in H₂SO₄, *Corrosion Prevention and Control.* 1999; 46: 157-162.
- 38. Lakhtin Y M. Engineering physical metallurgy and heat treatment. Mir. Publ: 1977.
- 39. https://www.metalsupplies.com/properties-of-mild-steel/.
- 40. https://sciencing.com/mechanical-properties-mild-steel-6618717.html.
- 41. Ramesh S, Rajeswari S, Maruthamuthu S. Effect of inhibitors and biocide on corrosion control of Mild steel in natural aqueous environment. *Materials Letters*. 2003; 57: 4547–4554.
- 42. https://www.mynewsdesk.com/in/indiamart/pressreleases/important-features-and-uses-of-mild-steel-939736.
- Quraishi M A, Sardar R, Jamal D. Corrosion inhibition of Mild steel in hydrochloric acid by some aromatic hydrazides. *Mater. Chem. Phys.* 2001; 71(3): 309-313.
- 44. Satpati A K, Ravindran P V. Electrochemical study of the inhibition of corrosion of stainless steel by 1, 2, 3-benzotriazole in acidic media. *Materials Chemistry and Physics*. 2008; 109: 352–359.

- 45. Aramaki K, Fujioka E. Spectroscopic investigations on the inhibition mechanism of propargyl alcohol for iron corrosion in hydrochloric acid at elevated temperatures. *Corrosion*. 1997; 53(4): 319-326.
- 46. Yurt A, Balaban A, Kandemir S U, Bereket G, Erk B. Investigation on some Schiff bases as HCl corrosion inhibitors for carbon steel. *Mater. Chem. Phys.* 2004; 85(2): 420-426.
- 47. Mu G, Li X, Qu Q, Zhou J. Molybdate and tungstate as corrosion inhibitors for cold rolling steel in hydrochloric acid solution. *Corrosion Science*. 2006; 48(2): 445-459.
- 48. Hughes A E, Gorman J D, Paterson P J K. The characterization of Ce- Mo-based conversion coatings on Al-alloys: Part I, *Corrosion Sci.* 1976; 38(11): 7-9.
- 49. Ilevbare G O, Burstein G T. The inhibition of pitting corrosion of stainless steels by chromate and molybdate ions. *Corrosion Science*. 2003; 45: 1545–1569.
- 50. Banerjee S N, Misra S. 1, 10,-Phenanthroline as corrosion-inhibitor for mild-steel in sulfuric acid solution. *Corrosion*. 1989; 45(9): 780-783.
- 51. Khaled K F, Hackerman N. Ortho-substituted anilines to inhibit copper corrosion in aerated 0.5 M hydrochloric acid. *Electrochimica Acta*. 2004; 49 (3): 485-495.
- 52. Bayol E, Kayakirilmaz K, Erbil M. The inhibitive effect of hexamethylene tetramine on the acid corrosion of steel. *Materials Chemistry and Physics*. 2007; 104(1): 74-82.
- 53. Boffardi B P. Control of Environmental Variables in Water-Re circulating Systems. *Corrosion*. ASM Handbook. ASM International: 1987.
- 54. Popova A, Sokolova E, Raicheva S, Christov M. AC and DC study of the temperature effect on Mild steel corrosion in acid media in the presence of benzimidazole derivatives. *Corrosion Science*. 2003; 45(1): 33-58.

- 55. Lebrini M, Lagrenee M, Traisnel M, Gengembre L, Vezin H, Bentiss F. Enhanced corrosion resistance of Mild steel in normal sulfuric acid medium by 2,5-bis(n-thienyl)-1,3,4- thiadiazoles: Electrochemical, X-ray photoelectron spectroscopy and theoretical studies. *Allied Surface Science*, 2007; 253(23): 9267-9276.
- 56. Bouklah M, Hammouti B, Aouniti A, Benhadda T. Thiophene derivatives as effective inhibitors for the corrosion of steel in 0.5 M H₂SO₄, *Progress in Organic Coatings*. 2005a; 53(4): 292-296.
- 57. Galal A, Atta N F, Al-Hassan M H S. Effect of some thiophene derivatives on the electrochemical behavior of AISI 316 austenitic stainless steel in acidic solutions containing chloride ions: II, Effect of temperature and surface studies.

 *Materials Chemistry and Physics. 2005; 89(1): 28-37.
- 58. Herrag L, Chetouani A, Elkadiri S, Hammouti B, Aouniti A. Pyrazole derivatives as corrosion inhibitors for steel in hydrochloric acid. *Portugaliae Electrochimica Acta*. 2008; 26: 211-220.
- 59. Gomma. Influence of copper cation on inhibition of corrosion for steel in presence of benzotriazole in sulfuric acid. *Materials Chemistry and Physics*. 1998b; 55(2): 131-138.
- 60. Abdennabi A M S, Abdulhadi A I, Abu-Orabi S T, Saricimen H. The inhibition action of 1(benzyl) 1-H-4, 5-dibenzoyl-1, 2, 3-triazole on Mild steel in hydrochloric acid media. *Corrosion Science*. 1996; 38(10): 1791-1800.
- 61. Fouad B, Michel T, Leon G, Michel L. A new triazole derivative as inhibitor of the acid corrosion of Mild steel: electrochemical studies, weight loss determination, SEM and XPS. *Allied Surface Science*. 1999a; 152(3-4): 237-249.

62. Ahmed S K, Ali W B, Khadom A A. Synthesis and investigations of heterocyclic compounds as corrosion inhibitors for Mild steel in hydrochloric acid. *Int J Ind Chem.* 2019; 10: 159–173.

CHAPTER – II

Review of Literature

Metals and alloys have been used in a wider spectrum of applications, therefore corrosion research is crucial. Many organic compounds have figured prominently in suppressing the corrosion process. In acidic, alkaline and neutral corrosive environments, heterocycles are the leading competitors and corrosion inhibition is principally influenced by the nature of the compounds as well as the corrosive environment. The anti-corrosive characteristics of some nitrogen containing heterocyclic compounds have been intensively investigated in Mild steel corrosion under various corrosive circumstances.

2.1. Corrosion protection study by Imidazole derivatives

N. W. Odozi et al [1] carried out the anticorrosive impact of '2, 4-di-tert-butyl-6-(1h-phenantro [9, 10-d] imidazol-2-yl) phenol' using weight loss and hydrogen evolution techniques on Mild steel in 0.5 % H₂SO₄. They suggested that the adsorption process followed the Temkin model through a physical adsorption mechanism with a maximum efficiency of 68.45 %. They also reported that the corrosion rate increases with increasing temperature while decreasing with increasing inhibitor concentration and the DFT calculations were used to calculate some electronic properties of the inhibitor molecules to determine the relationship between the inhibition power and molecular structure of the examined inhibitors.

O. Fergachi et al [2] have emphasized that the corrosion inhibition investigation of '2(-4(chlorophenyl-1H-benzo[d]imidazol)-1-yl) phenyl) methanone' on Mild steel in 1M HCl by electrochemical and spectroscopy method. They discovered that the inhibitory efficiency of the protector was 98.9% at 10⁻³ M concentration and

that it was a mixed-type inhibitor. The development of a complex between the inhibitor molecule and iron (II) ions on the metal surface hinders the process. The experimental results were in good accord with the theoretical assessments conducted by the DFT technique.

H. Hopfl et al [3] investigated the corrosion inhibition potential of '1-(2-aminoethyl)-2-imidazolidinethione'. They used DFT calculations and an X-ray crystallographic approach to determine the corrosion inhibition performance. H. R. Obayes et al [4] have conducted the DFT study with the B3LYP functional basis set to compare the theoretical evaluations of three isomers: 'benzimidazole', '2-methylbenzimidazole' and '2-mercaptobenzimidazole'. They concluded that nitrogroup containing inhibitors had lower effectiveness, but amino group-containing inhibitors had a higher inhibition rate.

Using gravimetric, electrochemical polarization and impedance methods, P. Dohare et al [5] investigated the inhibition action of three substituted imidazole compounds: '2-(3-methoxyphenyl)-4,5-diphenyl-1H-imidazole', '2,4,5-triphenyl-1H-imidazole', and '(3-nitrophenyl)-4,5-diphenyl-1Himidazole'. They found that the methoxy substituted inhibitor inhibited more effectively than the nitro substituted inhibitor with a maximum efficacy of 97.5 % at 100 mg. L⁻¹. The binding energy of the inhibitor molecules was calculated using molecular dynamics and DFT simulations. SEM measurements supported the development of the protective coating.

2.2. Quinoline derivatives as corrosion inhibitors

R. G. Sundaram et al [6] analyzed the anticorrosive effect of '8-quinoline sulphonyl chloride' on Mild steel in the 1M HCl medium using gravimetric and electrochemical methods. They demonstrated that the inhibition efficacy and surface coverage increased with an increase in concentration and that the adsorption process

followed the Langmuir model. The inhibitor slowed the cathode reaction according to Tafel plots. By adsorption of inhibitor molecules on the Mild steel surface, SEM and EDX analyses were utilized to assess the surface morphology. The computational inhibition efficiency investigation of three compounds namely, 'ethyl2-(8-hydroxyquinolin-5-yl) methyl) amino) acetate', '5-((benzylamino) methyl) quinolin-8-ol' and '5-(azidomethyl) quinolin-8-ol' has been described by E.A Erazua et al [7]. The results obtained from DFT calculations disclosed with increasing E_{HOMO}, softness, electrophilicity, electrons transferred from protectors to metal specimen, initial molecule metal interaction energy, energy change during electron back donation and decreasing E_{LUMO}, chemical hardness, energy gap, and dipole moment, the inhibition efficiency increased.

T. Laabaissi et al [8] carried out the electrochemical and theoretical studies to investigate the anti-corrosion behavior of '(E)-3-(4-methylstyryl) quinoxalin-2(1*H*)-one' against Mild steel in the 1M HCl media. They concluded that the inhibitor obeyed the Langmuir model and had optimal effectiveness of 91%. The inhibitor operated as a mixed type inhibitor according to the polarization investigation and the inhibition process was validated by the impedance study. Quantum chemical calculations were utilized to correlate the inhibitor's resistant power and molecular structure as well as to show that the experimental and theoretical evaluations were in harmony.

A. El Janati et al [9] investigated the protective efficacy of '6-nitro-1,4- di(prop-2-yn-1-yl)quinoxaline-2,3(1*H*,4*H*)-dione' on Mild steel corrosion in 1M HCl media using mass loss, electrochemical and DFT experiments and found that the highest inhibition rate was 95%. The Langmuir model was discovered to explain the inhibitory adsorption process and the inhibitor functioned as a mixed-type inhibitor. The corrosion protection capability was demonstrated using thermo dynamical and

activation characteristics such as Gibbs free energy, equilibrium constant and adsorption activation energy. DFT calculations were in good consonance with the experimental results.

2.3. Anti - corrosive performance of Azine derivatives

By using the mass loss technique and scanning electron microscopy, A. Kadhim et al [10] investigated the inhibitory efficacy of '2-Methyl-4*H*-benzo[1,3]oxazin-4-one' and '3-amino-2-methyl quinazoline-4(3*H*)-one'. The findings revealed that the corrosion inhibition process is influenced by the quantity of nitrogen present and also the molecular weight of the inhibitors examined.

S. Zhang et al [11] have proposed the anti-corrosion character of pyrazine derivatives in 15% HCl using mass loss, electrochemical, SEM and EDX analysis. The results revealed that the tested inhibitors are mixed-type inhibitors with chemical adsorption. They also discovered that the new pyrazine compounds acted as efficient defenders as the rising concentration of inhibitors in an acidic environment.

Applying electrochemical polarization and impedance spectroscopy techniques, the protective efficiency of azine and thiazine dyes such as Azure, Neutral Red, Eosinate, Toluidine Blue, Phenosafranin and Rhodanile Blue on Mild steel in the 1M HCl acid solution has been studied by E. E. Ebenso et al [12]. The procured findings revealed that the inhibition potential increased with an increase in concentration. They also concluded that thiazine dyes outperform azine dyes in terms of corrosion resistance which had been linked to the existence of multiple hydrogen bond donor centers in the inhibitor molecules.

The Mild steel corrosion inhibition activity of '1-((3,6-di(pyridin-2-yl)pyrdazin-4-yl)methyl)-indoline-2,3-dione', '4-(morpholinomethyl)-3,6-(pyridin-2-yl)pyridazine' and '3,6-di(pyridin-2-yl)-4-(p-tolyl)-pyridazine' in 1M HCl medium via weight loss,

electrochemical polarization, impedance and theoretical studies have been investigated by M. Filali et al [13]. All of the studies indicated that the efficacy of inhibitors increased as the concentration raised and the inhibitors were mixed-type inhibitors followed that the Langmuir model. It was also discovered that the inhibitor'1- ((3, 6-di(pyridin-2-yl)pyrdazin-4-yl)methyl)-indoline-2,3-dione' had better corrosion-prevention ability than the other inhibitors. The results achieved through experimental methods were quite comparable to those found through theoretical studies.

2.4. Corrosion mitigation performance of pyrimidine derivatives

Resit Yildiz [14] has investigated the corrosion resistance behavior of 2,4-Diamino-6-hydroxypyrimidine from 0.5 to 10 Mm concentration on Mild steel in the 1M HCl using linear polarization resistance, electrochemical measurements, quantum chemical calculations and scanning electron microscope techniques. From the observed data, he concluded that the adsorption process appeared to match the Langmuir model and the inhibitory mechanism. The anticorrosive activity of '6-(4-methoxyphenyl)-1-phenyl-2- thioxo-2,3-dihydro-1*H*-spiro[indoline-3,4-pyrimidine]-2-one' and '6-(4-methoxyphenyl)-1-phenyl-2-thioxo-2,3-dihydro-1*H*-spiro[indoline-3,4-pyrimidine]-2-one' on Mild steel corrosion in the 15% HCl solution has been inspected by M. Yadav et al [15]. They discovered that the studied inhibitors were mixed-type inhibitors that followed the Langmuir isotherm and SEM, FTIR, XPS and DFT analyses confirmed the ability to defend against corrosive environments.

S. Ambrish et al [16] used standard techniques such as weight loss, electrochemical impedance spectroscopy and potentiodynamic polarization to investigate the inhibition performance of Chromeno pyrimidine derivatives '8,8-Dimethyl-5-p-tolyl-8,9-dihydro- 1H-chromeno pyrimidine-2,4,6 (3H,5H,7H)-trione' and '8,8-Dimethyl-5-phenyl- 8,9- dihydro-1H-chromeno pyrimidine-2,4,6

(3*H*,5*H*,7*H*)-trione' for N80 steel in 15% hydrochloric acid solution. They revealed that Chromeno pyrimidine derivatives were effective corrosion inhibitors with 96.4 % inhibition efficiency and that adsorption with metal surfaces did involve both physical and chemical interactions. They also discovered that AFM and XPS spectra corroborated the mixed mode of inhibitoryaction and the adsorbed inhibitor film.

Khaled et al [17] have explored the anti-corrosive characteristics of three pyrimidine-bichalcophene derivatives '5-([2,20 -Bifuran]-5-ylmethylene)-1,3-dimethyl pyrimidine-2,4,6(1*H*,3*H*,5*H*)-trione', '5-([2,20-Bithiophen]-5-methylene)-1,3-dimethyl pyrimidine-2,4,6(1*H*,3*H*,5*H*)-trione' and '5-([2,20-Bithiophen]-5-yl methylene)-1,3-di ethyl-2-thioxodihydropyrimidine-4,6(1*H*,5*H*)-dione' in the 1M HNO3 via standard procedures. They discovered that increasing the concentrations of pyrimidine derivatives and the temperature of the medium enhanced the inhibitory effect. The polarization investigations revealed that the pyrimidine-bichalcophenes functioned as mixed inhibitors and the experimental results were validated using computational chemistry approaches such as quantum-chemical and molecular dynamics simulation techniques.

2.5. Triazole derivatives as effective corrosion protectors

Utilizing the mass loss and electrochemical experiments, A. A. Abd-Elaal et al [18] investigated the corrosion inhibited efficiency of '5-(phenyl)-4*H*-1,2,4-triazole-3-thiol', '3-(decylthio)-5-phenyl-1*H*-1,2,4-triazole', and '3-(benzylthio)-5-phenyl-1*H*-1,2,4-triazole'. They exposed that the inhibitors inhibited both the anodic and cathodic reactions; however, polarization was more towards the cathode according to the experimental data. D. Shevtsov et al [19] have analyzed the electrochemical and full-scale efficiency testing procedures to investigate the copper corrosion inhibition in neutral chloride solution using '3-sulphinylalkyl-5-amino-1*H*-1,2,4-triazole'. All of the

data revealed that the examined inhibitor was effective against corrosion degradation and that its protective capacity was twelve times more than when it was absent. Furthermore, the full-scale test in the 1% HCl solution revealed that the deterioration rate was reduced by 10 to 20 times even at 5mM inhibitor concentration.

In the 1M HCl acid solution, A. E. zquez et al [20] investigated the inhibitory impact of triazole—theophylline compounds on 'API 5LX52' steel. They found that increasing inhibitor concentrations resulted in the maximum corrosion inhibition rate and an impedance measurement revealed that the hampered efficiency for all inhibitor compounds was about 90% at 50 ppm. The examined inhibitors functioned as stronger inhibitors in the acidic corrosive media, according to SEM and EDS studies. A. M. Hassan et al [21] have discussed the carbon steel corrosion in hydrochloric acid medium with two triazole compounds namely; 'N-(furan-2-ylmethylene)-1*H*-1,2,4-triazole-3-amine' and 'N-(thiophene-2-ylmethylene)-1*H*-1,2,4-triazole-3-amine' by gravimetric method. They reported that both the inhibitors exhibited a high inhibition rate in the acid medium and obeyed the Langmuir isotherm. On carbon steel, they found that the thiophene-containing triazole was more efficient than the furancontaining triazole.

For the analysis of carbon steel corrosion with benzothiazole derivatives, A. S. Fouda et al [22] have utilized the mass loss, electrochemical polarization, impedance and frequency modulation techniques. They found that inhibition efficiencies increased with increasing concentrations of benzothiazole inhibitors but decreased with increasing temperature. Further, they proposed that the inhibitors were mixed-type inhibitors that followed the Temkin model. O.A. Kozaderov et al [23] have studied the hindered efficacy of '3-(piperidin-1-yl)- 5-amino-1*H*-1,2,4-triazole', '3-(4-phenyl piperazin-2-yl)-5-amino-1*H*-1,2,4-triazole' and '3-(4-benzylpiperazin-1-yl)-5-amino-

1*H*-1,2,4-triazole' on copper corrosion in chloride media using efficiency testing methods. The study findings concluded that the protective efficacies for all of the inhibitors observed were around 30-60% with the higher efficiency are been depicted by '3-(piperidin-1-yl)-5-amino-1*H*-1,2,4-triazole' in neutral medium and acidic chloride environment and the DFT calculations providing the correlation of inhibition activity and the molecular structure of the studied inhibitors.

The assessment of corrosion inhibition activity on '3-Amino-1,2,4-triazole-5-thiol' and cerium chloride for 'AA2024-T3' steel in NaCl medium was investigated by I. I. Udoh et al [24]. All of the data showed that the investigated inhibitor system had outstanding synergistic efficacy in a corrosive environment which was further demonstrated using the scanning vibrating electrode technique and X-ray photoelectron spectroscopy. R. G. Olvera et al [25] have discussed the corrosion inhibitive performance of 'mono-1,2,3-triazole derivatives' of pyrimidine nucleobases series against steel corrosion in 1M HCl medium and discovered the inhibitors to be promising inhibitors on steel corrosion in acid media.

O. A. Hazazi et al. [26] have observed that 4-amino-5-methyl-4*H*-1,2,4-triazole-3-thiol and halides had a synergistic impact against Mild steel corrosion in 0.5M H₂SO₄. The halide ions had a strong hindering impact on the inhibitor molecule according to the findings of the experiments. As the inhibitor concentration increased, the protection rate of Mild steel and the associated surface coverage values surged. In addition, the synergistic action followed the order Cl⁻, Br⁻, I⁻ on the inhibitor molecule and the adsorption process followed the Temkin model.

'(1-(4-nitrophenyl)-1*H*-1,2,3-triazol-4-yl)methanol','(1-(4-aminophenyl)-1*H*-1, 2,3-triazol-4-yl)methanol','1-(4-nitrophenyl)-5-methyl-1*H*-1,2,3-triazole-4-carboxy late,ethyl1-(4-aminophenyl)-5-methyl-1*H*-1,2,3-triazole-4-carboxylate' and '1-(5-

methyl-1-(4-nitrophenyl)-1*H*-1,2,3-triazol-4-yl)ethanone' were utilized for corrosion mitigation in the acidic atmosphere through mass reduction and electrochemical procedures were achieved by G. O. Resende et al [27]. They reported that at the optimal concentration, the protection rates were over 90% and that the inhibition process followed the Langmuir model which included both physisorption and chemisorption.

Jianfei Yu et al [28] have studied the corrosion mitigation ability of '3-amino-5-mercapto-1,2,4-triazole' on copper in a 3.5 % NaCl solution via gravimetric and electrochemical techniques. They claimed that raising the inhibitor concentration reduced the rate of corrosion. They also discovered that the inhibitor slowed both the anode and cathode reactions and that the Langmuir isotherm revealed a chemically adsorbed process. A. Nahle et al. [29] have examined the inhibitory characteristics of ethyl 2-(4-phenyl-1*H*-1,2,3-triazol-1-yl) acetate and 2-(4-phenyl-1*H*-1,2,3-triazol-1-yl) acetohydrazide on Mild steel corrosion in the 1M HCl solution. According to the researchers, both inhibitors exhibited a maximum efficacy of 95.3% and 95 % at 200 respectively. According to the Langmuir model, the examined protectors were physically and chemically adsorbed on the steel surface in the corrosive medium.

'1-[(4-ethyl-2-phenyl-4,5-dihydro-1,3-oxazol-4-yl)methyl]-4-phenyl-1*H*-1,2,3-triazole' and '1-[(4-ethyl-2-phenyl-4,5-dihydro-1,3-oxazol-4-yl)methyl]-5-phenyl-1*H*-1,2,3-triazole' were studied for Mild steel corrosion by mass loss and electrochemical methods and this work was analyzed by H. Rahmani et al [30]. Since the phenyl group position was altered from 5 to 4, the inhibitor 'Ph4' demonstrated the best efficacy at a 10-3 M of 95% according to the data. They also declared that the temperature tool revealed mitigation in impeded performance at high temperatures and that the DFT predictions were highly associated with the experimental results. In an acidic solution, C. M. Fernandes et al [31] have investigated the inhibited effectiveness of 1-benzyl-4-

phenyl-1H-1,2,3-triazole on Mild steel corrosion. The temperature investigation revealed that the inhibitor was chemically adsorbed on the steel surface, and the electrochemical tests revealed that the optimal inhibition efficacy was 81.7 % at 2.13 mmol⁻¹. The efficiency of the protector molecule on the steel surface in an acidic environment has been confirmed using the AFM analysis.

P. S. Desai et al [32] have proved that the anti-corrosive effects of '3-(piperazin-1-yl) benzo (d) isothiazole' and 'Hydroxybenzotriazol' on Mild steel corrosion in the 1M HCl solution and found that the hindered efficiencies ranged from 66-77 % at 25 mM to 33-44 % at 5 mM. The Langmuir, Freundlich and Temkin isotherms were followed during the adsorption processes at elevated temperatures. M. Scendo et al [33] have used inhibitor 3-amino-5-methylthio-1*H*-1,2,4-triazole to investigate the corrosion rate on 'C45 Mild steel' in an acid chloride environment. The examined inhibitor effectively suppressed both anodic oxidation and cathodic reduction processes according to electrochemical polarization data. They also discovered that the Temkin isotherm was the best fit for this physical adsorption process and they have used an inverted metallographic microscope to confirm the surface film in the presence of an inhibitor.

F. Bentiss et al [34] accounted for the relative learn of deterioration inhibition performance of 4-aminotriazole and 4*H*-triazoles in the 1M HCl and 0.5 M H₂SO₄ acid medium. They concluded that both inhibitors were efficient corrosion inhibitors in both acid media with the 4-aminotriazole inhibitor having a higher inhibitory efficacy than the 4H triazole. Additionally, both inhibitors decreased the rate of corrosion in the 1M HCl when compared to the 0.5 M H₂SO₄ solution. According to the electrochemical analysis, both of the examined inhibitors were mixed-type inhibitors that followed the Langmuir model.

D.S. Chauhan et al [35] used non-electrochemical tests, electrochemical methods and a surface morphology study to evaluate the effect of triazole modified chitosan macromolecule on carbon steel corrosion in HCl solution and perceived that the maximum level of protection achieved was 95 %. With both physisorption and chemisorption, the obstructed mechanism was the Langmuir model. The polarization methods revealed that the inhibitor molecule was mixed kind with corrosion doctors and more concentrated towards the cathode. DFT computations and MD simulations corroborated the experimental findings. The anti-corrosive effect of 'benzotriazole', '1,2,4-1*H*-triazole', 'tolyl triazole', and '5-chloro-1,2,3-benzotriazole' on copper corrosion was studied using corrosion testing methods such as electrochemical, ellipsometry, salt fog, wetting angle measurement and recurrent moisture condensation conditions. The research findings concluded that the inhibition was achieved by the formation of a nano-thin coating on the copper surface after 24 hour or longer exposure period to the inhibitors vapor treatment and the chloro derivative had the maximum protection according to O.A. Goncharova et al [36].

Using electrochemical method, A. Orhan et al [37] have demonstrated the ability of '4-Allyl–5-pyridin-4-yl-4H-1,2,4-triazole-3-thiol' to prevent Mild steel against corrosion in the 1M H₂SO₄ acid solution. The results revealed that as the inhibitor concentration increased, the efficiency rate increased and the inhibition was caused by the development of a protective coating on the Mild steel surface. B. E. Ibrahimi et al [38] have investigated the correlation between molecular structure and the relative hindered efficiency using quantum chemical analysis with the 'B3LYP/6-31G and [d,p]' technique. The triazole compounds '1,2,4 triazole,' '3-amino 1,2,4 triazole,' and '3,5-diamino 1,2,4 triazole,' were used as corrosion inhibitors on the copper surface and the experimental data were well correlated with the quantum

chemical study for the gaseous and aqueous parts of the investigated inhibitors, particularly for unprotonated species.

Y. I. Kuznetsov et al [39] have studied the relationship between the passivity and hydrophobicity of triazole molecules on the copper surface in a neutral chloride solution environment. The Frumkin isotherm demonstrated the monolayer adsorption with free energy values for the inhibition process ranging from 51 to 70 KJ/mol. The inhibitors effectively slowed the anodic oxidation process on the copper surface in a neutral chloride solution according to the findings.

The inhibitory activity of '3-amino-1, 2, 4-triazole' on copper exposed in the borax buffer media has been determined by Y. Wan et al [40]. The achieved efficacy was around 97% at 30mg.L⁻¹ according to the findings. The electrochemical and photo electrochemical measurements were in agreement, revealing that the inhibitor was an effective inhibitor on the copper surface in the borax medium and the improved corrosion prevention activity of the inhibitor compound was validated using Raman scattering spectroscopy. The Langmuir analysis was used to predict the adsorption mechanism which was determined to be physisorption.

2.6. Inhibition characteristics of pyrazole derivatives against corrosion

Z. T. Khudhair et al [41] used the mass loss approach to demonstrate the corrosion mitigation behavior of newly developed pyrazole derivatives on Mild steel in IM sulfuric acid solution. Likewise, the corrosion prevention ability of pyrazole ligands such as '1,4-bis(3,5-dimethylpyrazol-1-yl)butane', '1,3-bis(3,5-dimethyl pyrazol-1-yl) propane' and '1,3-bis(3,5-dimethylpyrazol-1-yl)propane-2-ol' and '[Cu₂(m3-SCN)₂(m-bbd)]n', '[Cu₂ (m3-SCN)₂(m-bdpp)]n', and '[Cu₂Hg(m2-SCN)₂(bdpo)₂ (CH3COO)₂] n' on Mild steel that had deteriorated in the 1M H₂SO₄ solution was examined by A. Masoumi et al [42]. They discovered that Pyrazole ligands had a modest impact

(38–78 %) on Mild steel corrosion, but their metal complexes had a stronger inhibitory efficacy (higher than 85%). Conversely, in corrosive environments, bimetallic compounds showed greater inhibition than monometallic compounds.

S. El Arrouji et al [43] investigated the inhibitory characteristics of 'N1, N1- bis (2-(bis ((3,5-dimethyl-1*H*-pyrazol-1-yl) methyl) amino)ethyl)-N2, N2-bis ((3,5-dimethyl-1*H*-pyrazol-1-yl) methyl) ethane-1,2-diamine' and 'diethyl 1,1'-(4-acetylphenyl) azanediyl) bis (methylene)) bis (5-methyl-1*H*-pyrazole-3-carboxylate)' for Mild steel in the 1M HCl solution employing chemical and electrochemical methods. According to the researchers, both inhibitors prevent anodic and cathodic corrosion currents and the corrosion inhibition mechanism follows the Langmuir model. The development of thin films has been confirmed by SEM and EDS investigations.

H. Chahmout et al [44] evaluated the stainless steel corrosion of '1-amino- 5,10-dioxo-3-(p-tolyl)-5,10-dihydro-1*H*-pyrazolo[1,2-b]phthalazine-2-carbonitrile' and '1-amino-3-(2-chlorophenyl)-5,10-dioxo-5,10-dihydro-1*H*-pyrazolo[1,2-b] phthalazine-2-carbonitrile in 2M H₂SO₄ solution by the electrochemical, Scanning Electron Microscope and Energy Dispersion X-ray spectroscope analyses. Both compounds operated as anodic defenders and followed the Langmuir model according to the findings. The corrosion resistance behavior of '2,4-diamino-5-(5-amino-3-hydroxy-1 *H*-pyrazole-1-carbonyl)thiophene-3-carbonitrile' and '1-(2,4-diamino-5-(5-amino-3-hydroxy-1*H*pyrazole-1-carbonyl)thiophen-3-yl) propan-1-one' has been discovered by M. S. Motawea et al [45] on carbon steel corrosion in the 1M HCl solution by standard procedure techniques. The results revealed that the evaluated inhibitor had a stronger anticorrosive response with chemisorption and followed the Langmuir model.

In a tetramethylammonium hydroxide solution for copper at pH 14, A. Goswami et al [46] examined the corrosion inhibition capabilities of 'pyrazole' and 'benzotriazole'. According to Micro pattern corrosion screening outcomes and electrochemical impedance methods, 1 mM Pyrazole in 'tetramethylammonium hydroxide solution' inhibited copper corrosion more strongly than 10 mM benzotriazole. They also discovered that Pyrazole-treated Cu surfaces are more hydrophilic than the triazole compound based on water contact angle measurements and XPS confirmed the formation of the copper-pyrazole complex.

The influence of corrosion inhibitors such as '3,5-diphenyl-4,5-dihydro-1*H*-pyrazole-1-carbothioamide' and '5-(3-methoxyphenyl)-3-phenyl-4,5dihydro-1*H*-pyrazole-1-carbothioamide' on Mild steel corrosion in the 1M HCl solution was examined by H. B. Ouici et al [47]. According to their verdicts, the effectiveness of inhibition increased with increasing concentration and the adsorption process followed the Langmuir isotherm model with both physical and chemical adsorptions. Combining mass loss, polarization, and impedance methods, R.S. Abdel Hameed et al [48] investigated whether 'S-acyclic nucleosides of pyrazolo[3,4-d]pyrimidine-thiones' performed as efficient corrosion protection for carbon steel in the 1M HCl solution. They discovered that the inhibitor caused a decrease in the open circuit potential and a mixed type protector.

M. El Azzouzi et al [49] identified the corrosion inhibiting action of '1,1'(pyridine-2,6-dihylbis(methylene))bis(5-methyl-1-*H*-pyrazole-3-carboxylicacid' in the
1M HCl solution for Mild steel using appropriate techniques. They revealed that the
protective capability of the explored protector improved with increasing concentration
and that it followed the Langmuir isotherm. I. Merimi et al [50] used mass loss,
electrochemical polarization and impedance methods to investigate the corrosion

inhibition contribution of pyrazole and bi pyrazole derivatives in an acidic environment. They concluded that the inhibitory activity of the tested inhibitors was primarily influenced by the composition of metals, substituent group and corrosive environment. They employed the DFT approach to correlate experimental and theoretical data.

The protective performance of 'N1,N1-bis(2-(bis(3,5-dimethyl-1*H*-pyrazol-1-yl) methyl)amino)ethyl)-N2,N2-bis(3,5-dimethyl-1*H*-pyrazol-1-yl)methyl)ethane-1,2-diamine' for Mild steel in the 0.5 M H₂SO₄ acidic atmosphere has been explored by S. El Arouji et al [51]. According to the thermal analysis, the studied inhibitor functioned as a mixed kind inhibitor and obeyed the Langmuir adsorption isotherm.

Using suitable methodologies, A. Thakur et al [52] investigated the anti-corrosion characteristics of '1-[benzyl-(2-cyano-ethyl)-amino]-methyl-5-methyl-1*H*-pyrazole-3- carboxylic acid methyl ester', '3,5-diphenyl-4,5-dihydro-1*H*-pyrazole-1-carbothioamide', '2*H*-pyrazole-triazole' and '5-Chloro-1-Phenyl-3-methyle Pyrazolo-4-methinethiosemicarbazone' on different metals and alloys.

L. Herrag et al [53] investigated the corrosion inhibition capacity of '1-[benzyl-(2-cyano-ethyl)-amino]-methyl-5-methyl-1*H*-pyrazole-3-carboxylic acid methyl ester' and 1-[benzyl-(2-cyano-ethyl)-amino]-methyl-5-methyl-1*H*-pyrazole-3-carboxylic acid ethyl ester' on Mild steel corrosion in the 1M HCl solution using mass loss and electrochemical techniques. They observed that for inhibitors containing ethyl ester, the ideal efficacy was about 98.5 % at 10⁻³ M and that the hampered efficacy of both the tested protectors decreased with higher temperatures.

N. K. Gupta et al [54] conducted experimental and theoretical analyses to explore the potential of '6-amino-3-methyl-2-oxo-1*H*-spiro[indoline-3,4-pyrano[2,3-c]pyrazole]-5-carbonitrile and 6-amino-3-methyl-2-oxo-1-phenyl-1*H*-spiro[indoline-

3,4-pyrano[2,3-c]pyrazole]-5-carbonitrile' to protect Mild steel against corrosion in the 1M HCl solution with maximum efficiency of 95.65% and 96.95 % at 200 ppm respectively. They led to the revelation that the inhibitors were mixed type, followed the Langmuir model and morphological studies validated the formation of thin films. To conclude, both experimental and theoretical studies demonstrated that both inhibitors were effective against the corrosive environment. Y. Kaddouri et al [55] revealed the inhibitory impact of '4-(bis((3,5-dimethyl-1*H*-pyrazol-1-yl) methyl) amino) benzonitrile' and '4-(bis((1*H*-pyrazol-1-yl) methyl) amino) benzonitrile' for Mild steel in the 1M HCl solution using mass loss, polarization, and impedance experiments. They observed that at 10⁻³ mol.L⁻¹, the corrosion resistance was 92.4 % and 92.3 % respectively and that the explored inhibitor was a mixed sort inhibitor. They also revealed that the hindered effect of both the protectors procured from experimental methods was validated by DFT analysis.

F. Boudjellal et al [56] investigated '3,5-disubstituted pyrazole carbothioamide' as a powerful corrosion inhibitor on Mild steel in an acidic environment using conventional techniques. They discovered that the corrosion inhibition mechanism was based on the Langmuir model which incorporated physicochemical adsorption and that the inhibitory efficiency was determined by DFT.

'4,4'-(1,4-phenylene)bis(6-amino-3-methyl-2,4-dihydropyrano[2,3-c]-pyrazole-5-carbonitrile' and '4,4'-(1,4-phenylene)bis(6-amino-3-methyl-1-phenyl-1,4-dihydro pyrano[2,3-c]pyrazole-5-carbonitrile' were utilized to preserve Mild steel in an acidic environment and it has been studied by P. Singh et al [57]. They found that the tested inhibitors were efficient defenders against Mild steel corrosion in an acidic environmentbased on the experimental and theoretical conclusions.

Employing electrochemical and surface investigation, M A. M. El-Haddad et al [58] employed 'Laurhydrazide N-propan-3-one' as a corrosion inhibitor for Mild steel dissolution in 5M HCl solution at different temperatures. They showed that the explored inhibitor acted as an effectual protector in acidic solutions based on kinetic, thermodynamic and time-dependent functional theory. A. Sehmi et al [59] have analyzed the corrosion suppression behavior of '5-(4-(dimethylamino) phenyl)-3-phenyl-4,5-dihydro-1*H*-pyrazole-1-carboxamide' and '(E)-5-(4-(dimethylamino) phenyl)-3-(4-(dimethylamino)styryl)-4,5-dihydro-1*H*-pyrazole-1-carboxamide' using appropriate techniques. They concluded that the examined protectors were mixed-sort inhibitors and that the inhibition mechanism followed the Langmuir model. The formation of a protective layer was validated using SEM and the correlation between experimental and theoretical consistency was explored by DFT analysis.

The effect of protectors '5-(4-Chlorobenzoyloxy)-1-phenyl-1*H*-pyrazole-3-carboxylate' and '5-(4-methoxyphenyl)-3-(4-methylphenyl)4,5-dihydro-1*H*-pyrazol-1-yl-(pyridin-4-yl)methanone' on Mild steel corrosion in the 15% HCl solution was investigated by M. Yadav et al [60]. At 250 ppm, the protective effect was 92 and 95.9% respectively and the adsorption mechanism was chemisorption according to the Langmuir model. They further claimed that SEM, EDX and AFM examinations were used to determine the reduction performance of examined protectors.

Using chemical, electrochemical, and theoretical analyses, A.Thomas et al [61] studied the inhibitory activity of '5-chloro-3-methyl-1-phenyl-1*H*-pyrazole-4-carbalde hyde' for Mild steel in the 1M HCl. The examined inhibitor worked effectively in an acidic environment, according to kinetic thermodynamic measurements and molecular dynamics simulations confirmed the interaction of inhibitor with the steel surface.

Using a gravimetric approach, Z. T. Khudhair et al [62] found several novel pyrazole compounds namely; 'ethyl 6-amino-3-methyl-4-(p-tolyl)-2,4-dihydropyrano [2,3,C]pyrazole-5-carboxylate', 'ethyl 6-amino-3-methyl-4(phenyl)-2,4-dihydro-pyrano [2,3,C]pyrazole-5-carboxylate', 'ethyl 6-amino-3-methyl-4-(3-nitrophenyl)-2,4-dihydro-pyrano[2,3,C]pyrazole-5-carboxylate' as Mild steel corrosion defenders in the 1M H₂SO₄ solution. All of the tested inhibitors performed as a capable defender against Mild steel corrosion in acid medium according to the experimental and theoretical findings.

The chemical, electrochemical, DFT, MD and surface morphological experiments to assess the corrosion mitigation capability of 'ethyl 6-amino-3-methyl-4-(p-tolyl)-2,4- dihydropyrano[2,3,C]pyrazole-5-carboxylate', 'ethyl 6-amino-3-methyl-4-(3-nitrophenyl)-2,4-dihydro- pyrano[2,3,C]pyrazole-5-carboxylate', 'ethyl 6-amino-3-methyl-4-(3-nitrophenyl)-2,4-dihydro- pyrano[2,3,C]pyrazole-5-carboxylate' for Mild steel were conducted by P. Doharea et al [63].

The corrosion mitigating performance of 'ethyl 6-amino-3-methyl-4-(p-tolyl)-2,4- dihydropyrano[2,3,C]pyrazole-5-carboxylate', 'ethyl 6-amino-3-methyl-4(phenyl)-2,4-dihydro-pyrano[2,3,C]pyrazole-5-carboxylate', 'ethyl 6-amino-3-methyl-4-(3-nitro phenyl)-2,4-dihydro- pyrano[2,3,C]pyrazole-5-carboxylate' on Mild steel corrosion using chemical electrochemical, DFT, MD and surface morphological studies have been explored by G. Singh et al [64]. The results produced by the above mentioned methodologies proved the overall inhibitory activity of the tested protectors.

2.7. Corrosion-resistant behavior of piperidine derivatives

A. Ousslim et al [65] tested the anti-corrosive characteristics of '4-benzyl piperidine', '1,6-bis(4-benzylpiperidine-1-carboxamide)hexane', and 'bis(4-benzyl piperidine)thiuram disulfide' against Mild steel in 5.5M phosphoric acid as corrosive

medium via chemical and electrochemical methodologies. They discovered that the corrosion behavior was hindered primarily due to the chemical structure and concentration of the investigated inhibitors which was acquired through electronic data.

G. Vengatesh et al [66] used acceptable approaches to evaluate the corrosion control capability of '2,4,6,11-tetraphenyl-9-oxa-1,5-diazatricyclo [5.3.1.03.8] undecane', '2,4,6,11-tetraaryl (4-methoxyphenyl)-9-oxa-1,5-diazatricyclo [5.3.1.03.8] undecane', '2,4,6,11-tetraaryl (4-chlorophenyl)- 9-oxa-1,5-diazatricyclo [5.3.1.03.8] undecane', '2,4,6,11-tetraaryl-p-tolyl-9-oxa-1,5-diazatricyclo [5.3.1.03.8] undecane' and '2,4,6,11-tetraaryl (4-fluorophenyl)-9-oxa-1,5-diazatricyclo [5.3.1.03.8] undecane' for copper metal in the 1M HNO3 solution. They discovered that methoxy substituted piperidine was more effective than the others by its electron-donating ability. They utilized SEM, AFM, FTIR and Monte Carlo simulation analyses in the acidic environment to demonstrate the hampered performance against copper corrosion.

Using Density Functional Theory, Y. Karzazi et al [67] demonstrated inhibitors such as '5-(1,3-benzodioxol-5-yl)-1-(piperidin-1-yl)penta-2,4-dien-1-one' and '5-(1,3-benzodioxol-5-yl)-1-(piperidin-1-yl)pent-2-en-1-one' have been worked as the efficient defenders for Mild steel corrosion. Ilim et al [68] used mass loss, polarization, and impedance experiments at various temperatures to examine the 'oligomer of 4-vinylpiperidine' as a corrosion protector in a brine solution with and without kerosene. They discovered that the protective ability of examined protector were around 62% in the absence of kerosene and 58 % in the existence of kerosene. They also discovered that the inhibited efficacy enhanced with increasing temperature and concentration at varying concentrations implying that the adsorption mechanism was chemisorption.

G. T. Xavier et al [69] evaluated the protective properties of '2, 6-diphenylpiperidin-4-ones' with various kinds of substituents using gravimetric and electrochemical methods at various temperatures. They also employed the mass loss approach with different halide ions to enhance the inhibitor's protective qualities with SEM analysis confirming the findings. C. B. Pradeep Kumar et al [70] used suitable approaches to examine the inhibitory efficiency of several recently synthesized 'piperidine sulphonamides' on Mild steel corrosion. The investigated inhibitors were revealed to be effective defenders against Mild steel corrosion relying on activation energies, thermo dynamical factors, SEM and quantum chemical analyses.

The piperidine derivatives '(4-hydrazono-3-Methyl-2,6-diphenyl-piperidin-1-yl) -ethanoic acid hydrazide', '5-(2,6-Diphenyl-3-methyl-4-hydrazono-piperidin-1-yl methyl)-3H-[1,3,4]oxadiazole-2-thione' and '4-Amino-5-(2,6-diphenyl-3-methyl-4-hydrazono-piperidin-1-ylmethyl)-4H-[1,2,4]triazole-3-thiol' on brass corrosion in natural seawater were studied by X. Joseph Raj et al [71]. They reported that the studied inhibitors functioned efficiently at increasing concentrations according to thermodynamic study, SEM and quantum chemical analysis. Using the electrochemical investigations, K. B. Samardzija et al [72] described the corrosion mitigation behavior of 'piperidine', '2-methylpiperidine', '3-methylpiperidine', 'cis-2,6-dimethylpiperidine', '3,5-dimethylpiperidine', '3-hydroxy piperidine', '4-hydroxypiperidine', '4-amino piperidine'. They discovered that piperidine and piperazine derivatives were more effective against corrosive environments than other compounds. They also concluded that all the inhibitors inhibited both anodic and cathodic currents and that the Langmuir model was followed.

The corrosion inhibition efficacy of '1-(5- fluoro-2-(methylthio) pyrimidine-4-yl)piperidine-4-yl)-2,5-dimethoxybenzenesulfonamide', '(1-(5-fluoro-2-(methylthio)

pyrimidine-4-yl) piperidine-4-yl)-4-nitrobenzenesulfonamide', '(1- (5-fluoro-2-(methyl thio) pyrimidine-4-yl) piperidine-4-yl)-3-methoxybenzenesulfonamide' was analyzed by K. Sava et al [73] via Quantum investigation and molecular dynamics simulation. Based on their molecular electronic features, the tested protectors were determined to be effective anti-corrosive competitors.

'N'-(2-(2-oxomethylpyrrol-1-yl)ethyl)piperidine' was used as corrosion inhibitors on Mild steel degradation in the 1M HCl solution through the mass loss technique by A. A. Alamiery et al [74]. They reported that the efficacy of the examined protector increased with increasing concentration, the adsorption process followed the Langmuir adsorption isotherm and the thin film generation has been validated by SEM examination. To study the impact of 'piperidone-4' on Mild steel deterioration in the 1M H_2SO_4 solution, K. F. Hamak et al [75] employed electrochemical polarization measurement. They observed that the presence of N, S atoms, π electron system, and piperidine constituent of the tested inhibitor had a significant impact on its inhibitory capacity.

According to mass loss, polarization, and impedance techniques, K. Rathidevi et al [76] evaluated the inhibition performance of '3, 5-diethyl 2, 6-diphenyl p-chloro Piperidin-4-one' for Mild steel in the 1M sulphuric acid environment and concluded that the examined inhibitor functioned as an active defender. S. Muralidharan et al [77] employed appropriate methodologies to explore the protection ability of '3-methyl-2,6-diphenyl piperidin-4-one' and '2-phenyl decahydroquinoline-4-one' on Mild steel deterioration in the 1M sulphuric acid medium. The results demonstrated that the explored inhibitors were effective protectors and that the adsorption process followed the Temkin isotherm model.

G. M. Muzakir et al [78] investigated the corrosion inhibitory capacity of some '1-(4-(2-allylphenoxy)butyl)piperidin-1-ium halides' on Mild steel corrosion using gravimetric, electrochemical and SEM techniques. They concluded that the explored inhibitors functioned effectively in the hydrogen sulphide saturated water salt hydrocarbon condition.

2.8. References

- 1. Odozi N W, Babalola J O, Ituen E B, Eseola A B. Imidazole derivative as novel effective inhibitor of Mild steel corrosion in aqueous sulphuric acid. *American Journal of Physical Chemistry*. 2015; 4(1-1): 1-9.
- Fergachi O, Benhiba F, Rbaa M, Touir R, Ouakki M, Galai M, Lakhrissi B, Oudda H, Touhami M E. Experimental and Theoretical Study of Corrosion Inhibition of Mild steel in 1.0 M HCl Medium by 2(-4(hloro phenyl-1H- benzo [d]imidazol)-1-yl)phenyl)methanone. *Materials Research*. 2018; 21(6):e20171038.
- 3. Hopfl H, Gomez B, Palou R M. Microwave-assisted Synthesis, Crystal and Molecular Structure, and DFT Study of 1-(2-aminoethyl)-2-imidazolidinethione. *J. Mex. Chem. Soc.* 2005; 49(4): 307-311.
- 4. Obayes H R, Alwan G H, Alobaidy A M, Al-Amiery A A, Kadhum A A H, Mohamad A B. Quantum chemical assessment of benzimidazole derivatives as corrosion inhibitors. *Chemistry Central Journal*. 2014; 8(21):1-8.
- Dohare P, Quraishi M A, Lgazc H, Salghi R. Electrochemical DFT and MD Simulation Study of Substituted Imidazoles as Novel Corrosion Inhibitors for Mild steel. *Portugaliae Electrochimica Acta*. 2019; 37(4): 217-239.
- Sundaram R G, Sundaravadivelu M. Anticorrosion Activity of 8-Quinoline Sulphonyl Chloride on Mild steel in 1M HCl Solution. *Journal of metallurgy*. 2016; 8095206: 9.
- 7. Erazua E A, Adeleke B B. A Computational Study of Quinoline Derivatives as Corrosion Inhibitors for Mild steel in Acidic Medium. *J. Appl. Sci. Environ. Manage*. 2019; 23(10): 1819-1824.
- 8. Laabaissi T, Benhiba F, Rouifi Z, Missioui M, Ourrak K, Oudda H, Ramli Y, Wara I, Allali M, Zarrouk A. New quinoxaline derivative as a green corrosion inhibitor

- for Mild steel in mild acidic medium: Electrochemical and theoretical studies. *Int. J. Corros. Scale Inhib.* 2019; 8(2): 241–256.
- Janati A E, Kandri Rodi Y, Mokhtari M, Rahman I A, Alaoui I, Chahdi F O,
 Ouzidan Y, Steli H, Elmsellem H, Hammouti B. 6-Nitro-1,4-di(prop-2-yn-1-yl)
 quinoxaline-2,3(1H,4H)-dione (NQPr)-a novel corrosion inhibitor for Mild steel in
 hydrochloric acid environment. *Int. J. Corros. Scale Inhib.* 2019; 8(3):702–716.
- 10. Kadhim A, Al-Okbi A K, Jamil D M, Qussay A, Al-Amiery A A, Gaaz T S, Kadhum A A H, Mohamad A B, Nassir M H. Experimental and theoretical studies of benzoxazines corrosion Inhibitors. *Results in Physics*. 2017; 7: 4013–4019.
- 11. Zhang S, Li H, Wang L, Liu D, Ping E, Zou P, Ma T, Li N. New Pyrazine Derivatives as Efficient Inhibitors on Mild steel Corrosion in Hydrochloric Medium. *Chemical Engineering transactions*. 2016; 55: 289-294.
- 12. Ebenso E E, Kabanda M M, Murulana L C, Singh A K, Shukla S K. Electrochemical and Quantum Chemical Investigation of Some Azine and Thiazine Dyes as Potential Corrosion Inhibitors for Mild steel in Hydrochloric Acid Solution. *Ind. Eng. Chem. Res.* 2012; 51: 12940–12958.
- 13. Filali M, El Hadrami E M, Ben-tama A, Hafez B, Abdel-Rahman I, Harrach A, Elmsellem H, Hammouti B, Mokhtari B, Stiriba S E, Julve M. 3,6-Di(pyridin-2-yl)pyridazine derivatives as original and new corrosion inhibitors in support of Mild steel: Experimental studies and DFT investigational. *Int. J. Corros. Scale Inhib.* 2019; 8(1): 93–109.
- 14. Yildiz R. Adsorption and inhibition effect of 2,4-diamino-6-hydroxypyrimidine for Mild steel corrosion in HCl medium: experimental and theoretical investigation. *Ionics*. 2019; 25:859–870.

- 15. Yadav M, Sinha R R, Kumar S, Sarkar T K. Corrosion inhibition effect of spiropyrimidinethiones on Mild steel in 15% HCl solution insight from: electrochemical and quantum studies. *RSC Advances*. 2015; 1-52.
- 16. Ambrish S, Chauhan A K R, Singh D, Quraishi M A, Sava K. Anti-corrosion investigation of pyrimidine derivatives as green and sustainable corrosion inhibitor for N80 steel in highly corrosive environment: Experimental and AFM/XPS study. Sustainable Chemistry and Pharmacy. 2020; 16: 100257.
- 17. Khaled M, Ismail M, El-Hossiany A, Fouda A. Novel pyrimidine-bichalcophene derivatives as corrosion inhibitors for copper in 1 M nitric acid solution. *RSC Adv*. 2021; 11(41): 25314-25333.
- 18. Abd-Elaal A A, Aiad I, Shaban S M, Tawfik S M, Sayed A. Synthesis and Evaluation of Some Triazole Derivatives as Corrosion Inhibitors and Biocides. *J Surfact Deterg*.2014;17:483–491.
- 19. Shevtsov D, Kozaderov O, Shikhaliev K, Komarova K, Kruzhilin A, Potapov A, Prabhakar C, Zartsyn I. 3-Sulphinyl-5-Amino-1*H*-1,2,4-Triazoles as Inhibitors of Copper Corrosion. *Appl. Sci.* 2019; 9: 4882.
- 20. Espinoza-Va zquez A, Rodriguez-Gomez F J, Martinez-Cruz I K, Angeles- Beltran D, Negron-Silva G E, Palomar-Pardave M, Lomas Romero L, Perez- Martinez D, Navarrete-Lopez A M. Adsorption and corrosion inhibition behaviour of new theophylline–triazole-based derivatives for steel in acidic medium. *R. Soc. open sci.* 2019; 6: 181738.
- 21. Hassan A M, Heakal B H, Younis A, Bedair M A, Elbialy Z I, Abdelsalam M M. Synthesis of Some Triazole Schiff Base Derivatives and Their Metal Complexes under Microwave Irradiation and Evaluation of Their Corrosion Inhibition and Biological Activity, *Egypt. J. Chem.* 2019; 62(9): 1603 1624.

- 22. Fouda A S, Diab M, El-Sonbati M A, Hassan S A. Benzothiazole derivatives as corrosion inhibitors for carbon steel in 1M phosphoric acid (H₃PO₄) solutions.

 African Journal of Pure and Applied Chemistry. 2013; 7(2): 67-78.
- 23. Kozaderov O A, Shikhaliev K S, Prabhakar C, Shevtsov D S, Kruzhilin E.S. Komarova A A, Potapov A Y, Zartsyn I D. Copper corrosion inhibition in chloride environments by 3-(*N*-hetaryl)-5-amino-1*H*-1,2,4-triazoles. *Int. J. Corros. Scale Inhib.* 2019; 8(2): 422–436.
- 24. Udoh I I, Shi H, Liu F, Han E. Synergistic Effect of 3-Amino-1,2,4-triazole-5-thiol and Cerium Chloride on Corrosion Inhibition of AA2024-T3. *Journal of the Electrochemical Society*. 2019; 166(6): C185-C195.
- 25. Olvera R G , Espinoza-Vazquez A, Negron-Silva G E, Palomar-Pardave M E, Romero-Romo M A, Santillan R. Multicomponent Click Synthesis of New 1,2,3-Triazole Derivatives of Pyrimidine Nucleobases: Promising Acidic Corrosion Inhibitors for Steel. *Molecules*. 2013; 18: 15064-15079.
- 26. Hazazi O A, Fawzy A, Awad M. Synergistic Effect of Halides on the Corrosion Inhibition of Mild steel in H₂SO₄ by a Triazole Derivative: Kinetics and Thermodynamic Studies. *Int. J. Electrochem. Sci.* 2014; 9: 4086 4103.
- 27. Resende G O, Teixeira S F, Figueiredo I F, Godoy A A, Lougon D J, Cotrim B A, Souza F C. Synthesis of 1,2,3-Triazole Derivatives and Its Evaluation as Corrosion Inhibitors for Carbon Steel. *International Journal of Electrochemistry*. 2019; 6759478: 12.
- 28. Yu J, Feng Q, Yu Y. Inhibition of copper corrosion in 3.5 percent NaCl solutions by triazole derivative. *Anti-Corrosion Methods and Materials*. 2009; 56(5): 275–279.

- 29. Nahle A, Salim R, El Hajjaji F. Novel triazole derivatives as ecological corrosion inhibitors for Mild steel in 1.0 M HCl: experimental & theoretical approach. RSC Adv. 2021; 11(7):4147-4162.
- 30. Rahmani H, Ismaily Alaoui K, Emran K M, El Hallaoui A, Taleb M, El Hajji S, Labriti B, Ech-chihbi E, Hammouti B, El-Hajjaji F. Experimental and DFT Investigation on the Corrosion Inhibition of Mild steel by 1, 2, 3- triazole Regioisomers in 1M hydrochloric Acid Solution. *Int. J. Electrochem. Sci.* 2019; 14: 985 998.
- 31. Fernandes C M, Alvarez L X, Santos N E, Maldonado Barrios A C, Ponzio E A. Green synthesis of 1-benzyl-4-phenyl-1H-1,2,3-triazole, its application ascorrosion inhibitor for Mild steel in acidic medium and new approach of classical electrochemical analyses. *Corrosion Science*. 2019; 149: 185–194.
- 32. Desai P S, Indorwala N S. Inhibitory action of Thiazole and Triazole on Mild steel Corrosion in Hydrochloric acid Solutions. *Res. J. Chem. Sci.* 2015; 5(3): 30-36.
- 33. Scendo M, Staszewska-Samson K. Assessment of the Inhibition Efficiency of 3-amino-5-methylthio-1*H*-1,2,4-triazole Against the Corrosion of Mild steel in Acid Chloride Solution. *Int. J. Electrochem. Sci.* 2017; 12: 5668 5691.
- 34. Bentiss F, Traisnel M, Lagrenee M. Inhibitor effects of triazole derivatives on corrosion of Mild steel in acidic media. *British Corrosion Journal*. 2000; 35(4): 315-320.
- 35. Chauhan D S, Quraishi M A, Sorour A A, Saha S K, Banerjee P. Triazole-modified chitosan: a biomacromolecule as a new environmentally benign corrosion inhibitor for carbon steel in a hydrochloric acid solution. *RSC Adv.* 2019; 9:14990–15003.

- 36. Goncharova O A, Luchkin A Y, Andreev N N, Andreeva N P, Vesely S S. Triazole derivatives as chamber inhibitors of copper corrosion. *Int. J. Corros. Scale Inhib.* 2018; 7(4): 657–672.
- 37. Orhan A, Ercan D, Koparir P, Soylemez A. Corrosion Inhibition of Mild steel by4-Allyl-5-pyridin-4-yl-4*H*-1,2,4-triazole-3-thiol. *Chem Sci Trans*. 2012; 1(2): 463-469.
- 38. El Ibrahimi B, Soumoue A, Jmiai A, Bourzi H, Oukhrib R, Elmouaden K, El Issami S, Bazzi L. Computational study of some triazole derivatives (un- and protonated forms) and their copper complexes in corrosion inhibition process. *Journal of Molecular Structure*. 2016; 1-19.
- 39. Kuznetsov Y I, Agafonkina M O, Shikhaliev H S, Andreeva N P, Potapov A Y. Adsorption and passivation of copper by triazoles in neutral aqueous solution. *Int. J. Corros. Scale Inhib.* 2014; 3(2):137–148.
- 40. Wan Y, Qin Z, Xu Q, Chen M, Min Y, Li M. Corrosion Inhibition Activity and Adsorption behavior of 3-Amino-1, 2, 4-Triazole on copper. *Int. J. Electrochem. Sci.* 2017; 12:10701 10713.
- 41. Khudhair Z, Shihab M. Preparation and Investigation of Some New Pyrazole Derivatives as Corrosion Inhibitors for Mild steel in Acidic Media. *Journal of Al-Nahrain University-Science*. 2016; 19 (2): 33-42.
- 42. Masoumi A, Hossaini Sadr M, Soltani B. Pyrazole ligands and their monometallic and bimetallic complexes: synthesis, characterization, and application as novel corrosion inhibitors. *J Adhes Sci Technol.* 2020; 34(23): 2569-2589.

- 43. El Arrouji S, Ismaily Alaoui K, Zerrouki A, EL Kadiri S, Touzani R, Rais Z, Filali Baba M, Taleb M, Chetouani A, Aouniti A. The Influence of Some Pyrazole Derivatives on the Corrosion Behavior of Mild steel in 1M HCl Solution. *J. Mater. Environ. Sci.* 2016; 7(1): 299-309.
- 44. Ouakki M, Chahmout H, Sibous S. Novel pyrazole derivatives as inhibitors of stainless steel in 2.0M H2SO4 media: Electrochemical Study. *Mediterranean Journal of Chemistry*. 2020; 10(3): 239-252.
- 45. Motawea M, Abdelaziz M. Some pyrazole derivatives as corrosion inhibitors for carbon steel in hydrochloric acid solutions. *European Journal of Chemistry*. 2015; 6(3): 342-349.
- 46. Goswami A, Koskey S, Mukherjee T, Chyan O. Study of Pyrazole as Copper Corrosion Inhibitor in Alkaline Post Chemical Mechanical Polishing Cleaning Solution. ECS Journal of Solid State Science and Technology. 2014; 3(10): 293-297.
- 47. Ouici H, Benali O, Guendouzi A. Experimental and quantum chemical studies on the corrosion inhibition effect of synthesized pyrazole derivatives on Mild steel in hydrochloric acid. *Research on Chemical Intermediates*. 2016; 42(9): 7085-7109.
- 48. Abdel Hameed R, Shamroukh A. Synthesis, characterization, and evaluation of some acyclic S-nucleosides of pyrazolo[3,4-d]pyrimidine-thiones as corrosion inhibitors for carbon steel in hydrochloric acid. *International Journal of Corrosion and Scale Inhibition*. 2017; 6(3): 333–348.

- 49. El Azzouzi M, Aouniti A, El Massaoudi M et al. Inhibition effect of 1,1′- (pyridine-2,6-dihylbis(methylene))bis(5- methyl-1-H-pyrazole-3-carboxylic acid) on the corrosion of Mild steel in 1 M HCl. Part A: Experimental study. *International Journal of Corrosion and Scale Inhibition*. 2017; 6 (4): 463–475.
- 50. Merimi I, Touzani R, Aouniti A, Chetouani A, Hammouti B. Pyrazole derivatives efficient organic inhibitors for corrosion in aggressive media: A comprehensive review. *International Journal of Corrosion and Scale Inhibition*. 2020; 9(4): 1237–1260.
- 51. EL Arouji S, Alaoui Ismaili K, Zerrouki K, El Kadiri S, Rais Z, Filali Baba M, Taleb M, Emran K, Zarrouk A, Aouniti A, Hammouti B. Inhibition effects of a new syntheses pyrazole derivative on the corrosion of Mild steel in sulfuric acid solution. *Der Pharma Chemica*. 2015; 7(10): 67-76.
- 52. Thakur A, Kumar A. Corrosion inhibition activity of Pyrazole derivatives on metals and alloys in acidic environment: A review. *Journal of Emerging Technologies and Innovative Research*. 2019; 6(1): 339-343.
- 53. Herrag L, Chetouani A, Elkadiri S, Hammouti B, Aouniti A. Pyrazole Derivatives as Corrosion Inhibitors for Steel in Hydrochloric Acid. *Portugaliae Electrochimica Acta*. 2008; 26: 211-220.
- 54. Gupta N, Haque J, Salghi R, Lgaz H, Mukherjee A, Quraishi M. Spiro [indoline-3,4'-pyrano[2,3-c]pyrazole] Derivatives as Novel Class of Green Corrosion Inhibitors for Mild steel in Hydrochloric Acid Medium: Theoretical and Experimental Approach. *J Bio Tribocorros*. 2018; 4(2).

- 55. Kaddouri Y, Takfaoui A, Abrigach F, El Azzouzi M, Zarrouk A,El-Hajjaji F, Touzani R, Sdassi H. Tridentate Pyrazole Ligands: Synthesis, Characterization and Corrosion Inhibition properties with Theoretical investigations. *Journal of Materials and Environmental Sciences*. 2017; 8 (3): 845-856.
- 56. Boudjellal F, Ouici H, Guendouzi A, Benali O, Sehmi A. Experimental and theoretical approach to the corrosion inhibition of Mild steel in acid medium by a newly synthesized pyrazole carbothioamide heterocycle. *J Mol Struct.* 2020; 1199:127051.
- 57. Singh P, Kumar M, Quraishi M, Haque J, Singh G. Bispyranopyrazoles as Green Corrosion Inhibitors for Mild steel in Hydrochloric Acid: Experimental and Theoretical Approach. *ACS Omega.* 2018; 3 (9):11151-11162.
- 58. El-Haddad M, Bahgat Radwan A, Sliem M, Hassan W, Abdullah A. Highly efficient eco-friendly corrosion inhibitor for Mild steel in 5 M HCl at elevated temperatures: experimental & molecular dynamics study. *Sci Rep.* 2019; 9 (1):1-15.
- 59. Sehmi A, Ouici H B, Guendouzi A, Ferhat M, Benali O, Boudjellal F. Corrosion Inhibition of Mild steel by newly Synthesized Pyrazole Carboxamide Derivatives in HCl Acid Medium: Experimental and Theoretical Studies. *Journal of the Electrochemical Society.* 2020; 167: 155508.
- 60. Yadav M, Sinha R, Sarkar T, Tiwari N. Corrosion inhibition effect of pyrazole derivatives on Mild steel in hydrochloric acid solution. *J Adhes Sci Technol*. 2015; 29 (16): 1690-1713.

- 61. Thomas A, Rugmini Ammal P, Joseph A. A comprehensive study of Mild steel corrosion in the aggressive acidic environment using CMPPC, a substituted pyrazole derivative. *Chemical Papers*. 2020.
- 62. Khudhaira Z T, Shihaba M S. Study of Synergistic Effect of Some Pyrazole Derivatives as Corrosion Inhibitors for Mild steel in 1 M H2SO4. Surface Engineering and Applied Electrochemistry. 2020; 56(5): 601–609.
- 63. Doharea P, Ansaria K R, Quraishia M A, Obotb I B. Pyranpyrazole derivativesas novel corrosion inhibitors for Mild steel useful for industrial pickling process: Experimental and Quantum Chemical study. *Journal of Industrial and Engineering Chemistry*. 2017; 52:197–210.
- 64. Singh G, Chandra P, Sachan N. Chemistry and Pharmacological Activities of Pyrazole and Pyrazole Derivatives: A Review. *Int. J. Pharm. Sci. Rev. Res.* 2020; 65(1): 201-214.
- 65. Ousslim A, Bekkouch K, Chetouani A et al. Adsorption and corrosion inhibitive properties of piperidine derivatives on Mild steel in phosphoric acid medium. *Res Chem Intermed*, 2013.
- 66. Vengatesh G, Sundaravadivelu M. Experimental and theoretical evaluation of new piperidine and oxaquinuclidine core containing derivatives as an efficient corrosion inhibitor for copper in nitric acid medium. *Journal of adhesion science and technology*. 2022; 28:1-32.
- 67. Karzazi Y, Alaoui Belghiti M E, Dafali A, Hammouti B. A theoretical investigation on the corrosion inhibition of Mild steel by piperidine derivatives in hydrochloric acid solution. *Journal of Chemical and Pharmaceutical Research*. 2014; 6(4):689-696.

- 68. Ilim I, Bahri S, Simanjuntak W, Syah Y M, Bundjali B, Buchari B. Performance of oligomer 4-vinylpiperidine as a carbon dioxide corrosion inhibitor of Mild steel. *Journal of Materials and Environmental Sciences*. 2017; 8 (7): 2381-2390.
- 69. Xavier G T, Thirumalairaj B, Jaganathan M. Effect of Piperidin-4-ones on the Corrosion Inhibition of Mild steel in 1N H₂SO₄. *International Journal of Corrosion*. 201; 410120: 15.
- 70. Kumar C, Mohana K, Muralidharan H. Electrochemical and thermodynamicstudies to evaluate the inhibition effect of synthesized piperidine derivatives on the corrosion of Mild steel in acidic medium. *Ionics*. 2014; 21(1): 263-281.
- 71. Raj X, Rajendran N. Inhibition effect of newly synthesised piperidine derivatives on the corrosion of brass in natural seawater. *Protection of Metals and Physical Chemistry of Surfaces*. 2013; 49(6): 763-775.
- 72. Babic-Samardzija K, Khaled K, Hackerman N. N-heterocyclic amines and derivatives as corrosion inhibitors for iron in perchloric acid. *Anti-Corrosion Methods and Materials*. 2005; 52(1): 11-21.
- 73. Sava K, Guo L, Kaya C, Tuzun B, Obot I B, Touir R, Islam N. Quantum chemical and molecular dynamic simulation studies for the prediction of inhibition efficiencies of some piperidine derivatives on the corrosion of iron. *Journal of the Taiwan Institute of Chemical Engineers*. 2016; 1–8.
- 74. Alamiery A A. Study of Corrosion Behavior of N'-(2-(2-oxomethylpyrrol-1-yl)ethyl)piperidine for Mild steel in the Acid Environment. *Biointerface Res Appl Chem.* 2021; 12(3): 3638-3646.
- 75. Fahed Hamak K. Synthesis, Characterization, Biological Evaluation and anticorrosion activity of some new bis-piperidone Derivatives. *Int J Adv Biol Biom Res.* 2013;1(2):186-196.

- 76. Rathidevi K, Jalajaa D. Corrosion Inhibition of Chlorine Substituted Piperidin– 4– One on Mild steel in Sulphuric Acid Medium. *International Journal of Science and Research*. 2016; 5(4):1852-1857.
- 77. Muralidharan S, Chandrasekar R, Iyer S V K. Effect of piperidones on hydrogen permeation and corrosion inhibition of Mild steel in acidic solutions. *Proc. Indian Acad. Sci. (Chem. Sci.).* 2000; 112(2):127–136.
- 78. Muzakir G M, Rza M B, Bahador S H, Musa G H. Allylphenoxypiperidinium halides as corrosion inhibitors of carbon steel and biocides. *Turk J Chem.* 2020; 44: 670 686.

CHAPTER - III

Aim and Scope

3.1. Scope of the present investigation

Metals and their alloys have traditionally been used to manufacture frame buildings, machinery parts, pipelines, bridges, nuclear power plants, water systems, furnaces, automobile cabs, gates, fences, signs, cars, furniture, wires and nails and cook wares due to their lower cost, availability, impact strength, weldability, ductility, electrical and thermal characteristics. However, they corrode swiftly in many circumstances, resulting in massive economic and societal losses. As a consequence, understanding corrosion and appropriate corrosion-resistance strategies are critical in this context. Although a variety of corrosion inhibitors have been used to diminish the deterioration impact, the necessity for protectors is increasing by the day due to the high cost of preventive maintenance, metal replacement costs, efficiency loss, fire hazards and toxic explosions from corroded materials. In a sense, heterocyclic compounds have long been recognized as effective defenders.

Moreover, metals will be utilized as long as humans exist and inhibitors will be necessary until metals are no longer used. Therefore, the role of heterocyclic compounds is a key requirement for mitigating Mild steel corrosion in all the corrosive conditions in the forthcoming periods.

3.2. Aim of the present work

The objectives of the present investigation are

- ➤ To synthesize five heterocyclic inhibitors namely; 4-(4-Methoxy-phenyl)-1-phenethyl-1*H*-[1,2,3]triazole(MPPT), 1-benzyl-4-(naphthalen-2-yl)-1*H*-1,2,3-triazole (BNT), *N*-methyl-N-phenyl-3-(phenylsulfonyl)-1*H*-pyrazole-5-carboxamide (MPSC), 5-Benzyl 3-ethyl 1*H*-pyrazole-3, 5-dicarboxylate (BEPD), N-(4-(piperidin-1-ylsulfonyl)phenyl)acetamide (PSPA).
- ➤ To characterize the synthesized heterocycles by the melting point, ¹H NMR and ¹³C NMR techniques.
- ➤ To forecast the resistant performance of the selected inhibitors using mass loss, electrochemical polarization and impedance methods in the 1M hydrochloric acid as the corrosive atmosphere at room temperature.
- > To explore the corrosion kinetics includes Activation Energies and Arrhenius factor at elevated temperatures.
- ➤ To analyze and thermodynamic parameters such as enthalpy of adsorption and entropy of adsorption at raised temperatures.
- ➤ To predict the suitable adsorption isotherm and feasibility of the corrosion process in view of the change in Gibbs free energy and adsorption equilibrium constants.
- > To understand the inhibition mechanism with the help of quantum chemical study.
- ➤ To confer the surface morphology by Scanning Electron Microscope, Energy Dispersive X-ray spectroscopy and Atomic Force Microscope techniques.

CHAPTER - IV

Experimental Methods

4.1. Experimental Methods of Corrosion Inhibitors

4.1.1. Materials

All the chemicals used for inhibitor synthesis were purchased from Sigma-Aldrich and commercially available solvents and reagents are used any further purification.

4.1.2. Experimental Methods

(a). Synthesis of 4-(4-Methoxy-phenyl)-1-phenethyl-1*H*-[1,2,3]triazole

(i). (2-Azido-ethyl)-benzene

Sodium azide (1.97g, 29.91 mmol) was added to phenethyl bromide (4.1a) (5 mL, 19.93 mmol) dissolved in 50 mL of dimethylsulphoxide (DMSO) and stirred overnight at room temperature. Following the completion of the reaction as confirmed by thin-layer chromatography (TLC), water was gradually added to the reaction mixture. The product was produced as clear oil via hexane extraction which was washed with brine solution and dried with anhydrous sodium sulphate [1, 2].

(ii). 1-(2-bromo-vinyl-4-methoxy-benzene)

In the presence of piperidine catalyst (0.24 mL, 3.28 mmol), malonic acid (4.1d) (6.8 g, 65.57 mmol) was added to a solution of 4-methoxy benzaldehyde (4.1c) (4.9 mL, 32.79 mmol) in pyridine (25 mL) and the reaction mixture was refluxed at 120°C for 4 hours. When the reaction was concluded, the reaction mixture was then poured into the cooled 10 % aqueous hydrochloric acid followed by filtering and washing with water yielded a white precipitate of 3-(4-methoxyphenyl)-acrylic acid (4.1e) [3]. Subsequently, N-bromosuccinimide (7.5 g, 42.09 mmol) was added to the mixture of

compound (4.1e) (5 g, 28.06 mmol) and Tetra butyl ammonium bromide (1.8 g, 5.61 mmol). The reaction was allowed to heat for 30 min at 90°C. The resulting crude was purified by column chromatography to obtain 1-(2-Bromo-vinyl-4-methoxybenzene) (4.1f) [4].

(iii). 4-(4-Methoxy-phenyl)-1-phenethyl-1*H*-[1,2,3]triazole

At 110 °C, a mixture of phenethyl azide (4.1b) (4.4 mL, 28.16 mmol), 1-(2-Bromo-vinyl-4-methoxy-benzene) (4.1f) (3 g, 14.08 mmol), CuO nanoparticles (0.56 g, 7.04 mmol) and piperidine (30 mL) was heated for 12 hours. The mixture was cooled to room temperature once the reactants had vanished and the crude product (4.1g) was purified using column chromatography [5] (Scheme - 4.1).

Scheme.4.1. Synthesis of 4-(4-Methoxy-phenyl)-1-phenethyl-1*H*-[1,2,3]triazole

(b). Synthesis of 1-benzyl-4-(naphthalen-2-yl)-1*H*-1,2,3-triazole

(i). (azidomethyl) benzene

Sodium azide (1.98g, 30.48 mmol) was added to Benzyl bromide (4.2a) (5mL, 20.32 mmol) in 50 mL DMSO and stirred overnight at room temperature. Water was progressively added to the reaction mixture after the reaction was confirmed by thin-layer chromatography. The reaction mixture was progressively diluted with water. The corresponding product was generated as clear oil by hexane extraction that was washed with brine solution and dried with anhydrous sodium sulphate [1, 2].

(ii). 2-(2-bromovinyl) naphthalene

Malonic acid (4.2d) (10.8 mg, 64.02 mmol) was added to a solution of 2-naphthaldehyde (4.2c) (5g, 32.01 mmol) in pyridine (25 mL) in the presence of a piperidine catalyst (0.25 mL, 3.2 mmol) and the reaction mixture was refluxed at 120°C for 4 hours. The reaction mixture was then poured into the cooled 10% HCl (aq) solution, filtered and washed with water to produce a white precipitate of 3-(naphthalen-2-yl) acrylic acid (4.2e) [3]. NBS (6.74 g, 37.85 mmol) was then added to the compound (4.2e) (5 g, 25.23 mmol) and TBAB (1.62g, 5.04 mmol). 2-(2-bromo vinyl) naphthalene (4.2f) was obtained by heating the reaction mixture at 90°C for 30 minutes and then evaporating the solvent [4].

(iii). 1-benzyl-4-(naphthalen-2-yl)-1*H*-1,2,3-triazole

A solution of benzyl azide (4.2b) (3.7 mL, 25.74 mmol), 2-(2-bromovinyl) naphthalene (4.2f) (3g, 12.87 mmol), CuO nanoparticles (0.51 g, 6.44 mmol) and piperidine (30 mL) were heated at 110 °C for 12 hours. The mixture was cooled to room temperature after the reaction was completed. Column chromatography was used to purify the resultant crude product (4.2g) [5] (Scheme - 4.2).

Scheme.4.2. Synthesis of 1-benzyl-4-(naphthalen-2-yl)-1*H*-1,2,3-triazole

$(c). \ Synthesis\ of\ N-methyl-N-phenyl-3-(phenylsulfonyl)-1 \\ H-pyrazole-5-carboxamide$

(i). 2-diazo-N-methyl-N-phenylacetamide

To the mixture of 2-bromoacetyl bromide (4.3b) (19.9 mL, 42.45 mmol), N-methyl aniline (4.3a) (3 mL, 28.30 mmol) and acetonitrile (50 mL), potassium bicarbonate (8.49g, 84.9 mmol) was added and stirred for 30 minutes at 0°C. The reaction mixture was quenched with water and extracted with dichloromethane. Brine solution was used to wash the organic phase, dried over with anhydrous sodium sulphate and the corresponding bromo derivative (4.3c) was procured by solvent evaporation. In addition, to the chilled (0°C) combination of 2-bromo-N-methyl-N-phenylacetamide (4.3c) (2g, 8.76 mmol) in Tetrahydrofuran (40 mL), N.N'-Ditosylhydrazine [TsNHNHTs] (5.96 g, 17.52 mmol), 1,8-diazabicyclo[5.4]-1,8-diazabicyclo[5.4]-1,8-d.0] Undec-7-ene [DBU] (6.8 mL, 43.8 mmol) was gently added at room temperature for 30 minutes with steady stirring. After that, the reaction mixture

was quenched with saturated sodium bicarbonate solution and ethyl acetate extraction was performed. The organic phase was washed with brine solution and dried with anhydrous sodium sulphate providing 2-diazo-N-methyl-N-phenylacetamide (4.3d) [6].

(ii). N-methyl-N-phenyl-3-(phenylsulfonyl)-1*H*-pyrazole-5-carboxamide

1, 4 - Dioxane (10 mL) was added to a combination containing (vinyl sulfonyl) benzene (4.3e) (2.88 g, 17.12 mmol), 2-diazo-N-methyl-N-phenylacetamide (4.3d) (1.5 g, 8.56 mmol,), Oxone (1.31 g, 8.56 mmol) and Cetyltrimethylammonium bromide [CTAB] (3.12 g, 8.56 mmol) in the presence of oxygen atmosphere. N-methyl-N-phenyl-3-(phenylsulfonyl)-1*H*-pyrazole-5-carboxamide (4.3f) was obtained by adding water to the reaction mixture, followed by ethyl acetate extraction and drying over anhydrous sodium sulphate [7] (Scheme - 4.3).

Scheme.4.3.Synthesis of N-methyl-N-phenyl-3-(phenylsulfonyl)-1*H*-pyrazole-5-carboxamide

(d). Synthesis of 5-benzyl 3-ethyl 1*H*-pyrazole-3, 5-dicarboxylate

(i). benzyl 2-diazoacetate

Potassium bicarbonate (8.01 g, 80.13 mmol) was added to a mixture of 2-bromoacetyl bromide (4.4b) (18.7 mL, 40.07 mmol), benzyl alcohol (4.4a) (3 mL, 26.71 mmol) and acetonitrile (50 mL) with constant stirring for 30 minutes at 0°C. The reaction mixture was quenched with water and extracted with dichloromethane. Before being dried on anhydrous sodium sulphate, the organic phase was washed with brine solution. The corresponding benzyl 2-bromoacetate (4.4c) was acquired by solvent evaporation. Further, to the cooled (0°C) mixture of the compound (4.4c) (2mL, 6.03 mmol) in THF (40 mL), TsNHNHTs (4.1g, 12.06 mmol) and DBU (4.8 mL, 30.15 mmol) was added slowly with constant stirring for 30 minutes at the room temperature. Thereafter, the reaction mixture was quenched with saturated sodium bicarbonate solution and ethyl acetate was used to extract it. The organic phase was washed in brine solution and dried with anhydrous sodium sulphate, yielding benzyl 2-diazoacetate (4.4d) [6].

(ii). 5-benzyl 3-ethyl 1*H*-pyrazole-3, 5-dicarboxylate

Under an oxygen atmosphere, 1, 4 - dioxane (10 mL) was added to a mixture of ethyl acrylate (4.4e) (1.5 mL, 15.68 mmol), benzyl 2-diazoacetate (4.4d) (1.5 mL, 7.84 mmol), Oxone (1.2 g, 7.84 mmol) and CTAB (2.85 g, 7.84 mmol). Following completion of the reaction, water was added to the reaction mixture which was then extracted with ethyl acetate and dried over anhydrous sodium sulphate and the product was obtained (4.4f) as a white solid [7] (Scheme- 4.4).

Scheme.4.4.Synthesis of 5-benzyl 3-ethyl 1*H*-pyrazole-3, 5-dicarboxylate

(e). Synthesis of N-(4-(piperidin-1-ylsulfonyl) phenyl) acetamide

(i). (4-acetamidobenzene sulfonyl chloride)

In a cooled condition, Chlorosulfonic acid (13 mL, 61.61 mmol) was added dropwise to Acetanilide (4.5a) (3g, 21.87 mmol) and stirred well for 3 hours. The reaction mixture was then poured into the broken ice and extracted with carbon tetrachloride once the reaction was completed. After washing the mixed organic layers with the dilute sodium carbonate solution, 4-acetamidobenzene sulfonyl chloride (4.5b) was procured by solvent evaporation. [8].

(ii). N-(4-(piperidin-1-ylsulfonyl) phenyl) acetamide

The reaction of 4-acetamidobenzene sulfonyl chloride (4.5b) (1.5 g, 6.41 mmol) and piperidine (7.0 mL, 9.63 mmol) in dichloromethane for 30 minutes at room temperature yielded N-(4-(piperidin-1-ylsulfonyl) phenyl) acetamide (4.5c). The resulting product was rinsed in water, filtered and dried [9-11]. (Figure 4.5)

Scheme.4.5. Synthesis of N-(4-(piperidin-1-ylsulfonyl) phenyl) acetamide

4.1.3. Characterization

(a). 4-(4-Methoxy-phenyl)-1-phenethyl-1*H*-[1,2,3]triazole(4.1g)

Appearance : White solid

Melting point : 139-141 °C

¹H NMR (500 MHz, CDCl₃ δ (ppm)) : 7.70 (d, J = 8, 2H), 7.39 (s, 1H), 7.33-7.25 (m,

3H), 7.16 (d, J=4, 2H), 6.95 (d, J = 8, 2H),

4.64 (t, J = 8, 2H), 3.84 (s, 3H), 3.26 (t, J = 8,

2H)

¹³C NMR (125 MHz, CDCl₃ δ (ppm)) : 159.6, 147.4, 137.1, 128.8, 128.7, 127.1, 127.0,

123.4, 119.2, 114.2, 55.3, 51.7

(b). 1-benzyl-4-(naphthalene-2-yl)1*H*-1,2,3-triazole (4.2g)

Appearance : White solid

Melting point : 176-178 °C

¹H NMR (500 MHz, CDCl₃) δ (ppm) : 8.31 (s, 1H), 7.89-7.82 (m, 4H), 7.78 (s, 1H),

7.49-7.47 (m, 2H), 7.46-7.42 (m, 3H), 7.36-

7.34 (*m*, 2H), 5.62 (*s*, 2H)

¹³C NMR (125 MHz, CDCl₃) δ (ppm) : 148.3, 134.7, 133.5, 133.2, 129.2, 128.9, 128.6,

128.2, 128.2, 127.8, 126.4, 126.1, 124.4,

123.8, 119.8, 54.3

(c). N-methyl-N-phenyl-3-(phenylsulfonyl)-1*H*-pyrazole-5-carboxamide (4.3f)

Appearance : White solid

Melting point : 192-194°C

¹H NMR (500 MHz, CDCl₃) δ (ppm) : 7.87 (d, J = 8 Hz, 2H), 7.59-7.47 (m, 7H), 7.26 (d

J = 4 Hz, 2H), 3.45 (s, 3H)

¹³C NMR (125 MHz, CDCl₃) δ (ppm) : 157.9, 153.2, 142.6, 140.5, 136.7, 133.6, 133.32

130.4, 129.6, 129.1, 127.9, 127.6, 108.2, 38.6

(d). 5-benzyl-3-ethyl 1*H*-pyrazole-3, 5-dicarboxylate (4.4f)

Appearance : White solid

Melting point : 88-90°C

¹H NMR (500 MHz, CDCl₃) δ (ppm) : 7.42-7.37 (m, 2H), 7.36-7.27 (m, 4H), 5.36 (s,

2H) 4.40(q, J = 8 Hz, 2H), 1.37 (t, J = 8 Hz,

3H)

¹³C NMR (125 MHz, CDCl₃) δ (ppm) : 160.3, 160.2, 139.9, 135.1, 128.7, 128.6, 128.5,

111.5, 67.2, 61.7, 14.2

(e). N-(4-(piperidin-1-ylsulfonyl) phenyl) acetamide (4.5c)

Appearance : Milky white solid

Melting Point : 108-110 °C

¹H NMR (500 MHz, CDCl₃) δ (ppm) : 7.73-7.68 (m, 4H), 7.27 (bs, 1H), 2.98 (t, J = 4

Hz, 4H), 2.22 (s, 3H), 1.66-1.61 (pen, 4H),

1.44-1.39 (p, 2H)

 13 C NMR (125 MHz, CDCl₃) δ (ppm) : 168.7, 141.9, 131.0, 128.9, 119.3, 46.9, 25.1,

24.7, 23.5

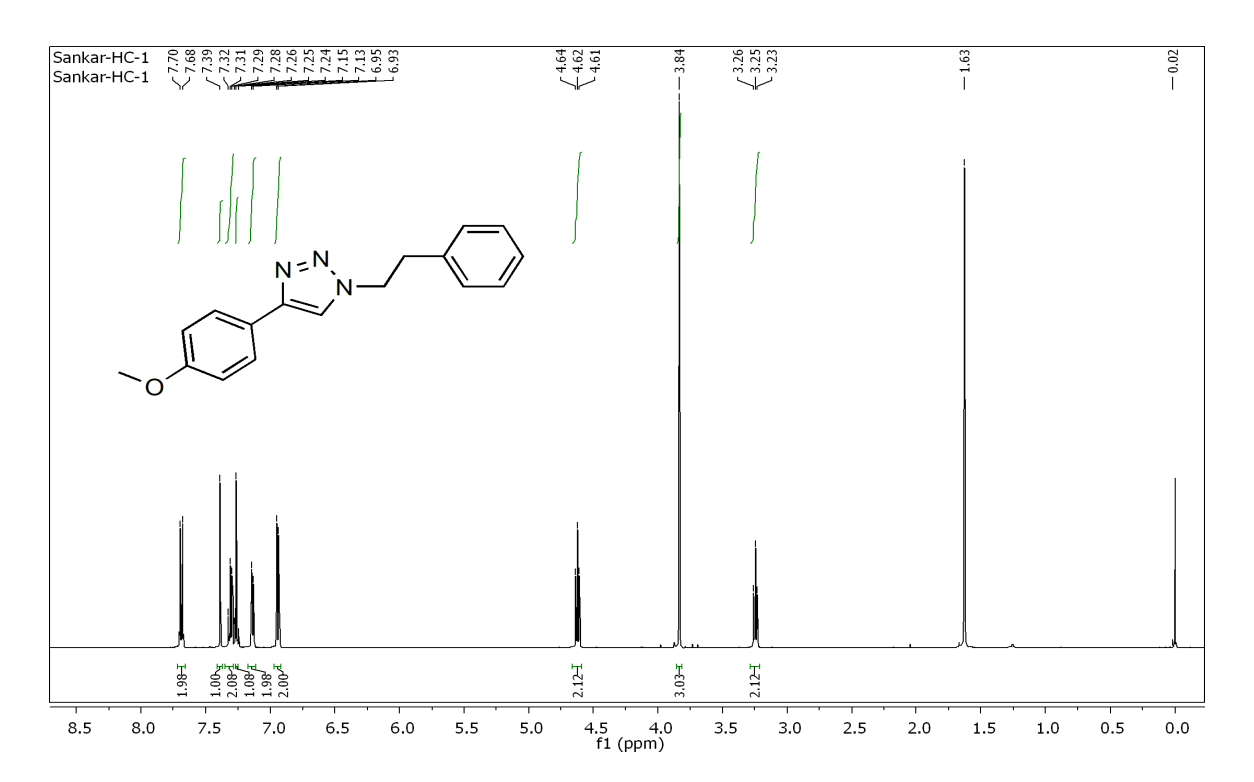


Fig.4.1. 1 H NMR spectrum of 4-(4-Methoxy-phenyl)-1-phenethyl-1H-[1,2,3] triazole

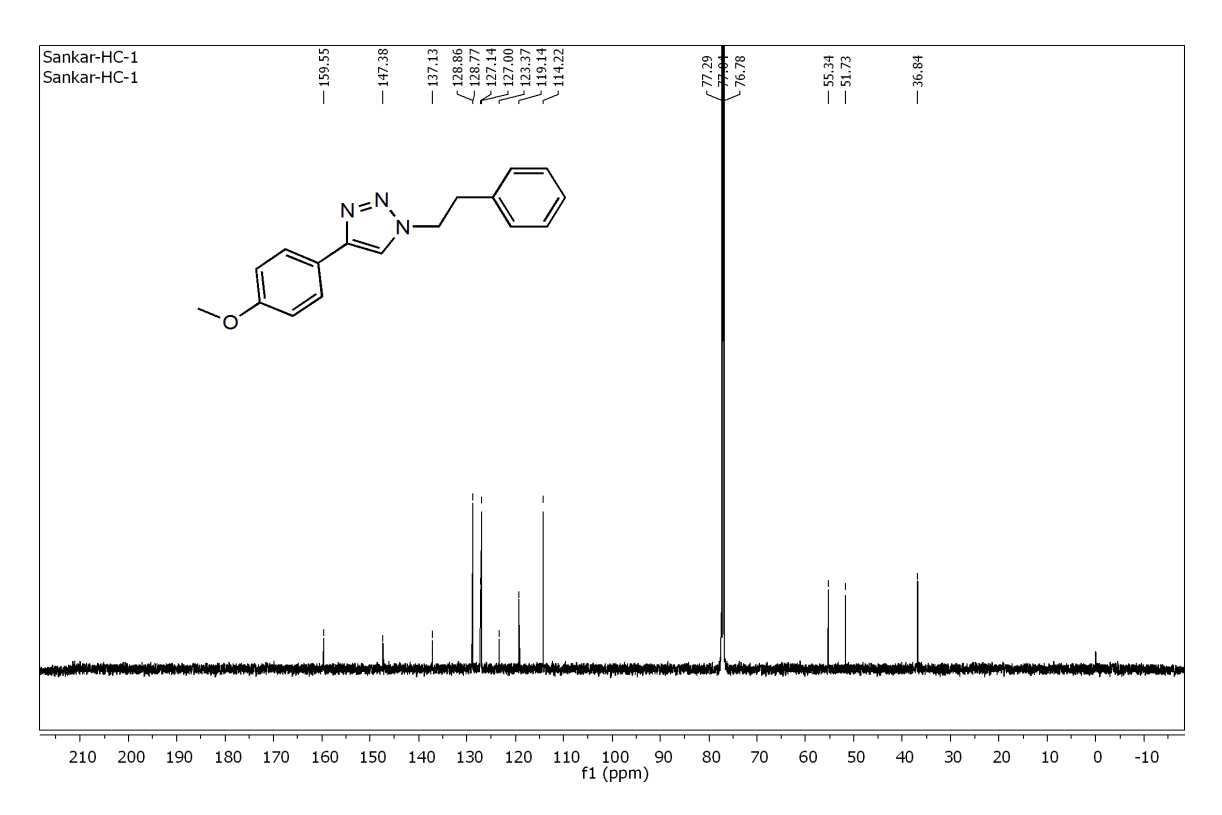
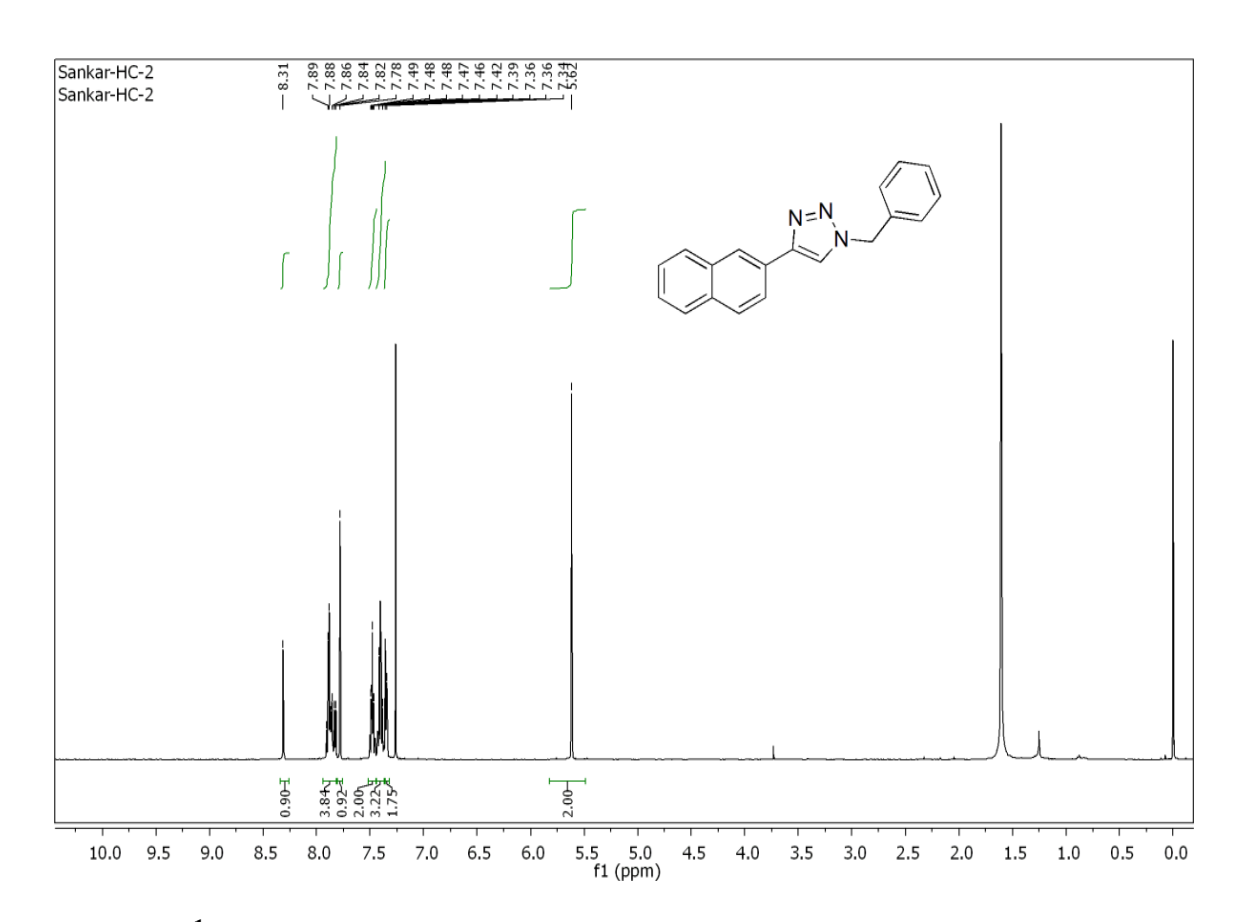


Fig.4.2. 13 C NMR spectrum of 4-(4-Methoxy-phenyl)-1-phenethyl-1H-[1,2,3] triazole



 ${\bf Fig. 4.3.^1H~NMR~spectrum~of~1-benzyl-4-(naphthalen-2-yl)-1} \\ H-1,2,3-triazole$

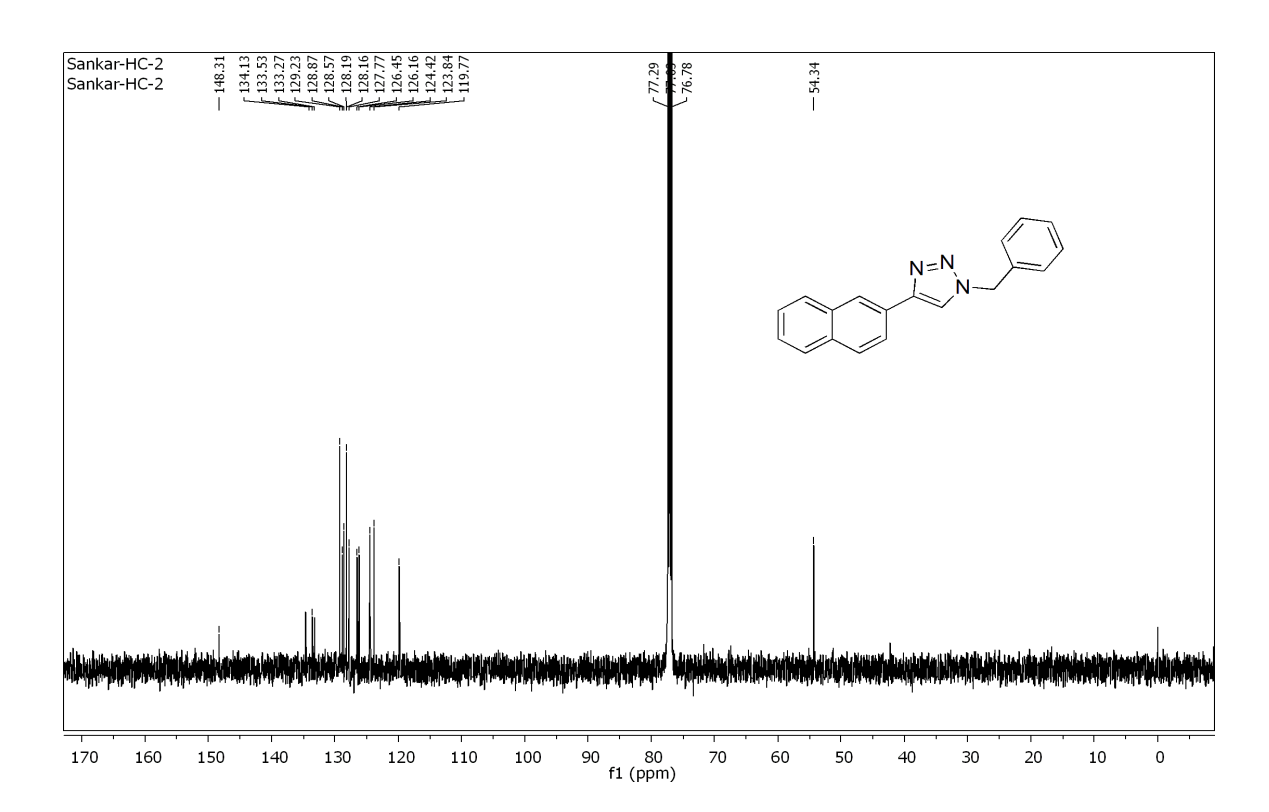
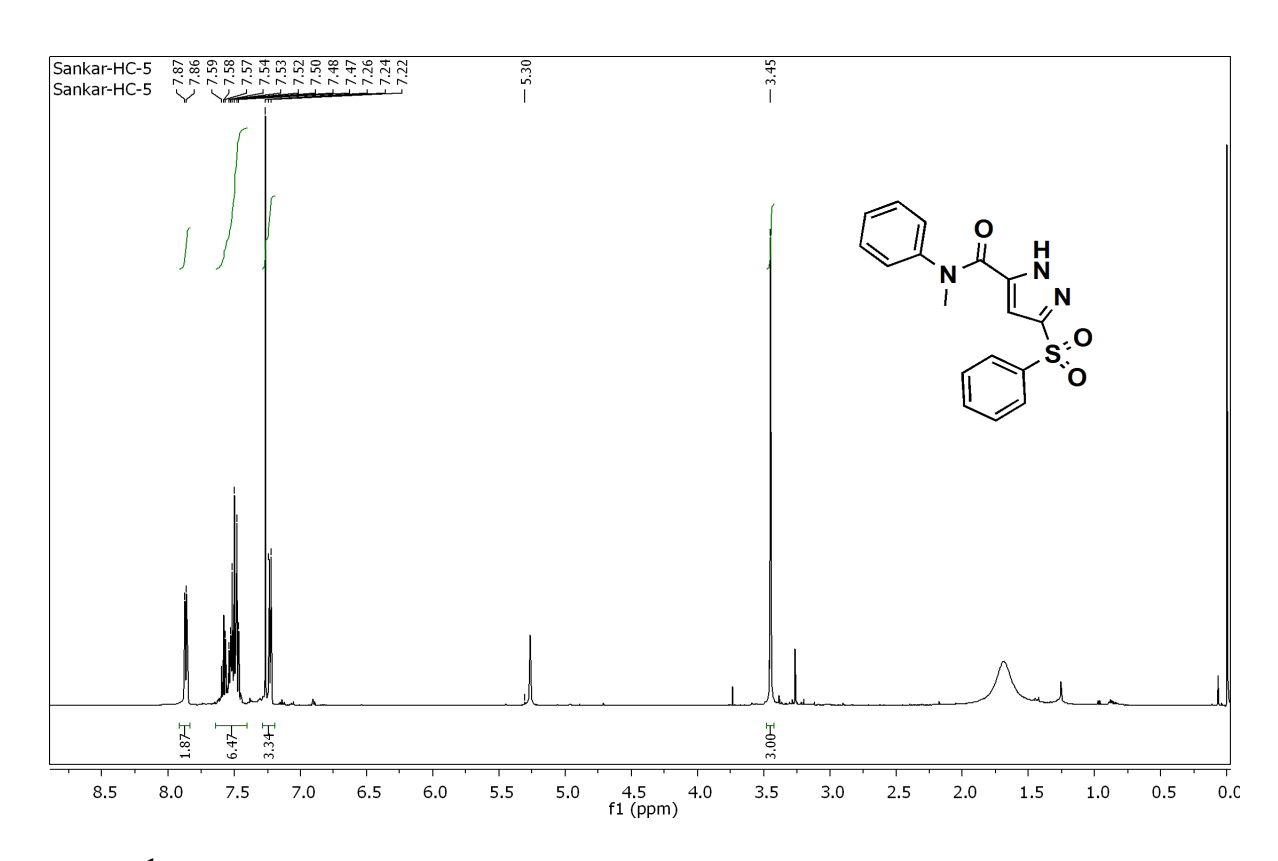


Fig.4.4. ¹³C NMR spectrum of 1-benzyl-4-(naphthalen-2-yl)-1*H*-1,2,3-triazole



 ${\bf Fig. 4.5.^1H~NMR~spectrum~of~N-methyl-N-phenyl-3-(phenylsulfonyl)-1} \\ {\bf H-pyrazole-5-carboxamide}$

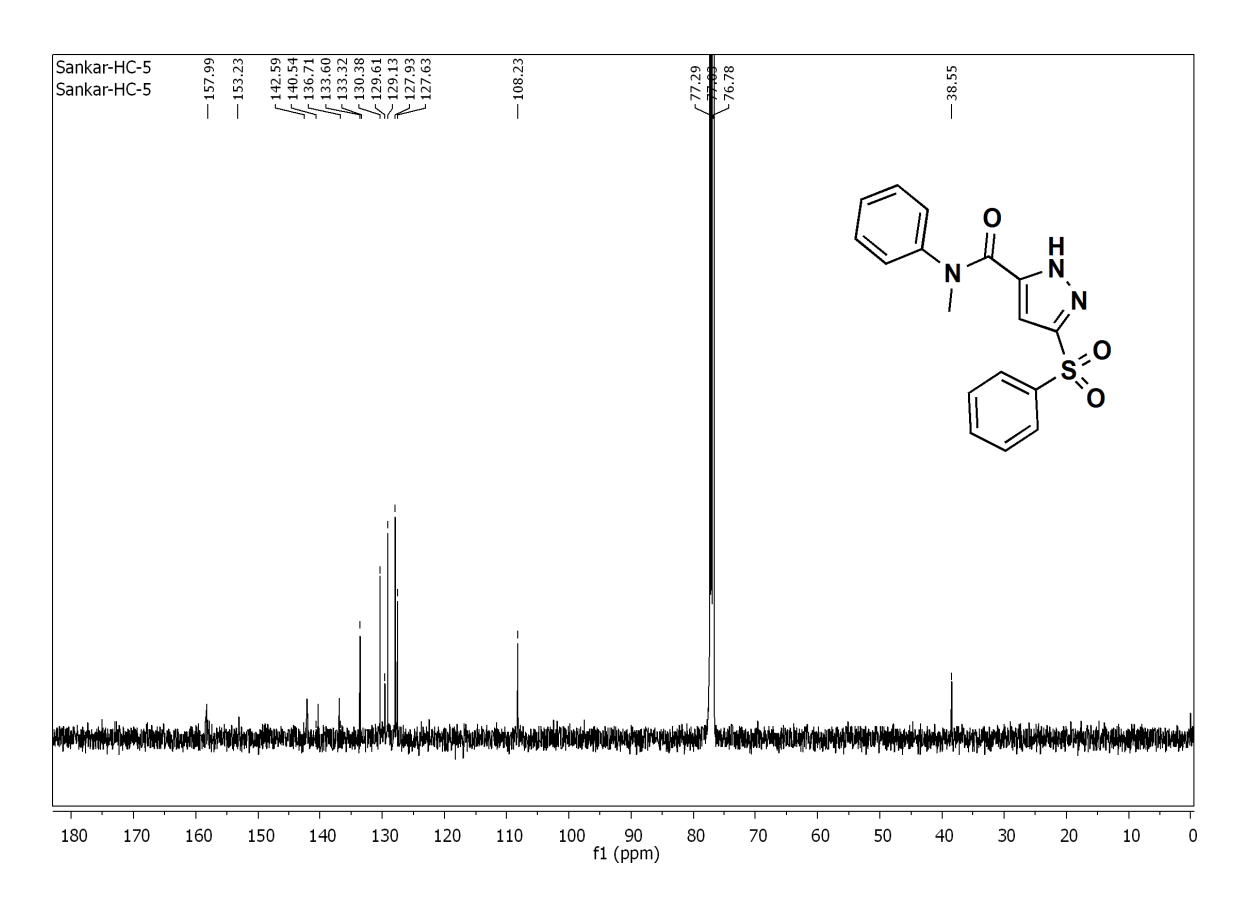


Fig.4.6. 13 C NMR spectrum of N-methyl-N-phenyl-3-(phenylsulfonyl)-1H-pyrazole-5-carboxamide

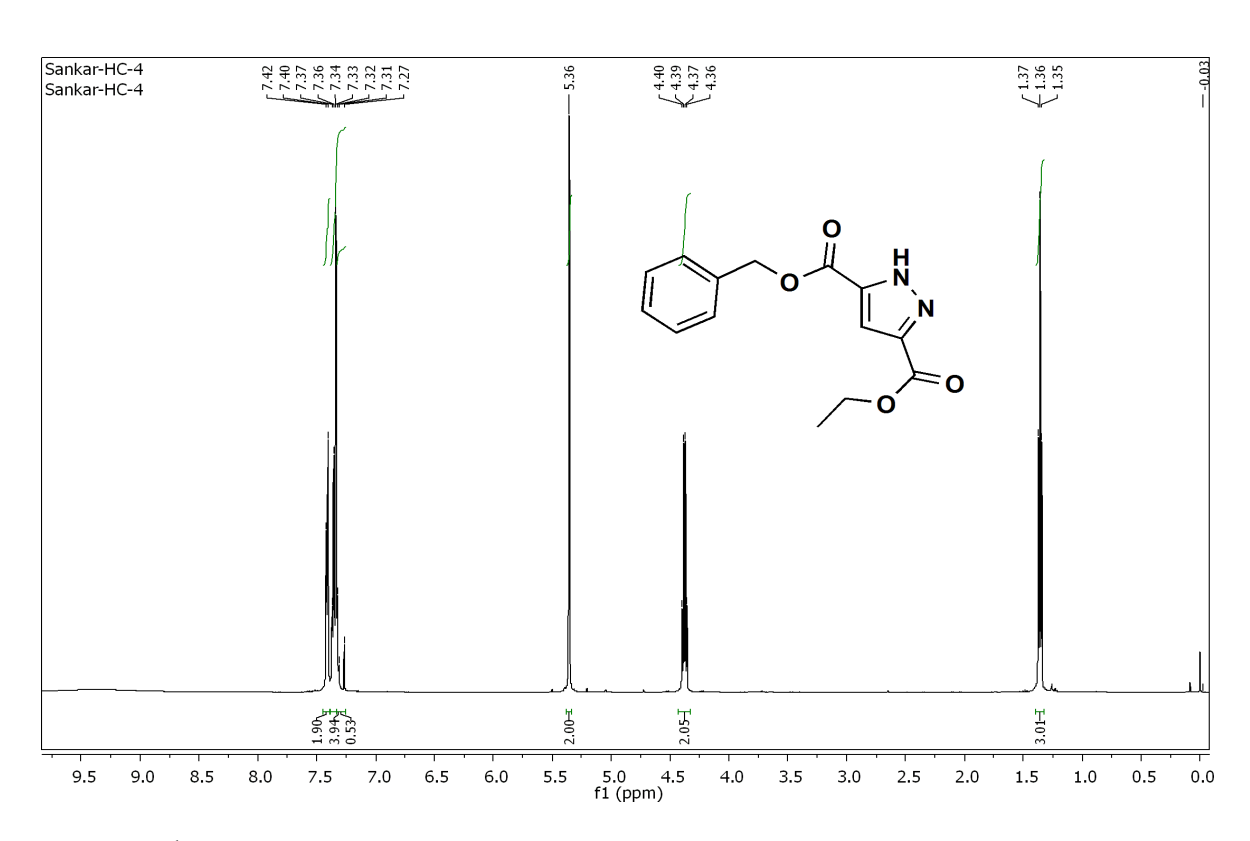


Fig.4.7. 1 H NMR spectrum of 5-benzyl 3-ethyl 1H-pyrazole-3, 5-dicarboxylate

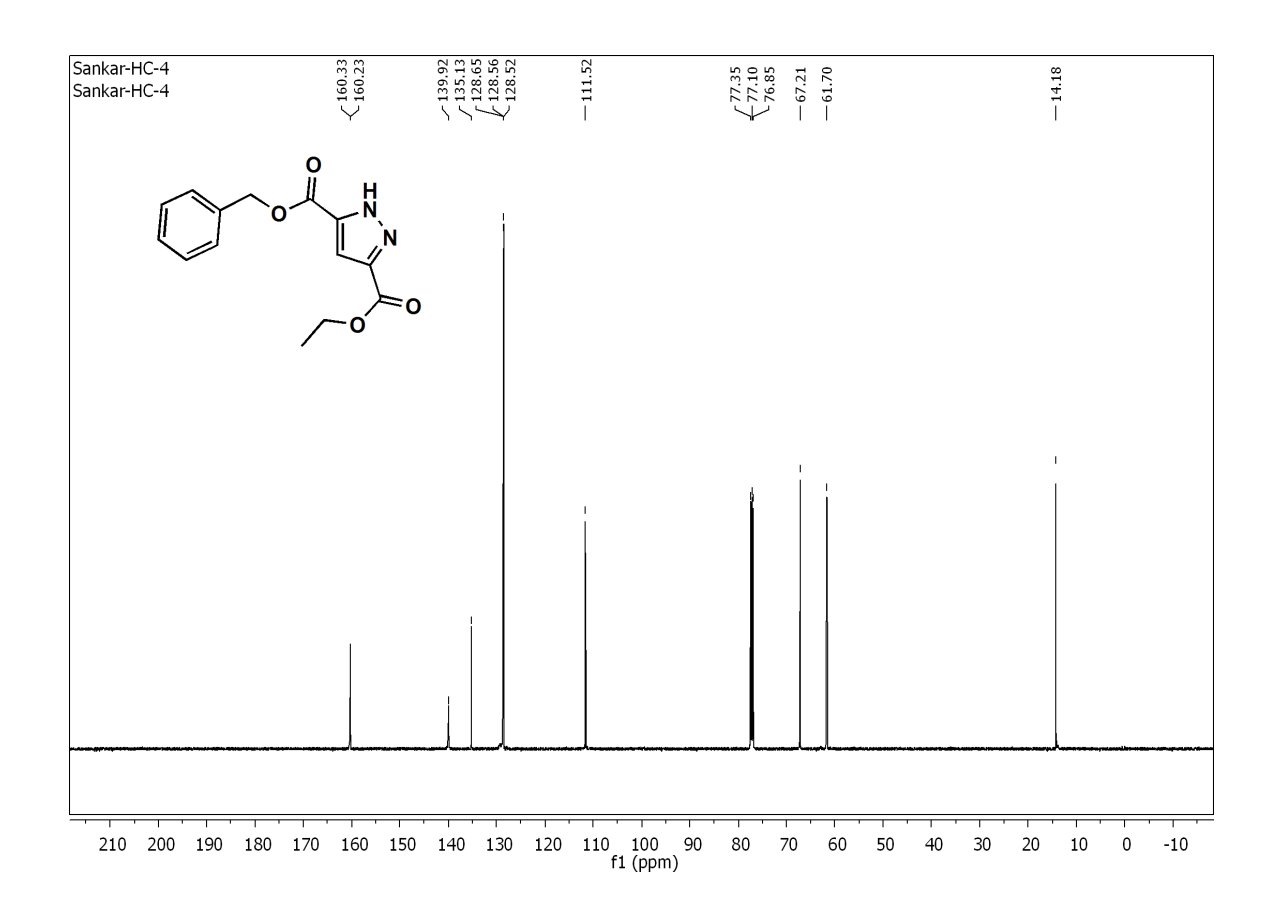


Fig.4.8. 13 C NMR spectrum of 5-benzyl 3-ethyl 1H-pyrazole-3, 5-dicarboxylate

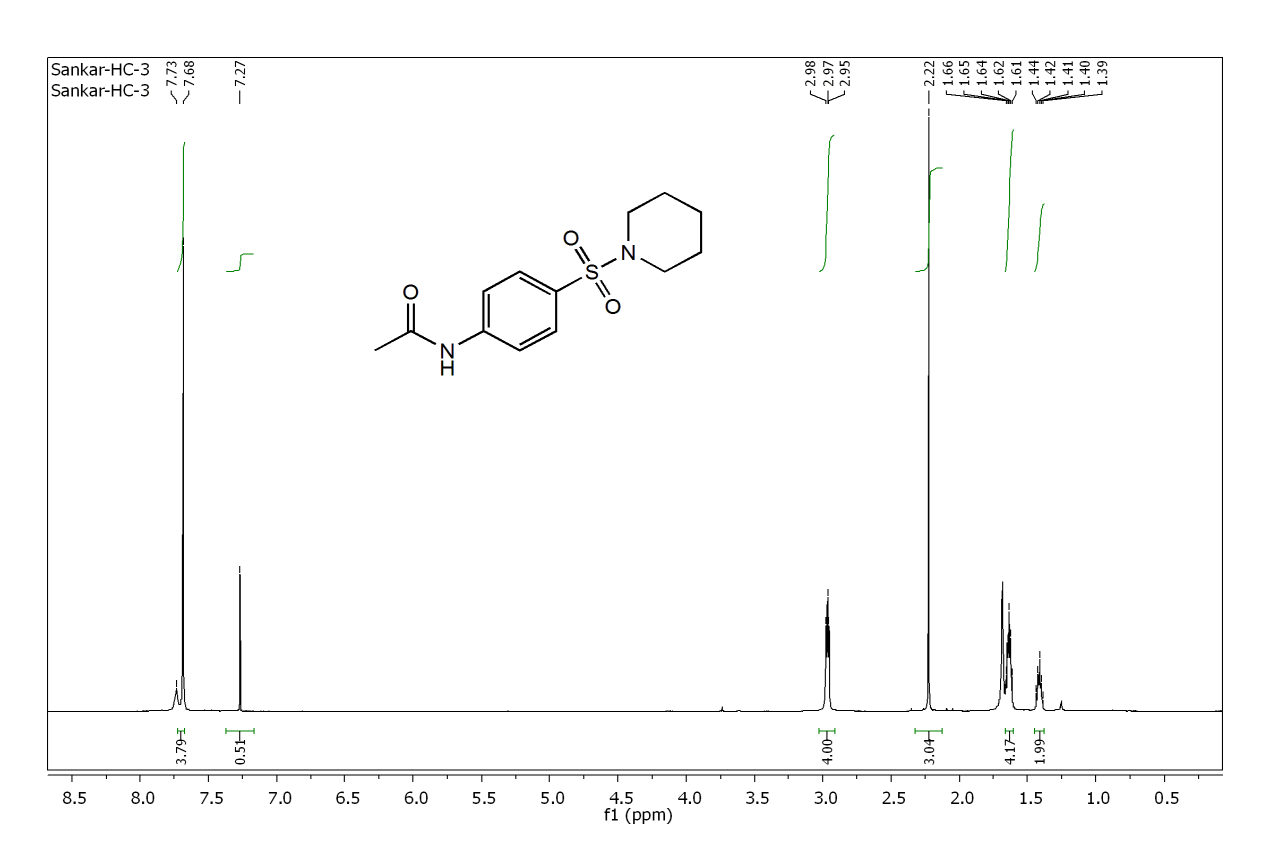


Fig.4.9.¹H NMR spectrum of N-(4-(piperidin-1-ylsulfonyl) phenyl) acetamide

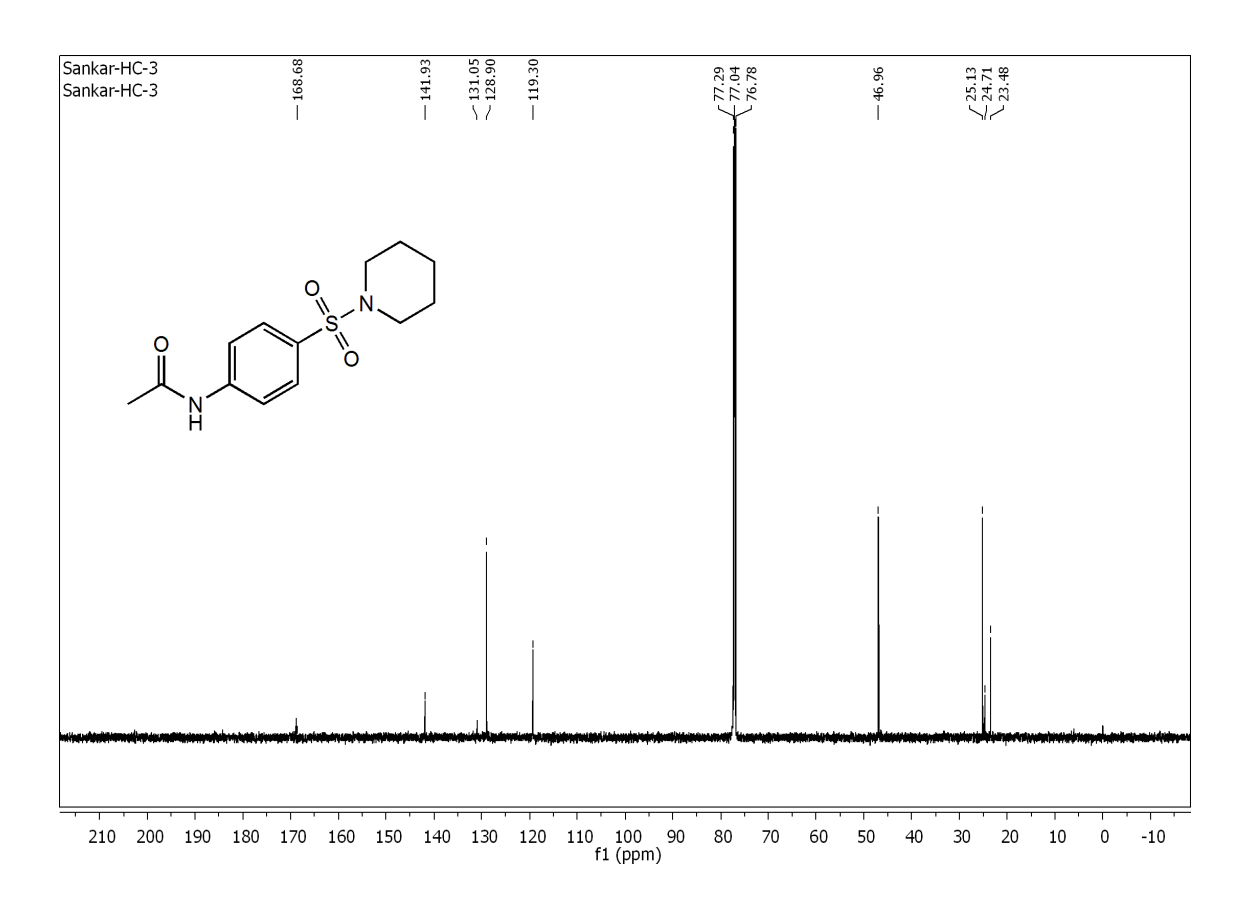


Fig.4.10. ¹³C NMR spectrum of N-(4-(piperidin-1-ylsulfonyl) phenyl) acetamide

4.2. Experimental Methods of Corrosion Investigation

4.2.1. Materials

(i). Mild steel

The specimens utilized in this study were commercially available IRSM41/97 grade Mild steel. The elemental analysis of the Mild steel specimens studied were S - 0.009%, Cu - 0.31%, P - 0.089%, Mn - 0.43%, C - 0.076%, Cr - 0.52%, Si - 0.319%, Al - 0.028%, Ni - 0.20% and Fe 99.69%.

(ii). Preparation of corrosive medium

The corrosive medium (1.0 M HCl) used in this investigation was made by diluting 84.8 mL of Analar HCl in one liter of double-distilled water.

(iii). Corrosion inhibitors

For corrosion studies, ethanol was used to prepare the desired concentrations of the synthetic inhibitors MPPT, BNT, MPSC, BEPD and PSPA.

4.2.1. Corrosion exploration

(i). Mass loss method

For the mass loss method, the rectangular-shaped Mild steel specimens enclosing the dimensions 5cm×2cm×0.2cm were employed. Mild steel specimens were prepared by different numbers (200, 400, 600, 800, 1200 and 1500 grades) of silicon carbide emery papers and the polished specimens were washed with distilled water, rinsed with ethanol and degreased with acetone [12].

The prepared Mild steel samples were weighed accurately before and after immersion in the 1M HCl corrosive solution in various concentrations of corrosion inhibitors for 6 hour contact time at room temperature. Subsequently, the specimens were taken out, washed, dried and then accurately weighed for the determination of corrosion parameters.

For this evaluation, the average weight loss was acquired by the three consecutive mass loss experiments in the above identical conditions [13, 14]. The corrosion factors such as the rate of corrosion (CR) inhibition efficiency (IE) and surface coverage (θ) were determined by the following equations (5.1), (5.2) and (5.3) respectively.

$$CR = \frac{\Delta W}{At}$$
 (5.1)

I. E(%) =
$$\left(\frac{W_0 - W}{W_0}\right) \times 100$$
 (5.2)

where ΔW is the average mass loss (mg), A is the total surface area (cm⁻²) and t is the exposure time (h) for the tested specimens with and without inhibitors in the 1M HCl medium.

$$\theta = \left(\frac{W_0 - W}{W_0}\right) \tag{5.3}$$

where W and W_0 reflect the average weight loss of Mild steel samples (mg) withand without inhibitor respectively.

(ii). Potentiodynamic polarization study

The electrochemical investigations were achieved by the CHI-66 model potentiostat with the conventional three-electrode assemblage. The reference and counter electrodes in these arrangements were a platinum foil and a standard calomel electrode. Meanwhile, 1 cm² of the Mild steel specimen was act as the working electrode in a corrosive context. For polarization measurements, the working electrode was exposed with and without inhibitors in the test solution for 30 minutes until the open circuit potential was reached. The polarization curves were obtained automatically by adjusting the potential of the electrode from –500 mV to +500 mV at a scan rate of 1 mV S⁻¹. At the intersection of Tafel lines, the corrosion current density (I_{corr}) values were obtained [15, 16]. Inhibition efficacy and the surface coverage values were measured with the following equation (5.4)

$$IE(\%) = \left[\frac{i_{corr} - i_{corr (inh)}}{i_{corr}}\right] \times 100$$
 (5.4)

where $I_{corr\ (inh)}$ and I_{corr} are the corrosion current densities in the presence and absence of inhibitors in the 1M HCl solution.

(iii). Impedance study

The electrochemical impedance analysis was carried out in the frequency range from 100 kHz to 10 MHz with the maximum amplitude of 5 mV, receiving AC signals at the open circuit potential. From the initial and final points of the Nyquist plots for

various concentrations of inhibitors, the investigational charge transfer resistance (R_{ct}) was obtained [17, 18]. The inhibition efficiency and electrical double layer capacity (C_{dl}) of the investigated inhibitors were determined from the charge transfer resistance values using equations (5.5) and (5.6) respectively.

I. E (%) =
$$\left[\frac{R_{ct (in h)} - R_{ct}}{R_{ct (in h)}}\right] \times 100$$
 (5.5)

$$C_{dl} = \frac{1}{2\pi \cdot f_{max} \cdot R_{ct}} \tag{5.6}$$

where $Rct_{(inh)}$ and Rct are the charge transfer resistance with and without inhibitor and f_{max} is the maximum peak frequency of the Nyquist plots.

(iv). Quantum chemical study

Quantum chemical study is a vital tool to comprehend the corrosion protection mechanism which is procured by the Density Functional Theory [DFT] using Gaussian 09W software with the B3LYP/6-31G (d, p) basis set. Herein, the efficiency of the investigated inhibitors is directly associated with the Frontier molecular orbital [FMO] energies, such as Ehomo and Elumo which can be inferred from the optimized geometry of the inhibitors. The following equations (5.7 - 5.14) can be used to extract the additional important electronic properties from the frontier molecular orbital energies: Energy gap (Δ E), Ionization energy (I), Electron affinity (A), Absolute electronegativity (χ), Global hardness (η), Globale softness (σ), Fraction of electron transferred (Δ N) and Back donation (Δ E_{Backdonation}) respectively. All of the

aforementioned features facilitate the finding of the reactivity and stability of the examined protector and the inhibitor-metal interactions [19-21].

$\Delta E = E_{HOMO} - E_{LUMO}$	(5.7)
$I = -E_{HOMO}$	(5.8)
$A = -E_{LUMO}$	(5.9)
$\chi = -\frac{1}{2} \left(E_{\text{LUMO}} + E_{\text{HOMO}} \right)$	(5.10)
$\eta = -\frac{1}{2} \left(E_{\text{HOMO}} - E_{\text{LUMO}} \right)$	(5.11)
$\sigma = \frac{1}{\eta}$	(5.12)
$\Delta N = \frac{\Phi - \chi_{inh}}{[2(\eta_{Fe} + \eta_{inh})]}$	(5.13)
$\Delta \mathrm{E}_{\mathrm{(backdonation\)}} = -rac{\eta}{4}$	(5.14)

(v). Morphological investigation

The corrosion products which generally rust on the metal surfaces were examined using a set of equipments as illustrated below.

(a). Scanning Electron Microscope analysis (SEM)

The morphology of Mild steel samples was investigated in the 1M HCl solution for 6 hours at room temperature with and without inhibitor using a scanning electron microscope [ZEISS] [22, 23].

(b). Energy-dispersive X-ray spectroscopy (EDX)

Electron Dispersive X-ray analysis is one of the most important ways for identifying the components present on the Mild steel surface. Using an Energy

Dispersive X-ray Analyzer unit coupled to a SUPRA 55 Field Emission Scanning Electron Microscope [FESEM], the corrosion inhibition process of Mild steel specimens with and without inhibitor in the 1M HCl solution for 6 hours contact time at room temperature was investigated [24, 25].

(c). Atomic force microscope analysis (AFM)

An atomic force microscope was used to assess the surface roughness of metals with and without inhibitor in the 1M HCl solution during a 6 hour exposure time at room temperature. These findings highlighted some intriguing concerns about the usefulness of inhibitors in preventing Mild steel specimen deterioration in corrosive conditions [26, 27].

4.3. References

- 1. Scriven E F V, Turnbull K. Azides: Their preparation and synthetic uses. *Chem. rev.* 1988; 88: 297-368.
- 2. Zhu Wand Ma D. Synthesis of aryl azides and vinyl azides *via* proline promoted CuI-catalyzed coupling reactions. *Chem. comm.* 2004; 888-889.
- Pandey A K, Sharma R, Shivahare R, Arora A, Rastogi N, Gupta S, Chauhan P M S
 J. Synthesis of Perspicamide A and Related Diverse Analogues: Their Bioevaluation as Potent Antileishmanial Agents. *J.Org. Chem.* 2013; 78: 1534–1546.
- 4. Ganguly N C, De P, Dutta S. Mild Regioselective Monobromination of Activated Aromatics and Heteroaromatics with *N*-Bromosuccinimide in Tetrabutylammonium Bromide. *Synthesis*. 2005; 7: 1103-1108.
- 5. Paul Raj J, Ganga Prasad D, Vajjiravel M, Karthikeyan K, Elangovan J. CuO-Nanoparticles Catalyzed Synthesis of 1,4-Disubstituted-1,2,3-Triazoles from Bromoalkenes. *J. Chem. Sci.* 2018; 130 (44): 1-6.
- 6. Toma T, Shimokawa J, Fukuyama T. *N, N'*-Ditosylhydrazine: a convenient reagent for facile synthesis of diazoacetates. *Org. Lett.* 2007; 9: 3195-3197.
- 7. Paul Raj J, Gangaprasad D, Karthikeyan K, Rengasamy R, Kesavan M, Venkateswarulu M, Vajjiravel M, Elangovan J. A new route to synthesis of substituted pyrazoles through oxidative [3+2] cycloaddition of electron deficient alkenes and diazocarbonyl compounds. *Tetrahedron Lett.* 2018; 59(51): 4462-4465.
- 8. Smiles S, Stewart J. p-Acetaminobenzenesulfonyl chloride. *Organic Syntheses*. Wiley: New York. 1941;8-10.

- 9. Ilies M, Vullo D, Pastorek J. Carbonic Anhydrase Inhibitors. Inhibition of Tumor Associated Isozyme IX by Halogeno sulfanilamide and Halogenophenyl aminobenzolamide Derivatives. *J Med Chem.* 2003; 46 (11): 2187-2196.
- 10. Patel P, Ramalingan C, Park Y. Synthesis and antimicrobial evaluation of guanylsulfonamides. *Bioorg Med Chem Lett.* 2007; 17 (23): 6610-6614.
- 11. De Castro Barbosa M, de Albuquerque Melo G, da Silva Y. Synthesis and pharmacological evaluation of N-phenyl-acetamide sulfonamides designed as novel non-hepatotoxic analgesic candidates. *Eur J Med Chem.* 2009; 44 (9): 3612-3620.
- 12. Verma D K, Ebenso E E, Quraishi M A, Verma C. Gravimetric, electrochemical surface and density functional theory study of acetohydroxamic and benzohydroxamic acids as corrosion inhibitors for copper in 1 M HCl. *Results in Physics*, 2019;13: 102194.
- 13. Li X, Ye Y, Liu T, Zheng W, Yang F, Zhao H, Wang L. Corrosion inhibition of Q235 steel in 1 M HCl using quaternized tetraaniline as a corrosion inhibitor. *Surf. Topogr. Metrol. Prop.* 2017; 5: 044001.
- 14. Obot I, Obi-Egbedi N. Adsorption properties and inhibition of Mild steel corrosion in sulphuric acid solution by ketoconazole: Experimental and theoretical investigation. *Corros Sci.* 2010; 52(1): 198-204.
- 15. Singh A K, Quraishi M A. Study of Some Bidentate Schiff Bases of Isatin as Corrosion Inhibitors for Mild steel in Hydrochloric Acid Solution. *Int. J. Electrochem. Sci.* 2012; 7: 3222-3241.
- 16. Saxena A, Prasad D, Haldhar R, Singh G, Kumar A. Use of Sida cordifolia Extract as Green Inhibitor for Mild steel in 0.5 M H₂SO₄. *J. Environ. Chem. Eng.*, 2018; 6: 694.

- 17. Hassan H, Abdelghani E, Amin M. Inhibition of Mild steel corrosion in hydrochloric acid solution by triazole derivatives. *Electrochim Acta*. 2007; 52 (22): 6359-6366.
- 18. Abdel-Aal M, Morad M. Inhibiting effects of some quinolines and organic phosphonium compounds on corrosion of Mild steel in 3M HCl solution and their adsorption characteristics. *British Corrosion Journal*. 2001; 36(4): 253-260.
- 19. Martinez S. Inhibitory mechanism of mimosa tannin using molecular modeling and substitutional adsorption isotherms. *Mater Chem Phys.* 2003; 77(1): 97-102.
- 20. Olasunkanmi L, Obot I, Kabanda M, Ebenso E. Some Quinoxalin-6-yl Derivatives as Corrosion Inhibitors for Mild steel in Hydrochloric Acid: Experimental and Theoretical Studies. *The Journal of Physical Chemistry C*. 2015; 119(28): 16004-16019.
- 21. Singh A, Ansari K, Haque J. Effect of electron donating functional groups on corrosion inhibition of Mild steel in hydrochloric acid: Experimental and quantum chemical study. *J Taiwan Inst Chem Eng.* 2018; 82: 233-251.
- 22. Ouakki M, Galai M, Rbaa M. Quantum chemical and experimental evaluation of the inhibitory action of two imidazole derivatives on Mild steel corrosion in sulphuric acid medium. *Heliyon*. 2019; 5(11): e02759.
- 23. Mulky L, Murthy V R, Rao P. An insight into inhibitory performance of Commiphora Mukul on corrosion of aluminum alloy under tribological conditions. *J Iran Chem Soc.* 2021; 18: 2953–2963.
- 24. Lgaz H, Salghi R, Chaouiki A, Shubhalaxmi, Jodeh S, Subrahmanya Bhat K. Pyrazoline derivatives as possible corrosion inhibitors for Mild steel in acidic media: A combined experimental and theoretical approach. *Cogent Engineering*. 2018;5: 1441585.

- 25. Gopi D, Sherif E, Surendiran M, Angeline Sakila D, Kavitha L. Corrosion inhibition by benzotriazole derivatives and sodium dodecyl sulphate as corrosion inhibitors for copper in ground water at different temperatures. *Surface and Interface Analysis*. 2015; 47(5): 618-625.
- 26. Oboz I B, Obi-Egbedi N O. Adsorption Properties and Inhibition of Mild steel Corrosion in Sulphuric Acid Solution by Ketoconazole: Experimental and Theoretical Investigation. *Corros. Sci.* 2010; 52: 198-204.
- 27. Qiang Y, Guo L, Zhang S, Li W, Yu S, Tan J. Synergistic effect of tartaric acid with 2,6-diaminopyridine on the corrosion inhibition of Mild steel in 0.5 M HCl. *Sci Rep.* 2016; 6(1): 33305.

CHAPTER - V

Corrosion investigation of 4-(4-methoxy-phenyl)-1-phenethyl-1*H*-[1,2,3]triazole(MPPT) on Mild steel in 1M HCl solution

As reported by the ASTM G31-72, the corrosion inhibition study was conducted by accurately weighed Mild steel samples before and after immersion in the 1M HCl corrosive solution in various concentrations (5, 10, 30, 50, 70 and 100 ppm) of 4-(4-Methoxy-phenyl)-1-phenethyl-1*H*-[1,2,3]triazole (MPPT) inhibitor for 6 hours contact time.

5. Results and Discussion

5.1. Mass loss examination

The mass loss approach was used to establish a correlation between the corrosion rate and the inhibition efficiency in the 1M HCl solution at room temperature as shown in (Fig. 5.1). It clearly shows that as the inhibitor concentration increases, the inhibition ability rises linearly while the corrosion rate drops.

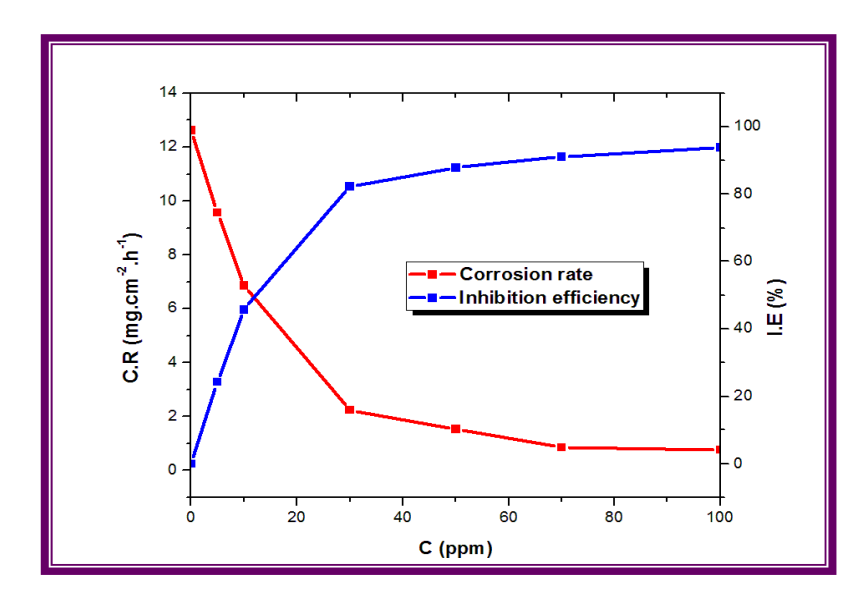


Fig.5.1.Correlation between the inhibition efficiency and the corrosion rate of MPPT in the 1M HCl solution

Additionally, corrosion statistics such as corrosion rate, inhibition efficiency and surface coverage are provided in Table 5.1. As the MPPT concentration increases, the weight loss of the steel specimen falls and the concomitant corrosion rate subsequently decreases from 12.629 to 0.7675 (mg cm⁻² h⁻¹) as shown in the tabular data. As the concentration of MPPT increases, the protective ability of Mild steel in corrosive media improves dramatically from 24.24 to 93.92%. The increasing values of surface coverage also pinpoint that the MPPT has a larger competence of protection over the metallic surface. Moreover, the optimal efficiency reaches up to 93.92% at 100 ppm concentration. All of the results from the mass loss analysis pointed to the examined MPPT acting as an effective protector in the 1M HCl media [1].

Table.5.1. Mild steel corrosion factors of MPPT in 1M HCl solution

Concentration	Weight loss	Corrosion rate	Inhibition	Surface
(ppm)	(mg)	(mg cm ⁻² h ⁻¹)	efficiency (%)	coverage (θ)
Blank	939.6	12.63	-	-
5	711.8	9.57	24.24	0.24
10	509.9	6.85	45.73	0.46
30	166.9	2.24	82.24	0.82
50	113.8	1.53	87.89	0.88
70	84.2	1.13	91.04	0.91
100	57.1	0.77	93.92	0.94

5.2. Potentiodynamic polarization investigation

(Fig.5.2) displays the Tafel lines for the test specimens in the absence and presence of various concentrations of MPPT in the 1M HCl medium at room temperature. The Tafel lines appear on both anodic and cathodic sites indicating that the presence of MPPT obstructs both the oxidation and reduction reactions on Mild steel in the acidic atmosphere.

Besides that, the acquired polarization parameters are presented in Table.5.2 confirming the preceding suggestion. In general, the difference in corrosion potential (E_0) values for the existence of inhibitor and the blank is greater than ± 85 mV suggesting that the inhibitor molecules are identified either as the cathode or anode inhibitor distinctively [2].

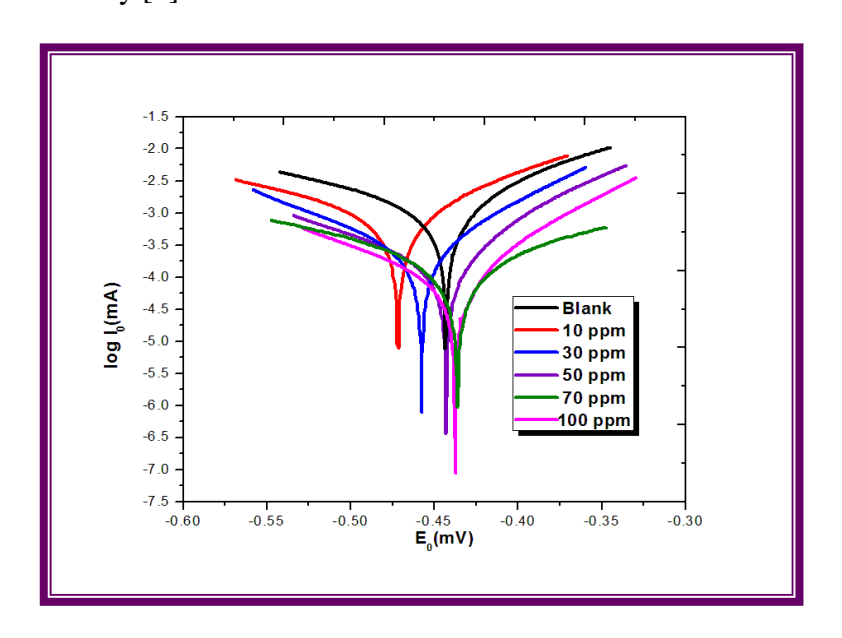


Fig.5.2. Tafel curves for MPPT in 1M HCl solution

As a result of this polarization investigation, the change in E_{corr} values from blank to optimum concentration ranges from -443 mV to -437.56 mV, demonstrating that the examined MPPT performed as a mixed type protector in an acidic environment which is substantiated by the Tafel slope values.

Tafel effect is observed on both the anodic and cathodic branches as shown by the Tafel slope values be and ba with the larger values of be reflecting cathodic preponderance. Furthermore, we can see that as the concentration of MPPT increases, the corrosion current density (I_{corr}) decreases from 1.746 to 0.098 mA illuminating that the corrosion current is retarded by the presence of MPPT molecules adsorbed onto the metallic surface [3]. Also, the maximum efficiency observed is 94.39% at 100 ppm

concludes that the MPPT inhibitor functioned as an effective anticorrosive defender in the 1M HCl medium.

Table.5.2. Polarization factors for MPPT on Mild steel corrosion in the 1M HCl solution

Conc.	Polarization parameters					
(ppm)	E ₀ (mV)	I ₀ (mA)	b _c (mV)	ba(mV)	IE (%)	
Blank	-443.00	1.746	249.63	116.96	-	
10	-471.69	1.312	233.64	125.50	24.86	
30	-457.53	0.296	118.11	78.36	83.0	
50	-443.02	0.205	147.80	72.12	88.26	
70	-436.62	0.132	125.41	71.24	92.42	
100	-437.56	0.098	120.90	67.79	94.39	

5.3. Impedance assessment

The increase in the diameter of Nyquist plots with the increasing MPPT concentration in the 1M HCl solution is seen in (Fig.5.3) implying that the addition of MPPT increases the charge transfer resistance capacity. Owing to the coarseness of the metal surface and inhomogeneity distribution of active sites for adsorption, as portrayed in (Fig.5.3), the semicircles acquired by impedance analysis are not perfect during the corrosion process [4].

Moreover, the impedance factors such as charge transfer resistance (R_{ct}), electrical double layer capacitance (C_{dl}) and inhibition efficiencies (I.E) are summarized in Table 5.3. It indicates that increased R_{ct} values from 9.95 to 155.23 Ω cm² with increasing MPPT concentrations suggest that charge transfer during the corrosion process is hampered by the acidic medium.

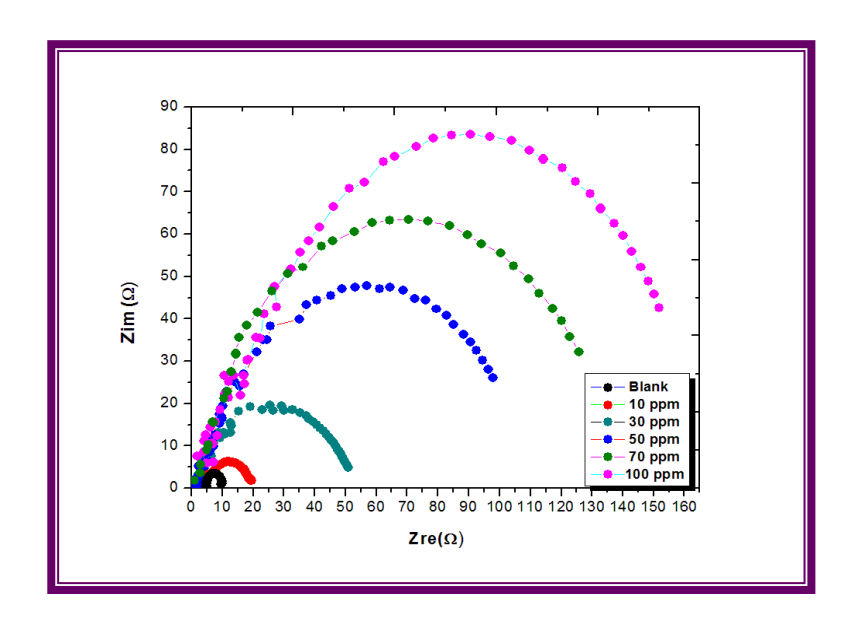


Fig.5.3. Impedance plots of MPPT in the 1M HCl solution

Furthermore, the decrease in C_{dl} values reveals that the electrical double layer at the metal-solution boundary is thicker, supporting the strong inhibitor-Mild steel interaction. We can also see that MPPT has a maximum protection efficacy of 93.59 % at 100 ppm and all of the impedance variables lead to MPPT having a high capacity to resist Mild steel corrosion in an aggressive environment.

Table.5.3. Impedance factors of MPPT on Mild steel corrosion in the 1M HCl solution

	Impedance parameters					
(ppm)	$\begin{array}{c} R_{ct} \\ (\Omega \text{ cm}^2) \end{array}$	C _{dl} (µF cm ⁻²)	I.E (%)			
Blank	9.95	3.334	0			
10	14.61	1.453	31.90			
30	50.97	0.158	80.48			
50	92.42	0.036	89.23			
70	129.43	0.018	92.31			
100	155.23	0.012	93.59			

5.4. Temperature effect on corrosion

The effect of temperature on Mild steel corrosion in the presence and absence of MPPT in 1M HCl at 305, 315, 325, and 335 K is shown in (Fig.5.4). It demonstrates that inhibition efficiency decreases at lower MPPT inhibitor concentrations such as 5 and 10 ppm, but at higher temperatures, all other MPPT inhibitor concentrations such as 30, 50, 70, and 100, exhibit a modest increase in hindered efficiencies. It clearly shows that both physical and chemical interactions on the Mild steel surface reduce the rate of corrosion.

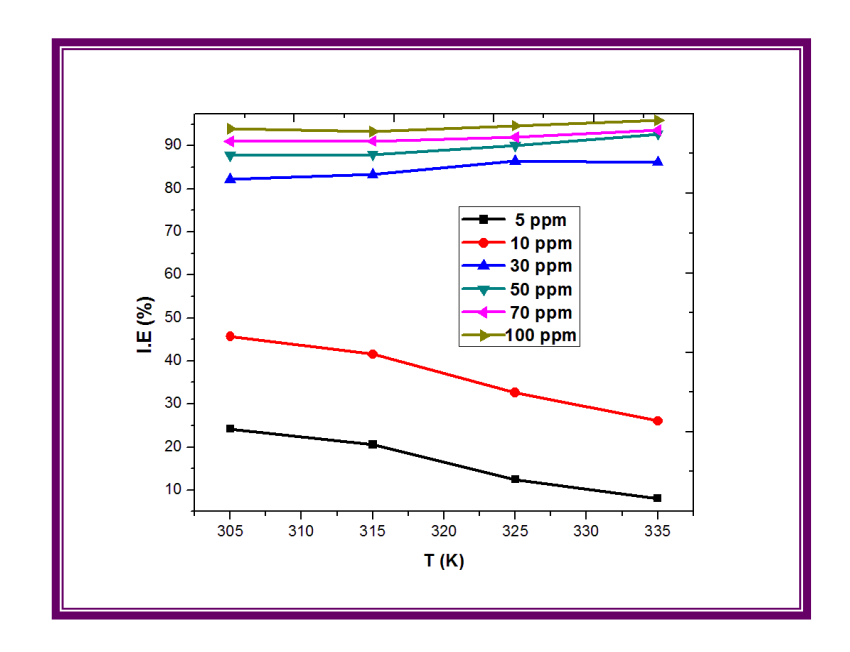


Fig.5.4. Inhibition efficiencies of MPPT in the M HCl solution at higher temperatures

Table.5.4 summarizes the corrosion metrics assessed such as corrosion rate and inhibition efficacy, together with the accompanying weight loss. We can deduce from the statistics that the decrease in I.E at 5 and 10 ppm signifies that the inhibitor is adsorbed on the steel surface via weak electrostatic attraction. However, when all other concentrations of MPPT increase, the protective ability increases implying that the protector molecule is adsorbed on Mild steel via chemical interaction. At 100 ppm in

1M HCl, the I.E values increase from 93.92 to 96.01 % confirming that the examined protector has a stronger protective capacity even at higher temperatures [5].

Table.5.4. Correlation between the temperatures and inhibition efficiencies of MPPT on Mild steel corrosion in 1M HCl solution

С	Weight loss(mg)			Weight loss(mg) Corrosion rate (mg cm ⁻² h ⁻¹)			Inhibition efficiency (%)					
(ppm)	305K	315K	325K	335K	305K	315K	325K	335K	305K	315K	325K	335K
Blank	939.6	1253.4	1932.5	2891.1	12.63	16.85	25.97	38.86	0	0	0	0
5	711.8	995.3	1691.4	2656.6	9.57	13.38	22.73	35.71	24.24	20.59	12.48	8.11
10	509.9	732.9	1301.5	2137.2	6.85	9.85	17.49	28.73	45.73	41.53	32.65	26.08
30	166.9	208.3	261.7	396.8	2.24	2.80	3.52	5.33	82.24	83.38	86.46	86.28
50	113.8	150.7	190.4	208.3	1.53	2.03	2.56	2.80	87.89	87.98	90.15	92.80
70	84.2	88.5	135.2	168.3	1.13	1.19	1.82	2.26	91.04	91.11	92.01	93.66
100	57.1	83.2	101.9	115.4	0.77	1.12	1.37	1.55	93.92	93.36	94.73	96.01

5.4.1. Kinetic and thermodynamic parameters

Based on the data achieved from the temperature study, the activation energy (E_a) and Arrhenius factor (A) can be determined by the Arrhenius equation (5.1)

$$\log CR = \log A - \frac{E_a}{RT} \tag{5.1}$$

where CR is the rate of corrosion, R is the gas constant and T is the temperature.

In addition, entropy (ΔS^0) and enthalpy (ΔH^0) values were calculated by the transition state equation (5.2)

$$\log\left(\frac{CR}{T}\right) = \log\left(\frac{RT}{Nh}\right) + \left(\frac{\Delta S^{0}}{2.303R}\right) - \left(\frac{\Delta H^{0}}{2.303RT}\right)$$
 (5.2)

where 'h' is Planck's constant and 'N' is Avogadro's number

The straight lines of Arrhenius plots are procured by plotting to 'log CR' vs '1000/T' with the slope ' $(-E_a/2.303R)$ ' and an intercept ' $(\log A)$ ' is shown in (Fig.5.5a). From the slope and intercept of Arrhenius plots, the activation energy (E_a)

and pre exponential factor (A) can be determined. In the same way, the particulars of the enthalpy and entropy can be attained by plotting 'log (CR/T)' versus '1000/T' from the transition state plots at various concentrations of the investigated MPPT as shown in (Fig.5.5b). The values of ΔH^0 and ΔS^0 are obtained from the slope '($-\Delta H^0/2.303R$)' and intercept '[(log (R/Nh) + $\Delta S^0/2.303R$]' of the straight lines from the transition state plots respectively.

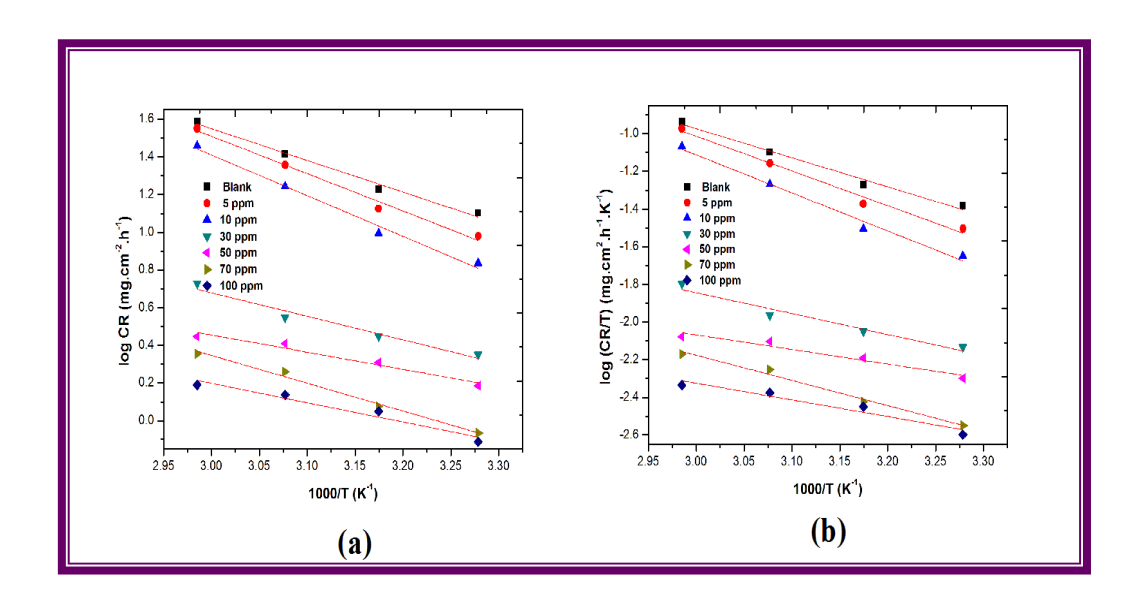


Fig.5.5. (a) Arrhenius plots and (b) Transition state plots of MPPT in the 1M HCl solution at raised temperatures

The kinetic and thermodynamic data achieved from the transition state plots and Arrhenius plots are summarized in Table 5.5. According to the tabulated data, E_a values range from 32.24 to 41.33 (KJ mol⁻¹) up to 10 ppm implying that the adsorption mechanism involves physisorption. Following that, it drops from 28.27 at 30 ppm to 17.47 (KJ mol⁻¹) at 100 ppm due to the enhanced inhibitor adsorption on Mild steel via the electron transfer mechanism, i.e., chemisorption, which lowers the energy barrier in the corrosion process. Further, the diminished A values support the inhibition process by chemisorption [6].

The E_a and ΔH^0 values in Table.5.5 decrease linearly with inhibitor concentration revealing that the hydrogen evolution process is related to a decline in net reaction volume [7]. Furthermore, the average difference of E_a - ΔH^0 is 2.66 (KJ mol⁻¹), which is equivalent to the average value of RT (2.61 KJ mol⁻¹) indicating that it is a unimolecular reaction and it is given by the following equation (5.3).

$$E_a - \Delta H^0 = RT \tag{5.3}$$

Table 5.5 further shows the positive ΔH^0 (29.59 to 14.81 KJ mol⁻¹) values mean that the corrosion process is endothermic and that the process of corrosion becomes harder in the presence of inhibitor. The decreasing ΔS^0 values from blank to optimal concentration (-193.91 to -197.57 JK⁻¹mol⁻¹) reveal that the disorderness decreases owing to more ordered adsorption of inhibitor molecule onto Mild steel, causing a drop in entropy at metal solution interface [8, 9]. It also means that the rate-determining step is based on the association process rather than the dissociation from the reactant to the activated complex. Therefore, we infer from the aforementioned data that the investigated inhibitor successfully mitigates corrosion degradation even at elevated temperatures in the 1M HCl solution.

Table.5.5. Kinetic and Thermodynamic data of MPPT on Mild steel corrosion in IM HCl solution

C (ppm)	E _a (KJ mol ⁻¹⁾	A	ΔH ⁰ (KJ mol ⁻¹)	$\begin{array}{c} \Delta S^0 \\ (JK^{-1}\ mol^{-1}) \end{array}$	E _a -RT
Blank	32.24	3.9948×10^6	29.59	-193.91	2.65
5	37.98	2.8880×10^7	35.32	-193.05	2.66
10	41.33	7.6824×10^7	38.67	-192.63	2.66
30	28.27	5.9744 X 10 ⁴	25.62	-196.09	2.65
50	23.92	2.6742×10^4	21.27	-197.23	2.66
70	19.67	1.9028×10^3	17.01	-197.32	2.66
100	17.47	1.5531×10^3	14.81	-197.57	2.66

5.4.2. Langmuir adsorption isotherm

The adsorption abilities on the metal surface of the inhibiting mechanism of the corrosion adsorption process are identified by the number of adsorption isotherm models. In this case, the most fitted model is the Langmuir isotherm and the adsorption parameters are acquired by the following the Langmuir isotherm equation (5.4)

$$\frac{C_{\text{inh}}}{\theta} = \frac{1}{K_{\text{ads}}} + C_{\text{inh}} \tag{5.4}$$

where C_{inh} is the concentration of the inhibitor, (θ) is the surface coverage and K_{ads} is the equilibrium adsorption constant.

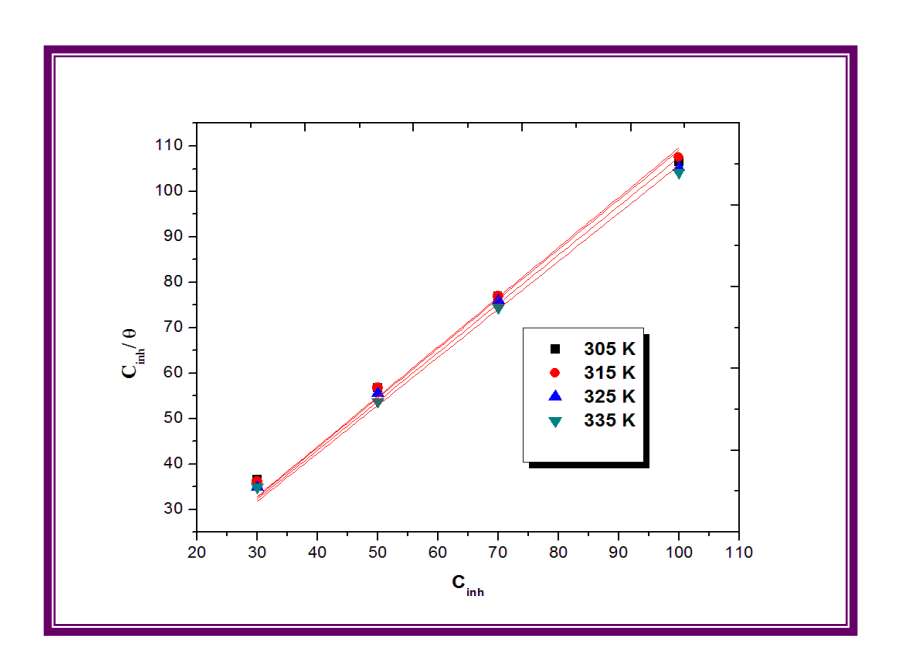


Fig.5.6. Langmuir isotherm of MPPT in 1M HCl solution

The straight lines were achieved by plotting (Cinh/) vs Cinh for various concentrations of MPPT at different temperatures as shown in (Fig.5.6) and the Langmuir parameters are listed in Table.5.6. The increase in K_{ads} values with

temperature for all the operational concentrations as shown in Table.5.6 demonstrates that MPPT has exceptional adhesion to metallic surfaces. Furthermore, the linear regression coefficient (R²) values are close to unity suggesting that the adsorption process is compatible with the Langmuir adsorption isotherm [10].

The values of standard free energy (ΔG^0) were calculated by equation (5.5)

$$\Delta G_{ads} = [-RT \ln(55.5 K_{ads})] \qquad (5.5)$$

where 'R' is the universal gas constant, 'T is the thermodynamic temperature, 55.5 is the concentration of water in probed solutions and 'K_{ads}' is the equilibrium adsorption constant.

Table.5.6. Langmuir parameters of MPPT on Mild steel corrosion at varioustemperatures

	Langmuir parameters			
T(K)	$\mathbf{K}_{ ext{ads}}$	ΔG (KJ.mol ⁻¹)	\mathbb{R}^2	
305	9192.87	-33.33	0.9973	
315	9129.92	-34.40	0.9982	
325	9337.94	-35.55	0.9985	
335	9469.7	-36.59	0.9986	

Moreover, the observed ΔG^0_{ads} ads values are negative, reflecting that the inhibition process is spontaneous and that the formation of the protective film is denser. According to the literature, physisorption is described by Gibbs free energy values around and below $-20~(kJ~mol^{-1})$ whereas chemisorption is described by Gibbs free energy values around or above $-40~(KJ~mol^{-1})$. Table 5.6 illustrates that the ΔG^0_{ads}

values range from -33.33 to -36.69 (KJ mol⁻¹), demonstrating that both electrostatic and chemical interactions are involved in the inhibition process [11].

5.5. Quantum chemical study

The optimal structure and Mulliken charges of the investigated inhibitor MPPT are shown in (Figs.5.7a-5.7b). Mulliken charges are commonly employed to highlight the inhibitor's adsorption center and coordination capabilities with the more negative atoms being identified as the inhibitor's adsorption sites. Herein, all of the heteroatoms that have greater negative values are listed in Table.5.7, signifying the presence of an adsorption core and strong inhibitory performance.

The neutral inhibitor molecule is protonated by abstracting hydrogen ions whereas Mild steel gets the negative charge in the HCl solution by absorbing chloride ions on its surface. The nitrogen atom designated as N₂₀ in the triazole moiety is identified as the molecule's protonation site due to its lower negative value. Thus, the protonated inhibitor molecule would interact with the negatively charged steel surface in the HCl environment resulting in electrostatic contact [12].

Table.5.7. Mulliken charges of hetero atoms present in MPPT

Hetero atoms	Mulliken charges
N ₂₀	-0.047
N ₂₁	-0.084
N ₂₂	-0.192
O ₃₄	-0.340

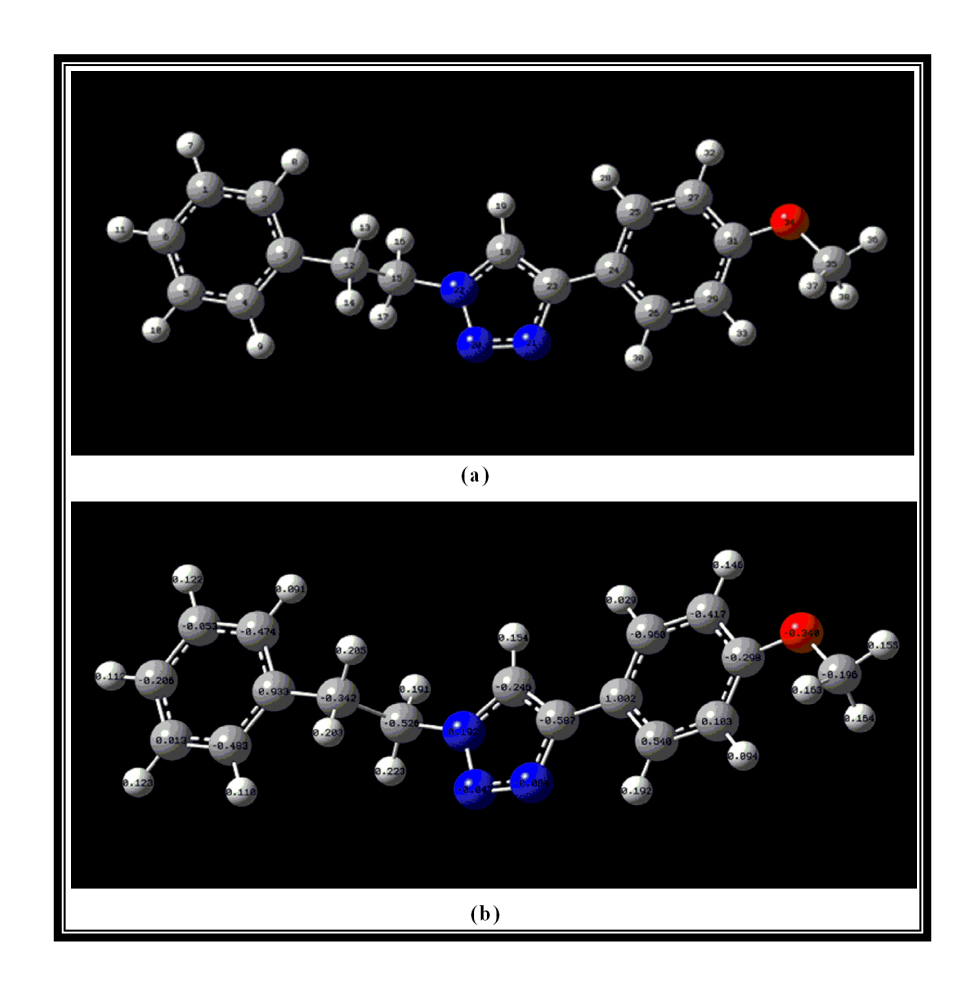


Fig.5.7. (a) Optimized structure and (b) Mulliken charges of MPPT

According to Frontier molecular orbital (FMO) Theory, the energy value of the highest occupied molecular orbital demonstrates the inhibitor's affinity for offering electrons to compatible acceptor molecules, whilst the energy value of the lowest unoccupied molecular orbital displays the inhibitor's ability to receive electrons from the metal via back donation [13-15]. The distribution of the FMO energies diagram (Ehomo and Elumo) is shown in (Fig.5.8a-5.8b).

As seen in (Fig.5.8a), the HOMO energy distribution extends the triazole moiety, benzene ring and oxygen atom of the inhibitor except for the phenethyl group, signaling that electrons are transported from those areas to the vacant d orbital of the iron atom gives strong coordination between them. As illustrated in (Fig.5.8b), the

LUMO's energy is centered on the phenethyl group, triazole moiety, and benzene ring, reflecting the development of a $d\pi$ -p π coordinate bond between Mild steel and inhibitor involving back donation of electrons from the iron atom to the protector.

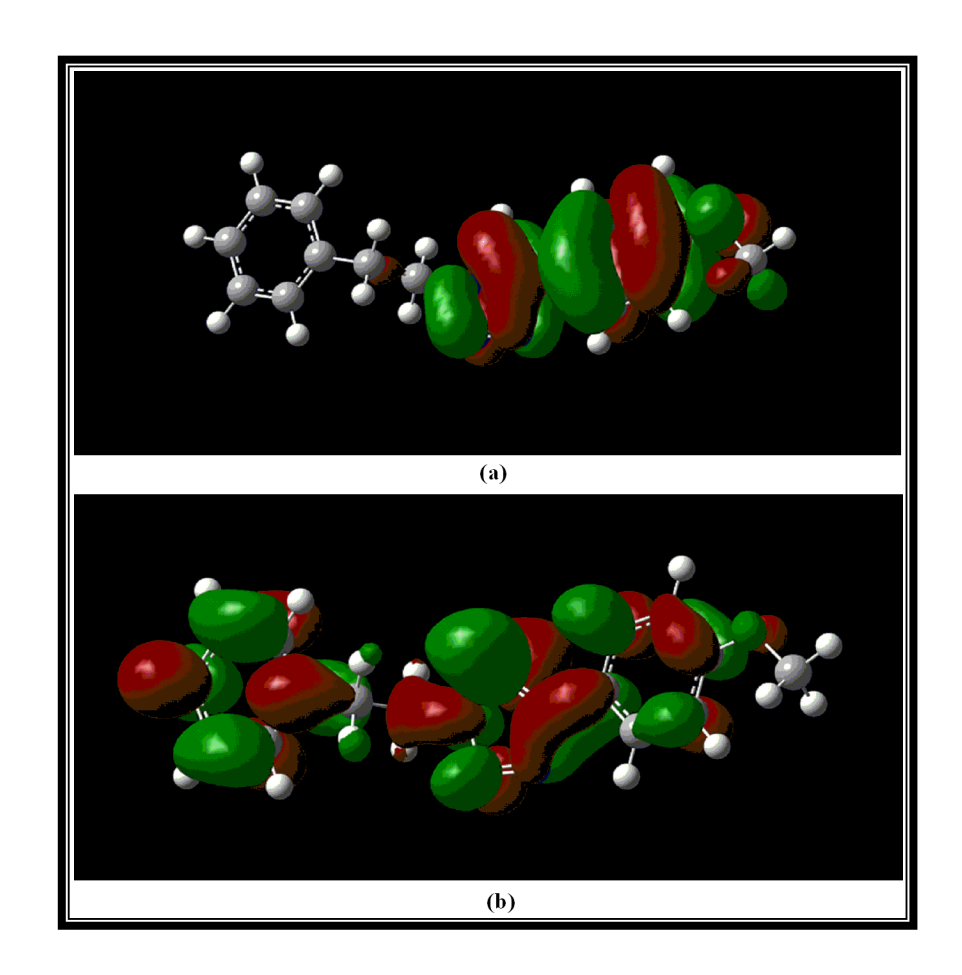


Fig.5.8. (a) HOMO and (b) LUMO electron density distribution of MPPT

Additionally, Ehomo, Elumo and other necessary factors such as ΔE , D, I, A, χ , η , σ and ΔN are displayed in Table.5.8. The larger negative energy value (-6.0095 eV) of the highest occupied molecular orbital connotes the highest chance of electron donation of the inhibitor. Conversely, the lower unoccupied molecular orbital's lower negative energy value (-1.0495 eV) reflects the inhibitor's tendency to receive electron pairs from metal through back bonding, according to the tabulated data.

Table.5.8. Electronic parameters of the investigated protector MPPT

Electronic parameters				
Еномо	-6.0095 (eV)			
Ешмо	-1.0495 (eV)			
Energy Gap (ΔE)	4.9 (eV)			
Dipolemoment (D)	4.04 D			
Ionization energy (I)	6.0094 (eV)			
Electron affinity (A)	1.0495 (eV)			
Absolute electronegativity (χ)	3.5295 (eV)			
Global hardness (η)	2.4799			
Global softness (σ)	0.4032			
Transferred electron fraction (ΔN)	0.2601			
Back donation (ΔE _{backdonation})	-0.62(eV)			

Hence, all of the electronic parameters derived from the DFT analysis demonstrated the reactivity of the MPPT as well as the harmony of experimental and theoretical evaluations [16-19].

5.6. Morphological Investigation

5.6.1. SEM study

SEM micrographs of polished Mild steel, unprotected, and protected metallic surfaces of MPPT in 1M HCl solution are shown in (Figs.5.9a - 5.9d). Before immersion in the corrosive solution, the exposed steel exhibits a smoother surface with minor scrapes, as seen in (Fig5.9a). In the absence of MPPT, rust production results in a sternly worn surface as seen in (Fig.5.9b). In addition, the smooth surface with the protective mass in the presence of MPPT can be seen in (Fig.5.9c&d) at 100 ppm. As an outcome of the SEM images, we can infer that the explored MPPT performed effectively in the hostile medium, confirming that corrosion is hindered by the development of a fine coating over the metallic surface in the 1M HCl solution [20].

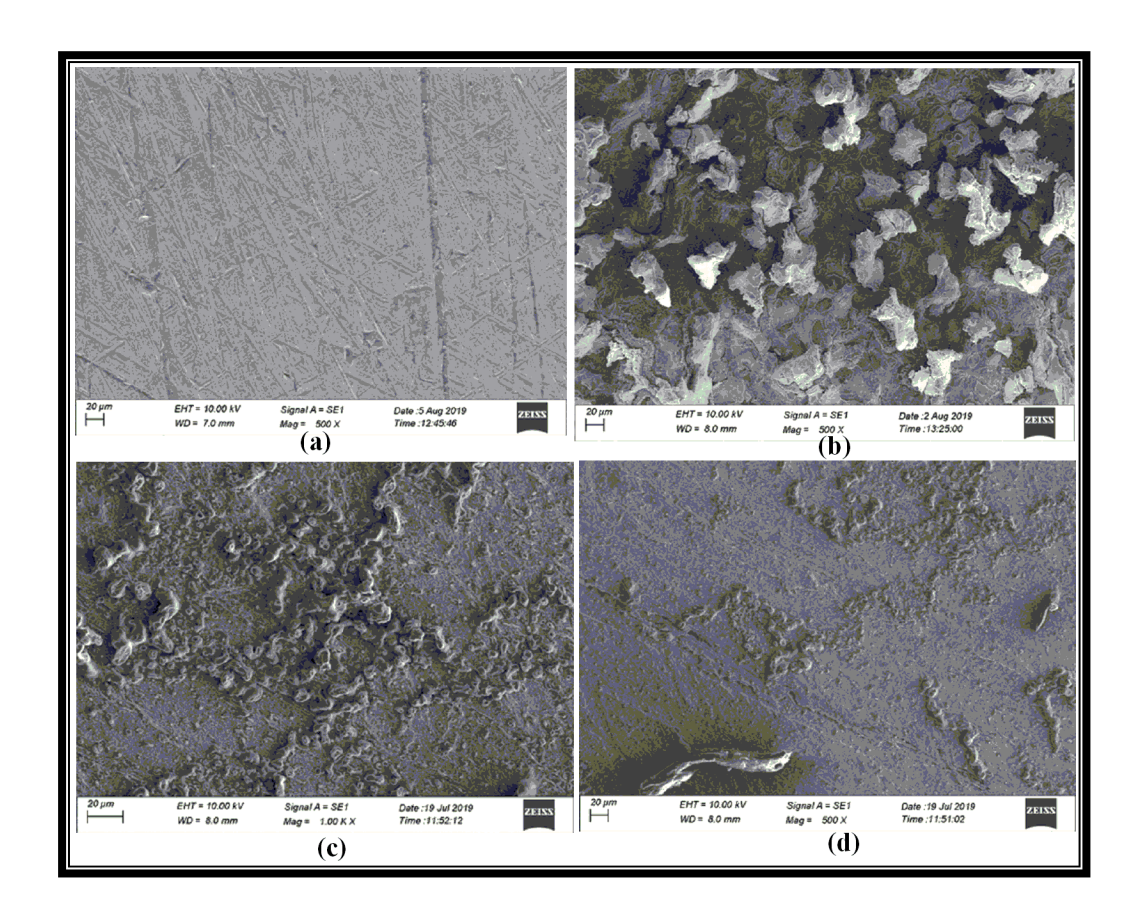


Fig.5.9. SEM micrographs for (a) bare steel surface, (b) unprotected surface, (c) & (d) protected surface with MPPT in 1M HCl solution

5.6.2. EDS study

The EDS interpretation of bare steel, unprotected and shielded Mild steel specimens with MPPT in 1M HCl solution at room temperature is shown in (Figs.5.10a–5.10c). C, O, N, and Fe are the primary elements found in the polished Mild steel as illustrated in the diagram (Fig.5.10a). In the absence of MPPT, the emergence of a chlorine peak along with the inspected elements (Fig.5.10b) reveals the heavily impacted steel surface due to rust accumulation. We can clearly see the presence of a nitrogen peak in the presence of MPPT in (Fig.5.10c) indicating that it shields the steel surface by sharing electrons from N and Oxygen to the Fe atom, which supports a chemical association.

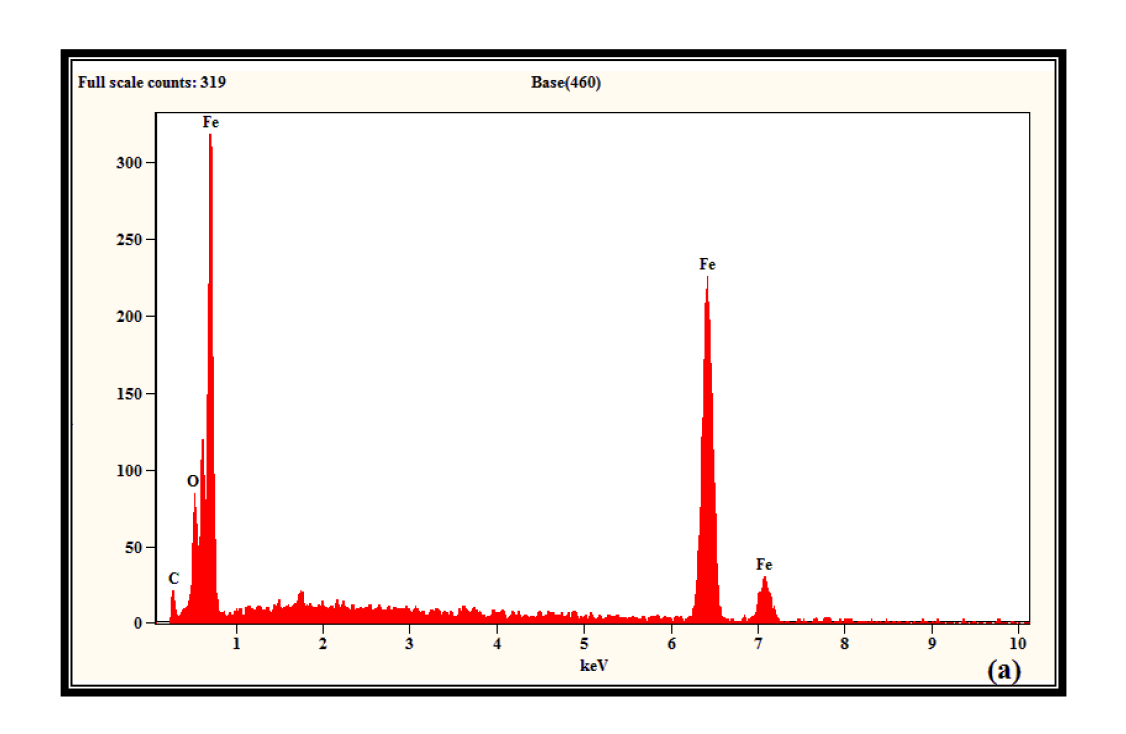


Fig.5.10a. EDX spectrum of bare steel

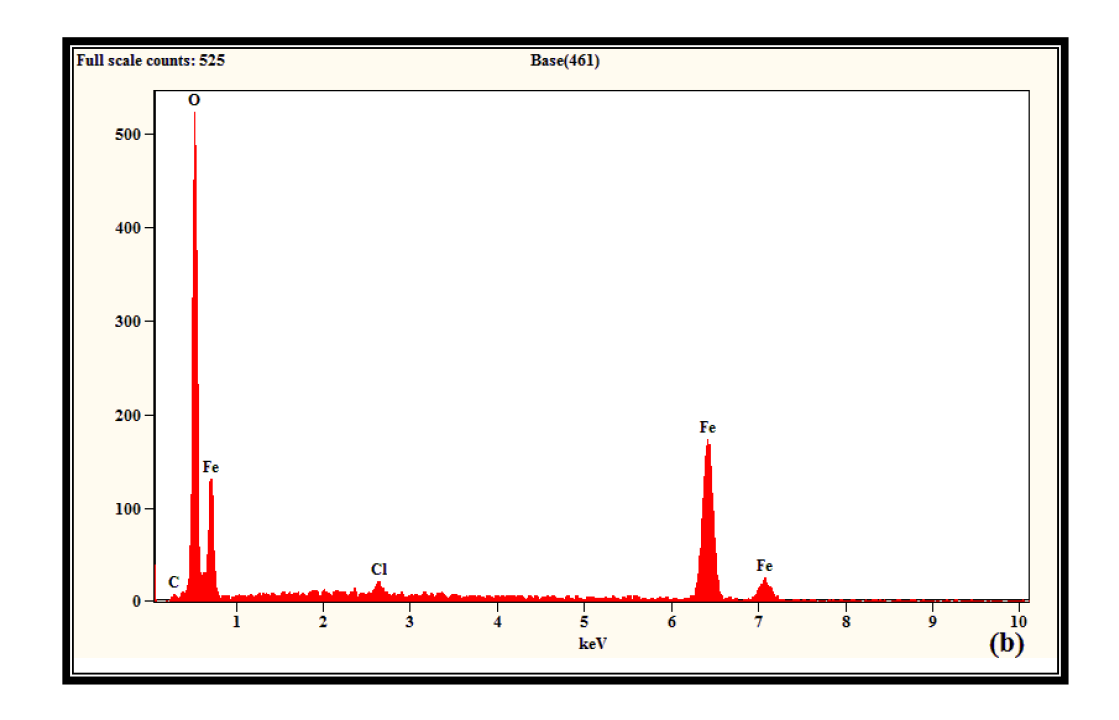


Fig.5.10b. EDX spectrum of Mild steel without MPPT in 1M HCl solution

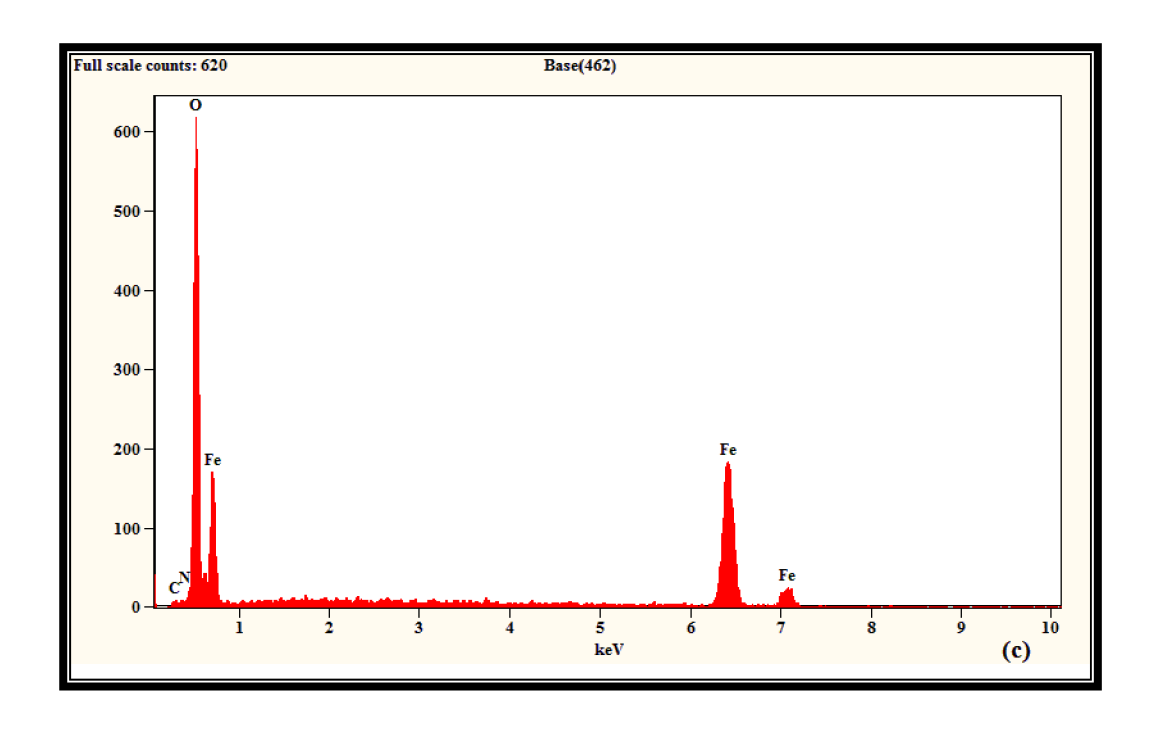


Fig.5.10c. EDX spectrum of Mild steel with MPPT in 1M HCl solution

The quantitative information derived from EDAX analysis, as shown in Table 5.9, also validates the corrosion protection. The weight percentages of N (1.25%) and O (12.73%) confirm that the corrosion sites of metallic surfaces are effectively blocked by forging a coordinating bond between MPPT and Mild steel in the 1M HCl medium [21].

Table.5.9. Elemental analysis of MPPT on Mild steel corrosion in 1M HCl solution

Samples	C	0	Cl	N	Fe
Bare steel	12.20	7.98	-	-	79.82
Unprotected Mild steel	5.84	43.44	1.06	-	49.66
Protected Mild steel with MPPT	10.46	12.73	-	1.25	75.56

5.6.3. AFM study

The AFM patterns of bare steel, uninhibited surface and inhibited surface of tested specimens with MPPT at 100 ppm are shown in (Figs.5.11a - 5.11c). The bare Mild steel surface exhibits a regular surface with little pits, as shown in (Fig.5.11a) whereas the unfettered metallic surface exposes a relatively rough and porous structure with large deep pores due to the corrosive environment, as shown in (Fig.5.11b). Additionally, the inhibited surface has a smoother region than the specimen submerged in corrosive media as seen in (Fig.5.11c) indicating that the roughness reduces with the presence of the MPPT molecule.

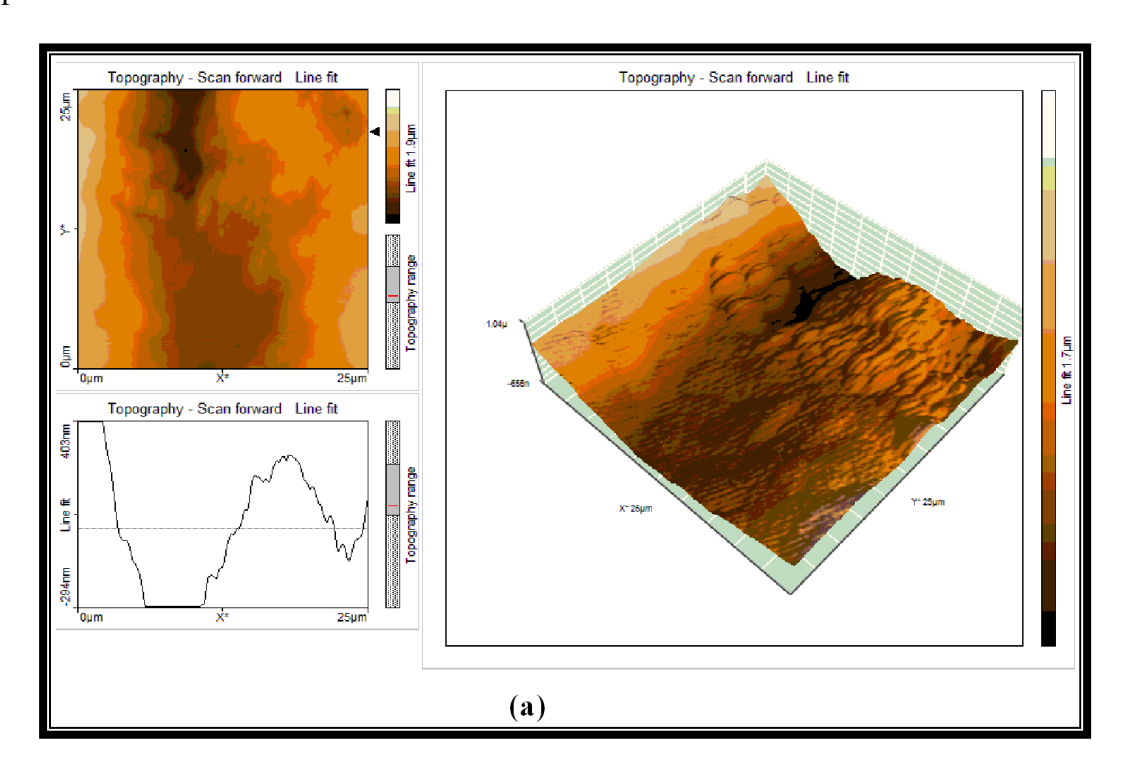


Fig.5.11a- AFM image of polished surface

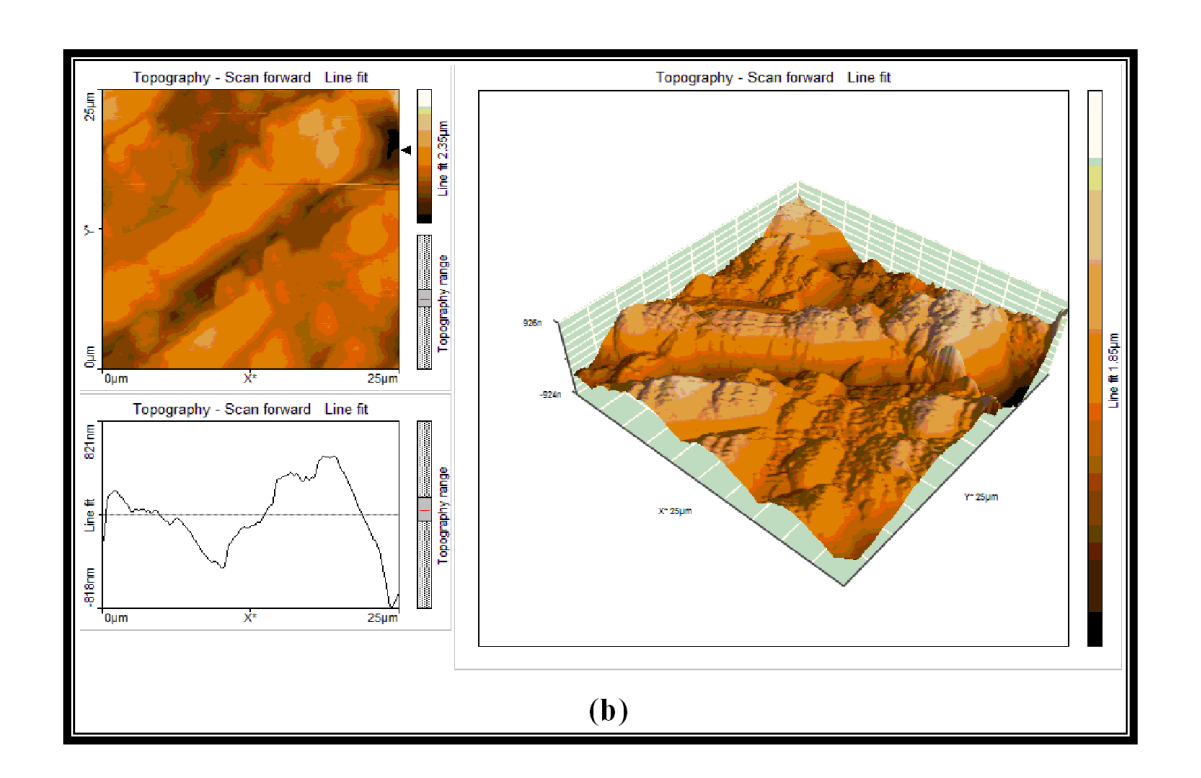


Fig.5.11b-AFM image of Mild steel in 1M HCl solution in the absence of MPPT

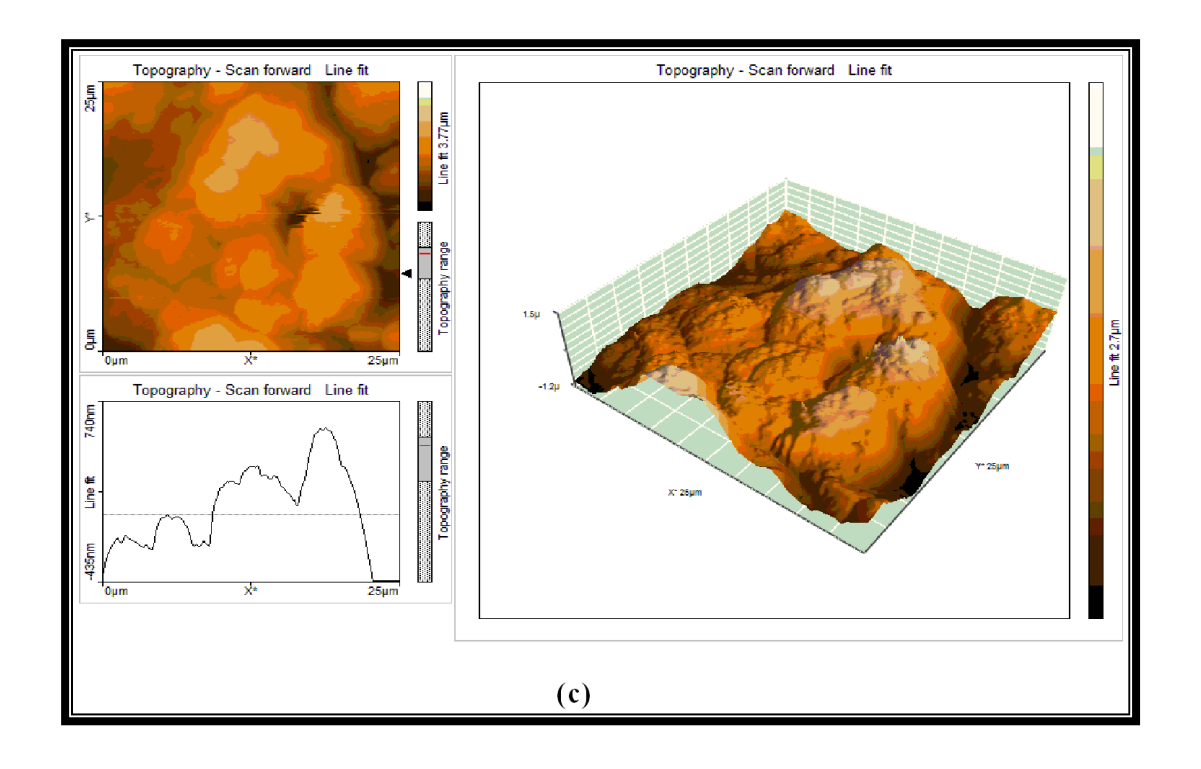


Fig.5.11c - AFM image of Mild steel in 1M HCl solution in the presence of MPPT

The acquired average roughness values of the Mild steel specimens before immersion, unprotected immersion, and protected immersion in acidic corrosive environments are 160.65 nm, 402.13 nm, and 188.08 nm, respectively, corroborating the surface protection. Similarly, bare steel, unprotected, and shielded Mild steel specimens have root mean square roughness values of 195.31 nm, 511.83 nm and 227.19 nm, respectively.

Table.5.10. Elemental analysis for MPPT on Mild steel corrosion in the IM HCl solution

Samples	Average Roughness	RMS roughness
Bampies	(R _a)nm	(R _q) nm
Polished Mild steel	160.65	195.31
Unprotected Mild steel	402.13	511.83
Protected Mild steel with MPPT	188.08	227.19

It is clear that the closeness of the investigated roughness data between the bare steel and protected surfaces exhibiting the roughness of the metallic surface is diminished by the adsorption of the MPPT protector. Accordingly, all the AFM findings corroborate the smoother protected surface due to the development of impenetrable and ordered barrier on the surface of the Mild steel [22].

5.7. References

- Hassan H H, Abdelghani E, Amin M A. Inhibition of Mild steel corrosion in hydrochloric acid solution by triazole derivatives Part I. Polarization and EIS studies. *Electrochimica Acta*. 2007; 52: 6359-6366.
- Ashassi-Sorkhabi H, Majidi M R, Seyyedi K. Investigation of Inhibitive Action of Amino Acids against Steel Corrosion in HCl Solution. *Applied Surface* Science. 2004; 225: 176-185.
- 3. Abdel-Aal M S, Morad M S. Inhibiting effects of some quinolines and organic phosphonium compounds on corrosion of Mild steel in 3M HCl solution and their adsorption characteristics. *British Journal of Corrosion*, 2001; 36(4): 253-260.
- 4. Nataraja S E, Venkatesha T V, Manjunatha K, Poojary B, Pavithra M K, Tandon H C. Inhibition of the corrosion of steel in hydrochloric acid solution by some organic molecules containing the methylthiophenyl moiety. *Corros. Sci.* 2011; 53(8): 2651-2659.
- 5. Popova A. Temperature effect on Mild steel corrosion in acid media in presence of azoles. *Corros. Sci.* 2007, 49(5), 2144- 2158.
- Liu Y, Zou C, Yan X, Xiao R, Wang T, Li M. β-Cyclodextrin Modified Natural Chitosan as a Green Inhibitor for Carbon Steel in Acid Solutions. *Ind Eng Chem Res.* 2015; 54(21): 5664-5672.
- 7. Ostovari A H, Peikari S M, Shadizadeh S R, Hashemi S J. Corrosion inhibition of Mild steel in 1M HCl solution by henna extract: A comparative study of the inhibition by henna and its constituents (Lawsone, Gallic acid, α-d-Glucose and Tannic acid). *Corros. Sci.* 2009; 51: 1935-1949.

- 8. Srimathi M, Rajalakshmi R, Subhashini S. Polyvinyl alcohol—sulphanilic acid water soluble composite as corrosion inhibitor for Mild steel in hydrochloric acid medium. *Arabian Journal of Chemistry*. 2014; 7(5): 647-656.
- Ferreira E S, Giacomelli C, Giacomelli F C, Spinelli A. Evaluation of the inhibitor effect of l-ascorbic acid on the corrosion of Mild steel. *Materials Chemistry and Physics*. 2004; 83(1): 129-134.
- Zarrouk B, Hammouti, Zarrok H, Salghi R, Dafali A, Bazzi L, Bammou L, Al-Deyab S. 3,7-Dimethylquinoxalin-2-(1H)-one for inhibition of acid corrosion of carbon steel. *Der Pharm. Chem.* 2012; 4(12): 5048-5055.
- 11. Kumari P, Rao S, Shetty P. Corrosion Inhibition of Mild steel in 2M HCl by a Schiff Base Derivative. Procedia Materials Science. 2014; 5: 499-507.
- 12. Singh P, Kumar M, Quraishi M, Haque J, Singh G. Bispyranopyrazoles as Green Corrosion Inhibitors for Mild steel in Hydrochloric Acid: Experimental and Theoretical Approach. *ACS Omega*. 2018; 3(9): 11151-11162.
- 13. Tao Z, Li Y, Peng Y, Su H, Han L, Liu G. Electrochemical studies of prothioconazole as a novel corrosion inhibitor for copper in acidic solutions. *RSC Adv.* 2020; 10(36): 21517-21529.
- 14. Umoren S, Obot I, Israel A. Inhibition of Mild steel corrosion in acidic medium using coconut coir dust extracted from water and methanol as solvents. *Journal of Industrial and Engineering Chemistry*. 2014; 20(5): 3612-3622.
- 15. Ansari K, Quraishi M. Experimental and computational studies of naphthyridine derivatives as corrosion inhibitor for N80 steel in 15% hydrochloric acid. *Physica E: Low-dimensional Systems and Nanostructures*. 2015; 69: 322-331.

- 16. Singh P, Makowska-Janusik M, Slovensky P, Quraishi M. Nicotinonitriles as green corrosion inhibitors for Mild steel in hydrochloric acid: Electrochemical, computational and surface morphological studies. *J Mol Liq.* 2016; 220: 71-81.
- 17. Mendonca G, Costa S, Freire V, Casciano P, Correia A, Lima-Neto P. Understanding the corrosion inhibition of carbon steel and copper in sulphuric acid medium by amino acids using electrochemical techniques allied to molecular modelling methods. *Corros Sci.* 2017; 115: 41-55.
- 18. Parr R, Szentpaly L, Liu S. Electrophilicity Index. *J Am Chem Soc.* 1999; 121(9):1922-1924.
- 19. Gomez B, Likhanova N, Domínguez-Aguilar M, Martínez-Palou R, Vela A, Gazquez J. Quantum Chemical Study of the Inhibitive Properties of 2-Pyridyl-Azoles. *The Journal of Physical Chemistry B*. 2006; 110(18): 8928-8934.
- 20. Tao Z, Zhang S, Li W, Hou B. Adsorption and Corrosion Inhibition Behavior of Mild steel by One Derivative of Benzoic-Triazole in Acidic Solution. *Ind Eng Chem Res.* 2010; 49(6): 2593-2599.
- 21. Rbaa M, Galai M, Benhiba F. Synthesis and investigation of quinazoline derivatives based on 8-hydroxyquinoline as corrosion inhibitors for Mild steel inacidic environment: experimental and theoretical studies. *Ionics (Kiel)*. 2018; 25(7): 3473-3491.

CHAPTER - VI

Anti-corrosive performance of '1-benzyl-4-(naphthalen-2-yl)-1*H*-1,2,3-triazole'(BNT) on Mild steel corrosion

The gravimetric analysis was performed using accurately weighed polished Mild steel specimens before and after immersion in the 1M HCl solution with 5, 10, 30, 50, 70 and 100 ppm concentrations of BNT for six hours exposure time.

6. Results and Discussion

6.1. Mass loss study

The relationship between the corrosion rates and the inhibition efficacy of various BNT concentrations in the 1M HCl solution is depicted in (Fig.6.1). As seen in (Fig.6.1), the inhibition effectiveness increases as the BNT concentration increases, and the corrosion rates decrease appropriately [1].

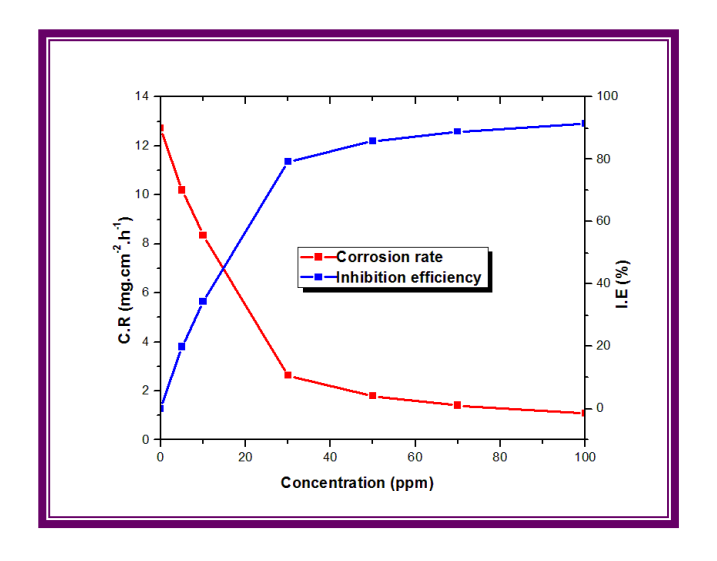


Fig.6.1.Correlation between the corrosion rates and the inhibition efficiencies for BNT on Mild steel specimens in 1M HCl solution

Table.6.1 shows the mean weight loss, corrosion rate, inhibition efficiency, and surface coverage data derived from the mass loss investigation. It is obvious that the CR value drops from 12.73 to 1.09 (mg cm⁻² h⁻¹), revealing that the examined protector suppresses the corrosion activity. Moreover, with the explored defender, the shielding capacity improves from 19.88 % at 5 ppm to 91.35 % at 100 ppm, signifying that BNT species defend a large area of the metal, as seen by the increasing values of surface coverage. The optimum efficacy was found to be 91.35 % at 100 ppm, showing that the adsorption of BNT species in an acidic environment significantly diminish Mild steel corrosion rates.

Table.6.1. Effect of BNT concentration on Mild steel corrosion in 1M HCl solution

Concentration (ppm)	Weight loss (mg)	Corrosion rate (mg cm ⁻² h ⁻¹)	Inhibition efficiency (%)	Surface coverage (θ)
Blank	946.8	12.73	-	-
5	758.6	10.19	19.88	0.20
10	626.5	8.36	33.83	0.34
30	197.7	2.64	79.12	0.79
50	134.5	1.80	85.79	0.86
70	105.6	1.42	88.85	0.89
100	81.9	1.09	91.35	0.91

6.2. Polarization study

Tafel polarization curves for different concentrations of BNT in 1M HCl solution are shown in (Fig.6.2). The observation that the Tafel lines move in both the anode and cathode areas indicates that the presence of BNT in the 1M HCl solution hampers electrochemical oxidation and reduction processes. The results of the polarization investigation are also described in terms of corrosion potential, corrosion current density, Tafel slopes, and inhibition efficiency (Table.6.2).

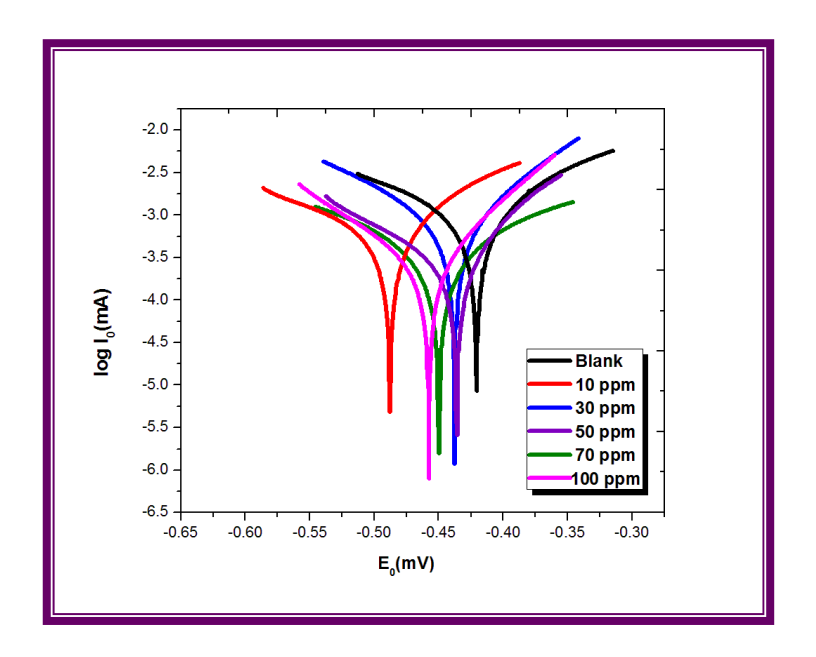


Fig.6.2.Tafel polarization curves for various concentrations of BNT on Mild steel samples in 1M HCl solution

The corrosion potential (E⁰) in the presence of the inhibitor is less than 85 mV as compared to the blank solution, showing that BNT is a mixed type inhibitor [2]. It is also evident from the values of Tafel slopes that the polarization moves on both sides but cathodic polarization is more predominant than the anodic move.

Besides that, the values of corrosion current density (I_0) decreased from 3.460 to 0.342 mA with the BNT concentrations which exposes that the corrosion currents are hindered by the adsorption of BNT on Mild steel specimens. Also, the optimum efficiency observed is 90.12% at 100 ppm. All the polarization findings conclude that BNT performed as a potential protector in the 1M HCl medium.

Table.6.2. Electrochemical polarization parameters of BNT on Mild steel in 1M HCl solution

	Polarization parameters							
C(ppm)	E ₀ (mV)	I ₀ (mA)	b _c (mV)	ba(mV)	IE (%)			
Blank	-420.613	3.46	995.82	254.55	-			
10	-487.864	2.05	297.82	262.02	40.90			
30	-437.671	0.63	672.88	561.31	81.68			
50	-436.141	0.56	153.55	102.96	83.96			
70	-449.694	0.41	248.32	154.85	88.08			
100	-458.956	0.34	161.80	78.76	90.12			

6.3. Impedance study

(Fig.6.3) exhibits the Nyquist plots for different concentrations of BNT in the 1M HCl solution and the diameter of the loops increases with increasing concentration of BNT which suggests the hindrance of charge transfer during the corrosion process in the presence of BNT. It also explains the obtained plots are not perfect circles owing to the roughness of the metallic surface and uneven distribution of active centers during the corrosion process [3].

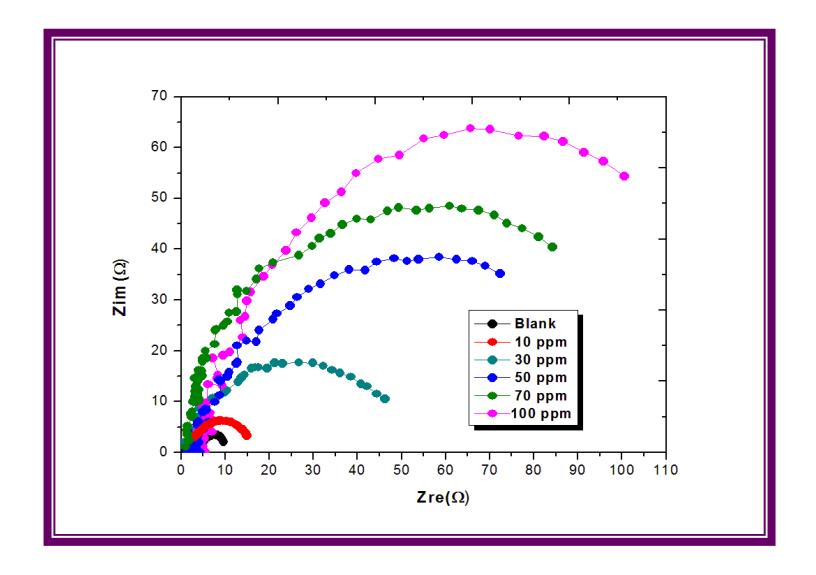


Fig.6.3.Nyquist plots for various concentrations of BNT on Mild steel samples in 1M HCl solution

Table.6.3 lists the parameters obtained by impedance analysis, such as Rct, Cdl, and IE. Table.6.3 displays that the presence of inhibitor ominously slowed the charge transfer progression in the corrosion reaction, with Rct values increasing from 9.52 to $100.55~\Omega~cm^2$. Correspondingly, the decreasing values of C_{dl} with an increase in BNT concentration also designates the increasing thickness of the electrical double layer at the metal solution interface prevents the metallic surface from rust formation in 1M HCl solution. Conclusively, the highest efficiency attained in this study is 90.60% which corroborates the investigated BNT is an efficient defender against Mild steel corrosion in an acidic medium.

Table.6.3. Electrochemical impedance parameters of BNT on Mild steel in 1M HCl

C	Impedance parameters						
	R ct	C dl	I.E				
(ppm)	$(\Omega \text{ cm}^2)$	(µF cm ⁻²)	(%)				
Blank	9.52	3.2095	0				
10	16.61	1.2369	42.69				
30	49.26	0.1626	80.67				
50	74.49	0.0513	87.22				
70	87.21	0.3114	89.08				
100	100.55	0.0241	90.53				

6.4. Temperature study

Experiments with various concentrations of BNT in 1M HCl solution at various temperatures ranging from 305K to 335K were carried out, and the association between temperature and IE is shown in (Fig.6.4).

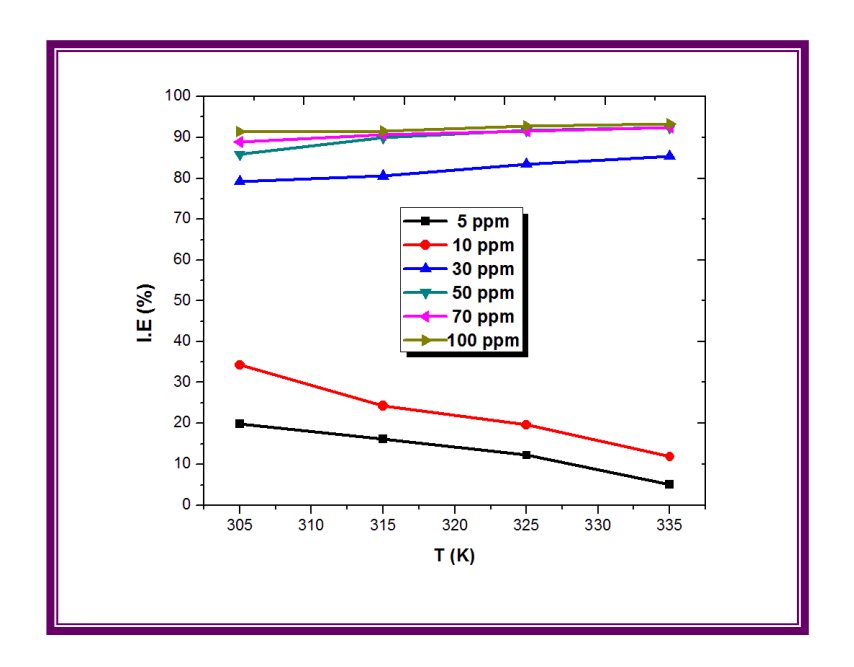


Fig.6.4.Effect of temperature on inhibition efficiencies for various concentrations of BNT on Mild steel specimens in 1M HCl solution

At the initial stage, the inhibition efficiencies for 5 and 10 ppm of BNT decrease with raising temperature suggesting that the inhibition process involves physisorption. In contrast, we can observe the modest increase in hindered efficiencies from 30 ppm to 100 ppm for all working temperatures implies that the adsorption mechanism is typical chemisorption. The experimental results shown in Table.6.4 substantiate the previously mentioned finding, with a maximum efficiency of 93.26 %. Hence, we infer that the rising efficiencies are due to chemisorption or a combination of physical and chemical interactions [4]. To conclude, even at increased temperatures in the 1M HCl environment, the adsorption process of BNT on Mild steel is preferred.

Table.6.4.Effect of temperature on the inhibition efficiencies for different concentrations of BNT on Mild steel in 1M HCl solution

Conc.	Weight loss(mg)			Corrosion rate (mg.cm ⁻² .h ⁻¹)			Inhibition efficiency (%)					
(ppm)	305K	315K	325K	335K	305K	315K	325K	335K	305K	315K	325K	335K
Blank	946.8	1533.1	2182.4	2856.1	12.73	20.61	29.33	38.39	0	0	0	0
5	758.6	1285.4	1916.2	2710.5	10.20	17.28	25.76	36.43	19.88	16.16	12.20	5.10
10	621.7	1160.2	1753.3	2515.2	8.36	15.59	23.57	33.81	33.83	24.32	19.66	11.78
30	196.2	298.3	361.7	416.8	2.64	4.01	4.86	5.60	79.12	80.54	83.43	85.38
50	133.5	153.7	181.4	216.3	1.79	2.07	2.44	2.91	85.79	89.97	91.69	92.43
70	105.6	143.6	175.50	207.60	1.42	1.93	2.36	2.79	88.85	90.63	91.96	92.73
100	81.3	131.2	158.1	192.1	1.09	1.76	2.13	2.58	91.35	91.44	92.76	93.26

6.4.1. Kinetic and Thermodynamic corrosion

Arrhenius equation (5.1) was used to calculate the activation energy (Ea) and pre-exponential factor (A). Also, (Fig.6.5a) shows the Arrhenius plots with straight lines which were created by plotting log CR Vs 1000/T with slope (Ea/R) and intercept (log A).

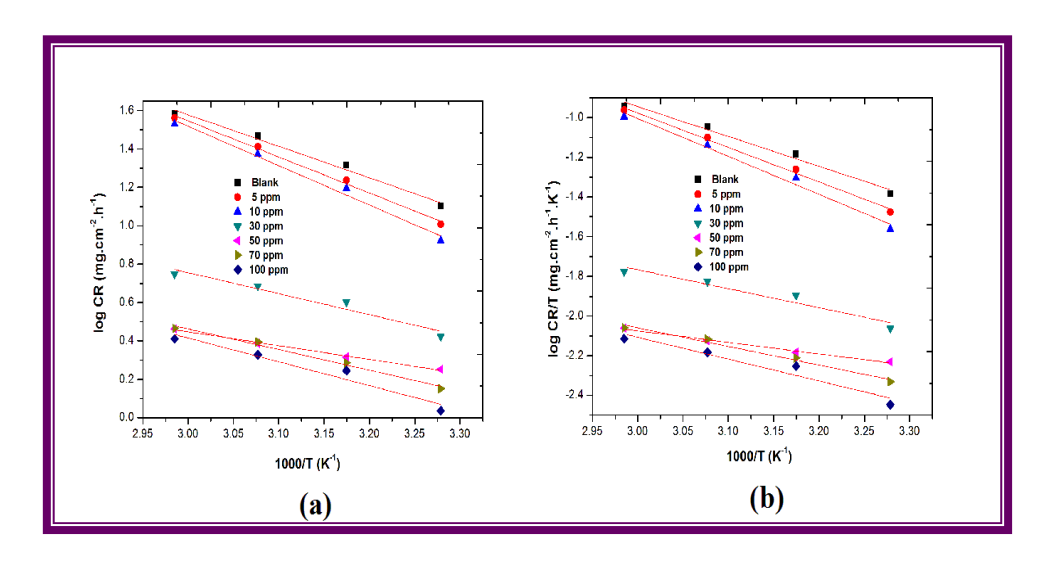


Fig.6.5. a) Arrhenius plots and (b) Transition state plots for various concentrations of BNT on Mild steel in 1M HCl solution

E_a and A values are calculated from the slope and intercept and are presented in Table.6.5. As seen in Table.6.5, decreasing activation energies from 31.39 to 13.76 (KJ mol⁻¹) correspond to increasing inhibitor concentrations, indicating chemical adsorption [5]. Furthermore, the lowering values of the Arrhenius factor suggest that the adsorption of BNT onto the metal surface efficiently prevents corrosion.

In the same way, the thermodynamic activation parameters such as entropy of activation (ΔS^0) and enthalpy of activation (ΔH^0) were determined from the transition state equation (6.2). Transition state plots are obtained by plotting to 'log CR/T' Vs '1000/T' with slope (- ΔH^0 /2.303R) and intercept [(log (R/Nh) + ΔS^0 /2.303R] of the straight lines as shown in (Fig.6.5b). The values of ΔH^0 and ΔS^0 are calculated from the slope and intercept respectively and the values for enthalpy of activation and entropy of activation are presented in Table.6.5.

Table.6.5. Thermodynamic activation parameters for BNT on Mild steel in 1MHCl solution

C (ppm)	E _a (KJ mol ⁻¹⁾	A	ΔH ⁰ (KJ mol ⁻¹)	$\begin{array}{c} \Delta S^0 \\ (JK^{-1}mol^{-1}) \end{array}$	E _a -RT
Blank	31.39	3.1304×10^7	28.73	-129.47	2.66
5	35.94	1.4910 X 10 ⁸	33.28	-116.50	2.66
10	39.24	4.6462 X 10 ⁸	36.59	-107.04	2.66
30	23.72	1.0866 X 10 ⁵	21.07	-174.73	2.66
50	20.94	1.3561 X 10 ⁵	18.28	-176.57	2.66
70	20.57	4.8495 X 10 ⁴	17.91	-183.29	2.66
100	13.76	4.0114×10^3	11.10	-204.00	2.66

It reveals the positive values of ΔH^0 indicating the adsorption process is endothermic and characteristic chemisorption [6]. The negative values of ΔS^0 suggest the entropy decreases at the metal solution interface due to the displacement of water molecules adsorbed on the metal surface by BNT species [7].

Further, Table 6.5.shows the difference between the values of E_a and ΔH^0 for all the concentrations are approximately equal to 2.61 KJ.mol⁻¹ (average value of RT) which gratifies the equation $E_a - \Delta H^0 = RT$ and it mention that the corrosion process is controlled by the thermodynamic activation parameters [8]. Hence, the effect of temperature on the adsorption process clearly explains the adsorption mechanism involving chemical interactions.

6.4.2. Langmuir adsorption isotherm

The mechanism of the corrosion inhibition process was described by many isotherm models and this adsorption process follows the Langmuir isotherm. The Langmuir isotherm parameters were achieved by the equation (6.4). The equilibrium constant values (K_{ads}) are obtained from the intercept of the straight lines by plotting ' C_{inh}/θ ' Vs ' C_{inh} ' for various concentrations of BNT at different temperatures are shown in (Fig.6.6) and recorded in Table.6.6.

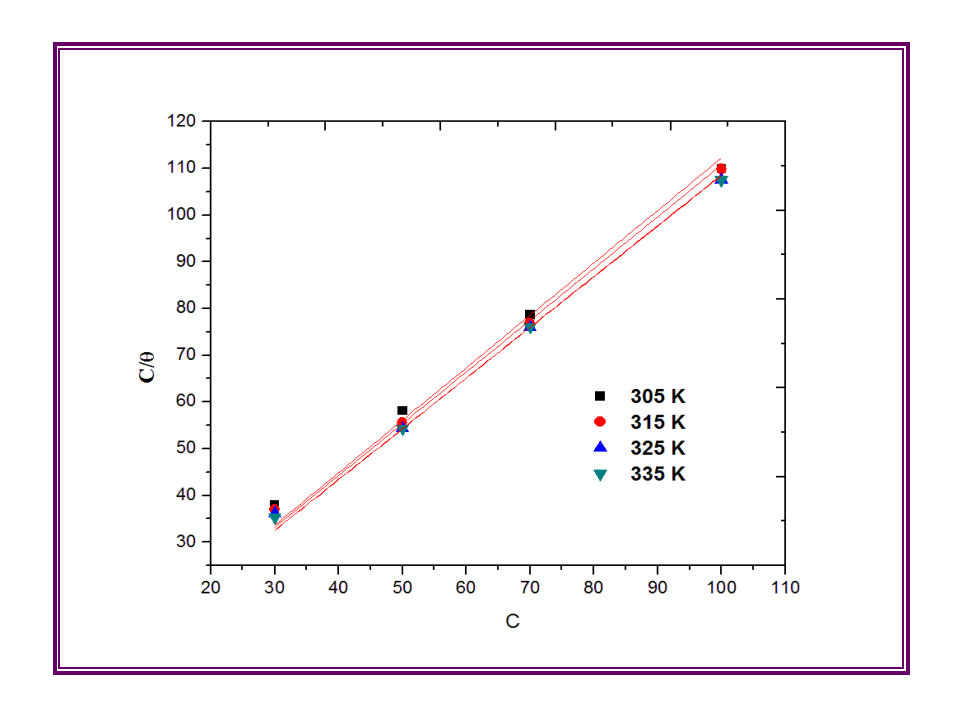


Fig.6.6. Langmuir isotherm for BNT on Mild steel in 1M HCl solution at different temperatures

From the tabulated results, the increasing values K_{ads} at raised temperatures suggest the strong adsorption and we can also perceive the linear regression coefficient (R²) values are closed to 1 which indicates that the adsorption process follows the Langmuir isotherm. Moreover, the adsorption standard free energy values (ΔG^0 ads) were determined using the equation (5.5) and listed in Table.6.6. It displays that the G^0 ads values varied from -33.25 to 36.61 KJ.mol⁻¹ indicating both physical and chemical adsorptions were involved in the adsorption process [9].

Table.6.6. Langmuir parameters for BNT on Mild steelin 1M HCl at different temperatures

	Langmuir parameters						
T (K)	Kads	ΔG (KJ mol ⁻¹)	R ²				
305	8912.42	-33.25	0.9975				
315	9006.66	-34.37	0.9986				
325	9206.83	-35.52	0.9987				
335	9222.97	-36.61	0.9992				

6.5. Quantum chemical investigation

(Figs.6.7a &6.7b) show the optimum structure as well as the Mulliken charges of the studied inhibitor BNT. The more negative atoms are recognized as the inhibitor's adsorption sites and Mulliken charges are typically used to emphasize the inhibitor's adsorption region and coordination characteristics [10-12].

Table.6.7. Mulliken charges of hetero atoms present in BNT

Hetero atoms	Mulliken charges
N ₂₁	-0.132
N ₂₂	0.048
N ₂₃	0.141

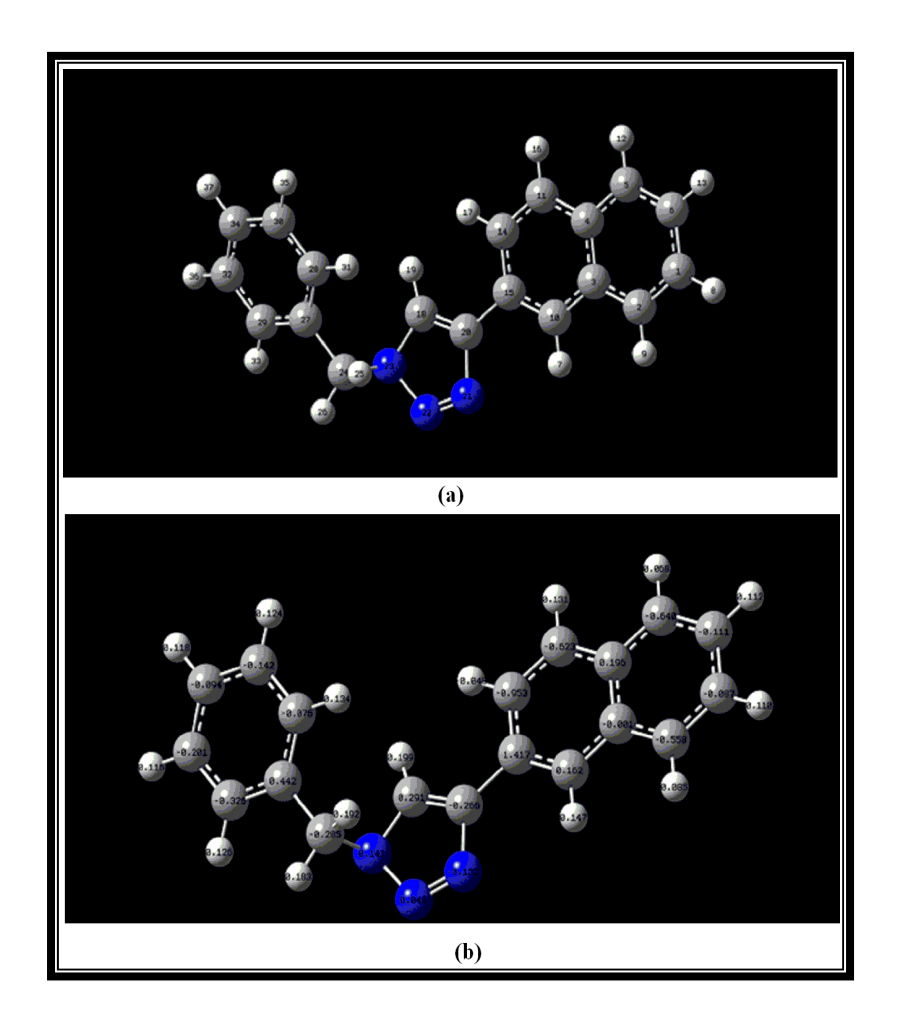


Fig.6.7. (a) Optimized structure and (b) Mulliken charges of BNT

In addition, the distribution of the Frontier molecular orbital energies diagram (Ehomo and Elumo) is shown in (Fig.6.8a-6.8b). The HOMO energy distribution spreads over on the naphthalene moiety and the triazole ring of the inhibitor as seen in (Fig.6.8a) implying that the electrons are transferred from those locations to the Mild steel for strong coordination. As shown in (Fig.6.8b), the LUMO's energy is centered on the naphthalene moiety indicating Mild steel to inhibitor back donation and exhibiting the inhibitor's significant anti-corrosion performance.

The inhibitory effect of the examined inhibitor is validated by the imperative electronic characteristics such as E_{HOMO} , E_{LUMO} , ΔE , D, I, A, χ , η , σ and ΔN are summarized in Table. 6.7. Here, the lower negative energy value (-1.8944 eV) of

the LUMO denotes the inhibitor's proclivity to accept electron pairs from metal via back bonding whereas the higher negative energy value (-7.3531 eV) of the HOMO denotes the inhibitor's highest probability of electron donation [14].

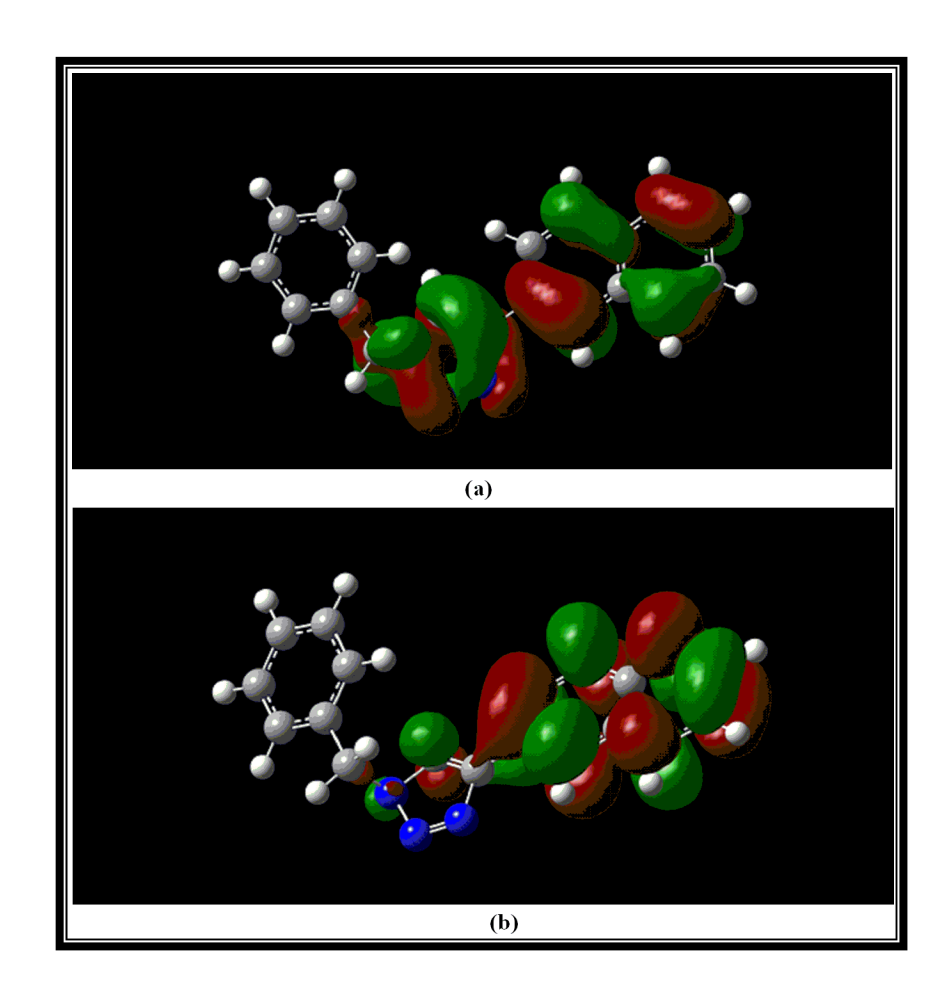


Fig.6.8. (a) HOMO and (b) LUMO distribution of BNT on Mild steel

As a consequence, all of the theoretical predictions reflect the experimental findings, showing that the tested BNT has a greater effect on Mild steel corrosion prevention [15, 16].

Table.6.8. Electronic parameters of the BNT molecule

Electronic parameters					
Еномо	-7.3531(eV)				
E _{LUMO}	-1.8944 (eV)				
Energy Gap (ΔE)	5.45 (eV)				
Dipolemoment (D)	2.5				
Ionization energy (I)	7.3531(eV)				
Electron affinity (A)	1.8944(eV)				
Absolute electronegativity (χ)	4.6237(eV)				
Global hardness (η)	2.7293				
Global softness (σ)	0.3663				
Transferred electron fraction (ΔN)	0.0359				
Back donation (ΔEbackdonation)	-0.6823(eV)				

6.6. Surface interpretation

6.6.1. SEM investigation

The SEM study of Mild steel without and with BNT in 1M HCl solution is shown in (Figs.6.9a-6.9d). Due to the particular formation of corrosion products on the steel surface, immersion of Mild steel in 1M HCl solution without BNT exposes several crevices and breaches as illustrated in (Fig.6.9a&b). Furthermore, (Fig.6.9c&d) depicts a smooth surface with some masses in the presence of BNT in 1M HCl solution, corroborating that the development of a thin film on the metallic surface against Mild steel corrosion is facilitated by BNT species adsorption in the corrosive medium [17,18].

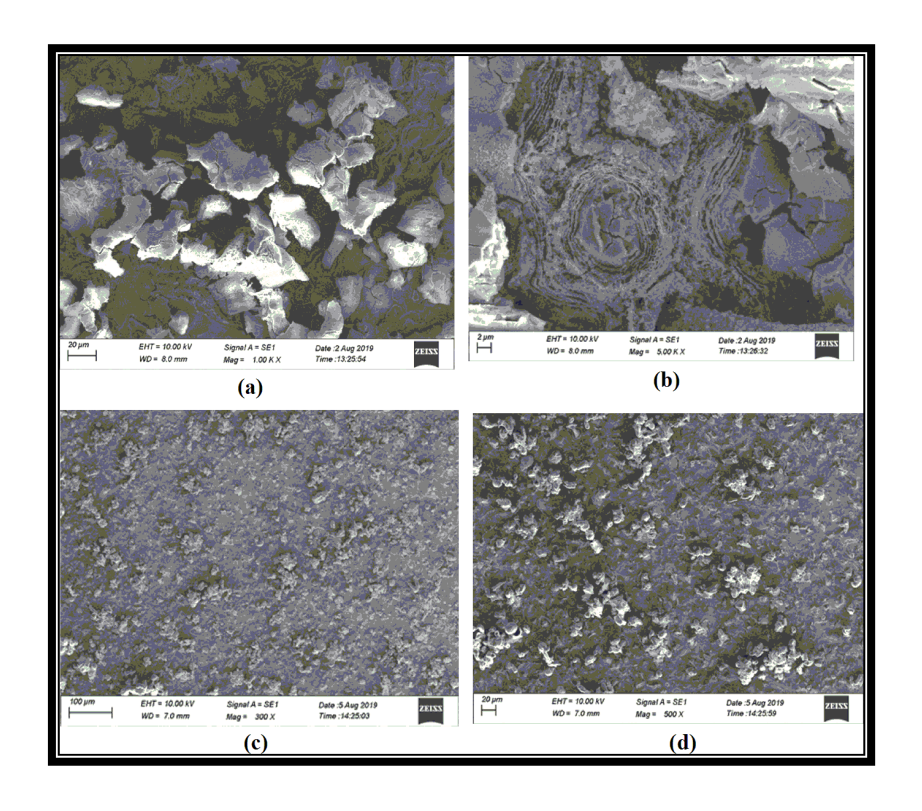


Fig.6.9.SEM images of Mild steel (a&b) unhindered surfaces (c&d) hinderedsurfaces with BNT in 1M HCl solution

6.6.2. EDX investigation

The electron dispersive spectra of Mild steel specimens in the absence and the presence of BNT are shown in (Figs.6.10a&b) respectively. The presence of a chlorine peak owing to rust development in the corrosive media without BNT is reflected in (Fig.6.10a). Furthermore, (Fig.6.10b) displays the nitrogen peak together with the investigated elements in the presence of BNT indicating that the adsorption of BNT molecule on the Mild steel surface reduces corrosion destruction.

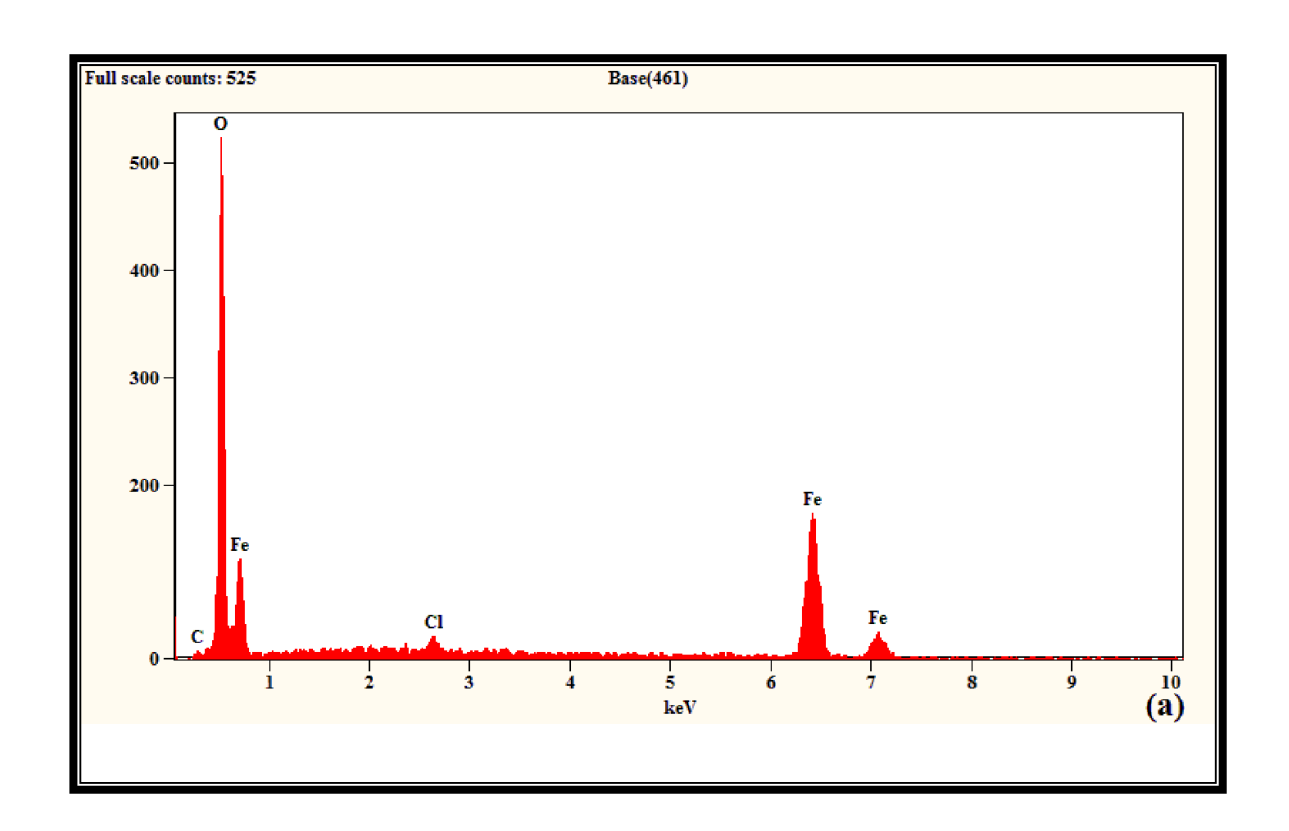


Fig.6.10a. EDX spectrum of Mild steel without BNT in 1M HCl solution

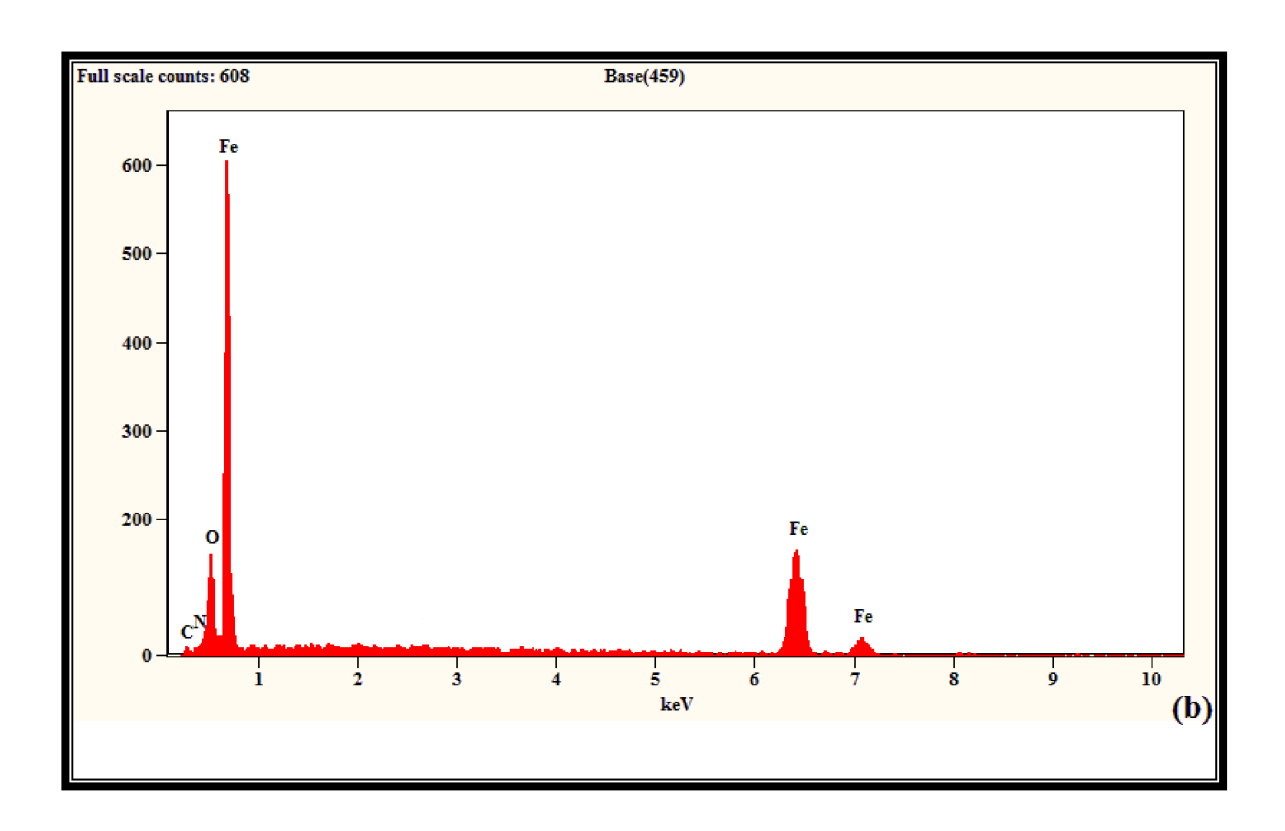


Fig.6.10b. EDX spectrum of Mild steel with BNT in 1M HCl solution

Furthermore, the quantitative EDX data of the analyzed steel specimens are recorded in Table.6.9, and the weight percentage values of N (1.39 %) support the corrosion behavior is hampered by the formation of a protective coating through nitrogen coordination with the steel surface in 1M HCl solution [19, 20].

Table.6.9. Elemental analysis of Mild steel with and without BNTin 1M HCl solution

Samples	С	0	Cl	N	Fe
Bare steel	12.20	7.98	-	-	79.82
Unprotected surface	5.84	43.44	1.06	1	49.66
Protected surface with BNT	13.21	9.73	-	1.39	75.67

6.6.3. AFM investigation

Table.6.10 displays the average roughness (R_a) and root mean square roughness (R_q) acquired from AFM observations. Inspection of Table.6.10 spectacles that the R_a values for polished Mild steel, specimens in the absence and presence of BNT are 160.65nm, 402.13 nm and 212.72nm while the corresponding R_q values are 195.31nm, 511.83 nm and 262.45 nm respectively. The larger values of roughness were noted for sternly dented by the corrosive medium. In the presence of the inhibitor, the roughness values are closer to the bare steel which corroborates that the corrosion deterioration is condensed by the adsorption of the inhibitor.

Table.6.10. AFM parameters of bare steel, unprotected and protected steel specimens in 1M HCl solution

Samples	Average Roughness (R _a)nm	RMS roughness (R_q) nm
Bare steel surface	160.65	195.31
Unprotected surface	402.13	511.83
Protected surface		
with BNT inhibitor	212.72	262.45

It is also evident from the AFM pattern (Figs. 6.11a & 6.11b) and the unprotected specimen reveals a rough surface due to acid attacks as shown in (Fig.6.11a) and the roughness of the steel surface is substantially reduced as shown in (Fig.6.11b) by the adsorption of BNT in 1M HCl solution [21, 22].

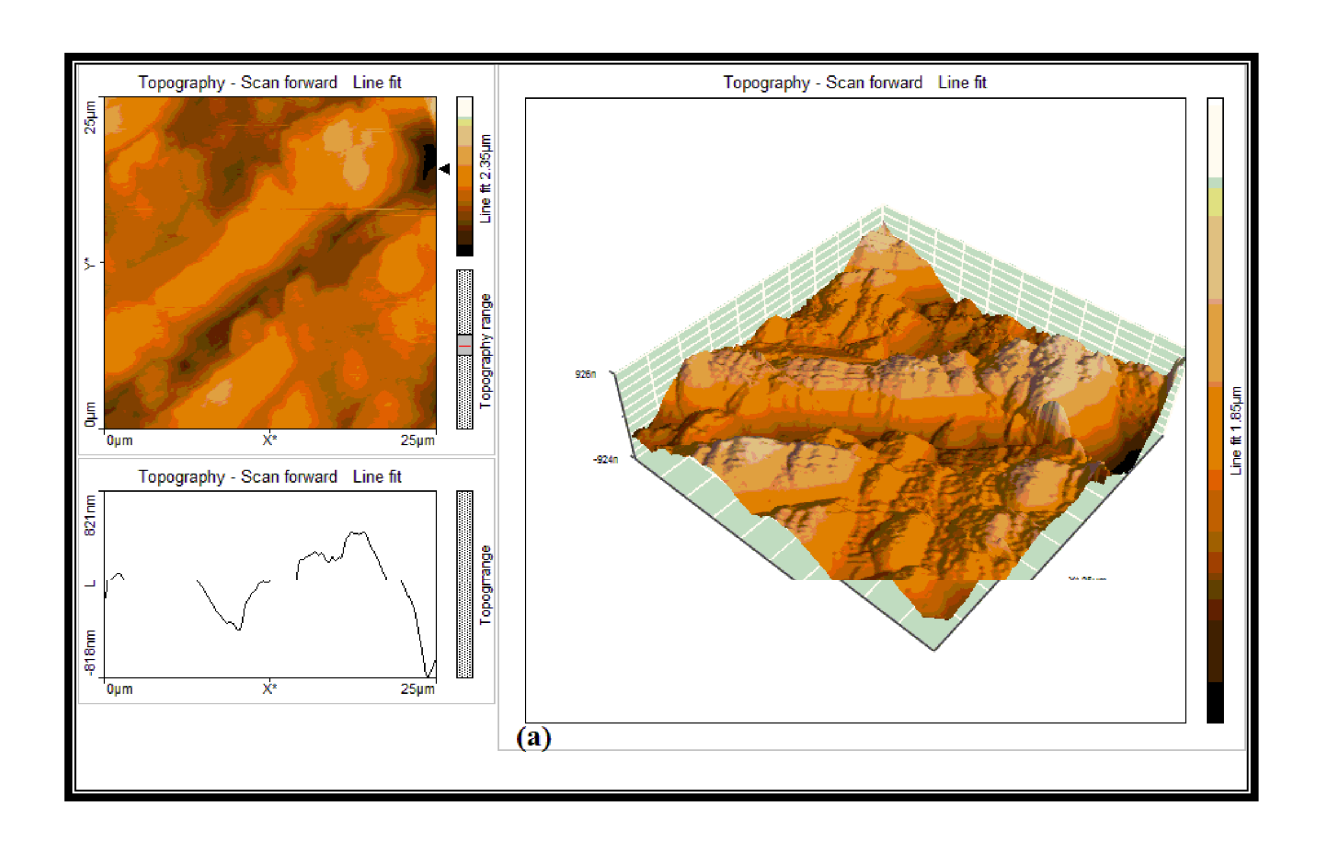


Fig.6.11a. AFM pattern of Mild steel without BNT in 1M HCl solution

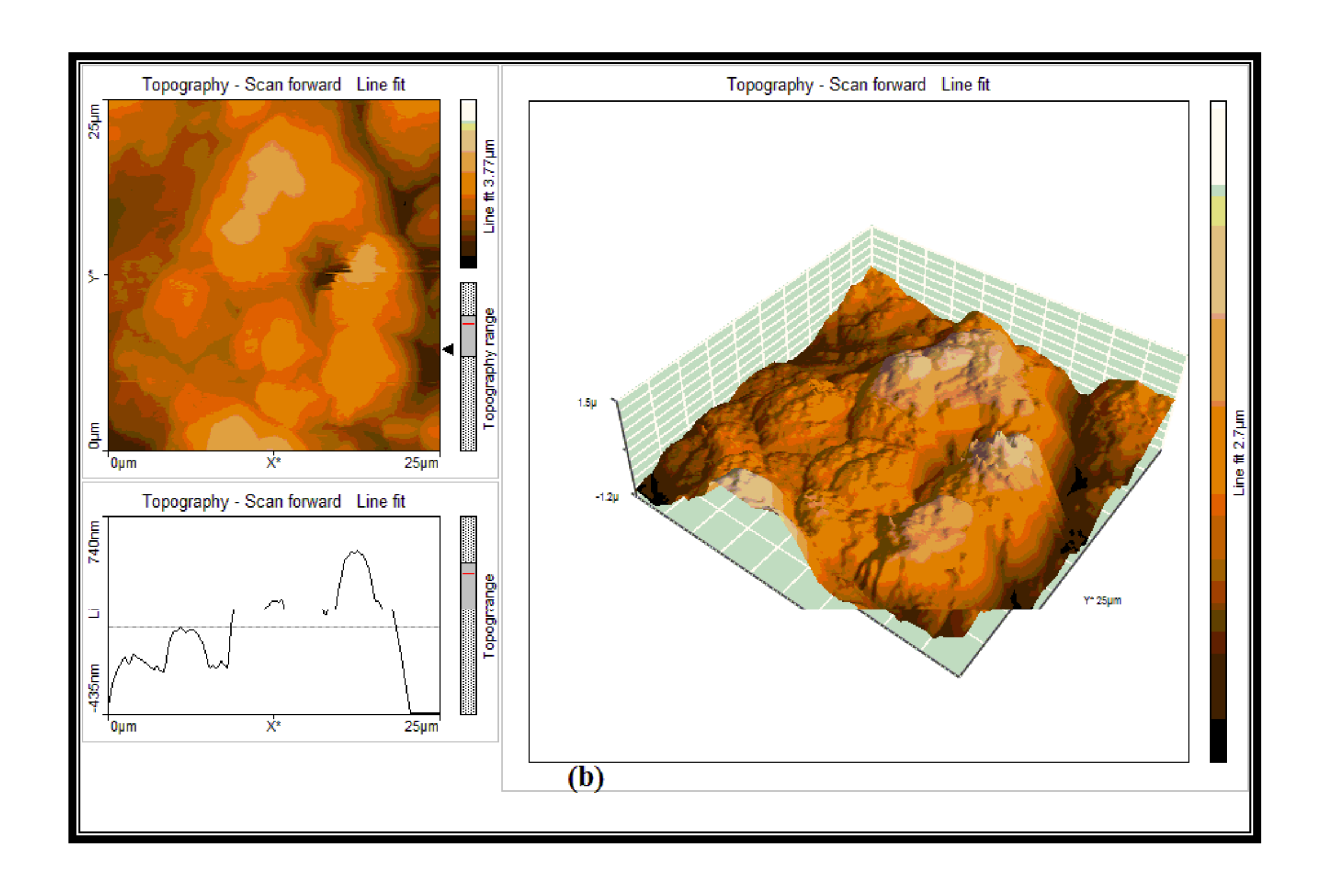


Fig.6.11b. AFM pattern of Mild steel with BNT in 1M HCl solution

Hence, morphological investigation corroborated that the corrosion rate is hindered by the development of the protective coating on Mild steel in the 1M HCl solution at room temperature.

6.7. References

- 1. Verma C, Olasunkanmia L O, Ebensoa E E, Quraishi M A. Substituents effect on corrosion inhibition performance of organic compounds in aggressive ionic solutions: A review. *J. Mol. Liq.* 2018; 251: 100–118.
- Ansari K R, Quraishi M A, Singh A. Corrosion Inhibition of Mild steel in Hydrochloric Acid by some Pyridine Derivatives: An Experimental and Quantum Chemical Study. J. Ind. Eng. Chem. 2015; 25: 89–98.
- 3. Haldhar R, Prasad D, Saxena A, Singh P. Valeriana wallichii root extract as a green & ustainable corrosion inhibitor for Mild steel in acidic environments: experimental and theoretical study. *Mater. Chem. Front.* 2018; 2: 1225–1237.
- 4. Ita B, Offiong O. The study of the inhibitory properties of benzoin, benzil, benzoin-(4-phenylthiosemicarbazone) and benzil-(4-phenylthiosemicarbazone) on the corrosion of Mild steel in hydrochloric acid. *Mater Chem Phys.* 2001; 70 (3): 330-335.
- 5. Dehri I, Zcan M O. The effect of temperature on the corrosion of Mild steel in acidic media in the presence of some sulphur-containing organic compounds. *Materials Chemistry and Physics*. 2006; 98 (2-3): 316–323.
- Martinez S, Stern I. Thermodynamic characterization of metal dissolution and inhibitor adsorption processes in the low carbon steel/mimosa tannin/sulfuric acid system. *Appl. Surf. Sci.* 2002; 199: 83 - 89.
- Abd El-Rehim S S, Refaey S A M, Taha F, Saleh M B, Ahmed R A. Corrosion inhibition of Mild steel in acidic medium using 2-amino thiophenol and 2cyanomethyl benzothiazole. *Journal of Applied Electrochemistry*. 2001; 31(4): 429–435.

- 8. Jafari H, Danaee I, Eskandari H, Rashv M. Combined computational and experimental study on the adsorption and Inhibition effects of N2O2 schiff base on the corrosion of API 5L Grade B steel in 1 mol/L HCl. Journal of Materials Science & Technology. 2014; 30: 239 252.
- Hosseini M, Mertens S F, Ghorbani M, Arshadi M R. Asymmetrical Schiff bases as inhibitors of Mild steel corrosion in sulphuric acidmedia. Materials Chemistry and Physics. 2003; 78(3), 800–808.
- 10. Gece G. The use of quantum chemical methods in corrosion inhibitor studies. Corrosion Science. 2008, 50(11), 2981–2992.
- 11. Henriquez-Roman J H, Padilla-Campos L, Paez M A. The influence of aniline and its derivatives on the corrosion behavior of copper in acid solution: a theoretical approach. *Journal of Molecular Structure*. 2005; 757 (1–3): 1–7.
- 12. Opez N L, Illas F. Ab initio modeling of themetal-support interface: the interaction of Ni, Pd, and Pt on MgO(100). *Journal of Physical Chemistry B*. 1998; 102(8): 1430–1436.
- 13. Obot I B, Macdonald D D, Gasem Z M. Density functional theory (DFT) as a powerful tool for designing new organic corrosion inhibitors. Part 1: An overview. *Corros. Sci.* 2015; 99: 1–30A.
- 14. Musa Y, Kadhum A A H, Mohamad A B, Rahoma A A B, Mesmari H. Electrochemical and quantum chemical calculations on 4,4-dimethyl oxazolidine-2-thione as inhibitor for Mild steel corrosion in hydrochloric acid. *Journal of Molecular Structure*. 2010; 969 (1–3): 233–237.
- 15. Gece G, Bilgic S. Quantum chemical study of some cyclic nitrogen compounds as corrosion inhibitors of steel in NaCl media. *Corrosion Science*. 2009; 51(8): 1876–1878.

- 16. Lesar A, Milosev I. Density functional study of the corrosion inhibition properties of 1,2,4-triazole and its amino derivatives. *Chemical Physics Letters*. 2009; 483(4–6): 198–203.
- 17. Tan B, Zhang S, Qiang Y, Guo L, Feng L, Liao C. A combined experimental and theoretical study of the inhibition effect of three disulfide-based flavoring agents for copper corrosion in 0.5 M sulfuric acid. *J. Colloid Interface Sci.* 2018; 526: 268–280.
- 18. Saxena A, Prasad D, Haldhar R, Singh G, Kumar A. Use of Sida cordifolia extract as green corrosion inhibitor for Mild steel in 0.5 M H₂SO₄. *J. Environ. Chem. Eng.* 2018; 6 (1): 694–700.
- 19. Shetty S K, Shetty A N. Eco-friendly benzimidazolium based ionic liquid as a corrosion inhibitor for aluminum alloy composite in acidic media. *J. Mol. Liq.* 2017; 225: 426–438.
- 20. Rbaa M, Galai M, Benhiba F, Obot I, Oudda H, Ebn Touhami M, Lakhrissi B, Zarrouk A. Synthesis and investigation of quinazoline derivatives based on 8-hydroxyquinoline as corrosion inhibitors for Mild steel in acidic environment: experimental and theoretical studies. *Ionics*, 2019a; 25 (7): 3473–3491.
- 21. Karthik G, Sundaravadivelu M, Rajkumar P, Manikandan M. Diaza-adamantane derivatives as corrosion inhibitor for copper in nitric acid medium. *Research on Chemical Intermediates*. 2014; 41: 7593–7615.
- 22. Chidiebere M A, Oguzie E E, Liu L, Li Y, Wang F. Ascorbic acid as corrosion inhibitor for Q235 Mild steel in acidic environments. *Journal of Industrial and Engineering Chemistry*. 2015; 26:182–192.

CHAPTER - VII

Corrosion mitigation performance of 'N-methyl-N-phenyl-3-(phenylsulfonyl)-1*H*-pyrazole-5-carboxamide' (MPSC)

The gravimetric assessment was conducted on accurately weighed polished Mild steel specimens before and after immersion in the 1M HCl solution for six hours at room temperature in the presence of MPSC concentrations of 5, 10, 20, 30, 40 and 50 ppm.

7. Results and Discussion

7.1. Gravimetric study

(Fig.7.1) manifests the inhibitor performance and the relative corrosion rates on Mild steel specimens in the 1M HCl solution at room temperature. It reveals that the protection efficiencies increase with an increase in MPSC concentration while the consequent corrosion rates decrease [1].

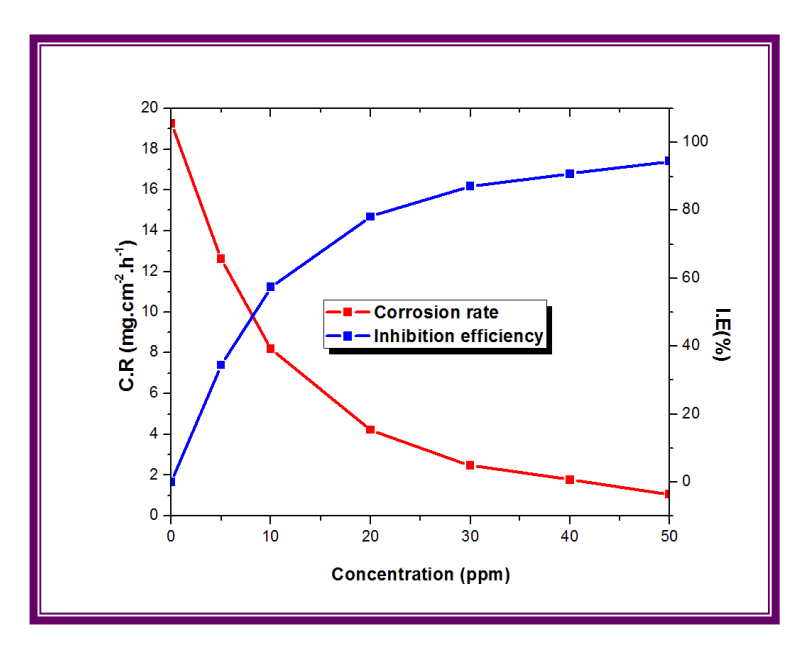


Fig.7.1. Correlation between the corrosion rates and the inhibition efficiencies of MPSC on Mild steel in 1M HCl solution

In addition, Table.7.1 provides corrosion variables such as corrosion rate and relative inhibition efficiency. It shows that when the concentration of MPSC increases, the rate of corrosion decreases from 19.25 to 1.07 (mg cm⁻² h⁻¹) indicating that corrosion effects are significantly suppressed in the 1M HCl solution. Disparately, I.E values increased from 34.45% to 94.46% at 50 ppm which depicts that the corrosion rates of the Mild steel specimens are remarkably reduced at an optimum concentration (50 ppm) of MPSC in 1M HCl solution.

Table.7.1. MPSC Corrosion data on Mild steel in 1M HCl solution

C ppm	CR (mg cm ⁻² h ⁻¹)	IE (%)	θ
Blank	19.2492	-	-
5	12.6177	34.45	0.34
10	8.1972	57.42	0.57
20	4.2141	78.11	0.78
30	2.4725	87.16	0.87
40	1.7722	90.79	0.91
50	1.0673	94.46	0.94

The escalating surface coverage (θ) values also specify that the MPSC defends the larger surface of the Mild steel from deterioration in the 1M HCl solution. Hence, the above verdicts suggest that the MPSC molecules interact actively with the Mild steel surface to mitigate the corrosion rates in the corrosive atmosphere.

7.2. Electrochemical polarization study

(Fig.7.2) exposes the Tafel polarization curves in the presence and absence of MPSC in the 1M HCl solution at room temperature. It is noticeable that polarization takes place on both anodic and cathodic sites as evidenced by the Tafel slope values provided in Table.7.2. Despite the existence of MPSC hindering anodic and cathodic

electrochemical processes, the cathodic results are conquered, and it serves as a mixed sort protector [2].

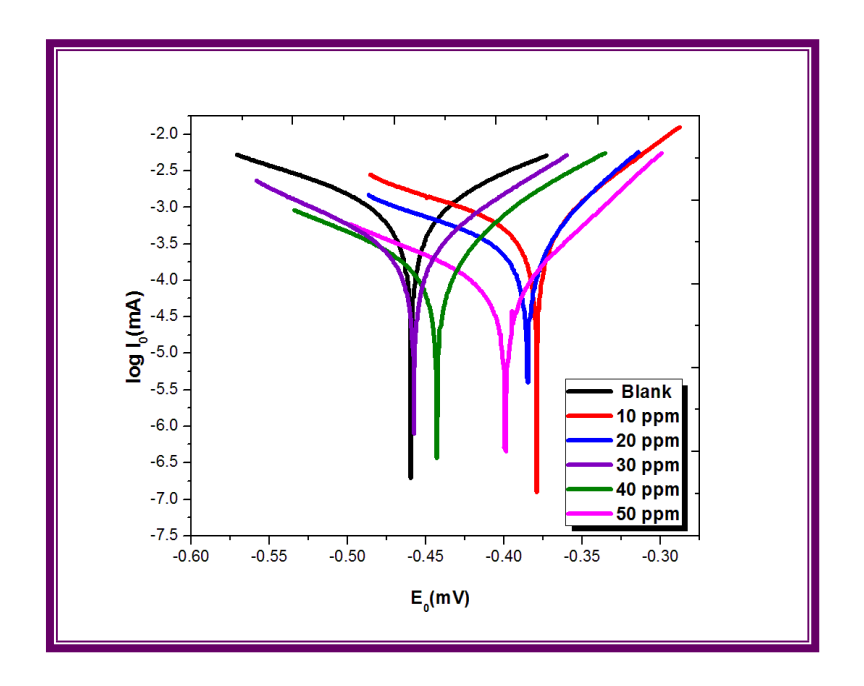


Fig.7.2.Tafel lines for various concentrations of MPSC on Mild steel in 1M HCl solution

The E₀, I₀, b_c, b_a, and I.E results calculated from the polarization examination are presented in Table.7.2. We can determine from the tabulated E₀ values that the studied protector has mixed sort behavior. The b_c and b_a values that support this concept are listed in Table.7.2. Furthermore, the I₀ value decreased from 1.372 to 0.0903 mA in response to an increase in MPSC concentration indicating that the corrosion degradation is effectively controlled by MPSC adsorption with a maximum inhibition efficacy of 93.42 % at 50 ppm.

Therefore, polarization information concludes that the electrochemical corrosion reactions are proscribed by the adsorption of MPSC on the Mild steel surface in 1M HCl solution.

Table.7.2. Polarization Parameters on Mild steel with and without MPSC in 1M HCl solution

С		Polarization parameters						
(ppm)	E ₀	\mathbf{I}_0	bc	ba	IE			
(ppm)	(mV)	(mA)	(mV)	(mV)	(%)			
Blank	-459.46	1.372	192.55	141.33	0.00			
10	-379.01	0.601	178.27	69.95	56.16			
20	-384.91	0.305	160.33	54.57	77.77			
30	-443.58	0.183	147.83	72.12	86.70			
40	-458.65	0.125	125.63	65.28	90.83			
50	-399.21	0.090	113.85	55.40	93.42			

7.3. Electrochemical impedance study

On exploring (Fig.7.3), the Nyquist plots altitude depending on the concentration of MPSC in the 1M HCl solution. The uppermost circle attained at the optimal concentration of MPSC depicts that the charge transfer is greatly resisted in the corrosive situation [3].

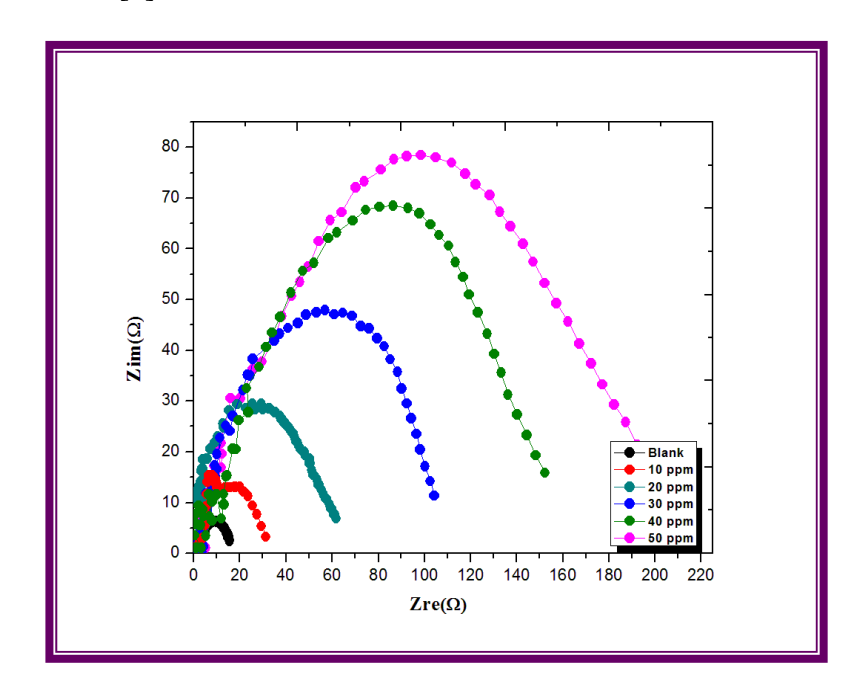


Fig.7.3. Nyquist plots for various concentrations of MPSC on Mild steel specimensin 1M HCl solution

The factors derived from the impedance investigation, such as R_{ct} , C_{dl} , and IE, are listed in Table.7.3. With an increase in MPSC concentration, the values of R_{ct} rose from 13.21 to 192.52 (Ω cm²) indicating that the charge transfer during the corrosion process is hindered by the formation of a prohibitive layer on the Mild steel surface. Alternatively, as the concentration of MPSC increased, C_{dl} values reduced from 1.628 to 0.011 (μ Fcm⁻²) revealing that metal surfaces are protected against corrosive environment. Furthermore, the optimum performance of 93.14 % reveals that MPSC is a potent defender against Mild steel corrosion in the 1M HCl solution.

Table.7.4. Impedance Parameters on Mild steel with and without MPSC in 1M

HCl solution

C	Impedance parameters					
C (ppm)	R_{ct} $(\Omega \text{ cm}^2)$	C _{dl} (μFcm ⁻²)	IE (%)			
Blank	13.21	1.628	0.00			
10	31.258	0.349	57.74			
20	61.912	0.085	78.66			
30	104.416	0.031	87.35			
40	150.255	0.015	91.21			
50	192.524	0.011	93.14			

7.4. Temperature analysis

As shown in (Fig.7.4), the mass reduction experiments were performed using distinct concentrations of MPSC at various temperatures (303, 313, 323, and 333 K) in the 1M HCl solution. Also, the procured corrosion rates and inhibition efficiencies are summarized in Table.7.4.

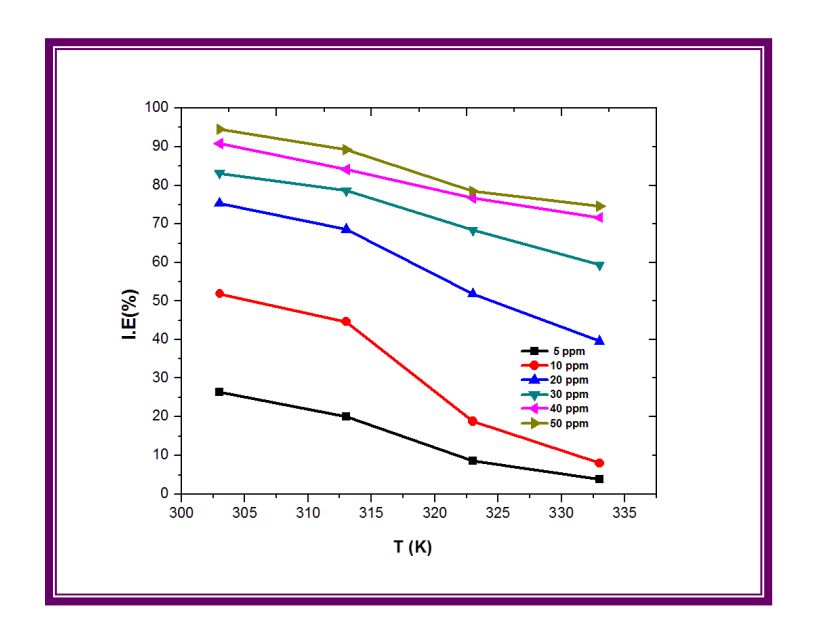


Fig.7.4.Temperature impact on inhibition efficiencies of Mild steel with and without MPSC in 1M HCl solution

Inspection of Table.7.4 reflects that the corrosion rates increase with an increase in temperature and the corresponding inhibition efficiencies decrease. The result that the corrosion rate increased from 1.07 to 12.43 (mg cm⁻² h⁻¹) when the inhibitor concentration was raised to 50 ppm suggests that the adsorption process is related to the electrostatic attraction between the inhibitor molecules and the Mild steel surface [4]. It's further reflected in the fact that at 50 ppm of MPSC in 1M HCl, the inhibitory effect dropped from 94.46 % to 74.52 %.

Table.7.5.Temperature study for various concentrations of MPSC on Mild steel in 1M HCl Solution

Conc.	Weight loss (mg)			Corrosion rate (mg cm ⁻² h ⁻¹)			Inhibition efficiency (%)					
(ppm)	303K	313K	323K	333K	303K	313K	323K	333K	303K	313K	323K	333K
Blank	1258.9	1383.4	2125.8	3191.1	19.25	21.15	32.50	48.79	0	0	0	0
5	825.2	1004.8	1812.2	2968.5	12.62	15.36	27.71	45.39	34.45	27.37	14.75	6.98
10	536.1	755.3	1525.4	2834.7	8.20	11.55	23.32	43.34	57.42	45.40	28.24	11.17
20	275.6	423.9	988.3	1967.4	4.21	6.48	15.11	30.08	78.11	69.36	53.51	38.35
30	161.7	295.8	642.1	1179.5	2.47	4.52	9.82	18.04	87.16	78.62	69.79	63.04
40	115.9	219.3	495.4	905.3	1.77	3.35	7.57	13.84	90.79	84.15	76.70	71.63
50	69.8	149.6	457.5	813.2	1.07	2.29	7.00	12.43	94.46	89.19	78.48	74.52

7.4.1. Corrosion kinetics and adsorption thermodynamics

Using the Arrhenius equation (5.1), the apparent activation energy (E_a) and Arrhenius factor (A) were derived for mass reduction observations at various temperatures. (Fig.7.5a) displays the Arrhenius plots procured by plotting to 'log CR' against '1000/T' with slope '(-Ea/2.303R)' and an intercept '(log A)'. The values of 'E_a' and 'A' were obtained from the slope and intercept of the straight lines respectively.

Table.7.6 contains kinetic variables such as Ea and A. Table.7.6 shows that when MPSC concentration increased, Ea values ascended from 26.83 to (KJ.mol⁻¹) demonstrating that the energy barrier rises during the corrosion inhibition process at higher temperatures. It mentions that the adsorption process is physical adsorption and it is further supported by the increasing values of the Arrhenius factor [5].

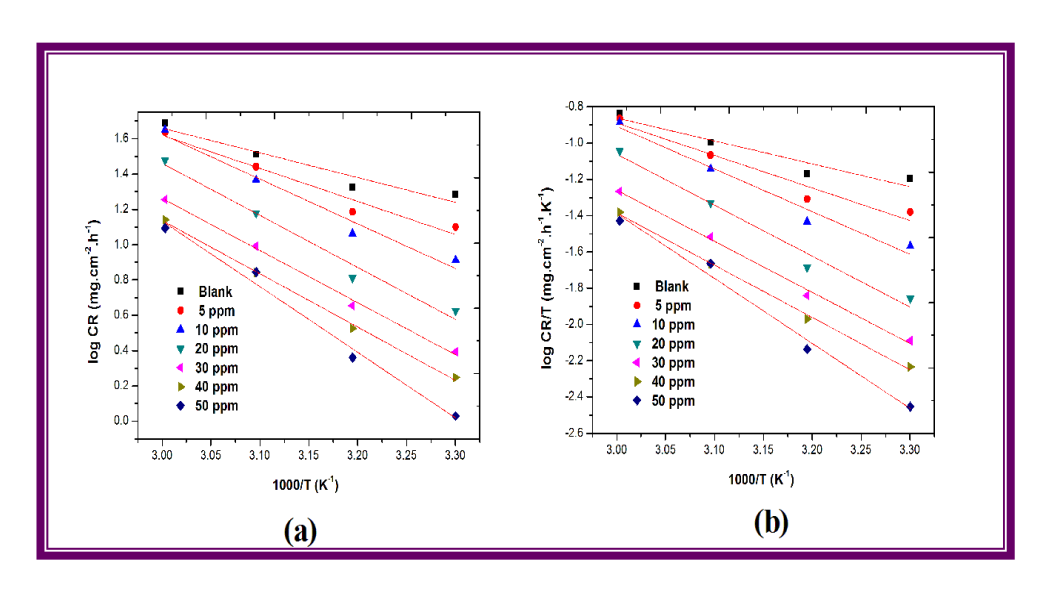


Fig.7.5. (a) Arrhenius plots and (b) Transition state plots for various concentrations of MPSC on Mild steel in 1M HCl solution

Table.7.6.Kinetic and Thermodynamic parameters of MPSC on Mild steel in 1M

HCl Solution at different temperatures

C (ppm)	E _a (KJ mol ⁻¹)	A	ΔH ⁰ (KJ mol ⁻¹)	$\begin{array}{c} \Delta S^0 \\ (JK^{\text{-}1}\text{mol}^{\text{-}1}) \end{array}$	Ea-RT
Blank	26.83	7.3198 X 10 ⁶	24.18	-141.51	2.64
5	36.97	2.6853×10^8	34.33	-111.57	2.64
10	47.62	1.1934 X 10 ¹⁰	44.98	-80.01	2.64
20	56.43	1.3121 X 10 ¹¹	53.78	-60.06	2.64
30	56.50	2.0044 X 10 ¹¹	53.88	-56.56	2.62
40	57.82	3.9627 X 10 ¹¹	55.18	-58.55	2.64
50	71.15	1.9186 X 10 ¹²	68.51	-18.62	2.64

(Fig.7.5b) represents the transition state plots for various concentrations of MPSC on Mild steel in the 1M HCl solution. Straight lines are achieved by the relationship of 'log CR/T' against '1000/T' with slope '(- $\Delta H^0/2.303R$)' and intercept '[(log (R/Nh) + $\Delta S^0/2.303R$]'. In addition, the slope and intercept of the transition state plots were used to obtain ΔH^0 and ΔS^0 values, which are presented in Table.7.6.

Positive values of ΔH^0 imply that the adsorption process is endothermic and the negative values of ΔS^0 moved to positive track imply that the randomness of the adsorption process is increased from blank to 50 ppm in an acidic environment [6]. Furthermore, the average value of Ea-H 0 (2.64 KJ mol $^{-1}$) is nearly identical to the value of RT (2.61 KJ mol $^{-1}$) indicating that the thermodynamic activation factors influence the corrosion adsorption process.

7.4.2. Temkin Adsorption isotherm

Various isotherms are employed to explain the interactions between inhibitor compounds and Mild steel; however, the Temkin isotherm is the best fit in this context and the logarithmic Temkin equation (7.1) is given below

$$\theta = \frac{-2.303 (\log C)}{2a} - \frac{2.303 (\log K)}{2a}$$
 (7.1)

Fig.7.6 represents the affiliation between the surface coverage and inhibitor concentration. Straight lines are obtained by plotting to ' θ ' against 'log C' with slope (-2.303/2a) and intercept (-2.303(log K) / 2a).

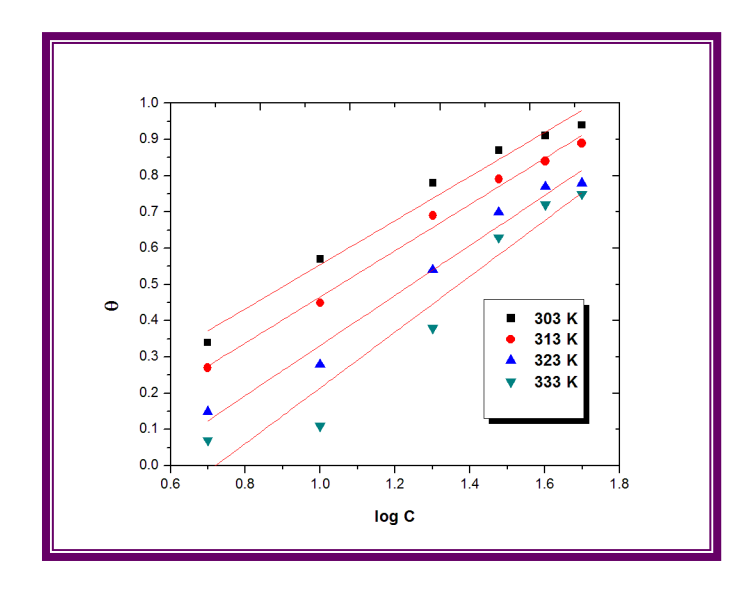


Fig.7.6.Temkin isotherm for various concentrations of MPSC on Mild steel in 1M HCl solution at different temperatures

Moreover, the attractive parameter 'a' and the adsorption constant ' K_{ads} ' are calculated from the slope and intercept in that order and presented in Table.7.7. The negative sign of the attractive parameter indicates that the repulsive force prevails in the adsorption process at elevated temperatures, implying that desorption occurs, and the K_{ads} values decreased from 81.84 to 19.08, suggesting that physisorption occurs. Besides that, the change in Gibb's free energy values was acquired by the equation (5.5). The negative ΔG values obtained here suggest that the adsorption process is spontaneous, and the values range from - 21.21 to -19.28 KJ.mol⁻¹ denoting that the adsorption is electrostatic and desorption occurs at a rising temperature. Furthermore, the regression coefficient values (R^2) are close to 1 representing that the Temkin model drives the adsorption process. [7].

Table.7.7. Temkin parameters of MPSC on Mild steel corrosion at raisedtemperatures

	Temkin isotherm						
T (K)	K _{ads}	ΔG ⁰ _{ads} (KJ.mol ⁻¹)	a	\mathbb{R}^2			
303	81.840	-21.21	-1.89	0.9758			
313	54.060	-20.84	-1.81	0.9906			
323	30.281	-19.94	-1.67	0.977			
333	19.079	-19.28	-1.50	0.9665			

7.5. DFT approach

The optimized structure and Mulliken charges of the examined protector are shown in (Figs.7.7a-7.7b). Also, Table.7.8 shows the Mulliken charges of the atoms involved in the inhibition process, indicating the presence of an adsorption center and the inhibitory efficiency of the MPSC inhibitor [8].

Table.7.8. Mulliken charges of atoms present in MPSC

Atoms	Mulliken charges
N ₁₁	-0.208
N ₁₃	0.029
N ₂₈	0.080
O ₆	-0.415
O ₁₅	-0.396
O ₁₆	-0.487
S ₁₄	0.923

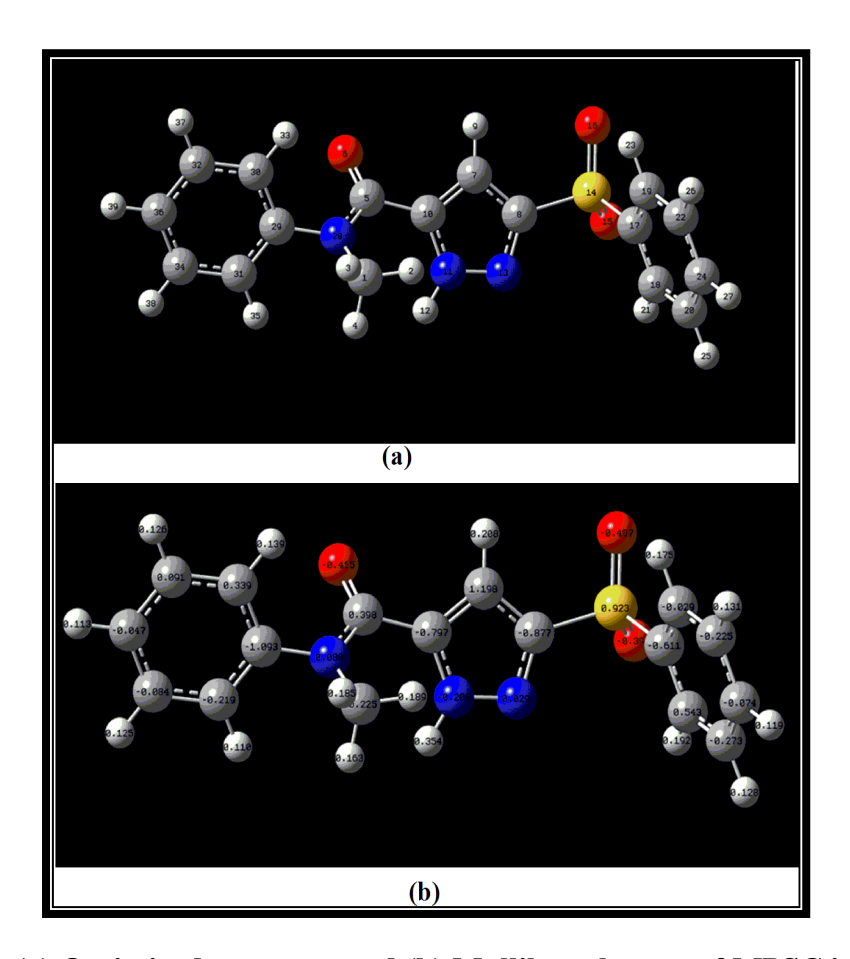


Fig.7.8. (a) Optimized structure and (b) Mulliken charges of MPSC inhibitor

Among all, the Nitrogen atom which is labeled as N_{11} (-0.208) in the pyrazole ring regarded the protonation site of the inhibitor in the HCl environment, evoking electrostatic attraction on a steel surface.

The HOMO energy distribution on the pyrazole moiety, benzene ring, -N-CH3 and -C=O groups of the inhibitor (Fig.7.8a) suggests that electrons might be transported from those spots to the Mild steel for coordination as seen in (Fig.7.8b). The LUMO's energy is focused at the -N-CH3, -C=O group, and pyrazole ring, as illustrated in (Fig.7.8b), signifying Mild steel to inhibitor back donation and high anti-corrosion performance [9-11].

The electronic properties such as E_{HOMO} , E_{LUMO} , ΔE , D, I, A, χ , η , σ and ΔN derived from DFT analysis are summarized in Table.7.9. The lower unoccupied molecular orbital has a lower energy value (-0.8778 eV), indicating the inhibitor's propensity for accepting electron pairs from metal via back bonding, whereas the highest occupied molecular orbital has a higher energy value (-5.7406 eV), indicating the inhibitor's highest probability of electron donation.

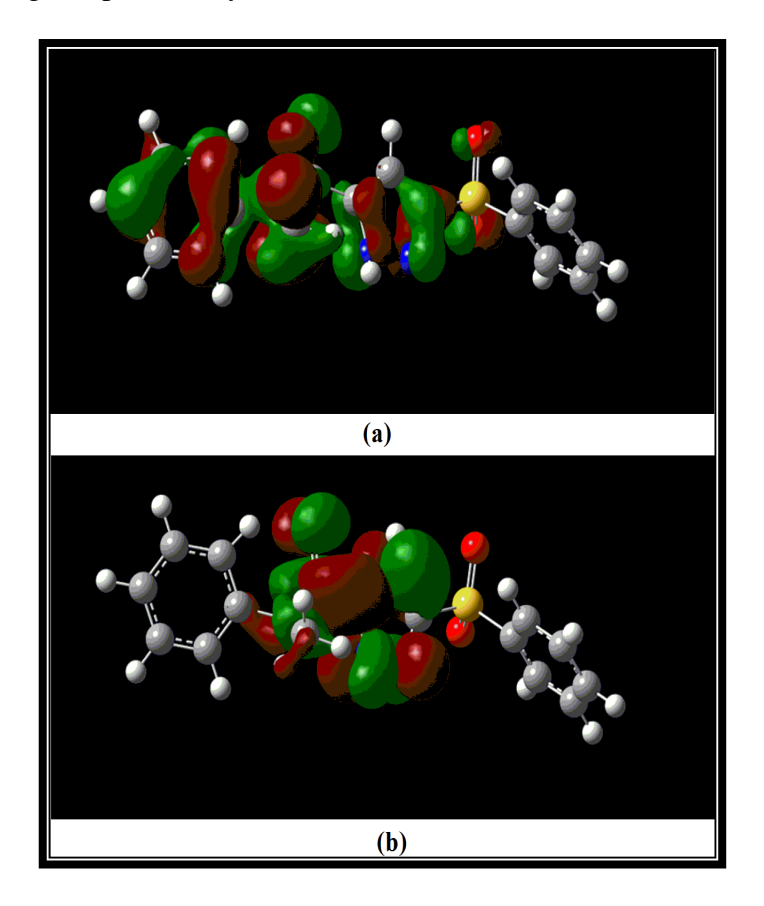


Fig.7.8.(a) HOMO and (b) LUMO of MPSC inhibitor

Table.7.9. Electronic parameters of the investigated protector MPSC

DFT constraints					
Еномо	-5.7406 eV				
Ешмо	-0.8778 eV				
Energy Gap (ΔE)	4.8 eV				
Ionization energy (I)	5.7406 eV				
Electron affinity (A)	0.8778 eV				
Absolute electronegativity (χ)	3.3092 eV				
Global hardness (η)	2.4314				
Global softness (σ)	0.4112				
Electrophilicity index (ω)	1.7731				
transferred electrons fraction (ΔN)	0.3106				
Back donation (ΔE _{backdonation})	-0.6078 eV				

The computed values of ΔE , D, I, A, χ , η , σ and ΔN also support the view that the MPSC is a potent inhibitor and the theoretical assessment is in line with the experimental findings [12].

7.6. Morphological interrogation

7.6.1. SEM analysis

The SEM photographs of polished Mild steel submerged in 1M HCl solution with MPSC are displayed in (Fig.7.9a&7.9b). The smooth surface with mass deposition in the presence of the protector resists the corrosive detriments by forming a passive coating on the Mild steel surface as can be seen in these images [13]. As a consequence, SEM micrographs revealed that the explored MPSC functions as an effective inhibitor in the 1M HCl solution.

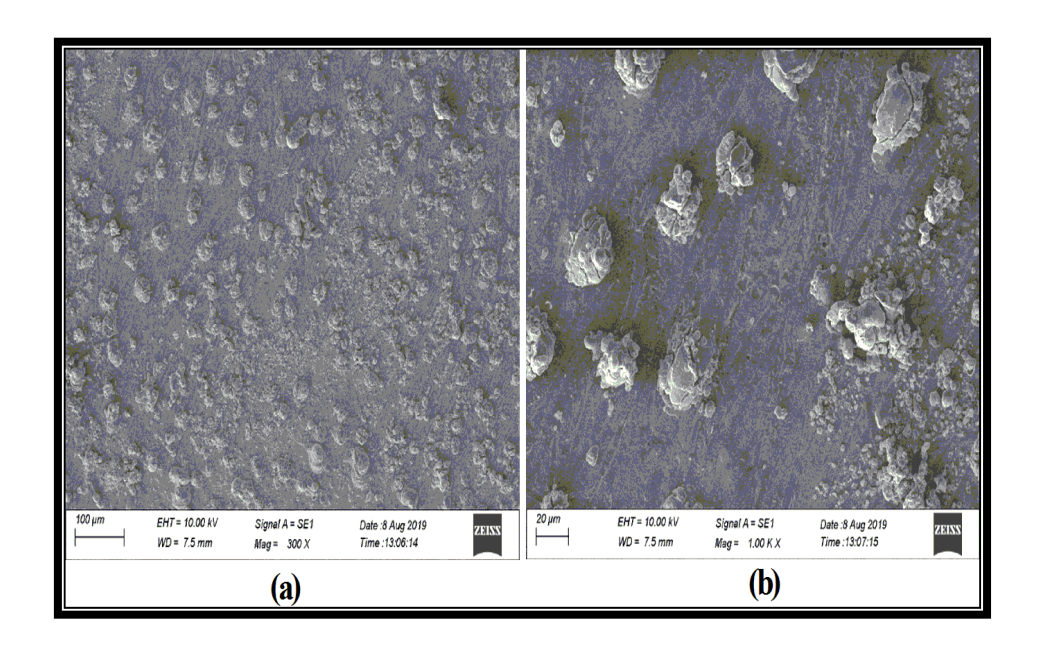


Fig.7.9 a&b. SEM images of the inhibited surface with MPSC in 1M HCl solution

7.6.2. EDX analysis

In 1M HCl solution, EDX evaluation of specimens without and with MPSC is displayed in (Fig.7.10a&7.10b). The presence of a chlorine peak in (Fig.7.10a)indicates that the corrosive scenario influenced the steel surface in the absence of an inhibitor in the 1M HCl solution. (Fig.7.10b) depicts that the presence of MPSC shields the steel surface, implying that a thin coating is forming on the Mild steel surface, as evidenced by the presence of a nitrogen peak in the spectrum. Thus, the corrosion inhibition accompanied by the sharing of lone pair electrons on the nitrogen andoxygen atoms to the empty d orbital of the iron atom is corroborated by the EDX study [14].

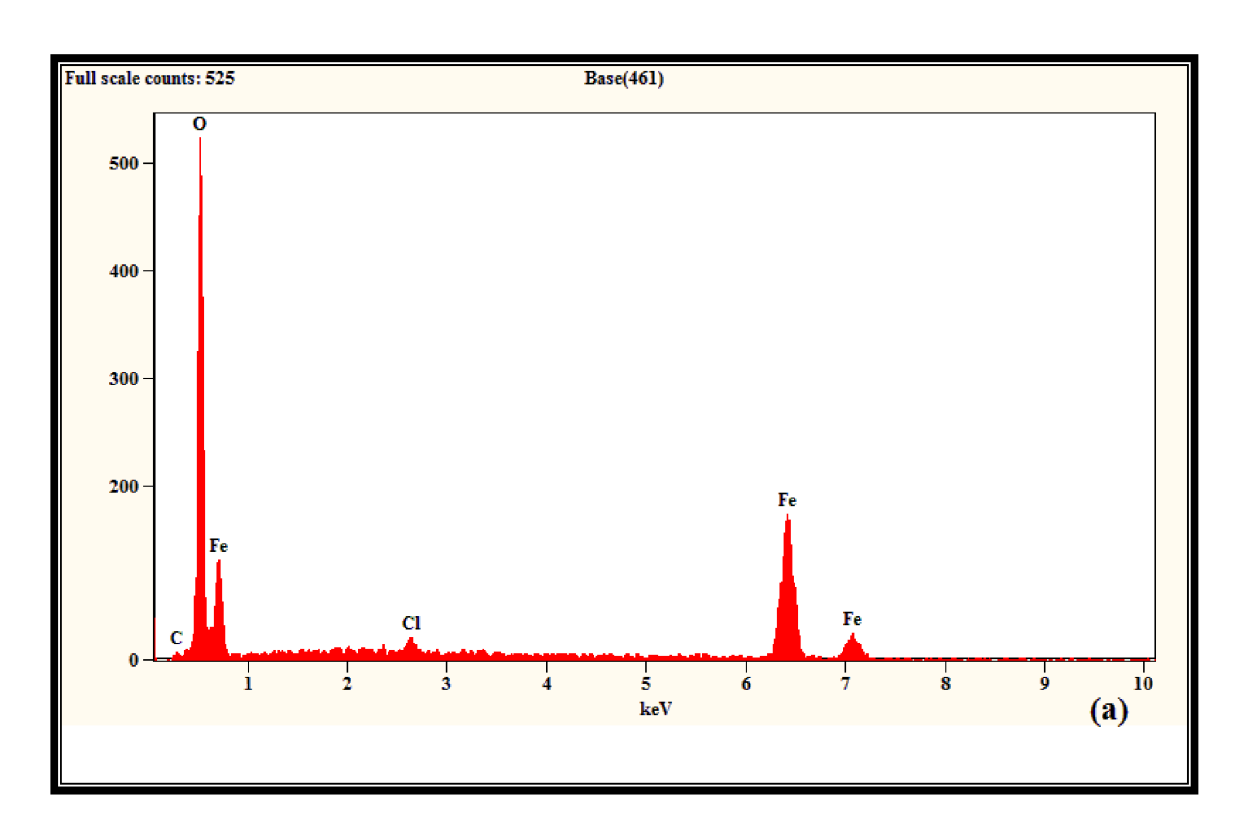


Fig.7.10a. EDX spectrum of uninhibited surface in 1M HCl solution

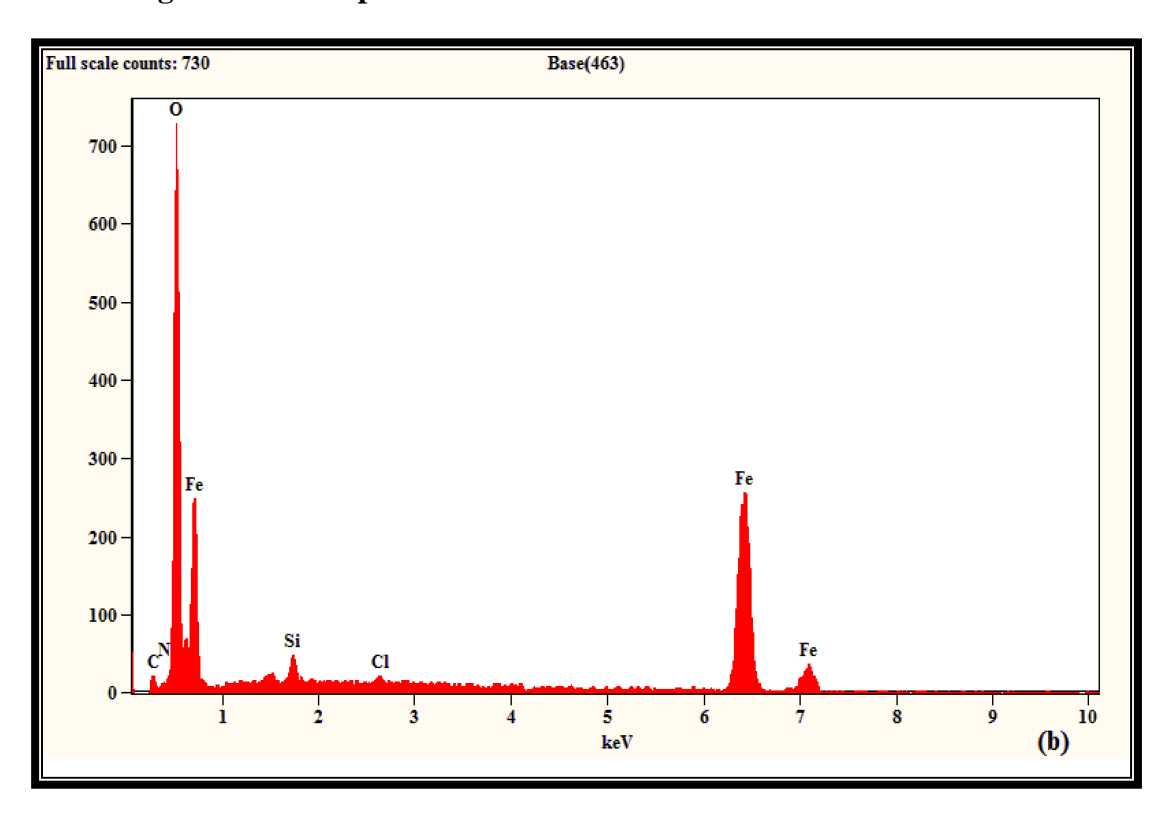


Fig.7.10b. EDX spectrum of inhibited surface with MPSC in 1M HCl solution

Furthermore, the quantitative EDX data of the analyzed steel specimens are shown in Table.7.10 indicating that the corrosion behavior is hampered by the development of a passive coat through N (1.24%) and O (20.97%) coordination with the steel surface in the 1M HCl solution [15].

Table.7.10. EDX parameters of the explored inhibitor MPSC

Samples	С	O	Cl	N	Si	Fe
Bare steel	12.20	7.98	-	-	-	79.82
Unprotected surface	5.84	43.44	1.06	-	-	49.66
Protected surface with						
MPSC	8.83	20.97	0.39	1.24	0.98	67.59

7.6.3. AFM Analysis

3D AFM images of polished steel, unprotected Mild steel and shielded Mild steel surfaces are shown in (Fig. 7.11a-7.11c). The smooth surface of the Mild steel surface is shown in (Fig.8.11a). In the absence of an inhibitor, corrosion in the 1M HCl solution causes severe surface damage, as seen in (Fig 7.11b). On the other hand, (Fig.7.11c) displays that the surface irregularity was drastically diminished in the presence of MPSC in the 1M HCl solution [15]. This analysis proves that the MPSC efficiently protects the surface of the Mild steel specimens from the corrosive environment.

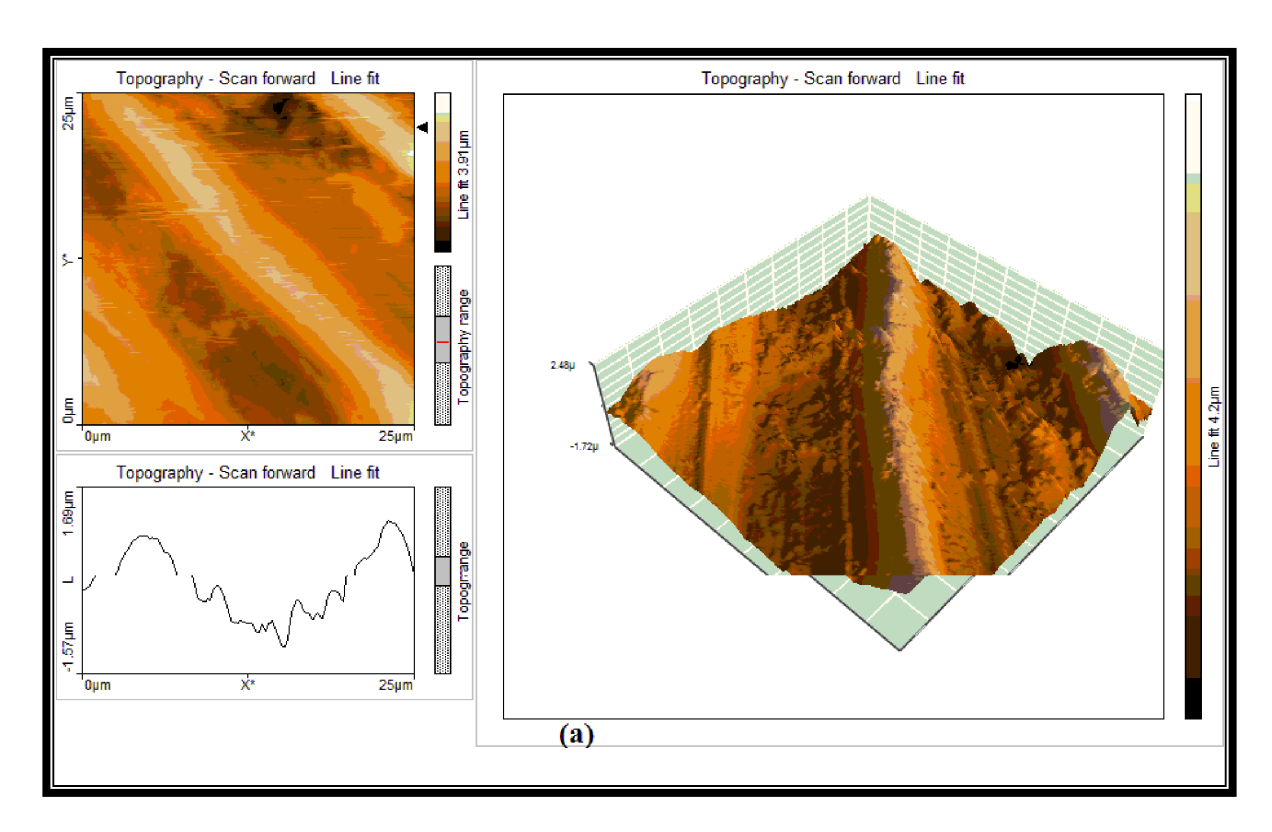


Fig.7.11a. 3D - AFM image of polished Mild steel 1M HCl solution

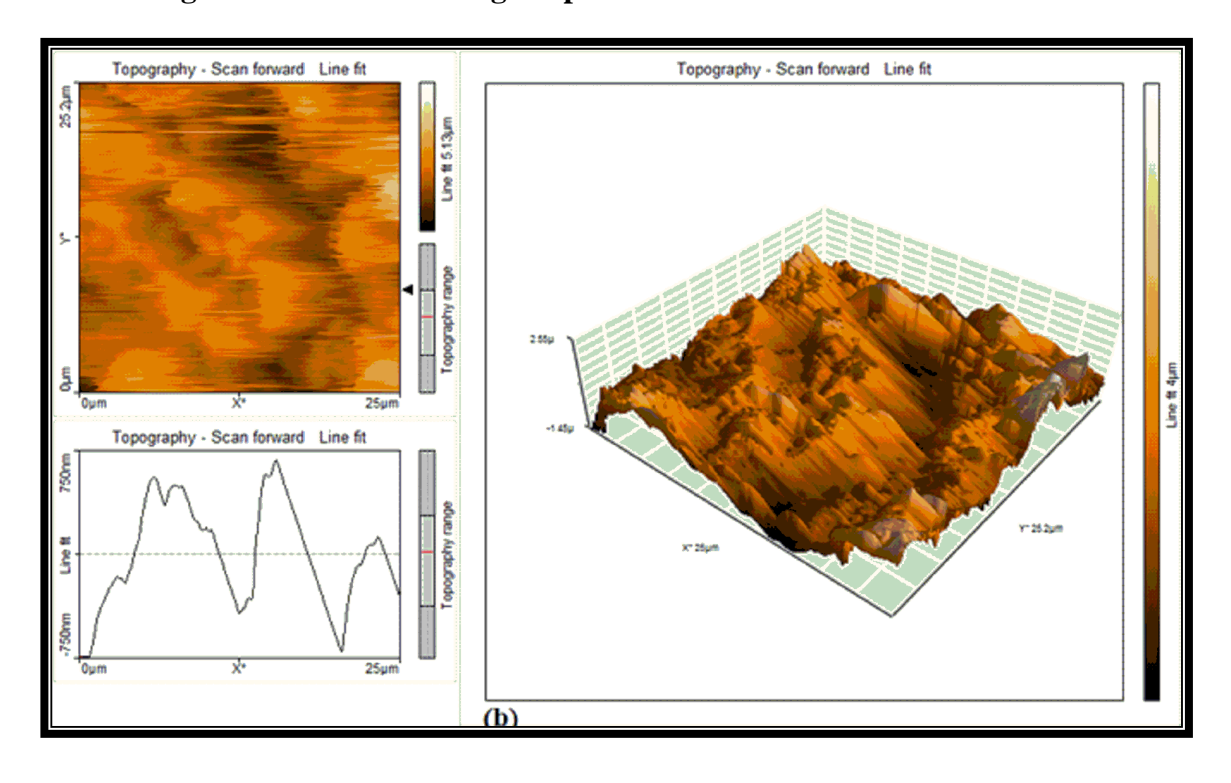


Fig.7.11b. 3D - AFM image of uninhibited Mild steel in 1M HCl solution

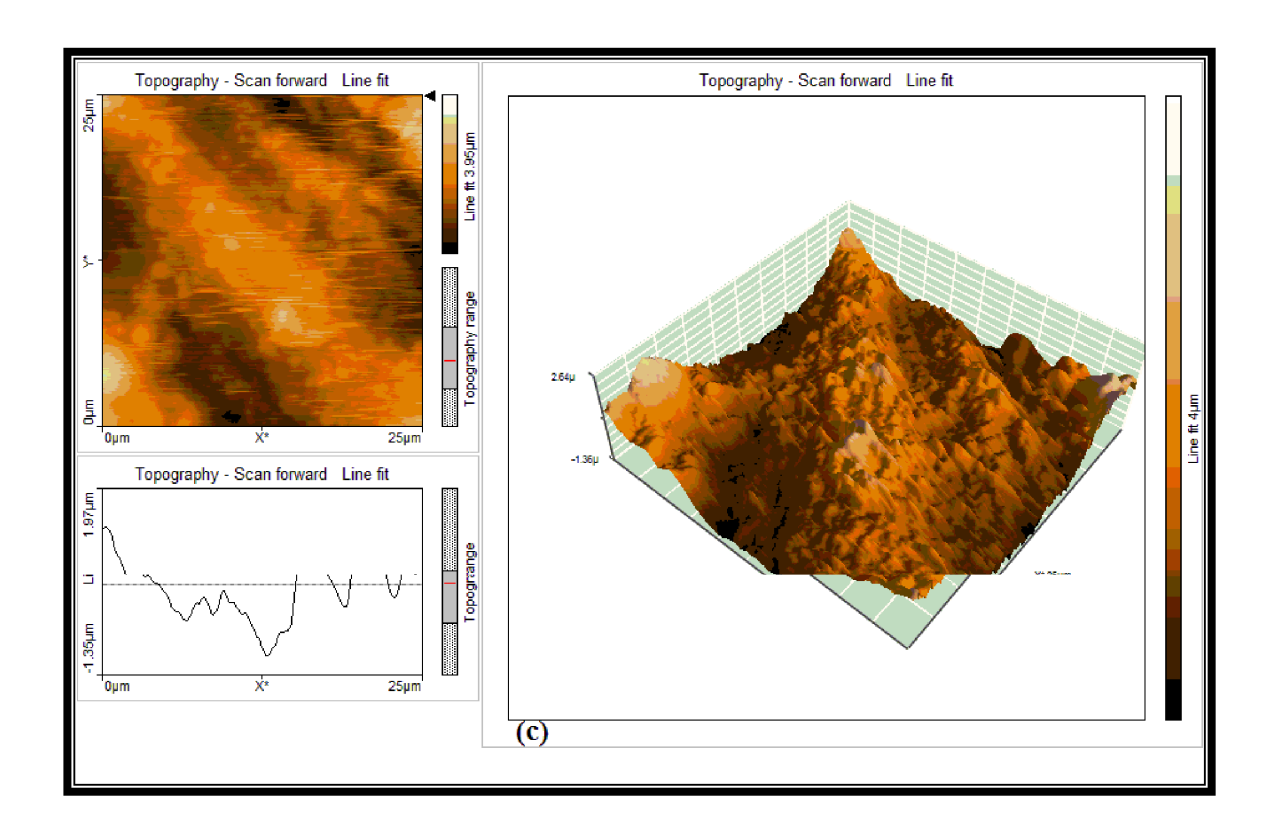


Fig.7.11c. 3D - AFM image of the inhibited surface with MPSC in 1M HCl

The corrosion protection is also supported by the Ra and Rq values obtained from the AFM investigation of Mild steel in the presence and absence of MPSC are provided in Table.7.11. The average roughness values for polished Mild steel specimens in the absence and presence of MPSC are 279.41nm, 418.32 nm and 334.33 nm respectively according to Table.7.10 whereas the corresponding RMS values are 332.27nm, 489.49 nm, and 386.47 nm.

The roughness with the highest values than the polished Mild steel was found to be extensively affected by the corrosive media. The inhibited surface has lower roughness values than the unprotected steel surface, revealing that the inhibitor's adsorption lowers corrosion assaults.

Table.7.11. AFM parameters of the examined inhibitor MPSC with and without MPSC in 1M HCl solution

Samples	Average Roughness	RMS roughness	
	(R _a)nm	$(\mathbf{R}_{\mathbf{q}})$ nm	
polished Mild steel	279.41	332.27	
unprotected steel surface	418.32	489.49	
Protected steel surface with MPSC	334.33	386.47	

All the explorations corroborated that the examined MPSC works as an effective protector on Mild steel corrosion in an acidic medium.

7.1. References

- Rbaa M, Galai M, Benhiba F. Synthesis and investigation of quinazoline derivatives based on 8-hydroxyquinoline as corrosion inhibitors for Mild steel inacidic environment: experimental and theoretical studies. *Ionics (Kiel)*. 2018; 25(7): 3473-3491.
- Louadi Y, Abrigach F, Bouyanzer A. Theoretical and Experimental Studies on the Corrosion Inhibition Potentials of Two Tetrakis Pyrazole Derivatives for Mild steel in 1.0 M HCl. *Portugaliae Electrochimica Acta*. 2017; 35(3): 159-178.
- 3. Singh A, Quraishi M. Inhibitive effect of diethylcarbamazine on the corrosion of Mild steel in hydrochloric acid. *Corros Sci.* 2010; 52(4): 1529-1535.
- 4. Al-Fakih A, Abdallah H, Aziz M. Experimental and theoretical studies of the inhibition performance of two furan derivatives on Mild steel corrosion in acidicmedium. *Materials and Corrosion*. 2018; 70(1): 135-148.
- 5. Dohare P, Quraishi M, Obot I. A combined electrochemical and theoretical study of pyridine-based Schiff bases as novel corrosion inhibitors for Mild steel in hydrochloric acid medium. *Journal of Chemical Sciences*. 2018; 130: 1-8.
- Singh A, Shukla S, Singh M, Quraishi M. Inhibitive effect of ceftazidime on corrosion of Mild steel in hydrochloric acid solution. *Mater Chem Phys.* 2011; 129 (1-2): 68-76.
- Ituen E, Akaranta O, James A. Evaluation of Performance of Corrosion Inhibitors Using Adsorption Isotherm Models: An Overview. Chemical Science International Journal. 2017; 18(1): 1-34.

- Huong D Q, Duong T, Nam P C. Experimental and theoretical study of corrosion inhibition performance of N-phenylthiourea for Mild steel in hydrochloric acid and sodium chloride solution. *J. Mol. Model.* 2019; 25: 204-213.
- 9. Umoren S, Obot I, Israel A. Inhibition of Mild steel corrosion in acidic medium using coconut coir dust extracted from water and methanol as solvents. *Journal of Industrial and Engineering Chemistry*. 2014; 20 (5): 3612-3622.
- 10. Ansari K, Quraishi M. Experimental and computational studies of naphthyridine derivatives as corrosion inhibitor for N80 steel in 15% hydrochloric acid. *Physica E: Low-dimensional Systems and Nanostructures*. 2015; 69: 322-331.
- 11. Singh P, Makowska-Janusik M, Slovensky P, Quraishi M. Nicotinonitriles as green corrosion inhibitors for Mild steel in hydrochloric acid: Electrochemical, computational and surface morphological studies. *J Mol Liq.* 2016; 220: 71-81.
- 12. Mendonca G, Costa S, Freire V, Casciano P, Correia A, Lima-Neto P. Understanding the corrosion inhibition of carbon steel and copper in sulphuric acid medium by amino acids using electrochemical techniques allied to molecular modelling methods. *Corros Sci.* 2017; 115: 41-55.
- 13. Tan B, Zhang S, Qiang Y. A combined experimental and theoretical study of the inhibition effect of three disulfide-based flavoring agents for copper corrosion in 0.5 M sulfuric acid. *J Colloid Interface Sci.* 2018; 526: 268-280.
- 14. Dohare P, Ansari K, Quraishi M, Obot I. Pyranpyrazole derivatives as novel corrosion inhibitors for Mild steel useful for industrial pickling process: Experimental and Quantum Chemical study. *Journal of Industrial and Engineering Chemistry*. 2017; 52: 197-210.

15. El-Haddad M, Bahgat Radwan A, Sliem M, Hassan W, Abdullah A. Highly efficient eco-friendly corrosion inhibitor for Mild steel in 5 M HCl at elevated temperatures: experimental & molecular dynamics study. *Sci Rep.* 2019; 9(1): 7730-7739.

CHAPTER-VIII

Corrosion protection characteristics of '5-benzyl 3-ethyl 1*H*-pyrazole-3, 5-dicarboxylate (BEPD) on Mild steel corrosion

Accurately weighed Mild steel samples before and after immersion in the 1M HCl corrosive solution with different concentrations (10, 20, 30, 40 and 50 ppm) of 5-benzyl 3-ethyl 1H-pyrazole-3, 5-dicarboxylate were used to determine corrosion inhibition for 6 hours contact time.

8. Results and Discussion

8.1. Mass loss study

The mass loss approach was used to establish a correlation between the corrosion rate and the inhibition efficiency in the 1M HCl solution at room temperature as demonstrated in (Fig. 8.1).

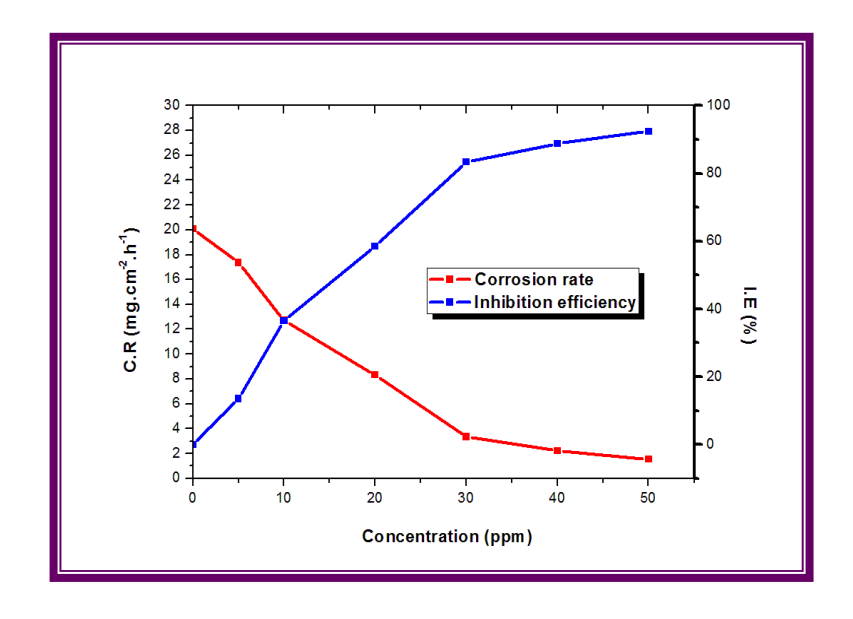


Fig.8.1. Relationship between the protection capacity and the corrosion rate of BEPD in the 1M HCl solution

The protective capability rises as the BEPD concentration increases, while the corrosion rate reduces, as demonstrated in (Fig. 8.1). Table.8.1 displays corrosion parameters such as corrosion rate, protective ability and surface coverage revealing that when BEPD concentration increases from blank to 50 ppm, the corrosion rate lowers dramatically (20.07 to 1.52 mg cm⁻² h⁻¹). In turn, as the concentration of BEPD increased, the IE value raised from 36.56 to 92.42 % with the maximum efficiency recorded at 50 ppm showing that the tested inhibitor resists Mild steel corrosion in the 1M HCl solution at ambient temperature [1, 2].

Table.8.1. Corrosion metrics of Mild steel corrosion with BEPD in 1M HCl

Concentration (ppm)	Weight loss (mg)	Corrosion rate (mg cm ⁻² h ⁻¹)	Inhibition efficiency (%)	Surface coverage (θ)
blank	1312.4	20.07	-	-
10	832.6	12.73	36.56	0.37
20	543.8	8.32	58.56	0.59
30	218.4	3.33	83.36	0.83
40	146.3	2.23	88.85	0.89
50	99.5	1.52	92.42	0.92

8.2. Electrochemical polarization investigation

The Tafel lines for test specimens in 1M HCl at room temperature in the absence and the presence of various concentrations of BEPD are shown in (Fig.8.2). The Tafel lines migrate on both anodic and cathodic sites as shown in (Fig.8.2) demonstrating that the inhibitor inhibited both anodic and cathodic electrochemical corrosion reactions [3].

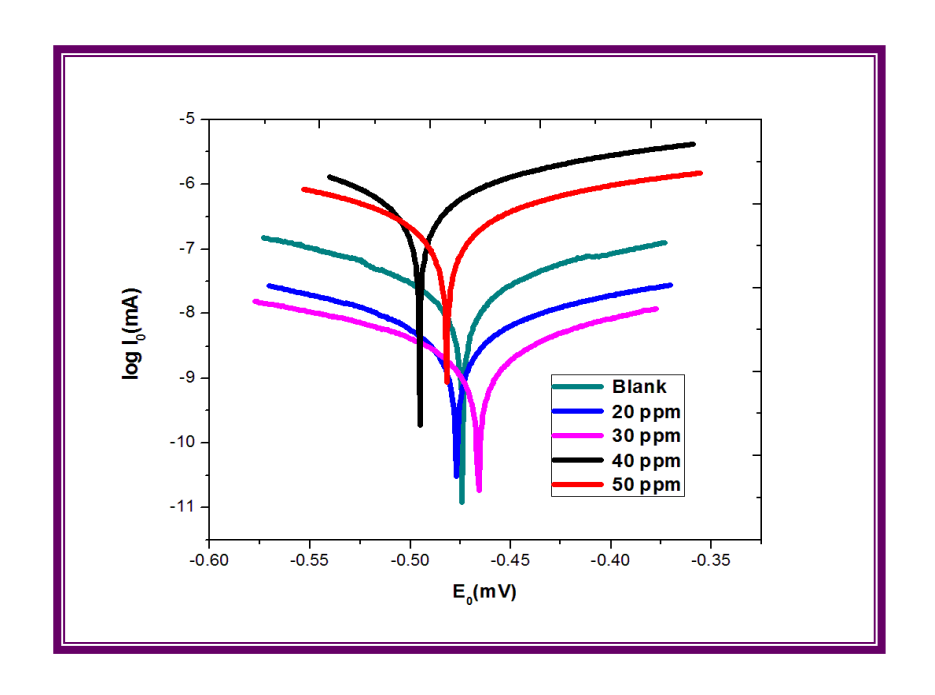


Fig.8.2. Tafel lines for BEPD on Mild steel corrosion in 1M HCl solution

Moreover, the polarization parameters presented in Table 8.2 display that as the concentration of BEPD increased, the values of I₀ declined substantially indicating that the corrosion rate is retarded by BEPD molecules adsorbed onto the metallic surface. Both anodic and cathodic moves are validated by the tabulated Tafel slope values resulting in the cathodic impact being more prominent [4, 5].

Table.8.2. Polarization factors of BEPD on Mild steel corrosion in 1M HCl

C	Polarization parameters					
(ppm)	E ₀ (mV)	I ₀ (mA)	b _c (mV)	ba(mV)	IE (%)	
blank	-492.35	6.309	303.11	78.34	0.00	
20	-485.51	2.695	271.35	99.15	57.28	
30	-474.58	1.124	200.47	249.18	82.18	
40	-476.80	0.761	246.60	282.61	87.93	
50	-465.75	0.509	258.187	242.103	91.92	

As a result of this polarization investigation, the E₀ values ranged from -492.35 mV to -465.75 mV representing that the examined BEPD operated as a mixed kind protector in an acidic environment. Additionally, the BEPD inhibitor has a maximum efficacy of 91.92% at 50 ppm signifying that it was a potent anticorrosive protector in the 1M HCl medium.

8.3. Electrochemical impedance investigation

The diameters of the Nyquist plots increase with an increase in BEPD concentration as shown in (Fig.8.3), implying that the addition of inhibitor to the corrosive medium resists the charge transfer.

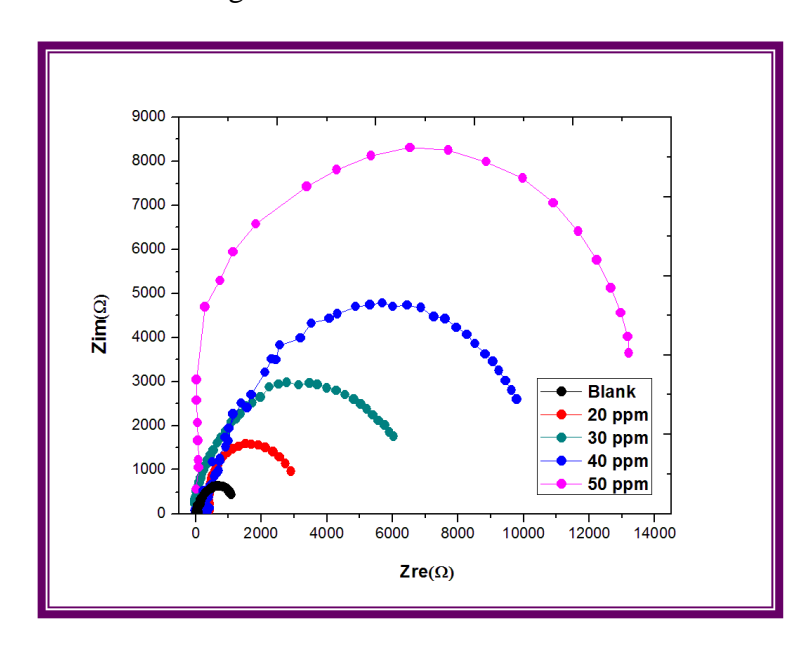


Fig.8.3. Impedance plots for BEPD on Mild steel corrosion in 1M HCl

The impedance parameters are listed in Table 8.3 show that the increase in R_{ct} (1092.58 to 13211.52 Ω cm²) with an increase in BEPD concentration which exposes the corrosion progression is diminished by the charge transfer impediment in the acidic medium. Additionally, the lower C_{dl} values (1.832 to 0.001 μF cm⁻²) suggest a larger electrical double layer at the metal-solution boundary implying the strong inhibition[6, 7].

Table.8.3. Impedance factors for BEPD on Mild steel corrosion in the 1M HCl

С	Impedance parameters					
(ppm)	R_{ct} $(\Omega \text{ cm}^2)$	C _{dl} (µFcm ⁻²)	I.E (%)			
Blank	1092.58	1.832	0			
20	2605.02	0.366	58.06			
30	6133.25	0.087	82.19			
40	9682.32	0.032	88.72			
50	13211.52	0.001	91.73			

We can also see from Table.8.3 that the BEPD has a maximum protection efficacy of 91.73 % at 50 ppm and all of the impedance parameters indicate that the examined protector has a high capacity to resist corrosion assaults in a hostile environment.

8.4. Thermal study on Mild steel corrosion

(Fig.8.4) demonstrates the influence of temperature on Mild steel corrosion in the presence and absence of MPPT in a 1M HCl atmosphere at 303, 313, 323, and 333 K. It illustrates that the corrosion process is influenced by the electrostatic interactions on the Mild steel surface in an acidic environment, as seen by the decrease in hampered efficiencies at increased temperatures for all BEPD inhibitor concentrations.

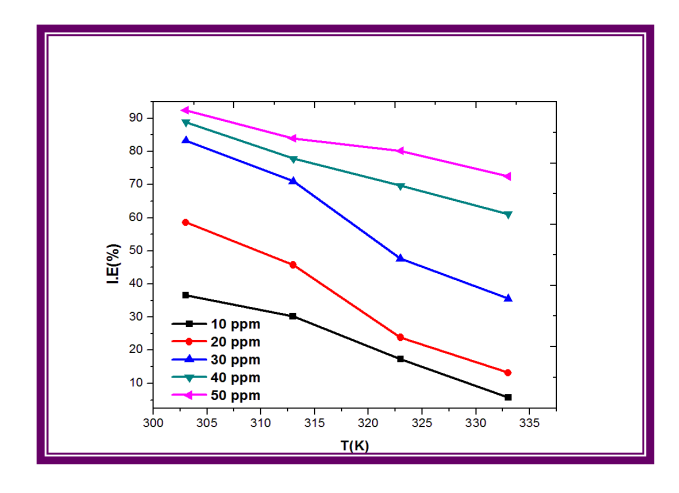


Fig.8.4. Relationship between the corrosion rate and the inhibition ability of the BEPD in 1M HCl solution at elevated temperatures

Table.8.4 summarizes the corrosion parameters assessed such as corrosion rate and inhibition efficacy. Based on the statistics, we can predict that the protective capability decreases as the temperature rises.

Temperature effects on corrosion as evidenced by the fact that the corrosion rate dropped from 1.52 to 13.17 mg cm⁻² h⁻¹. As a result of the preceding discussion, it was discovered that the decrease in efficiency (92.42 % to 72.44 %) with increasing BEPD concentration is mainly owing to the investigated inhibitor's desorption nature on the metal surface at higher temperatures, implying that the adsorption process is physisorption [8].

Table.8.4. Correlation between the temperatures and the inhibition efficiencies of BEPD on Mild steel corrosion in the 1M HCl solution

Conc. (ppm)	Weight loss (mg)			Corrosion rate (mg cm ⁻² h ⁻¹)			Inhibition efficiency (%)					
	303K	313K	323K	333K	303K	313K	323K	333K	303K	313K	323K	333K
Blank	1312.4	1451.6	2147.2	3125.8	20.07	22.20	32.83	47.80	0	0	0	0
10	832.6	1012.8	1774.7	2945.8	12.73	15.49	27.14	45.04	36.56	30.23	17.35	5.76
20	543.8	787.8	1635.5	2714.7	8.31	12.05	25.01	41.51	58.56	45.73	23.83	13.15
30	218.4	421.5	1124.8	2014.3	3.34	6.44	17.20	30.80	83.36	70.96	47.62	35.56
40	146.3	321.5	652.1	1214.7	2.24	4.92	9.97	18.57	88.85	77.85	69.63	61.14
50	99.5	231.8	425.3	861.5	1.52	3.54	6.50	13.17	92.42	84.03	80.19	72.44

8.4.1. Kinetic and thermodynamic parameters

Applying the data from the temperature study, the activation energy (E_a) and Arrhenius factor (A) can be calculated using the Arrhenius equation (5.1). Likewise, the transition state equation (5.2) was also used to determine the values of entropy change (ΔS^0) and enthalpy change (ΔH^0) .

(Fig.8.5a) shows the straight lines of Arrhenius plots obtained by plotting log CR versus 1000/T with the slope (–Ea /2.303R) and an intercept (log A) and the statistics of ΔS^0 and ΔH^0 can be derived from the transition state plots by plotting log (CR/T) vs 1000/T as illustrated in (Fig. 6.5b).

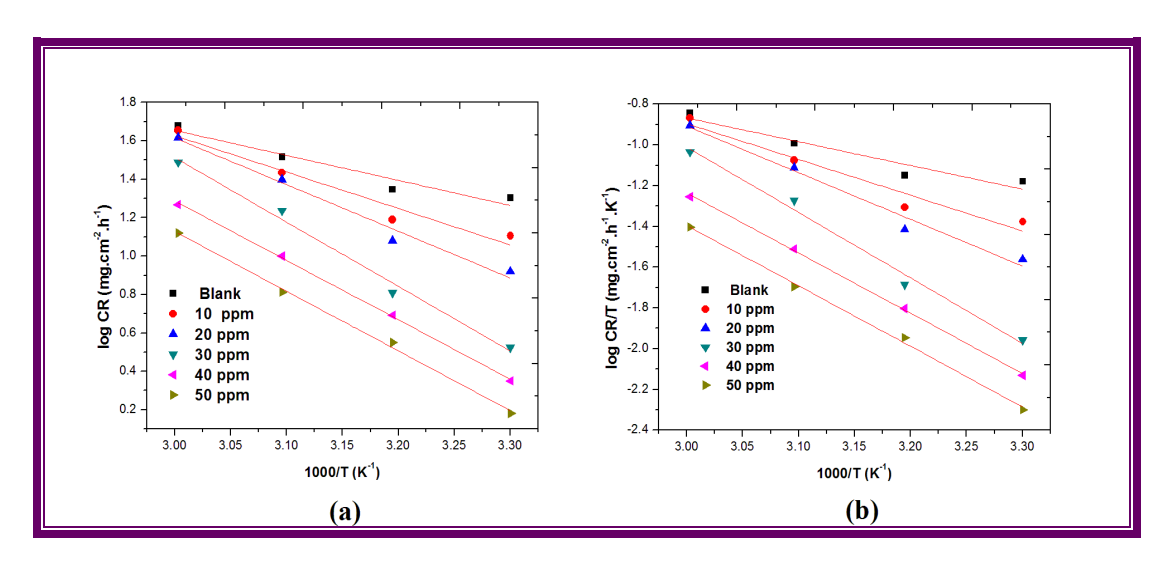


Fig.8.5 (a) Arrhenius plots and (b) Transition state plots for BEPD on Mild steel corrosion in 1M HCl solution

Table 8.5 summarizes the kinetic and thermodynamic parameters acquired from the transition state plots and Arrhenius plots. At all working temperatures, we can witness an increase in E_a (from 24.95 to 64.14 KJ mol⁻¹) with an increase in BEPD concentration, revealing that the energy barrier rises during the corrosion inhibition process at higher temperatures. It states that the adsorption process involves physical adsorption which is substantiated by increasing Arrhenius factor values [9-11]. The endothermic nature of the adsorption process is shown by the positive ΔH^0 values. Furthermore, positive transfer of ΔS^0 values from blank to optimum concentration indicates an increase in randomness in the adsorption process in an acidic environment [12, 13].

Table.8.5. Kinetic and Thermodynamic data of BEPD on Mild steel corrosion in 1M HCl solution

C (ppm)	E _a (KJ mol ⁻¹)	A	ΔH ⁰ (KJ mol ⁻¹)	$\begin{array}{c} \Delta S^0 \\ (JK^{-1}mol^{-1}) \end{array}$	E _a -RT
Blank	24.95	3.6812×10^6	22.32	-147.22	2.63
10	36.32	2.0796 X 10 ⁸	33.68	-113.67	2.64
20	46.51	7.9799 X 10 ⁹	43.87	-83.34	2.64
30	59.20	2.7542×10^{11}	56.56	-53.75	2.64
40	59.47	3.6305×10^{11}	56.85	-51.51	2.62
50	64.14	3.6308×10^{11}	61.50	-32.37	2.64

8.4.2. Freundlich adsorption isotherm

Freundlich model can be expressed as the following equation (8.1)

$$\log \theta = \log K + \frac{1}{n} \log C \tag{8.1}$$

where ' θ ' is the surface coverage, 'K' is the adsorption constant, 'n' refers to the adsorption intensity and 'C' refers to the concentration of the inhibitor. By plotting to '(log θ) vs (log C)' gives straight lines with slope (1/n) and intercept (log K) is shown in (Fig.8.6).

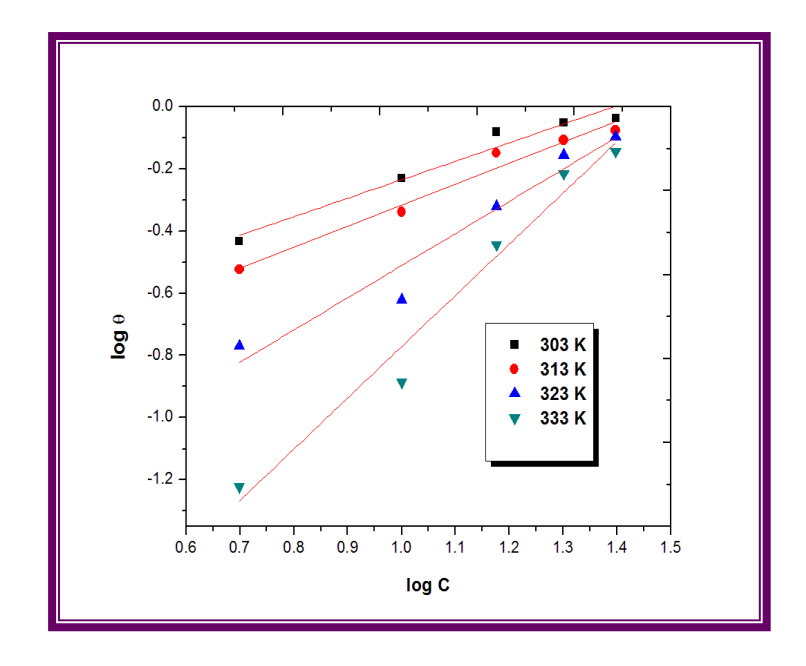


Fig.8.6.Freundlich isotherm of BEPD on Mild steel specimens in 1M HCl solution at different temperatures

Table.8.6 displays the values of adsorption intensity 'n' and the adsorption constant 'Kads' as a function of slope and intercept in that order. It suggests that declining K values (14.83 to 0.381) and adsorption intensity values < 2 imply that desorption occurs at higher temperatures [14]. ΔG values (-16.91 to -8.45 KJ.mol⁻¹) determined from the Gibb's free energy equation (5.5) are therefore included in Table.8.6, suggesting that the electrostatic adsorption process.

Table.8.6. Freundlich data of BEPD on Mild steel corrosion at elevatedtemperatures

	Freundlich parameters						
T (K)	$\mathbf{K}_{ ext{ads}}$	ΔG (KJ mol ⁻¹)	n	\mathbb{R}^2			
303	14.832	-16.91	1.68	0.9495			
313	10.224	-16.50	1.48	0.9659			
323	2.846	-13.59	0.97	0.9685			
333	0.381	-8.45	0.61	0.9669			

8.5. DFT investigation

The optimized structure, as well as the Mulliken charges of the BEPD inhibitor, is shown in (Fig.8.7a&b).

The Mulliken charges of all electronegative atoms in the inhibitor molecule are also provided in Table.8.7. The lower negative value specified by O₂₇ leads to the electrostatic interaction between the inhibitor and the iron surface, as seen in (Fig.8.7b) and tabulated data (Table.8.7).

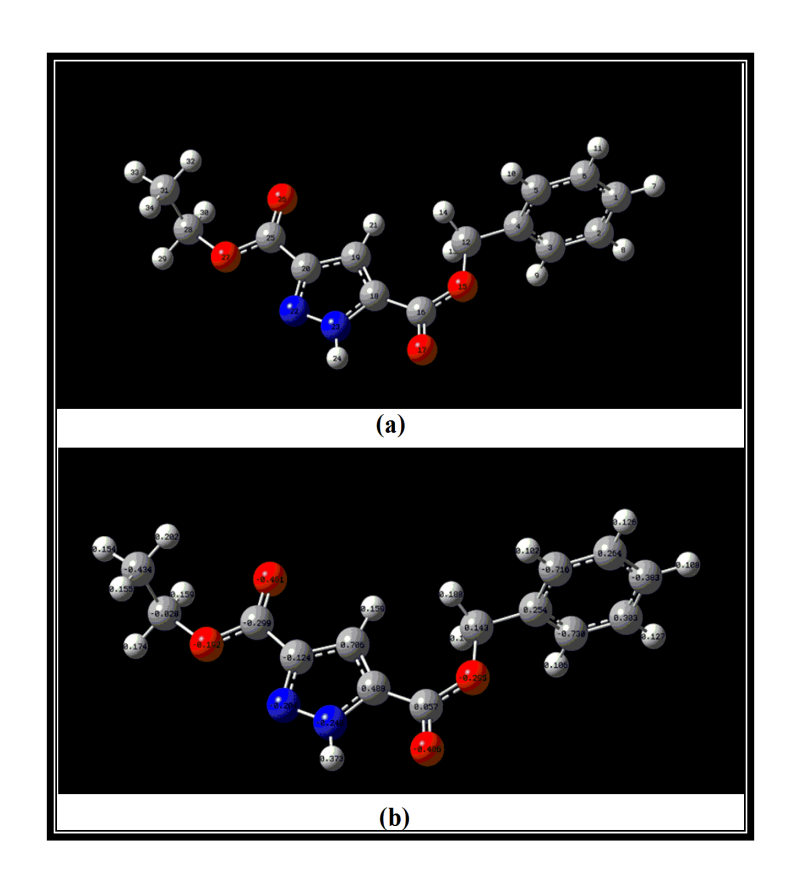


Fig.8.7. (a) Optimized structure and (b) Mulliken charges of BEPD

Table.8.7. Mulliken charges of the atoms present in the BEPD molecule

Atoms	Mulliken charges
O ₁₅	-0.295
O ₁₇	-0.405
O ₂₆	-0.451
O ₂₇	-0.192
N ₂₂	-0.204
N ₂₃	-0.248

In addition, (Fig.8.8a&b) depicts the HOMO and LUMO density distributions, respectively. The electron density distribution of HOMO in the inhibitor is primarily centered on the pyrazole moiety as well as all of the oxygen atoms present as shown in (Fig.8.8a) indicating that electrons transfer from these centers to the iron surface for strong coordination. Additionally, the electron density distribution of LUMO focuses on the benzyl portion of the molecule causing iron to inhibitor retro donation as seen in (Fig.8.8b).

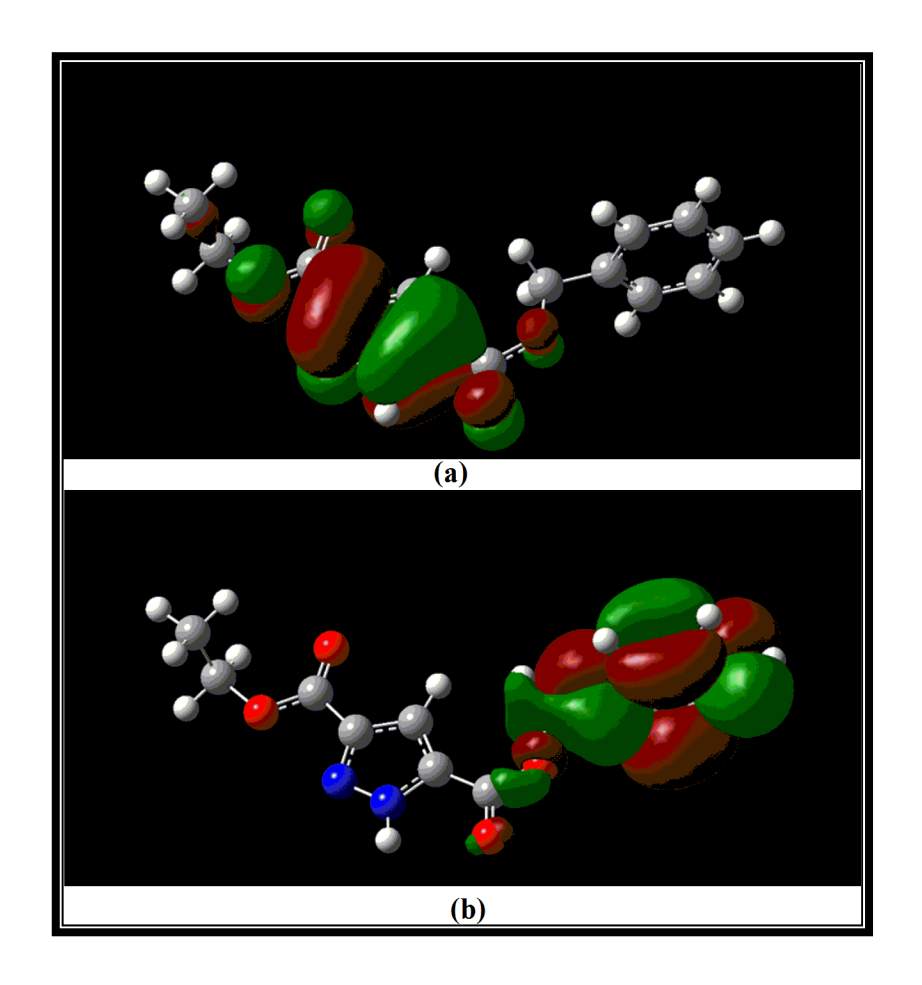


Fig.8.8. (a) HOMO and (b) LUMO distribution of BEPD

The E_{HOMO}, E_{LUMO} and all other essential electronic properties of the BEPD defender are displayed in Table.6.8. The inhibitor's tendencies to accept electron pairs from metal via back bonding are asserted by the lower negative energy value (-1.6522 eV) of the lower unoccupied molecular orbital, whereas the inhibitor's highest probability of electron donation is indicated by the higher negative energy value (-7.0702 eV) of the highest occupied molecular orbital [15, 16].

Table.8.8. Electronic parameters of the investigated BEPD

Electronic parameters						
Еномо	-7.0702(eV)					
Ешмо	-1.6522(eV)					
Energy Gap (ΔE)	5.4(eV)					
Dipolemoment (D)	3.6(D)					
Ionization energy (I)	7.0701(eV)					
Electron affinity (A)	1.6522(eV)					
Absolute electronegativity (χ)	4.3611(eV)					
Global hardness (η)	2.7089					
Global softness (σ)	0.3691					
Transferred electron fraction (ΔN)	0.0846					
Back donation (ΔE _{backdonation})	-0.6772(eV)					

The acquired electronic property values support the notion that BEPD is a potent inhibitor and the theoretical evaluation is in agreement with the experimental observations [17, 18].

8.6. Surface investigation

8.6.1. SEM examination

The corrosion impact on Mild steel in 1M HCl solution in the presence of BEPD inhibitor is shown in (Fig. 8.9a &b). It is evident that the formation of a passive film on the Mild steel specimen in the presence of an inhibitor prevents corrosion impairment. As a result, we can infer that the BEPD protector is effective in an acidic environment [19, 20].

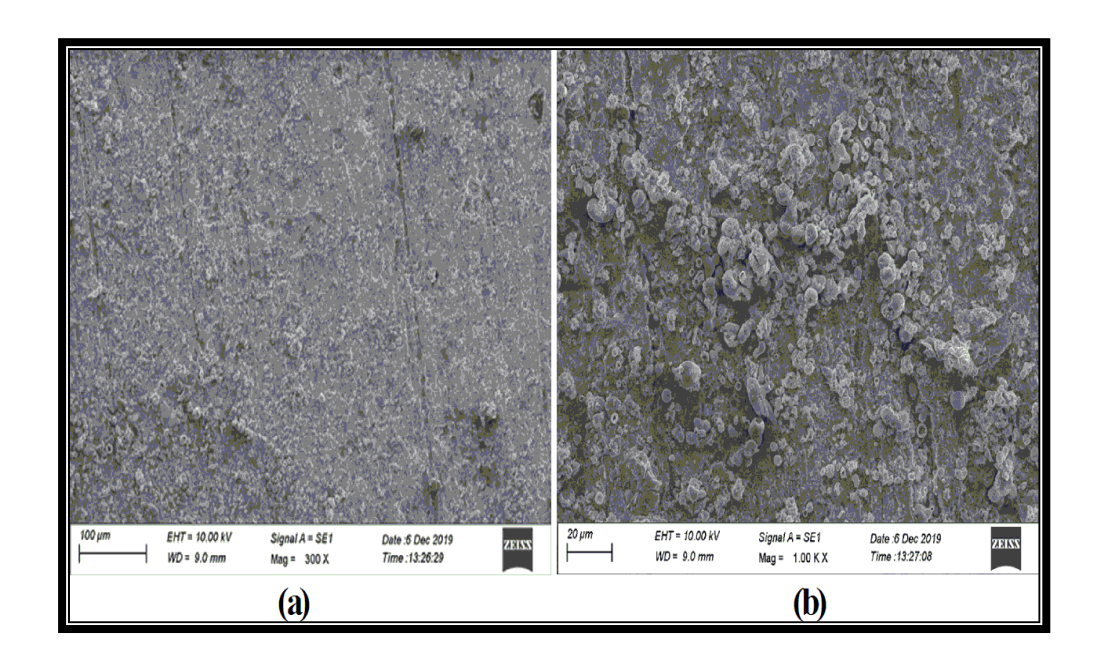
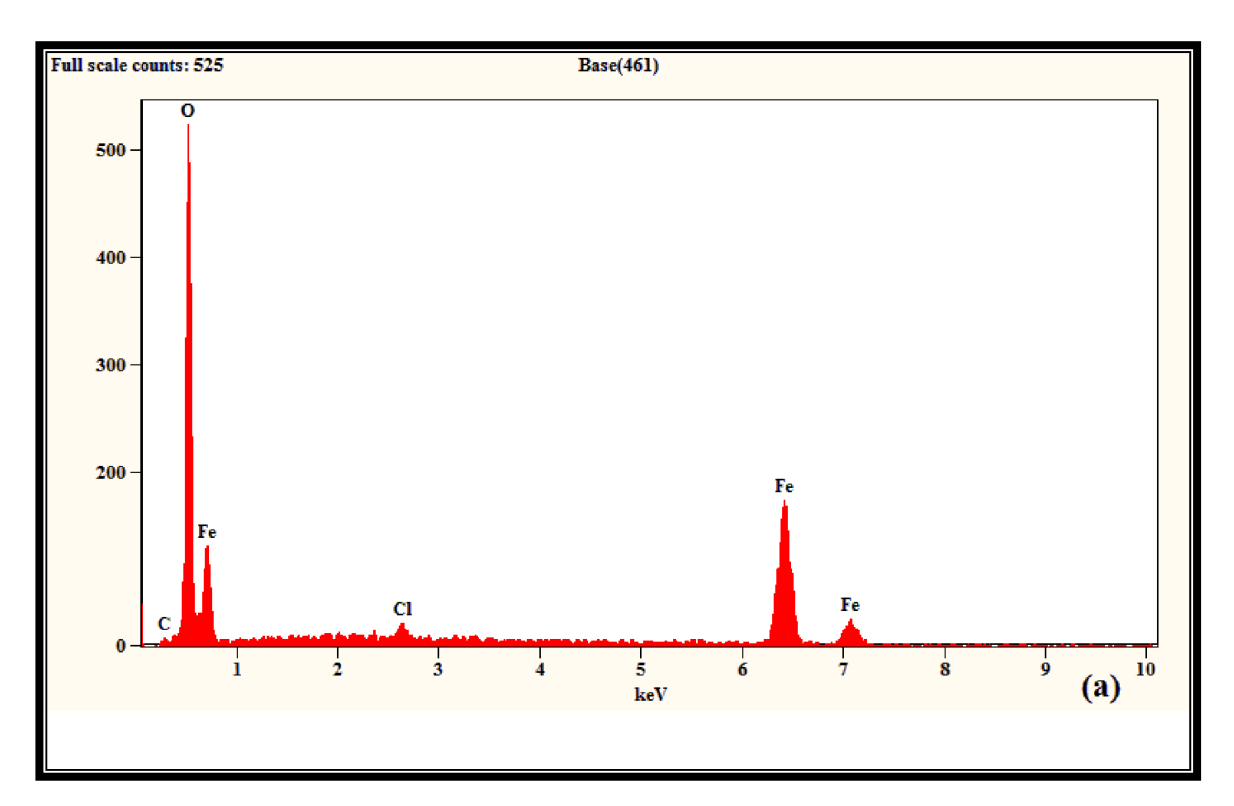


Fig.8.9a&b. SEM micrographs of Mild steel with BEPD in M HCl solution

8.6.2. EDAX examination

The EDAX spectra of Mild steel in the absence and presence of BEPD in 1M HCl solution are seen in (Fig.8.10a&b) respectively. The chlorine peak, together with the other components identified on the Mild steel specimen as shown in (Fig.8.10a) suggests that the steel surface has been substantially corroded. In addition, the absence of a chlorine peak and the presence of a nitrogen peak (Fig.8.10b) suggest that in the 1M HCl environment, the lone pair electrons coordinated with the metal surface inhibit corrosion degradation [21].

Furthermore, Table.8.9 shows the quantitative analysis of all discovered elements in the Mild steel specimens and the weight percentage of Nitrogen (1.21 %) and Oxygen (41.51%) confirms the corrosive inhibition process in the presence of BEPD. Thus, EDAX data demonstrated that corrosion reduction is accomplished by coordinating an inhibitor with the steel surface and acting as an effective protector.



 ${\bf Fig. 8.10a.\ EDAX\ spectrum\ of\ uninhibited\ surface\ in\ 1M\ HCl\ solution}$

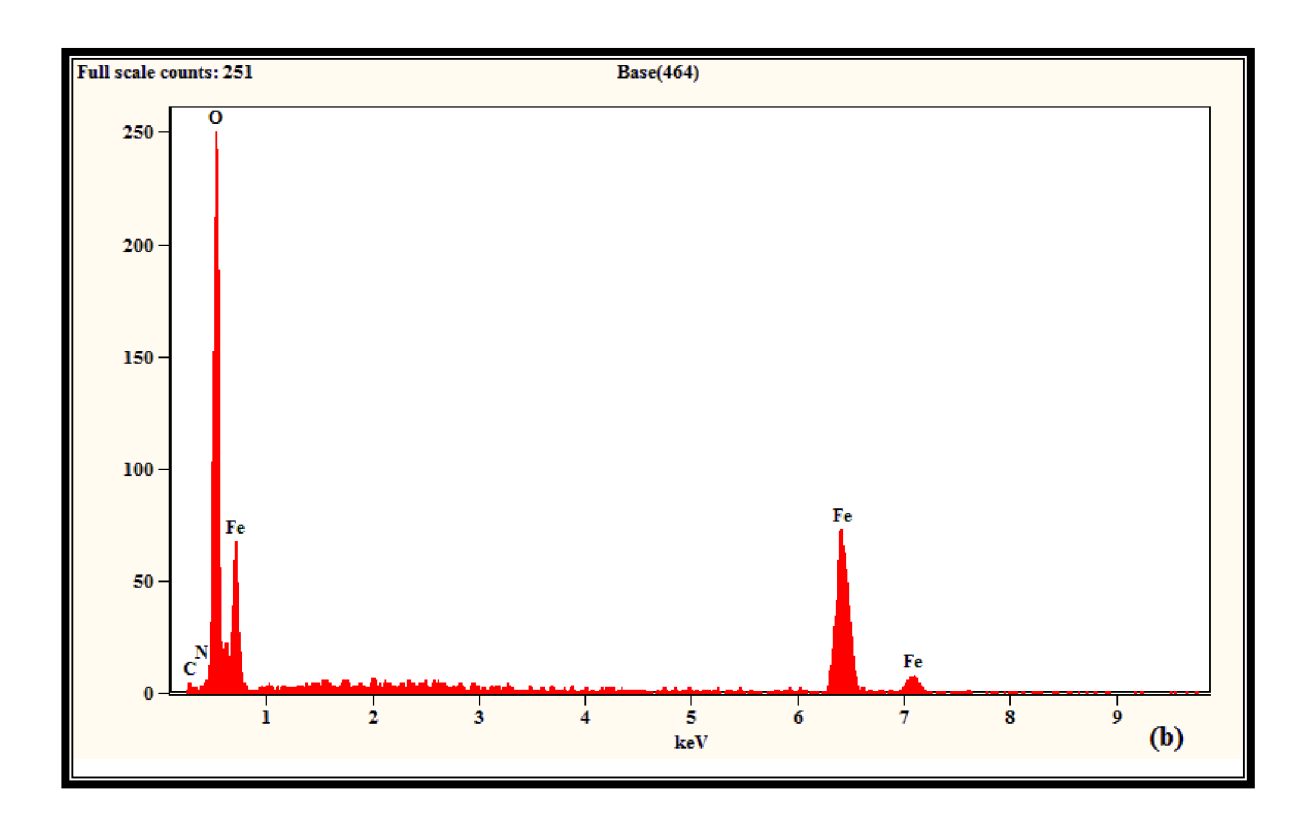


Fig.8.10b. EDAX spectrum of inhibited surface in 1M HCl solution

Table.8.9.EDAX data of the explored inhibitor BEPD

Samples	C	О	Cl	N	Fe
Bare steel	12.20	7.98	-	-	79.82
Unprotected surface	5.84	43.44	1.06	-	49.66
Protected surface with					
BEPD	3.38	41.51	-	1.21	53.9

8.6.3. AFM examination

The AFM pattern of Mild steel in the absence and presence of BEPD inhibitor in 1M HCl solution is shown in (Fig.8.11a&b) and the corresponding average roughness and root mean square values are provided in Table.8.10.

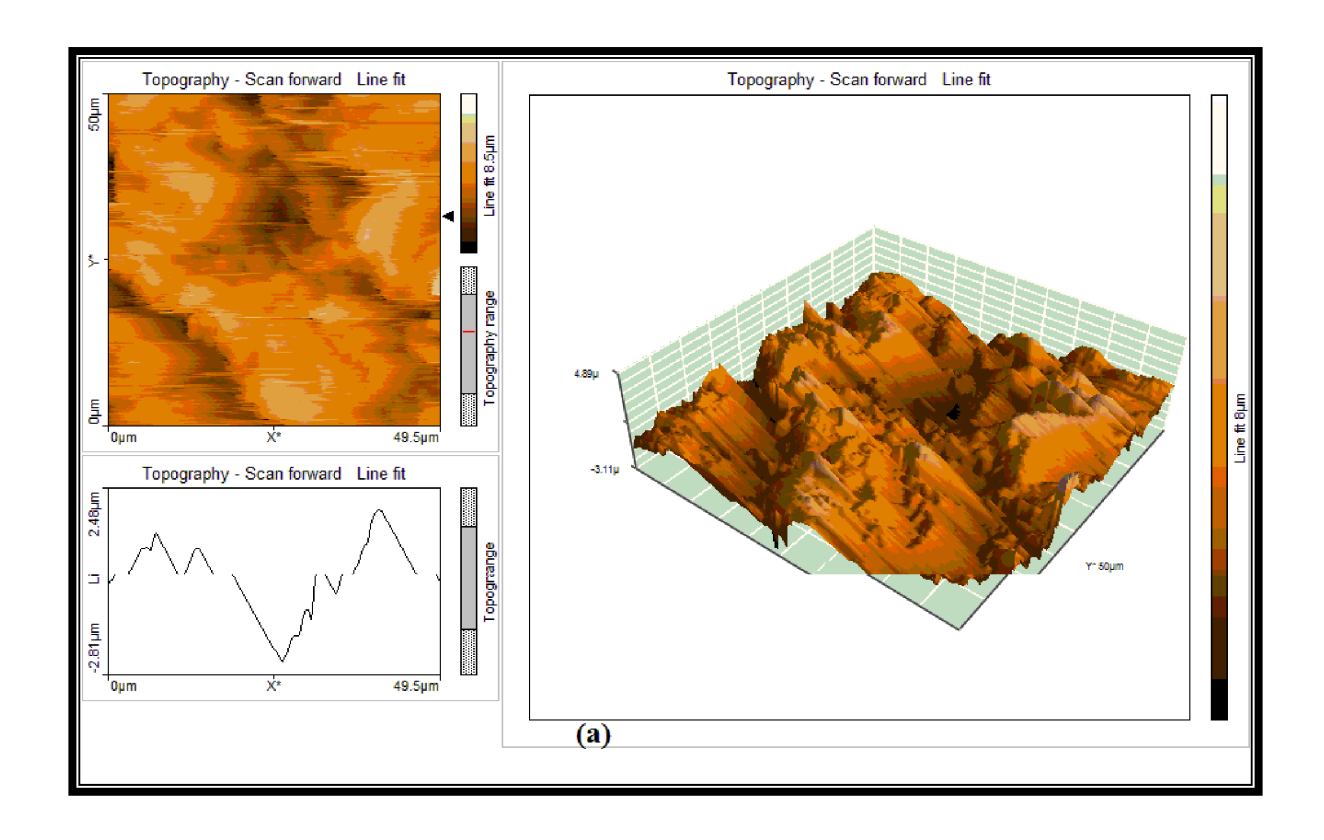


Fig.8.11a. 3D - AFM image of unprotected steel surface in 1M HCl solution

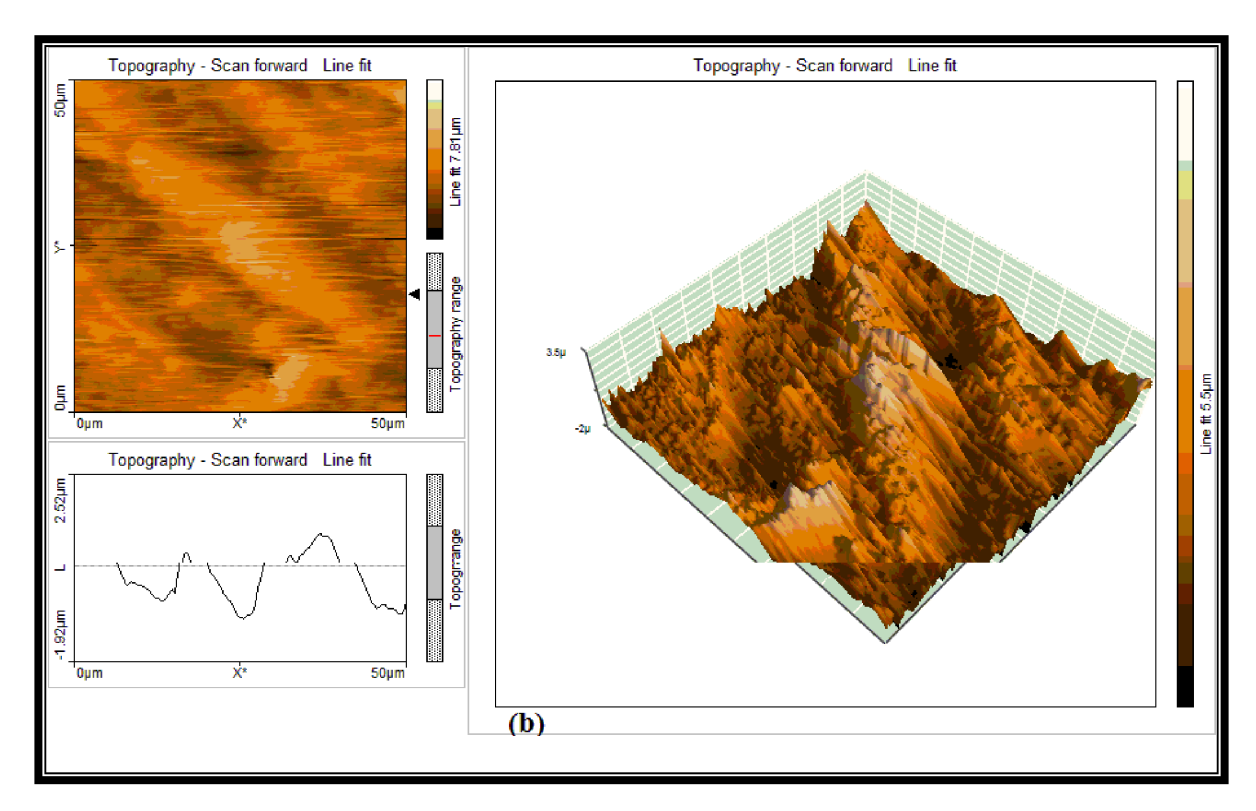


Fig.8.11b. 3D - AFM image of inhibited steel surface in the presence of BEPD in 1M HCl solution

The average roughness of bare steel, unprotected, and protected surfaces ate 651.27, 895.36, and 701.41nm, respectively indicating that the roughness is mitigated by the existence of the inhibitor. Accordingly, root mean square values 765.16, 1200.42, and 827.19 nm in that sequence confirm that the steel surface deterioration is suppressed by the addition of inhibitor [22, 23].

Table.8.10. AFM factors of Mild steel corrosion with and without BEPDin 1M HCl solution

Samples	Average Roughness	RMS roughness	
Sumpress .	(R _a)nm	(R _q) nm	
Bare steel	651.27	765.16	
Unprotected surface	895.36	1200.42	
Protected surface	701.41	827.19	

As a consequence, the examined BEPD was found to be an efficient inhibitor in the 1M HCl environment using AFM examination.

8.7. References

- Ouici H B, Belkhouda M, Benali O, Salghi R, Bammou L, Zarrouk A, Hammouti B. Adsorption and inhibition effect of 5-phenyl-1,2,4-triazole-3thione on C38 steel corrosion in 1 M HCl. Res. Chem. Intermed. 2015; 41: 4617-4625.
- 2. Singh A, Talha M, Xu X, Sun Z, Lin Y. Heterocyclic corrosion inhibitors for J55 steel in a sweet corrosive medium. *ACS Omega*. 2017; 2: 8177-8186.
- 3. Xu B, Yang W, Liu Y, Yin X, Gong W, Chen Y. Experimental and theoretical evaluation of two pyridine carboxaldehyde thiosemicarbazone compounds as corrosion inhibitors for Mild steel in hydrochloric acid solution. *Corros. Sci.* 2014; 78: 260-269.
- 4. Yurt A, Balaban A, Kandemir S U, Bereket G, Erk B. Investigation on some Schiff ases as HCl corrosion inhibitors for carbon steel. *Mater. Chem. Phys.* 2004; 85: 420-428.
- 5. Li W, He Q, Pei C, Hou B. Experimental and theoretical investigation of the adsorption behavior of new triazole derivatives as inhibitors for Mild steel corrosion in acid media. *Electrochim. Acta*, 2007; 52: 6386-6395.
- 6. Zhang Q B, Hua Y X. Corrosion inhibition of Mild steel by alkylimidazolium ionic liquids in hydrochloric acid. *Electrochim. Acta.* 2009; 54: 1881-1889.
- Erami R S, Amirnasr M, Meghdadi S, Talebian M, Farrokhpour H, Raeissi K.
 Carboxamide derivatives as new corrosion inhibitors for Mild steel protection in hydrochloride solution. *Corros. Sci.* 2019; 151: 190-197.
- 8. Singh A K, Quraishi M A. Investigation of the Effect of Disulfiram on Corrosion of Mild steel in Hydrochloric Acid Solution. *Corrosion Science*. 2010; 53(4): 1288-1297.

- 9. Clark P N, Jackson E, Robinson M. Effect of Thiourea and Some of its Derivatives on the Corrosion Behaviour of Nickel in 50% v/v (5·6M) Hydrochloric Acid. *British Corrosion Journal*, 1979; 14(1): 33-39.
- 10. Szauer T, Brandt A. On the role of fatty acid in adsorption and corrosion inhibition of iron by amine—fatty acid salts in acidic solution. *Electrochimica Acta*. 1981; 26 (9): 1257-1260.
- 11. Abdallah M. Rhodanine azosulpha drugs as corrosion inhibitors for corrosion of 304 stainless steel in hydrochloric acid solution. *Corrosion science*. 2002; 44(4): 717-728.
- 12. Anusuya N, Saranya J, Sounthari P, Zarrouk A, Chitra S. Corrosion inhibition and adsorption behaviour of some bis-pyrimidine derivatives on Mild steel in acidic medium. *J Mol Liq.* 2017; 225: 406-417.
- 13. Bousskri A, Anejjar M, Messali R, Salghi O, Benali Y, Karzazi S, Jodeh M, Zougagh S, Ebenso E E, Hammouti B. Corrosion inhibition of carbon steel in aggressive acidic media with 1-(2-(4-chlorophenyl)-2-oxoethyl)pyridazinium bromide. *J. Mol. Liq.* 2015, 211, 1000–1008.
- 14. El Hajjaji F, Abrigach F, Hamed, Hasan A R, Taleb M, Jodeh, Algarra M. Corrosion resistance of Mild steel coated with orgain material containing pyrazol moiety. *Coatings*. 2018; 8(10): 330-339.
- 15. Pang X, Guo W, Li W, Xie J, Hou B. Electrochemical, quantum chemical and SEM investigation of the inhibiting effect and mechanism of cipro- floxacin, norfloxacin and ofloxacin on the corrosion for Mild steel in hydrochloric acid. *Sci.China Ser.* 2012; 51(10): 928–936.

- 16. Khaled K.F. Corrosion control of copper in nitric acid solutions using some amino acids – A combined experimental and theoretical study. *Corros. Sci.* 2010; 52: 3225–3234.
- 17. Ben Hmamou D, Salghi R, Zarrouk A, Zarrok H, Hammouti B. Electrochemical and Gravimetric Evaluation of 7-methyl-2- phenylimidazo [1, 2- a] pyridine of Carbon Steel Corrosion in Phosphoric Acid Solution. *Int. J. Electrochem. Sci.* 2013; 8: 11526–11545.
- 18. Zarrouk A, Hammouti B, Dafali A, Bouachrine M, Zarrok H, Boukhris S, Aldeyab S S. A theoretical study on the inhibition efficiencies of some quinoxalines as corrosion inhibitors of copper in nitric acid. *J. Saudi Chem. Soc.* 2014; 18(5): 450–455.
- 19. Verma C, Olasunkanmi L O, Ebenso E E, Quraishi M A, Obot I B. Adsorption Behavior of Glucosamine-Based, Pyrimidine- Fused Heterocycles as Green Corrosion Inhibitors for Mild steel: Experimental and Theoretical Studies. J. Phys. Chem. 2016; 120: 11598–11611.
- 20. Singh P, Quraishi M A. Corrosion inhibition of Mild steel using Novel Bis Schiff's Bases as corrosion inhibitors: Electrochemical and Surface measurement. *Measurement*. 2016; 86: 114–124.
- 21. Toumiat K, Guibadj A, Taouti B M, Lanez T. Electrochemical study and computational details of copper corrosion inhibition by 1*H*-benzotriazole in 3wt. % Nacl medium. *Mor. J. Chem.* 2015; 3(4): 809-823.
- 22. Vashisht H, Bahadur I, Kumar S, Goyal M S, Kaur G, Singh G, Katata-Seru L, Ebenso E E. Synergistic interactions between tetra butyl phosphonium hydroxide and iodide ions on the Mild steel surface for corrosion inhibition in acidic medium. *J. Mol. Liq.* 2016; 224: 19–29.

23. Singh P, Srivastava V, Quraishi M A. Novel quinolone derivatives as green corrosion inhibitors for Mild steel in acidic medium: Electrochemical, SEM, AFM, and XPS studies. *J. Mol. Liq.* 2016; 216: 164–173.

CHAPTER - IX

Mild steel corrosion probe of 'N-(4-(piperidin-1-ylsulfonyl) phenyl)acetamide' (PSPA) in 1M HCl solution

The corrosion mitigation efficacy of N-(4-(piperidin-1-ylsulfonyl) phenyl) acetamide was evaluated on polished pre-weighed Mild steel specimens in the absence and presence of different concentrations of PSPA (5, 10, 15, 20, 25 and 30 ppm) in the 1M HCl solution for six-hour exposure duration and the results are discussed below.

9. Result and Discussion

9.1. Mass reduction technique

The correspondence between the corrosion rate and the inhibition efficiency is depicted in (Fig.9.1). The inhibitory capacity rises as the PSPA concentration increases whereas the corrosion rate decreases as shown in (Fig.9.1).

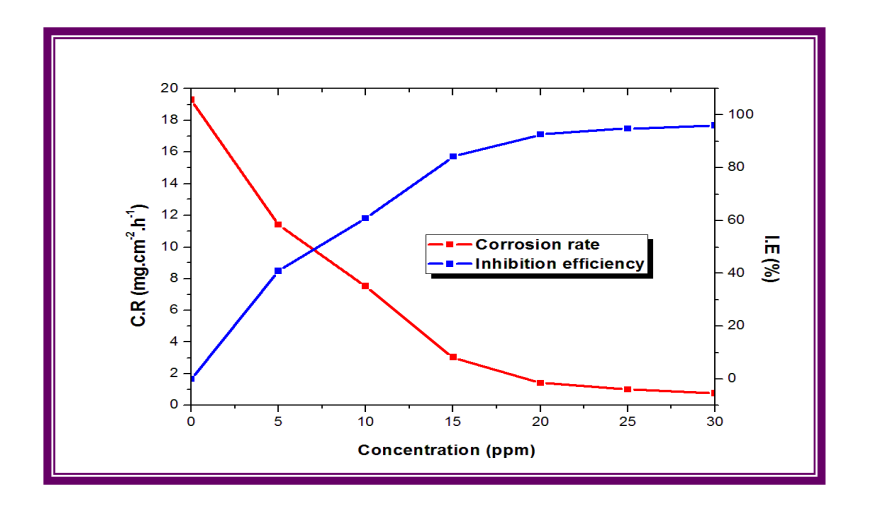


Fig.9.1.Correlation between the corrosion rates and inhibition efficiencies of PSPA on Mild steel in 1M HCl solution

Corrosion statistics such as rate of corrosion, inhibition efficiency and surface coverage are presented in Table.9.1. The outcomes demonstrate that as the PSPA

concentration is increased, the corrosion degradation diminishes and the inhibition efficiency increases linearly. At 30 ppm, the maximal effect is determined to be 96.06 % [1, 2].

Table.9.1. Effect of PSPA concentration on Mild steel corrosion in 1M HCl solution

Concentration (ppm)	Weight loss (mg)	Corrosion rate (mg.cm ⁻² .h ⁻¹)	Inhibition efficiency (%)	Surface coverage (θ)
Blank	1262.4	19.3028	-	-
5	746.2	11.4098	40.89	0.41
10	492.7	7.5336	60.97	0.61
15	198.4	3.0336	84.28	0.84
20	92.4	1.4128	92.68	0.93
25	65.3	0.9985	94.83	0.95
30	49.8	0.7615	96.06	0.96

As a result of the mass loss investigation, the investigated inhibitor is found to be an effective protector in the 1M HCl environment.

9.2. Electrochemical polarization technique

The polarization curves of various concentrations of PSPA in 1M HCl solution are displayed in (Fig.9.2). Electrochemical corrosion processes are suppressed at both anodic and cathodic regions as illustrated in (Fig.9.2) revealing that the explored inhibitor is a mixed-kind protector.

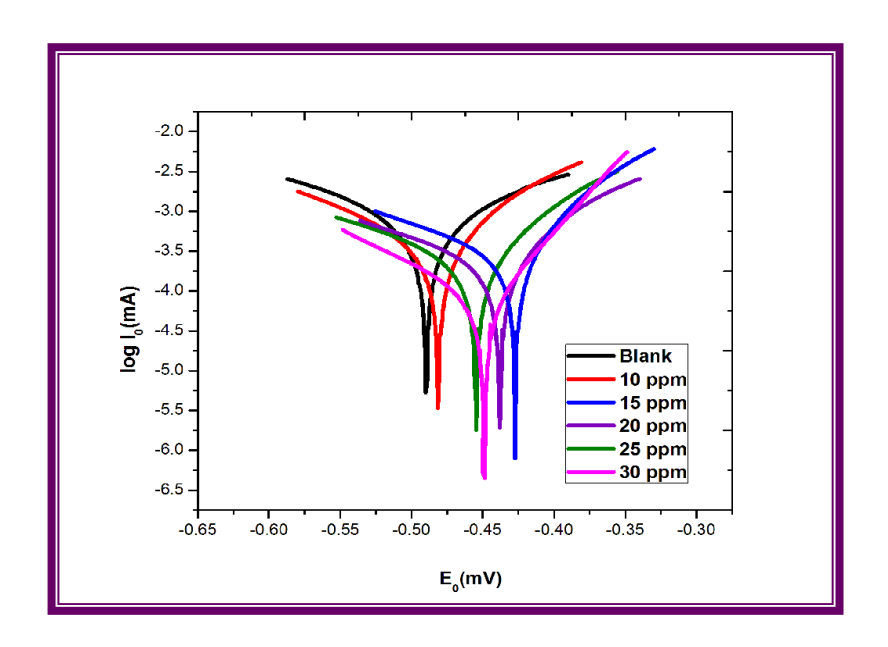


Fig.9.2.Electrochemical polarization curves for various concentrations of PSPA on Mild steel in 1M HCl solution

Further, Table.9.2 contains information about electrochemical polarization which depicts that when the concentration of PSPA increases the I_0 value lowers (1.893 to 0.0922 mA) indicating that PSPA controls corrosion with optimum protection of 95.13 %. Aside from that, the E_0 values represent that the protector is a mixed sort protector, which is supported by the Tafel slope values b_c and b_a [3, 4].

Table.9.2.Electrochemical polarization parameters for PSPA on Mild steel in 1M HCl solution

	Polarization parameters						
C (ppm)	E ₀ (mV)	I ₀ (mA)	$b_c(mV)$	b _a (mV)	IE (%)		
blank	-487.67	1.893	372.29	311.05	0		
10	-481.34	0.752	186.64	104.40	60.25		
15	-438.14	0.312	466.91	117.16	83.51		
20	-427.26	0.146	303.11	258.34	92.28		
25	-451.64	0.112	252.84	112.68	94.07		
30	-454.87	0.092	268.63	98.06	95.13		

The examined PSPA protector has a remarkable potential to mitigate Mild steel corrosion in 1M HCl solution according to the polarization investigation.

9.3. Electrochemical impedance technique

The impedance plots of various concentrations of PSPA inhibitor in the 1M HCl atmosphere are shown in (Fig.9.3). It demonstrates that since the concentration of PSPA rises, the diameter of the semicircle increases signaling that the charge transfer resistant capacity increases.

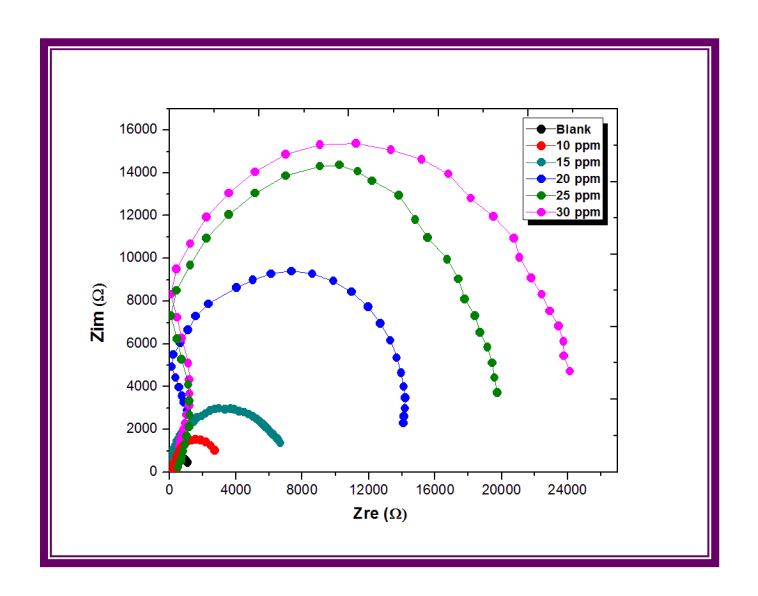


Fig.9.3.impedance plots for various concentrations of PSPA on Mild corrosion in 1M HCl solution

Moreover, Impedance data such as R_{ct} and C_{dl} are also listed in Table.9.3. The addition of PSPA significantly slows the electrochemical process as evidenced by the increasing values of R_{ct} (1061.25 to 23634.84 Ω cm²) and the stalling process is also confirmed by the increasing values of C_{dl} (1.516 to 0.0043 μF cm⁻²). The highest efficiency of this approach is 95.51 % at 30 ppm, confirming that the PSPA is a competent protector in 1M HCl solution [5, 6].

Table.9.3. Impedance parameters for PSPA on Mild steel corrosion in 1M HCl solution

C	Impedance parameters					
(ppm)	R_{ct} ($\Omega \text{ cm}^2$)	C _{dl} (µF cm ⁻²)	I.E (%)			
Blank	1061.25	0.516	0			
10	2702.55	0.299	60.73			
15	6674.58	0.076	84.10			
20	13044.23	0.013	91.86			
25	19159.97	0.0056	94.46			
30	23634.84	0.0043	95.51			

9.4. Effect on temperature

The mass loss experiment in 1M HCl solution at various temperatures (304, 314, 324, and 334 K) revealed a relationship between preventive efficiency and temperature as shown in (Fig.9.4). It is apparent that when the concentration of protector increases, the inhibitory effectiveness diminishes.

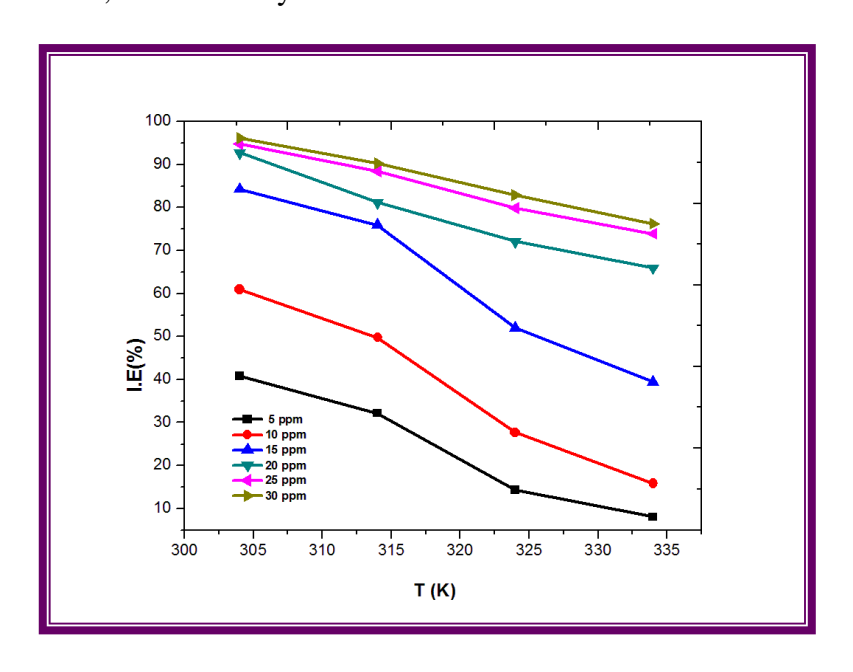


Fig.9.4.Temperature effect on inhibition efficiencies for Mild steel with and without PSPA in 1M HCl solution

Meanwhile, Table.9.4 summarizes the rate of corrosion and the effectiveness data of Mild steel corrosion at different concentrations of inhibitor. We conclude from the tabulated results that the protective ability of PSPA reduces at increased temperatures for all the concentrations implying that the adsorption mechanism is physisorption [7].

Table.9.4.Temperature Study for Various Concentrations of PSPA on Mild steel corrosion in 1M HCl Solution

Conc.	Weight loss (mg)			Corrosion rate (mg cm ⁻² h ⁻¹)			Inhibition efficiency (%)					
(ppm	304K	314K	324K	334K	304K	314K	324K	334K	304K	314K	324K	334K
Blank	1262.4	1365.3	2054.3	3015.2	19.30	20.88	31.41	46.10	0	0	0	0
5	746.2	925.3	1758.5	2772.4	11.41	14.15	26.89	42.39	40.89	32.23	14.40	8.05
10	492.7	685.3	1485.3	2536.2	7.53	10.48	22.71	38.78	60.97	49.81	27.70	15.89
15	198.4	328.7	985.7	1825.5	3.03	5.03	15.07	27.91	84.28	75.92	52.02	39.46
20	92.4	257.5	574.2	1025.8	1.41	3.94	8.78	15.69	92.68	81.14	72.05	65.98
25	65.3	157.4	413.8	787.1	1.00	2.41	6.33	12.04	94.83	88.47	79.86	73.90
30	49.8	132.6	352.1	715.3	0.76	2.03	5.38	10.94	96.06	90.29	82.86	76.28

9.4.1. Thermodynamic activation parameters

The mass loss experiment was used to determine the kinetic restraints such as activation energy and Arrhenius factor at various temperatures using the Arrhenius equation (5.1). The straight lines obtained by plotting 'log CR' versus '1000/T' with slope '(- E_a /2.303R)' and intercept '(log A)' can be seen in (Fig. 9.5). The slope and intercept of the Arrhenius plots were used to calculate the values of ' E_a ' and 'A'.

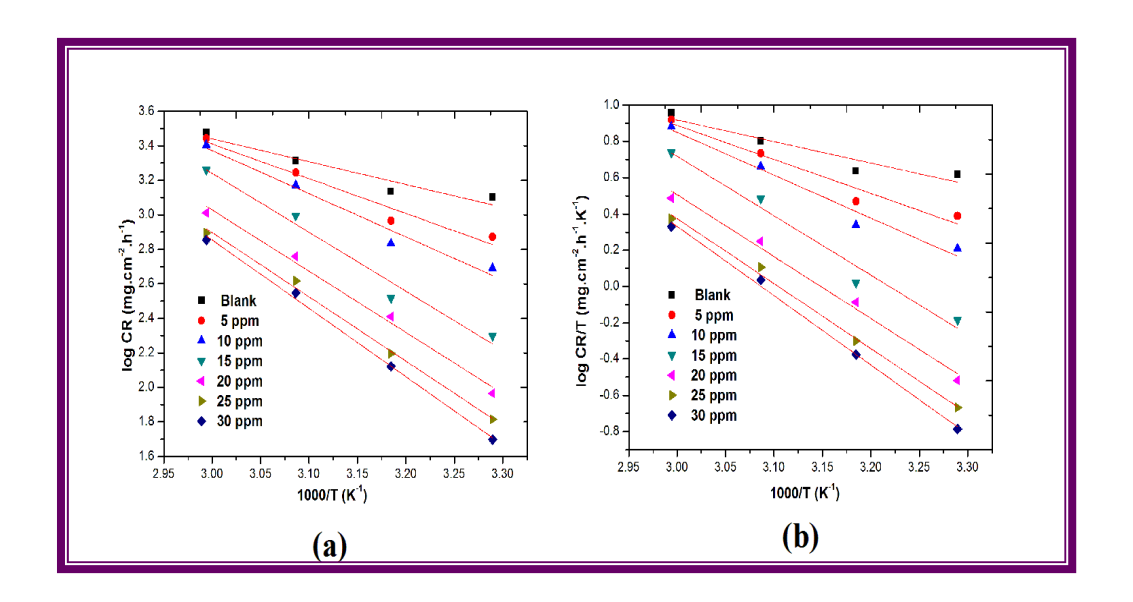


Fig.9.5. (a) Arrhenius plots and (b) Transition state plots for various concentrations of PSPA on Mild steel corrosion in 1M HCl solution

In addition, Table.9.5 shows the kinetic activation parameters ' E_a ' and 'A'. The escalating values of Ea (25.32 to 75.84 KJ mol^{-1}) with increasing inhibitor concentrations suggest that physisorption is followed by the adsorption process which is corroborated by the increasing values of A [8, 9].

Furthermore, ΔH^0 and ΔS^0 values were obtained by plotting 'log CR/T' versus '1000/T' with slope '(- ΔH^0 /2.303R)' and intercept '[(log (R/Nh) + ΔS^0 /2.303R)' using transition state equation (5.2). The ΔH^0 and ΔS^0 values from Table 9.5 suggest that the adsorption process is endothermic and that the randomness increases during the inhibition process respectively [10, 11].

Table.9.5.Kinetic and Thermodynamic Parameters of PSPA on Mild steel corrosion in 1M HCl Solution at different temperatures

C (ppm)	E _a (KJ mol ⁻¹)	A	ΔH ⁰ (KJ mol ⁻¹)	$\begin{array}{c} \Delta S^0 \\ (JK^{-1}mol^{-1}) \end{array}$	E _a -RT
blank	25.32	2.5603×10^8	22.68	-111.97	2.65
5	38.51	2.7854×10^{10}	35.86	-72.98	2.65
10	47.89	7.5335×10^{11}	45.24	-45.56	2.65
15	65.38	3.0549×10^{13}	62.74	4.37	2.65
20	67.94	4.7097×10^{13}	65.29	7.97	2.65
25	71.30	1.1695 X 10 ¹⁴	68.65	15.53	2.65
30	75.84	5.4450 X 10 ¹⁴	73.19	28.34	2.65

9.4.2. Freundlich adsorption isotherm

By plotting ' $(\log \theta)$ vs $(\log C)$ ' using the Freundlich equation (8.1), the adsorption parameters such as 'Kads' and 'n' were determined from the slope and intercept of the straight lines as shown in (Fig.9.6).

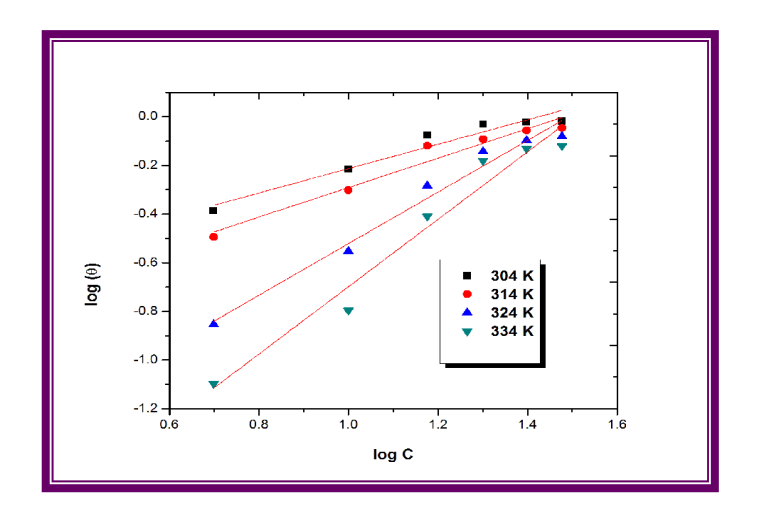


Fig.9.6.Freundlich isotherm of PSPA on Mild steel corrosion in 1M HCl solution at different temperatures

Table.9.6 shows that as temperature rises, decreasing Kads values (19.32 to 0.826) imply physical adsorption and decreasing 'n' values disclose desorption during the corrosion inhibition process in 1M HCl solution. Furthermore, the ΔG^0 values (-17.64 to -10.62 KJmol⁻¹) derived from Gibb's free energy equation (5.5) demonstrate that the adsorption process relies on physisorption in the absence and various

concentrations of PSPA in an acidic corrosive environment at elevated temperatures [12].

Table.9.6. Freundlich data of PSPA on Mild steel corrosion at elevated temperatures

Т	F	Freundlich parameters					
(K)	$\mathbf{K}_{\mathbf{ads}}$	ads ΔG (KJmol ⁻¹)		R ²			
304	19.320	-17.64	1.99	0.9331			
314	12.735	-17.13	1.65	0.9444			
324	2.624	-13.42	0.94	0.9697			
334	0.826	-10.62	0.72	0.955			

9.5. DFT investigation

The optimized structure and Mulliken charges of the explored PSPA inhibitor are shown in (Fig.9.7a&b).

Table.9.7. Mulliken charges of electro atoms present in PSPA

Atoms	Mulliken charges
O ₁₂	-0.173
O ₁₃	-0.272
O ₃₂	-0.366
S ₁₁	0.960
N ₁₄	-0.346
N ₃₀	-0.264

Table.9.7 specifies the Mulliken charges of the electronegative atoms in the molecule revealing that the inhibitor's coordination sites and protonation center are intact. The lower negative value of O₁₂ (-0.173) implies that it has a higher proclivity for protonation and can easily interact with negatively charged steel surfaces via physisorption [13]. Due to their lower negative values, the other mentioned atoms imply that electrons migrate from these locations to the iron's unoccupied d orbital for coordination through chemisorption [14].

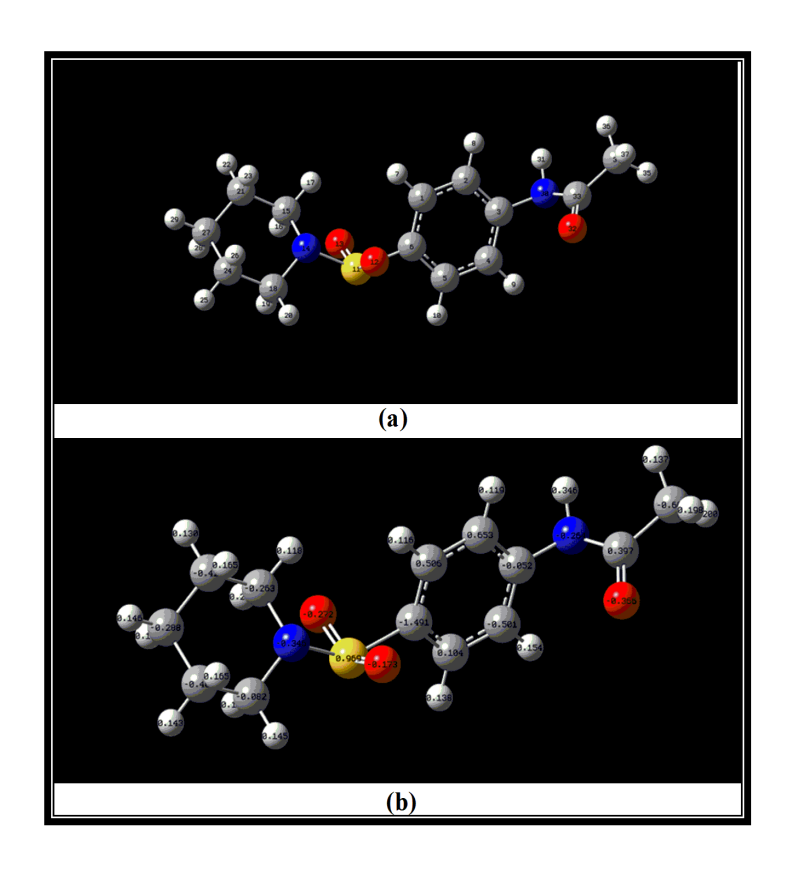


Fig.9.7. (a) Optimized structure and (b) Mulliken charges of PSPA

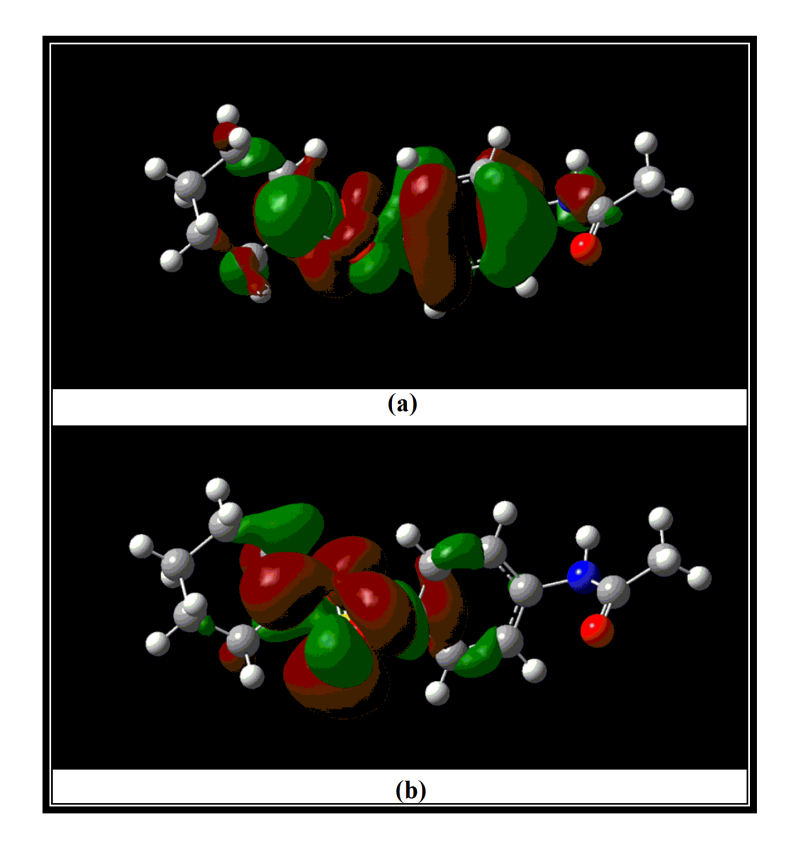


Fig.9.8. (a) HOMO and (b) LUMO distribution of PSPA

The electron density distribution of HOMO and LUMO is seen in (Fig.9.8 a&b). We can find in (Fig.9.8a), HOMO focuses on almost every portion of the inhibitor molecule indicating that those locations are the coordination sites for strong inhibition causing chemisorption. Conversely, LUMO focuses primarily on the nitrogen atom in the piperidine ring, the SO₂ group and the benzene ring, all of which are the focal point for accepting electrons from metal to inhibitor retro donation, resulting in chemisorption.

Table 9.8 shows the imperative electronic parameters such as E_{HOMO} , E_{LUMO} , ΔE , D, I, A, χ , η , σ and ΔN . E_{HOMO} (-5.523 eV) implies that electrons can be donated from the inhibitor to the Mild steel whereas E_{LUMO} (-0.8629 eV) suggests that electrons may be donated from the metal to inhibitor. The relationship between the inhibitor's molecular structure and activity is represented by other factors such as ΔE , D, I, A, χ , η , σ and ΔN . Altogether, the data revealed that PSPA has a high prospect of mitigating corrosion in an acidic environment [15].

Table.9.8. Electronic parameters of the PSPA molecule

Electronic parameters					
Еномо	-5.523(eV)				
Ешмо	-0.8629(eV)				
Energy Gap (ΔE)	4.66(eV)				
Dipolemoment (D)	4.3				
Ionization energy (I)	5.5229(eV)				
Electron affinity (A)	0.8628(eV)				
Absolute electronegativity (χ)	3.1929(eV)				
Global hardness (η)	2.3300				
Global softness (σ)	0.4291				
Transferred electron fraction (ΔN)	0.3491				
Back donation (ΔE _{backdonation})	-0.5825(eV)				

9.6. Surface exploration

9.6.1. SEM investigation

The protected surface of Mild steel specimens in the presence of PSPA in 1M HCl solution is shown in (Fig.9.9a&b). These figures clearly show the smoother surface and corrosive damages can be greatly diminished by the development of a protective layer in the existence of PSPA implying that the examined inhibitor effectively blocked corrosion degradation in an acidic environment [16].

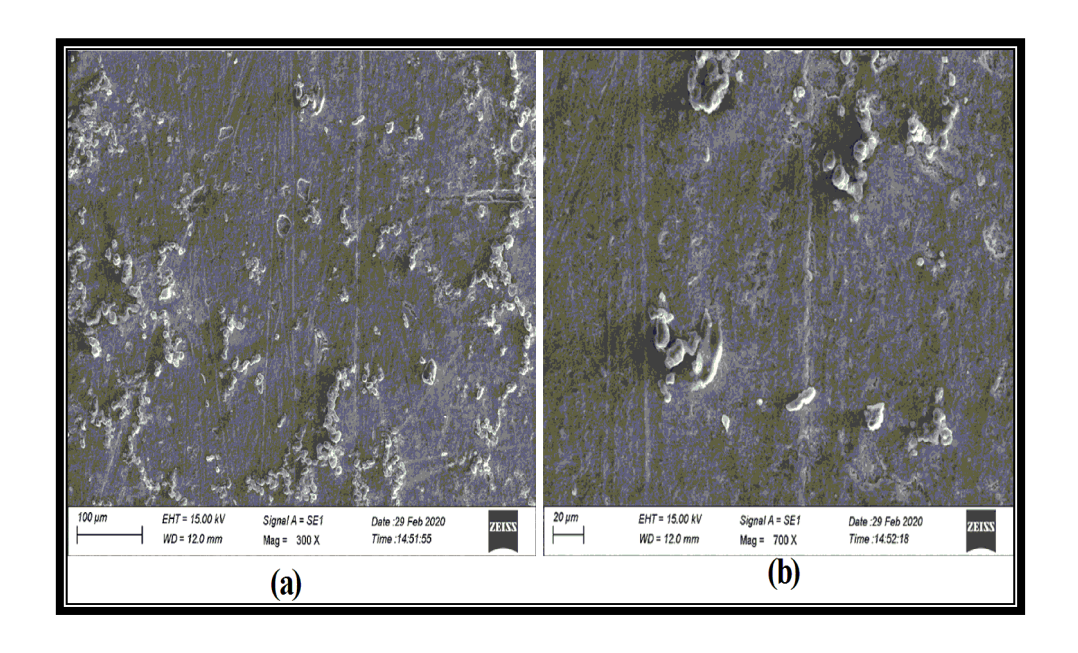


Fig.9.9a&b.SEM images of protected samples with PSPA in 1M HCl solution

9.6.2. EDX investigation

The elements found on the steel surface without and with an inhibitor in the 1M HCl solution are displayed in (Fig.9.10a&b). (Fig.9.10a) shows the chlorine peak together with the elements identified in bare steel implying that in the absence of PSPA, the corrosive solution impacted the steel surface. In addition, the presence of a Nitrogen peak in (Fig.9.10b) indicates that electrons transit from the inhibitor to the steel surface to prevent corrosion in the 1M HCl solution [17].

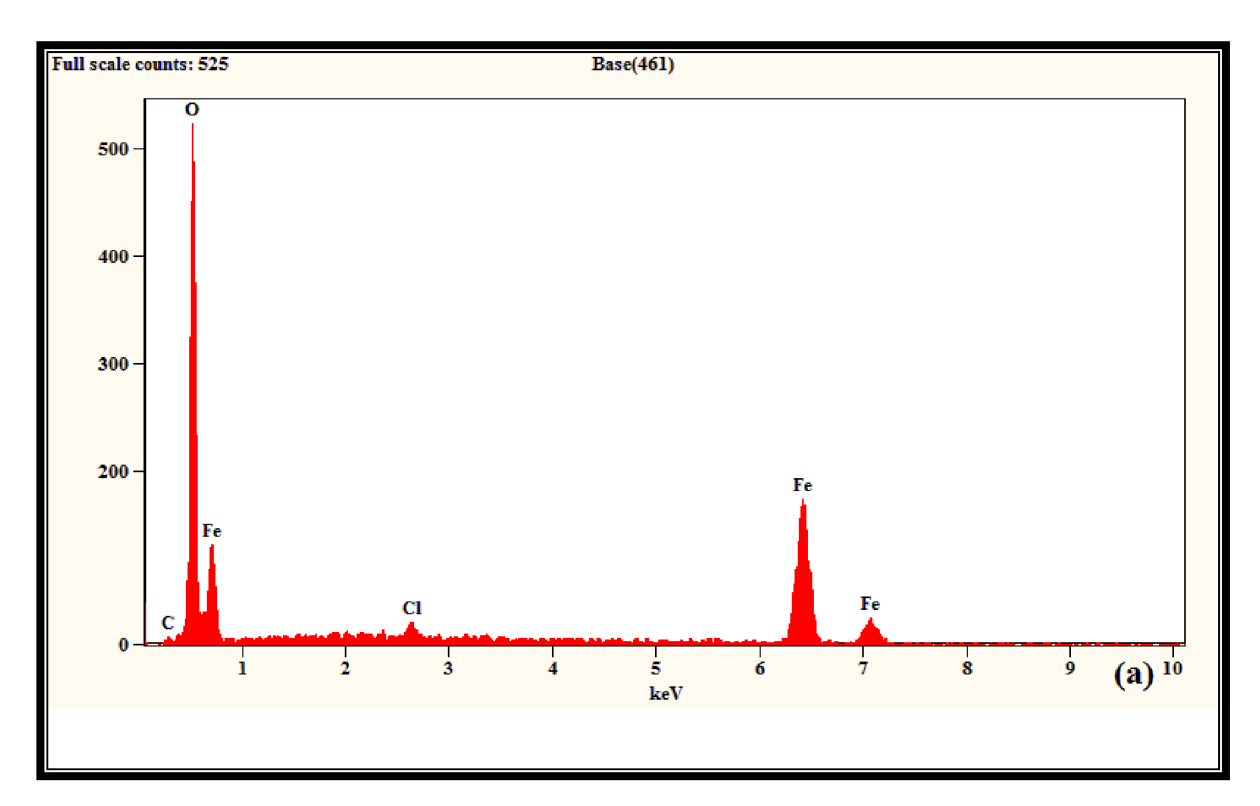


Fig.9.10a. EDX spectrum of Mild steel without PSPA in 1M HCl solution

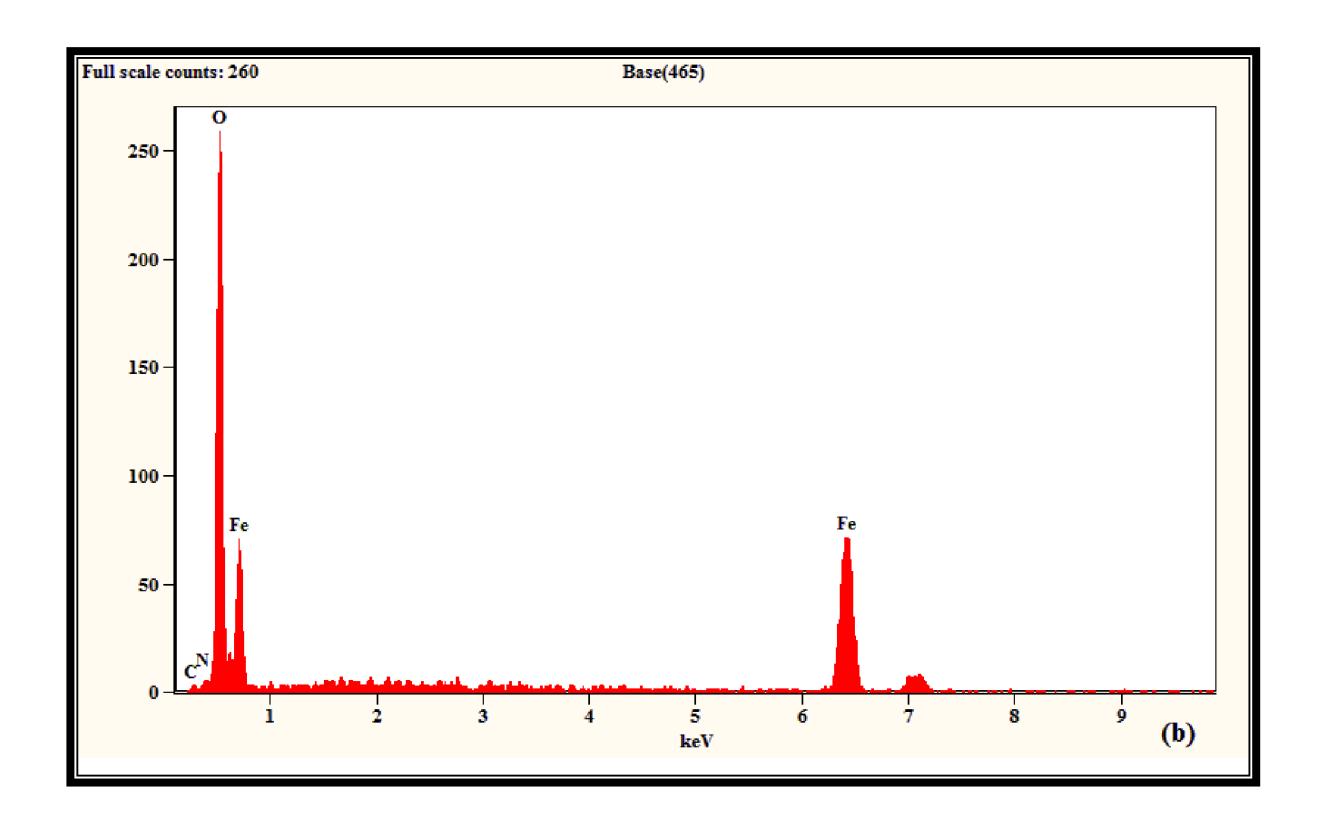


Fig.9.10b. EDX spectrum of Mild steel with PSPA in 1M HCl solution

The quantitative information of EDX in bare steel, without and with inhibitor, which is provided in Table.9.9, further validates PSPA's corrosion mitigation behavior on Mild steel. Hence, PSPA efficiently resists Mild steel corrosion in the 1M HCl solution, according to EDX data.

Table.9.9. Elemental analysis for polished, unprotected and protected steel specimen with PSPA in 1M HCl solution

Samples	С	0	Cl	N	Fe
polished Mild steel	12.20	7.98	-	-	79.82
unprotected Mild steel	5.84	43.44	1.06	1	49.66
protected Mild steel with PSPA	10.25	36.27	-	1.65	51.83

9.6.3. AFM investigation

(Figs.9.11a&b) display the AFM pattern of PSPA on Mild steel corrosion in the 1M HCl solution.

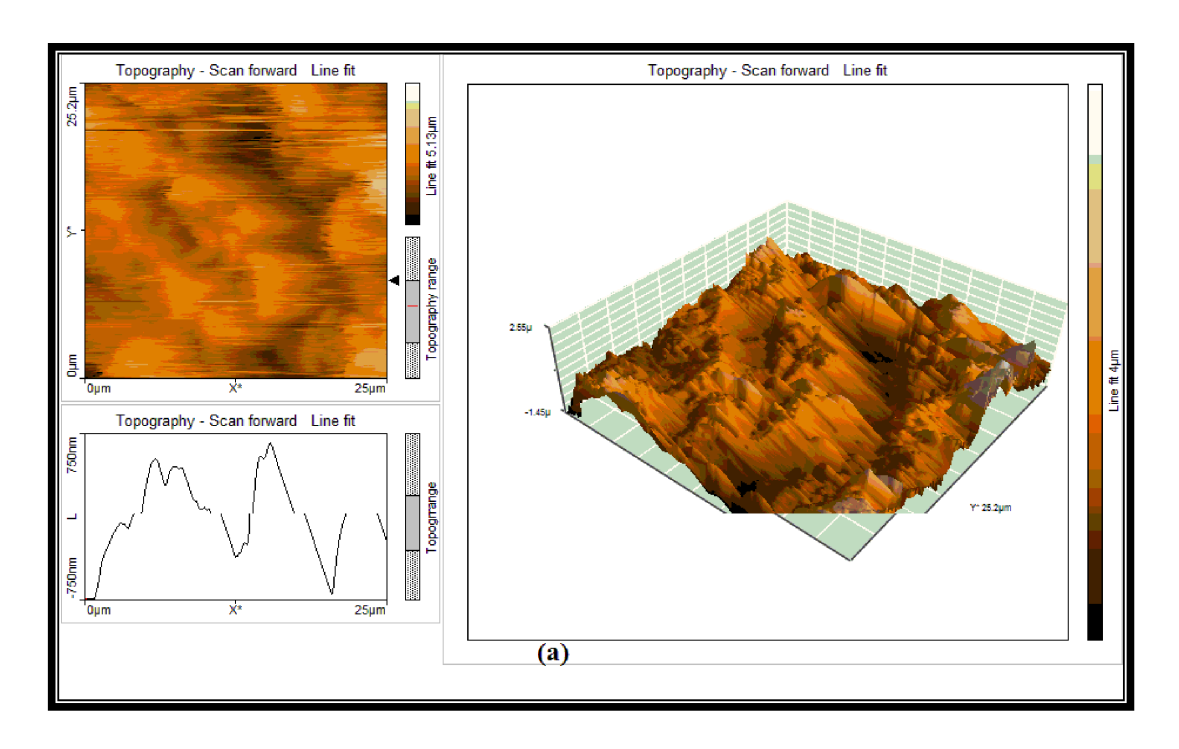


Fig.9.11a. AFM pattern of Mild steel without PSPA in 1M HCl solution

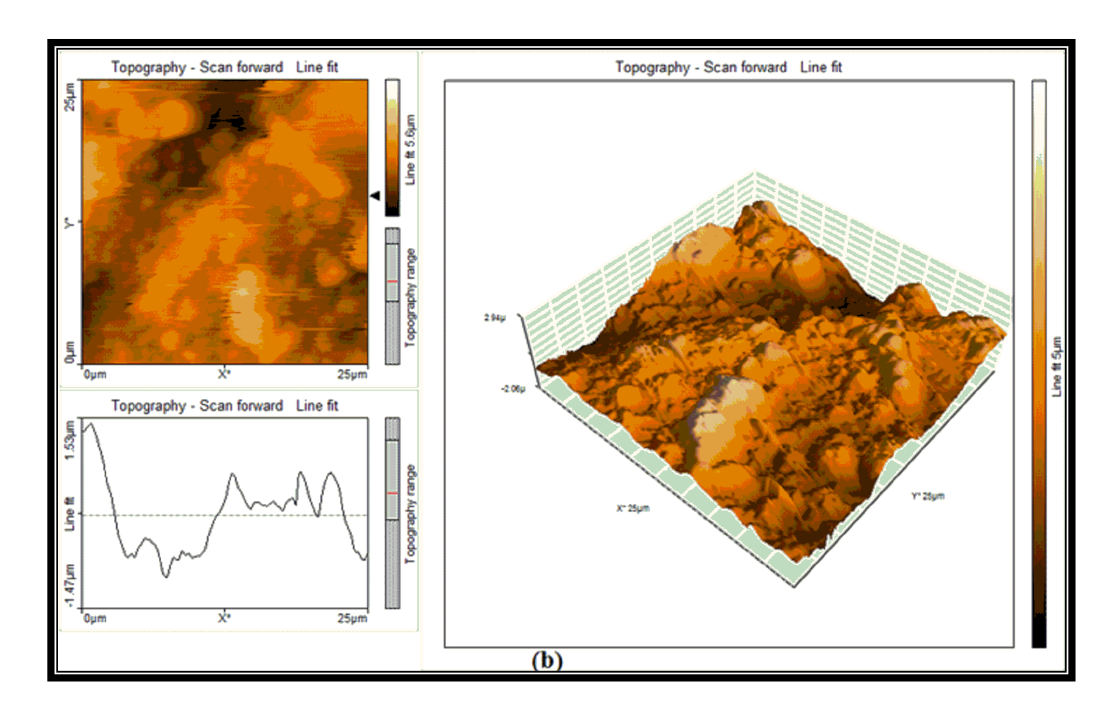


Fig.9.11b. AFM pattern of Mild steel with PSPA in 1M HCl solution

(Fig.9.11a) reveals the affected surface in the absence of inhibitor in 1M HCl solution and it is further explored by the average roughness and root mean square roughness values (418.32 and 489.49 nm) respectively as listed in Table.9.10. Moreover, (Fig.9.11b) exposes the surface reduction in the presence of inhibitor which is also validated by the Ra and Rq values (290.63 and 364.81nm) respectively [18 - 20].

Table.9.10. AFM parameters for bare steel, unprotected and protected steel specimens with PSPA in the 1M HCl solution

Complex	Average Roughness	RMS roughness	
Samples	(R _a)nm	$(\mathbf{R}_{\mathbf{q}})$ nm	
Polished Mild steel	279.41	332.27	
Unprotected surface	418.32	489.49	
Protected surface with PSPA	290.63	364.81	

Therefore, AFM information corroborated that the examined PSPA greatly suppressed the corrosion process and works as an efficient protector in the 1M HCl environment.

9.7. References

- 1. Li Y H, Deng S D, Fu H, Mu G N, Zhao N. Synergism between rare earth cerium (IV) ion and vanillin on the corrosion of steel in H₂SO₄solution: weight loss, electrochemical, UV–vis, FTIR, XPS and AFM approaches. *Appl. Surf. Sci.* 2008; 254: 5574–5586.
- 2. Ma H, Chen S, Liu Z, Sun Y. Theoretical elucidation on the inhibition mechanism of pyridine–pyrazole compound: a Hartree Fock study. *J. Mol. Struct.* 2006; 774:19–22.
- 3. Tao Z, Liu G, Li Y, Zhang R, Su H. Electrochemical investigation of tetrazolium violet as a novel copper corrosion inhibitor in an acid environment. ACS Omega. 2020; 5: 4415–4423.
- 4. Zhang S, Tao Z, Li W, Hou B. Substitutional adsorption isotherms and corrosion inhibitive properties of some oxadiazol–triazole derivative in acidic solution. *Corros. Sci.* 2010; 52: 3126–3132.
- 5. Gong Y, Wang F, Gao S, Zhang, Li H. Synthesis of new benzotriazole derivatives containing carbon chains as the corrosion inhibitors for copper in sodium chloride solution. *Ind. Eng. Chem. Res.* 2015; 54: 12242–12253.
- 6. Wang J. Inhibitor-concentration-induced extreme behavior in electrochemical parameters. *Chin. J. Oceanol. Limnol.* 1998; 16: 183–188.
- 7. Mishra A, Verma C, Lgaz H, Srivastava V, Quraishi M, Ebenso E E. Synthesis, characterization and corrosion inhibition studies of N-phenyl-benzamides on the acidic corrosion of Mild steel: experimental and computational studies. *J Mol Liq.* 2018; 251: 317–332.

- 8. Dehri I, Ozcan M. The effect of temperature on the corrosion of Mild steel in acidic media in the presence of some sulphur containing organic compounds.

 Mater. Chem. Phys. 2006; 98: 316-323
- 9. Li X, Deng S, Fu H, Mu G. Synergistic inhibition effect of rare earth cerium (IV) ion and anionic surfactant on the corrosion of cold rolled steel. *Corros. Sci.* 2008; 50: 2635-2645.
- 10. Haque J, Ansari K, Srivastav R V, Quraishi M A, Obot I B. Pyrimidine derivatives as novel acidizing corrosion inhibitors for N80 steel useful for petroleum industry: A combined experimental and theoretical approach. *Journal of Industrial and Engineering Chemistry*. 2017; 49: 176-188.
- 11. Herrag L, Chetouani A, Elkadiri S, Hammouti B, Aouniti A. Pyrazole Derivatives as Corrosion Inhibitors for Steel in Hydrochloric Acid. *Portugaliae Electrochimica Acta*. 2008; 26: 211-220.
- 12. Bouklah R, Hammouti B, Lagrenee M, Bentiss F. Thermodynamic properties of 2,5-bis(4-methoxyphenyl)- 1,3,4-oxadiazole as a corrosion inhibitor for Mild steel in normal sulfuric acid medium. *Corrosion Science*. 2006; 48 (9), 2831–2842.
- 13. Dutta A, Saha S K, Adhikari U, Banerjee P, Sukul D. Effect of substitution on corrosion inhibition properties of 2-(substituted phenyl) benzimidazole derivatives on Mild steel in 1 M HCl solution: a combined experimental and theoretical approach. *Corros. Sci.* 2017; 123: 256–266.
- 14. Mendoncca G L F, Costa S.N, Freire V N, Casciano P N S, Correia A N, de Lima-Neto P. Understanding the corrosion inhibition of carbon steel and copper in sulphuric acid medium by amino acids using electrochemical techniquesallied to molecular modelling methods. *Corros.Sci.* 2017; 115: 41–55.

- 15. Jing C, Wang Z, Gong Y, Huang H, Ma Y, Xie H, Li H, Zhang S, Gao F. Photo and thermally stable branched corrosion inhibitors containing two benzotriazole groups for copper in 3.5 wt% sodium chloride solution. *Corros.Sci.* 2018; 138: 353–371.
- 16. Abd El-Lateef H M, Abo-Riya M A, Tantawy A H. Empirical and quantum chemical studies on the corrosion inhibition performance of some novel synthesized cationic gemini surfactants on carbon steel pipelines in acid pickling processes. *Corros.Sci.* 2016; 108: 94–110.
- 17. Branzoi F, Branzoi V. Adsorption and Inhibitive Corrosion Properties of Some New Polymeric Compounds as Green Inhibitors on Carbon Steels in Cooling Water Systems. *Developments in Corrosion Protection*. 2014; 23: 233-242.
- 18. Ouakki M, Galai M, Rbaa M, Abousalem A S, Lakhrissi B, Rifi E H, Cherkaoui M. Quantum chemical and experimental evaluation of the inhibitory action of two imidazole derivatives on Mild steel corrosion in sulphuric acid medium. Heliyon. 2019; 20 (5): e02759.
- 19. Vashisht H, Bahadur I, Kumar S, Goyal M S, Kaur G, Singh G, Katata-Seru L, Ebenso E E. Synergistic interactions between tetra butyl phosphonium hydroxide and iodide ions on the Mild steel surface for corrosion inhibition in acidic medium. *J. Mol. Liq.* 2016; 224: 19–29.
- Singh P, Srivastava V, Quraishi M A. Novel quinolone derivatives as green corrosion inhibitors for Mild steel in acidic medium: Electrochemical, SEM, AFM and PS studies. *J. Mol. Liq.* 2016; 216:164–173.

CHAPTER - X

Summary and Conclusion

The explored inhibitors namely, 4-(4-Methoxy-phenyl)-1-phenethyl-1H-[1,2,3]triazole (MPPT), 1-benzyl-4-(naphthalen-2-yl)-1H-1,2,3-triazole (BNT), N-methyl-N-phenyl-3-(phenylsulfonyl)-1H-pyrazole-5-carboxamide (MPSC), 5-Benzyl 3-ethyl 1H-pyrazole-3, 5-dicarboxylate (BEPD), N-(4-(piperidin-1-ylsulfonyl)phenyl)acetamide (PSPA) were synthesized and characterized by melting point, ¹H NMR and ¹³C NMR. The corrosion assessment of all the synthesized inhibitors in the 1M HCl solution resulted in the following considerations.

Utilization of 4-(4-methoxy-phenyl)-1-phenethyl-1H-[1,2,3]triazole on Mild steel

- ➤ In the mass loss study, the corrosion rate of Mild steel dropped from 12.63 to 0.77 mg cm⁻² h⁻¹ while the inhibition efficiency increased from 24.24 to 93.92 % as the concentration of MPPT increased in 1M HCl solution at room temperature.
- ➤ In polarization studies, the value of corrosion current density (I₀) declined from 1.746 to 0.098 mA as the concentration of MPPT increased with a maximum efficiency of 93.49 %.
- ➤ According to the values of corrosion potential (E₀) and Tafel slopes (bc and ba), the inhibitor functioned as a mixed sort.
- The charge transfer value (R_{ct}) increased from 9.95 to 155.23 Ωcm^2 as MPPT concentration increased, and the inhibitory process was demonstrated by lower electrical double layer capacitance (C_{dl}) values (3.334 to 0.012 μF cm⁻²). A

- total of 93.59 % was protecte and the electrochemical results supported the moss loss findings
- ➤ In temperature investigations, the corrosion rate increased from 12.63 to 38.86 77 mg cm⁻² h⁻¹ as the temperature increased from 305 to 335 K and it was decreased dramatically from 38.86 to 1.55 77 mg cm⁻² h⁻¹ with various concentrations of MPPT at 335K. The observed prevention efficacy was 93.92, 93.36, 94.73 and 96.01 % at increased temperatures.
- ➤ Chemisorption can be seen in a decrease in activation energy (E_a) from 32.24 to 17.47 KJ mol⁻¹ which was supported by lowered Arrhenius factor (A) values.
- The endothermic reaction was indicated by the positive enthalpy ΔH^0 (29.59 to 14.81 KJ mol⁻¹).
- The decrease in disorderiness with increasing MPPT concentration was indicated by the negative ΔS^0 values (-193.91 to -197.57 JK⁻¹mol⁻¹).
- ➤ The Langmuir adsorption isotherm was exhibited by the linear regression coefficient value (R²) approaching 1 at all temperatures and the chemisorption process was revealed by the increase in K_{ads} value from 9124.09 to 9523.81.
- \triangleright Both the physisorption and chemisorption processes were indicated by the negative ΔG^0 (-33.33 to -36.59 KJ mol⁻¹).
- \triangleright The significant negative Mulliken charge of N₂₀ (-0.047) which causes electrostatic attraction between N₂₀ and Mild steel was identified as the protonation core of the MPPT in a quantum chemical investigation.
- The larger negative value of E_{HOMO} (-6.0095 eV) highlighted the inhibitor's electron donation core whereas the lower negative value of E_{LUMO} revealed the inhibitor's back donation of metal (-1.0495 eV).

- The electron distribution site in MPPT was indicated by the electron density distribution of HOMO which was focused on the triazole ring, benzene ring, and oxygen atom. Additionally, Elumo highlighted the phenethyl group, triazole moiety and benzene ring as the MPPT's electron reception site.
- \triangleright Electronic characteristics such as ΔE , D, I, A, χ , η , σ and ΔN revealed fascinating details regarding the reactivity and inhibitory mechanism of MPPT.
- ➤ The barrier layer development on the steel surface was proven by the SEM photographs with dispersed trenches in the absence of inhibitor and the smooth surface with foggy mass.
- ➤ Through the Nitrogen (1.25%) and Oxygen (12.73%) atoms of the MPPT, the EDX exploration validated the complex development on the Mild steel surface.
- The AFM analysis of Mild steel revealed extreme roughness in the absence of an inhibitor (Ra 402.13nm and Rq 511.83nm) which was significantly decreased in the presence of MPPT (Ra 188.08nm and Rq 227.19 nm) demonstrating the protector's corrosion-prevention ability.

Utilization of 1-benzyl-4-(naphthalen-2-yl)-1*H*-1,2,3-triazole on Mild steel

- ➤ With increasing concentrations of BNT at room temperature, the corrosion rate reduced from 12.73 to 1.09 77 mg cm⁻² h⁻¹ while the protective efficacy increased from 19.88 to 91.35 % in the mass loss investigation.
- ➤ The I₀ value decreased from 3.460 to 0.342 mA demonstrating BNT's inhibitory performance, with a maximum efficacy of 90.12 %, according to the polarization investigation.
- ➤ According to the values of E₀, bc and ba, the studied BNT is a mixed class protector.

- With the addition of BNT, the R_{ct} value increased from 9.52 to 100.55 Ωcm^2 indicating charge transfer impediment which was confirmed by the lowering values of C_{dl} (3.185 to 0.024 μF cm⁻²) with a maximum efficiency of 90.60 %.
- ➤ In the absence of BNT, the corrosion rate increased from 12.73 to 38.39 77 mg cm⁻² h⁻¹ while the protection capacity increased from 91.35 to 93.26 % at temperatures ranging from 305 to 335 K.
- ➤ The chemisorption process was suggested by the reduced value of E_a (31.39 to 13.76 KJ mol⁻¹) with an increase in BNT and the decreased value of A.
- The positive value of ΔH^0 obtained from the blank to the maximum concentration of BNT showed an endothermic reaction and the negative values of ΔS^0 indicated a drop in randomness at the metal solution interface.
- The adsorption process followed the Langmuir model and negative ΔG^0 values ranging from -31.25 to 36.61 KJ mol⁻¹ demonstrated that physicochemisorption was involved in the prevention mechanism.
- The N₂₁ atom was found as a protonation center in BNT, according to the quantum chemistry study. The electron donation sites discovered by the distribution of E_{HOMO} were the triazole moiety and the naphthalene ring, however, the naphthalene ring was recognized as a retro donation site by E_{LUMO}.
- The value of E_{HOMO} (-7.3531 eV) demonstrated the capacity to donate electrons to metal whereas the value of E_{LUMO} (-1.8944 eV) revealed the ability toreceive electrons from the metal to BNT. Other electronic metrics include $\Delta E_{,}D_{,}I_{,}A_{,}$ χ , η , σ and ΔN which represented inhibitory capability of BNT.
- The protective layer development with the disseminated matter on the Mild steel surface was substantiated by the SEM pictures, confirming the insoluble complex formation that successfully controlled Mild steel corrosion.

- ➤ The establishment of a barrier layer by Nitrogen (1.39%) coordination with Mild steel was established by the EDX study.
- ➤ The Ra (212.72 nm) and Rq (262.45 nm) values of Mild steel in the presence of BNT revealed that the roughness was greatly reduced by the formation of the protective barrier.

Utilization of N-methyl-N-phenyl-3-(phenylsulfonyl)-1H-pyrazole-5-carboxamide on Mild steel

- ➤ The corrosion rate value decreased from 19.25 to 1.07 77 mg cm⁻² h⁻¹ with an increase in MPSC in the mass loss technique, and the corresponding protection efficiency value increased from 34.45 to 94.46 %.
- ➤ The I₀ value decreased from 1.372 to 0.090 mA in the polarization analysis indicating that electrochemical corrosion processes were controlled as MPSC concentration increased. MPSC functioned as both anodic and cathodic protector, according to E₀, bc and ba values.
- \triangleright During the corrosion inhibition process, the increasing value of R_{ct} from 13.21 to 192.52 Ωcm² and the associated C_{dl} values reduced from 1.628 to 0.011 μF cm⁻² demonstrated the impediment of charge transfer with MPSC.
- At rising temperatures (303K to 333K), the corrosion rate increased from 1.07 to 12.4377 mg cm⁻² h⁻¹ without an inhibitor, and the IE value decreased from 94.46 to 74.52 % suggesting physisorption.
- ➤ The E_a value increased from 26.83 to 71.15 KJ mol⁻¹ as MPSC increased demonstrating that the energy barrier increased, implying physisorption, and the higher A value supported this notion.
- ightharpoonup The positive ΔH^0 values indicated endothermic and the positive change of ΔS^0 values indicated increased disorderness.

- \triangleright The adsorption process followed the Temkin model, and the lower K_{ads} value reflected physisorption. The repulsive forces predominate at elevated temperatures as evidenced by the negative values of the attractive parameter (a).
- ➤ According to density functional theory, the electrostatic attraction center of the mpsc was N₁₁. The value of E_{HOMO} (-5.7406 eV) indicated the probability of electron releasing whereas the value of E_{LUMO} (-0.8778 eV) denoted MPSC's electron receiving capacity.
- The electron density distribution of homo around the pyrazole moiety, benzene ring, O and N atoms of MPSC revealed possible electron-donating cores, whereas E_{LUMO} on the pyrazole ring, N and O atoms of MPSC suggested electron receiving sites. The ΔE , D, I, A, χ , η , σ and ΔN values were also supportive of the inhibitory mechanism.
- > SEM images demonstrated that the surface was entirely covered by the dispersed material in the presence of MPSC avoiding Mild steel deterioration.
- ➤ In EDX analysis, N (1.24 %) and O (20.97 %) atoms were found in the MPSC which formed a protective complex on the Mild steel surface.
- The AFM analysis revealed that in the presence of MPSC, the values Ra (334 nm) and Rq (386.47 nm) indicated decreased roughness.

Utilization of 5-benzyl 3-ethyl 1H-pyrazole-3, 5- dicarboxylate on Mild steel

Using the gravimetric technique, the corrosion rate decreased from 20.07 to 1.5277 mg cm⁻² h⁻¹ as the BEPD concentration increased, and the protective ability was enhanced from 36.56 to 92.42 %.

- ➤ The I₀ value decreased from 6.309 to 0.509 mA as the BEPD concentration was increased, illustrating that BEPD hindered corrosion processes. Similarly, BEPD's E₀, bc, and ba values revealed that both anodic and cathodic electrochemical processes were restricted with a maximum efficiency of 91.92%.
- The R_{ct} value increased from 1092.58 to 13211.52 Ωcm^2 as the C_{dl} value decreased (1.832 to 0.0014 μF cm⁻²) suggesting that BEPD contributed to the charge transfer process and the ideal efficacy observed was 91.73 %.
- ➤ The corrosion rate rose from 1.52 to 13.177 mg cm⁻² h⁻¹ for optimal concentration at temperatures ranging from 303K to 333K, according to thermal studies. At 50 ppm, the IE value dropped from 92.42 to 72.44 %, indicating physisorption.
- ➤ The rise in E_a from 24.95 to 64.14 KJ mol⁻¹ implied physisorption which was accompanied by the higher A values.
- The endothermic reaction was shown by positive ΔH^0 values and the increased disorderness was disclosed by the negative ΔS^0 values.
- The corrosion prevention process followed the Freundlich model, and the lower value of K_{ads} (14.83 to 0.38) revealed that weak electrostatic interactions were involved in the adsorption. The electrostatic interaction mechanism was further validated by the lowered adsorption intensity (n) values (1.68 to 0.61).
- ➤ According to DFT, the coordination sites were disclosed by the E_{HOMO} value (-7.0702 eV) and E_{LUMO} value (-1.6522 eV) whereas the electrostatic interaction was discovered at O₁₅ of the inhibitor.

- \triangleright The E_{HOMO} distribution on the pyrazole moiety and oxygen atom revealed the electron availability sites, whereas the E_{LUMO} distribution on the benzyl region of the inhibitor revealed the receiving core.
- ➤ In the presence of BEPD, SEM images demonstrated the formation of the protective coating.
- ➤ EDX analysis showed the existence of N (1.21%) and O (41.51 %) with BEPD suggested the coordination occurred through the mentioned atoms of the inhibitor to the Mild steel surface.
- The roughness reduction of steel surface with BEPD was evidenced by the Ra (701.41 nm) and Rq (825.19 nm) which reflected the prevention of Mild steel corrosion.

Utilization of N-(4-(piperidin-1-ylsulfonyl) phenyl) acetamide on Mild steel

- ➤ According to the mass reduction, as PSPA concentration increased, the corrosion rate decreased from 19.30 to 0.7677 mg cm⁻² h⁻¹ and the accompanying efficiency increased from 40.89 to 96.06 %.
- ➤ The polarization study revealed a drop in the I₀ value from 1.893 to 0.0 922 mA indicating that the inclusion of PSPA slowed down corrosion processes. The values of E₀ and Tafel slopes revealed the mixed sort nature of PSPA, with a maximum efficiency of 95.13 %.
- The increased R_{ct} value from 1061.25 to 23634.84 Ωcm^2 indicated that the charge transfer mechanism was successfully controlled with the PSPA concentration, which was corroborated by the decreased C_{dl} values (1.516 to 0.0043 $\mu F cm^{-2}$). The highest effectivity was 95.51 %.

- ➤ The corrosion rate increased from 0.76 to 10.94 77 mg cm⁻² h⁻¹ at temperatures ranging from 304K to 334K, according to the temperature study. Consequently, the IE value dropped from 96.06 to 76.28 % at 30 ppm.
- ➤ The increased values of E_a (25.32 to 75.84 KJ mol⁻¹) with increasing PSPA concentrations suggested physisorption which was also affirmed by the increasing values of A.
- ightharpoonup Positive ΔH^0 values indicated an endothermic process and the positive ΔS^0 values showed incressed disorderness.
- The lowered K_{ads} (19.32 to 0.826) and n (1.99 to 0.72) values showed electrostatic interaction, which was further supported by the negative ΔG^0 values (-17.64 to 10.62 KJ mol⁻¹).
- The probability of inhibitor to metal electron donation was shown by the E_{HOMO} value (-5.523 eV) whereas the possibility of metal to inhibitor back donation was revealed by the E_{LUMO} value (-0.8629 eV). The O_{12} atom was identified as the PSPA's protonation site.
- The presence of E_{HOMO} on practically every part of the inhibitor suggested electron donation cores, whereas E_{LUMO} concentrated on the N atom, SO₂ group and benzene ring, which was revealed as the focal point for electron reception cores.
- > SEM images revealed a smooth surface with the distributed particles in the presence of PSPA indicating the establishment of a barrier coating on the Mild steel surface.
- ➤ The atomic weight percentage readings of 1.65 % for N and 36.27 % for O atoms in EDX analysis revealed that chemisorption with Mild steel proceeded via N, O coordination.

➤ In the AFM examination, the roughness was significantly decreased in the presence of PSPA (Ra - 290.63 nm and Rq - 364.81 nm) indicating that corrosion degradation was successfully controlled in an acidic environment.

Eventually, all the specifics acquired from this endeavor validated that the impact of all the inhibitors against the Mild steel dissolution was magnificent and they were employed as proficient protectors in 1M HCl solution.

PAPER PUBLICATIONS

- 1. K. Vijayalakshmi and J. Elangovan, 1,2,3-Triazole derivative as a potential protector for mild steel corrosion in acid media: A kinetic and thermodynamic approach" *Journal of the Indian chemical society*, 2020, 97(9b), 1574-1583.
- 2. K Vijayalakshmi, N Punitha, R Rengasamy and J Elangovan, Effect of 1,2,3-triazole derivative on the dissolution performance of mild steel in 1M HCl medium, *Indian Journal of Chemical Technology*, 2021, 28, 421-428.

J. Indian Chem. Soc., Vol. 97, No. 9b, September 2020, pp. 1574-1583



1,2,3-Triazole derivative as a potential protector for mild steel corrosion in acid media: A kinetic and thermodynamic approach

K. Vijayalakshmi and J. Elangovan*

PG and Research Department of Chemistry, Rajah Serfoji Government College (Autonomous), Thanjavur-613 005, Tamil Nadu, India

(Affiliated to Bharathidasan University, Thiruchirappalli-620 024, Tamil Nadu, India)

E-mail: elangoorganic@gmail.com

Manuscript received online 29 June 2020, accepted 25 August 2020

The anticorrosive effect of a new triazole derivative 4-(4-methoxy-phenyl)-1-phenethyl-1*H*-[1,2,3]triazole (MPPT) on mild steel specimens exposed in 1 *M* HCl corrosive solution was inspected by the mass reduction, polarization and impedance methods. The thermodynamic parameters, corrosion kinetics, and adsorption isotherm studies of the examined MPPT were discussed at various temperatures. The polarization study discovered that MPPT was a mixed kind protector with more acidic existence and the electrochemical measurements were in fine concordance with the mass loss method. SEM, EDS, and AFM assessments corroborated the development of inhibitive barriers on the mild steel specimens.

Keywords: Adsorption, mild steel, triazole derivative, thermodynamic parameters, HCl.

Introduction

Mild steels are widely consumed materials for huge sectors due to their economically low cost, ease of production, machinability, weldability, etc. However, these handlings have been rigorously affected by the metallic corrosion in an aggressive environment¹. In consequence, numerous sectors are losing billions of dollars in their business. According to the recent reports of International Measures of Prevention, Applications of Corrosion Technology, and the Study of Corrosion Economics, the cost of corrosion in all sectors is about 3.4% in their Gross Domestic Product (GDP) and it is estimated recurrently by the National Association of Corrosion Engineers². Thus, corrosion is an expansive and expensive ecological issue around the globe, and corrosion prevention is the pivotal solution to recuperate the economic misery and lifespan concern. Despite innumerable endeavor have been made for curtailing the rate of corrosion, the most effective and universally utilized technique is the metal surfaces prevented by the adherence of inhibitor species^{3,4}.

In this circumstance, many inorganic and organic mol-

ecules have been made to protect metals against corrosion^{5,6}. However, organic inhibitors are observed as efficient defenders on account of their molecular structures, consuming low concentration, diminutive noxious and implausible ability to concoct protective layers in different corrosive environments^{7,8}. Besides that, heterocyclic compounds are excellent anticorrosive materials comprising π -electrons, heteroatoms such as nitrogen, oxygen, and sulfur to surge the protection from corrosion deterioration^{9,10}. Among a lot of heterocyclic candidates, triazole derivatives are one of the noteworthy numbers to avert such stringent detritions attributable to the presence of π -electrons and heteroatoms of the triazole moieties in various acidic and basic corrosive media. Numerous anti-corrosive studies have been widely conferred for 1,2,4-triazoles but not a great degree to 1,2,3triazole derivatives 11,12.

Thus, the present work intends to interrogate the corrosion inhibition efficacy of 4-(4-methoxy-phenyl)-1-phenethyl-1*H*-[1,2,3]triazole (MPPT) and Fig. 1 shows the structure of the MPPT molecule.

Vijayalakshmi et al.: 1,2,3-Triazole derivative as a potential protector for mild steel corrosion in acid media: etc.

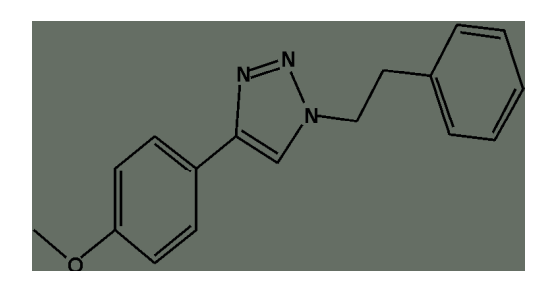


Fig. 1. Structure of MPPT.

Experimental

Materials:

According to ASTM E415-17, the elemental analysis of the mild steel specimens studied were S - 0.009%, Cu - 0.31%, P - 0.089%, Mn - 0.43%, C - 0.076%, Cr - 0.52%, Si - 0.319%, Al - 0.028%, Ni - 0.20%, and Fe - 99.69% (IRS M41/97 steel). The dimensions of mild steel specimens 5 cm×1 cm×0.2 cm were utilized for the gravimetric method and the test specimens were polished by different numbers of silicon carbide papers finally finished with a grade of 1500. Initially, mild steel samples were washed with distilled water, followed by ethanol then degreased with acetone. An aggressive medium of 1 M hydrochloric acid was prepared with 37% analaR HCl solution and bidistilled water ¹³.

The examined MPPT was synthesized in the laboratory¹⁴ and characterized by FTIR, ¹H and ¹³C NMR techniques. For further assessments, the desired concentrations of MPPT were prepared in ethanol.

Mass loss method:

As reported by the ASTM G31-72, the prepared mild steel samples were weighed accurately before and after immersion in 1 *M* HCl corrosive solution in various concentrations (10, 30, 50,100 ppm) of MPPT inhibitor for 6 h contact time at room temperature. Subsequently, the specimens were taken out, washed, dried and then accurately weighed for the determination of corrosion parameters¹⁵.

For this evaluation, the average weight loss was acquired by the three consecutive mass loss experiments in the above identical conditions. The corrosion factors such as inhibition efficiency (IE), surface coverage (θ) and the rate of corrosion (CR) were determined by eqs. (1), (2) and (3) respectively.

$$IE (\%) = \left(\frac{W_0 - W}{W_0}\right) \times 100 \tag{1}$$

$$\theta = \left(\frac{W_0 - W}{W_0}\right) \tag{2}$$

where W and W_0 reflect the average weight loss of mild steel samples (mg) with and without MPPT respectively.

$$CR = \frac{\Delta W}{At}$$
 (3)

where ΔW is the average mass loss (mg), A is the total surface area (cm⁻²) and t is the exposure time (h) for the tested specimens with and without MPPT in 1 M HCl medium.

Electrochemical methods:

Potentiodynamic polarization study:

The electrochemical investigations were achieved by the CHI-66 model potentiostat with the conventional three-electrode assemblage. The reference and counter electrodes in these arrangements were a platinum foil and a standard calomel electrode. Meanwhile, 1 cm 2 of the mild steel specimen was act as the working electrode in a corrosive context. For polarization measurements, the working electrode was exposed with and without MPPT in the test solution for 30 min until the open circuit potential was reached. The polarization curves were obtained automatically by adjusting the potential of the electrode from -500 mV to +500 mV at a scan rate of 1 mV s $^{-1}$ 16 .

At the intersection of Tafel lines, the corrosion current density (I_{corr}) values were obtained. Inhibition efficacy and the surface coverage values were measured with the following eqs. (4) and (5) respectively.

$$\theta = \left[\frac{I_{\text{corr}} - I_{\text{corr}(\text{inh})}}{I_{\text{corr}}} \right]$$
 (5)

where $I_{\text{corr}(\text{inh})}$ and I_{corr} are the current densities of corrosion with and without MPPT respectively.

Impedance study:

The electrochemical impedance analysis was carried out

in the frequency range from 100 kHz to 10 MHz with maximum amplitude of 5 mV, receiving AC signals at the open circuit potential.

From the initial and final points of the Nyquist plots for various concentrations of MPPT, the investigational charge transfer resistance ($R_{\rm ct}$) was obtained ¹⁷. The inhibition efficiency, surface coverage, and electrical double layer capacity ($C_{\rm dl}$) of the investigated MPPT were determined from the charge transfer resistance values using eqs. (6), (7) and (8) respectively.

IE (%) =
$$\left[\frac{R_{\text{ct(inh)}} - R_{\text{ct}}}{R_{\text{ct(inh)}}} \right] \times 100$$
 (6)

$$\theta = \left[\frac{R_{\text{ct (inh)}} - R_{\text{ct}}}{R_{\text{ct (inh)}}} \right]$$
 (7)

$$C_{\rm dl} = \frac{1}{2\pi . f_{\rm max} . R_{\rm ct}} \tag{8}$$

where $R_{\rm ct(inh)}$ and $R_{\rm ct}$ are the charge transfer resistance with and without MPPT and $f_{\rm max}$ is the maximum peak frequency of the Nyquist plots.

Surface morphology:

SEM analysis:

The micrographs of mild steel samples was interpreted by the scanning electron microscope with (100 ppm) and without MPPT in 1 M HCl solution for 6 h of immersion at room temperature¹⁸.

EDS analysis:

Electron Dispersive Spectrum analysis is one of the imperative methods to identify the elements present on the surface of the mild steels. In this regard, mild steel specimens were exposed with (100 ppm) and without MPPT in 1 M HCl solution for 6 h of contact time at room temperature ¹⁹.

AFM analysis:

Atomic Force Microscope was employed to inspect the surface roughness of the metals with (100 ppm) and without MPPT in 1 *M* HCl solution for 6 h exposure time at room temperature. These findings furnished some significant thoughts about the corrosion inhibiting performance of inhibitor on mild steel specimens in the corrosive atmosphere²⁰.

Results and discussion

Mass loss examinations:

Table 1 represents the corrosion data such as corrosion rate, inhibition efficiency, and surface coverage acquired from mass loss study in 1 *M* HCI solution at room temperature. Evaluation of Table 1 indicates that the corrosion rate diminishes with increasing concentration of MPPT suggesting the inhibitor species adsorbed on the surface of the mild steel specimens²¹. Moreover, the increasing values of surface coverage with increasing inhibitor concentration which also pinpoints that the MPPT has a larger competence of protection over the metallic surface. Moreover, the optimal efficiency reaches up to 93.92% at 100 ppm concentration suggesting the inspected MPPT act as an efficient protector in the 1 *M* HCI medium.

. Mildsteel corrosion factors	s for MPPT in 1 <i>M</i> H	CI solution
CR	IE	θ
$(mg cm^{-2} h^{-1})$	(%)	
12.63	_	-
6.85	45.73	0.46
2.24	82.24	0.82
1.53	87.89	0.88
0.77	93.92	0.94
	CR (mg cm ⁻² h ⁻¹) 12.63 6.85 2.24 1.53	(mg cm ⁻² h ⁻¹) (%) 12.63 – 6.85 45.73 2.24 82.24 1.53 87.89

Potentiodynamic polarization investigations:

Fig. 2 displays the Tafel lines for the test specimens in the absence and presence of various concentrations of MPPT in 1 M HCl medium at room temperature and the inhibition efficiencies for all the investigated concentrations are determined from the $I_{\rm corr}$ values. Meanwhile, the polarization parameters are summarized in Table 2 reveals that the values of corrosion current density ($I_{\rm corr}$) considerably dropped off with the rising concentration of MPPT which exposes the corrosion rate is curtailed by MPPT molecule adsorbed onto the metallic surface. Further, the tabulated values interpret that the Tafel polarization transpires to the anodic branch as well as the cathodic branch but the cathodic effect is predominent²².

In general, the difference in corrosion potential (E_0) values for the existence of inhibitor and the blank is greater than ± 85 mV suggested that the inhibitor molecules are identified either as the cathode or anode inhibitor distinctively²³.

Vijayalakshmi et al.: 1,2,3-Triazole derivative as a potential protector for mild steel corrosion in acid media: etc.

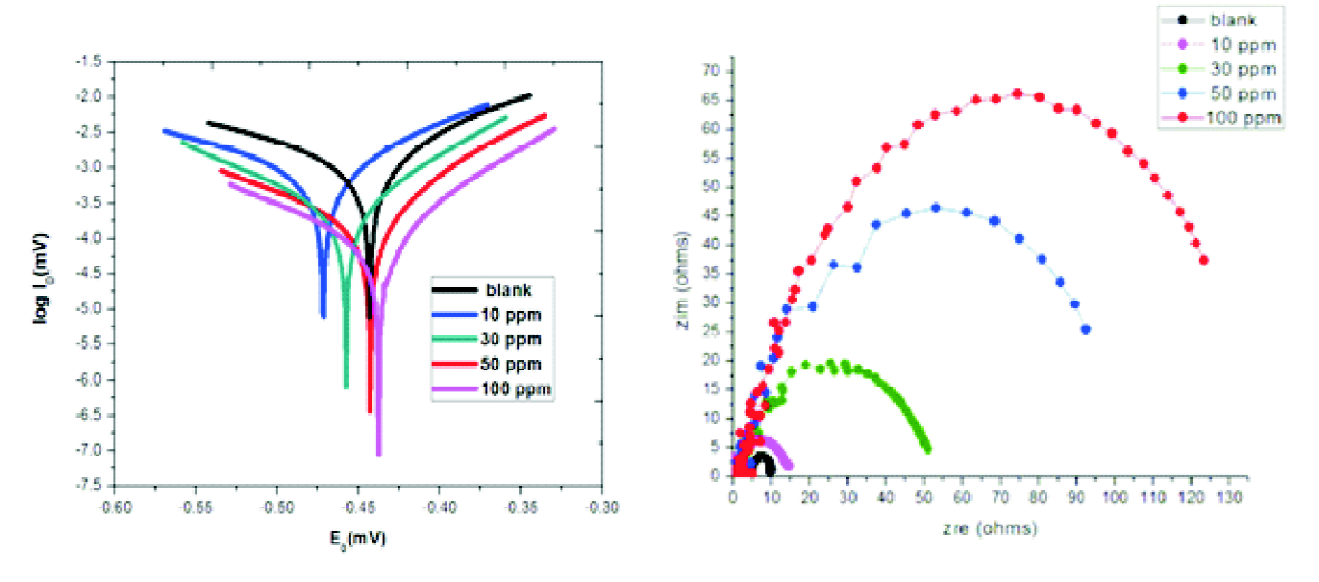


Fig. 2. Tafel curves and impedance plots for MPPT in 1 M HCl solution.

Conc.		Po	larization paramet	ters		Im	pedance paramete	ers
(ppm)	$\overline{E_0}$	<i>I</i> ₀	b _c	b _a	IE	R _{ct}	C _{dl}	I.E
	(mV)	(mA)	(mV)	(mV)	(%)	$(\Omega \text{ cm}^2)$	$(\mu F cm^{-2})$	(%)
Blank	-443.00	1746.00	249.63	116.96	_	9.95	3.334	-
10	-471.69	1312.00	233.64	125.50	24.86	14.61	1.453	31.90
30	-457.53	296.79	118.111	78.366	83.00	50.97	0.158	80.48
50	-443.02	205.02	147.80	72.12	88.26	92.42	0.036	89.23
100	-437.56	98.01	120.90	67.79	94.39	129.43	0.018	92.31

Accordingly, this polarization study demonstrates the shift in $E_{\rm corr}$ values is varied from 0.02 mV to 28 mV which reflects that the inspected MPPT performed as the mixed kind protector in an acidic environment. Also, the maximum efficiency observed is 94.39% at 100 ppm which concludes that the MPPT inhibitor functioned as an effective anticorrosive defender in the 1 M HCI medium.

Impedance assessments:

Fig. 2 spectacles the diameters of the Nyquist plots increase with increasing MPPT concentration which construes the reduction of the charge by the addition of MPPT in the corrosive medium. As shown in Fig. 2, the semicircles procured by the impedance analysis are not perfect during the corrosion process owing to the coarseness of the metal surface and inhomogeneity distribution of active sites for adsorption²⁴.

Table 2 illustrates that the increasing values of R_{ct} with

the rising concentration of MPPT which exposes the corrosion rate is mitigated by the hindrance of charge transfer in the acidic medium. Also, the lowering $C_{\rm cl}$ values reflect that the electrical double layer is larger at the metal-solution boundary which supports the strong inhibition. We can also notice that the maximum protection efficacy of MPPT is 92.31% at optimum concentration and all the impedance factors conclude that MPPT has a great ability from corrosion attacks in aggressive environment.

Temperature effect on corrosion:

Table 3 exposes that the investigational data of corrosion with and without MPPT in the 1 *M* HCl environment at different temperatures 305, 315, 325, and 335 K. It shows clearly the moderate rise in hindered efficiencies attained for all the higher concentrations of MPPT inhibitor at raised temperatures which stand for the corrosion rate is mitigated by the chemical interaction or both the physical and chemical

	Table 3. Co	rrelation between	the temperatures	s and inhibition e	ficiencies for MF	PPT on mildstee	Corrosion	
Conc.		CR (mg	$cm^2 h^{-1}$)			ΙE	(%)	
(ppm)	305 K	315 K	325 K	335 K	305 K	315 K	325 K	335 K
Blank	12.63	16.85	25.97	38.86	_	_	_	_
10	6.85	9.85	17.49	28.73	45.73	41.53	32.65	26.08
30	2.24	2.80	3.52	5.33	82.24	83.38	86.46	86.28
50	1.53	2.03	2.56	2.80	87.89	87.98	90.15	92.80
100	0.77	1.12	1.37	1.55	93.92	93.36	94.73	96.01

interactions on the mild steel surface²⁵.

Hence, the above discussion exposed that the hike in efficiencies is due to enhance in electron density of the adsorption center of MPPT which might be blocked the corrosion sites on the metal surface at elevated temperatures.

Kinetic and thermodynamic parameters:

Based on the data achieved from the temperature study, the activation energy (E_a) and Arrhenius factor (A) can be determined by the Arrhenius eq. (9);

$$\log CR = \log A - \frac{E_a}{2.303RT} \tag{9}$$

where CR is the rate of corrosion, R is the gas constant and T is the temperature.

In addition, entropy (ΔS^0) and enthalpy (ΔH^0) values were calculated by the transition state eq. (10);

$$\log\left(\frac{CR}{T}\right) = \log\left(\frac{RT}{Nh}\right) + \left(\frac{\Delta S^{0}}{2.303R}\right) - \left(\frac{\Delta H^{0}}{2.303RT}\right)$$
(10)

where 'h' is Planck's constant and 'N' is Avogadro's number.

The straight lines of Arrhenius plots are procured by plotting to log CR vs 1000/T with the slope $(-E_a/2.303R)$ and an intercept (log A) is shown in Fig. 3. From the slope and intercept of Arrhenius plots, the activation energy (E_a) and preexponential factor (A) can be determined. In the same way, the particulars of the enthalpy and entropy can be attained by plotting log (CR/T) versus 1000/T from the transition state plots at various concentrations of the investigated MPPT as shown in Fig. 3. The values of ΔH^0 and ΔS^0 are obtained

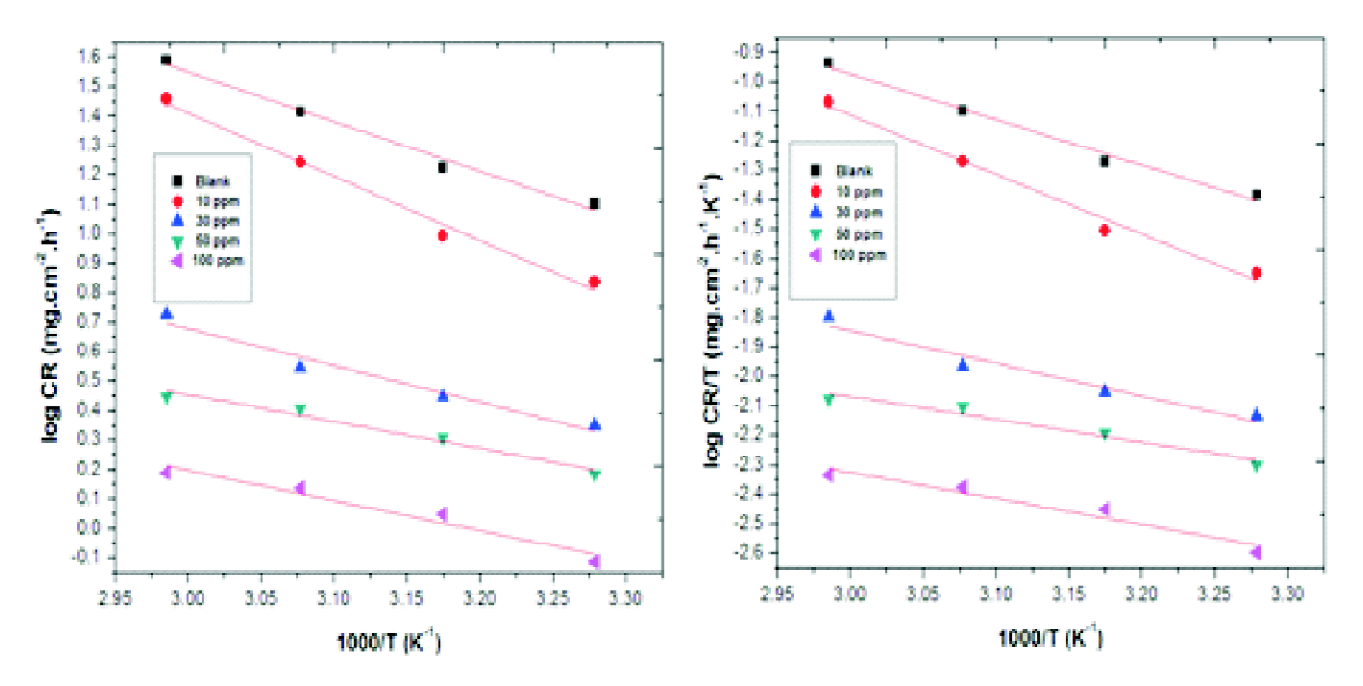


Fig. 3. Arrhenius and transition state plots for MPPT in 1 M HCl solution.

Vijayalakshmi et al.: 1,2,3-Triazole derivative as a potential protector for mild steel corrosion in acid media: etc.

from the slope $(-\Delta H^0/2.303R)$ and intercept [(log $(R/Nh) + \Delta S^0/2.303R$] of the straight lines from the transition state plots respectively.

The kinetic and thermodynamic data achieved from the transition state plots and Arrhenius plots are summarized in Table 4. Here, we can see a decrease in $E_{\rm a}$ with increasing MPPT concentration at all worked temperatures which indicate that the adsorption process is characteristic chemical adsorption. Meanwhile, the diminished A values support the inhibition process by the formation of the defensive coating on the mild steel surface by MPPT molecule²⁶. We also notice from Table 4 that the positive ΔH^0 values reflect the corrosion process is endothermic and also suggests that the dissolution process of mild steel is difficult²⁷. The negative values of ΔS^0 expose that the decrease in entropy on the mild steel corrosion²⁸.

Table 4. Thermodynamic-kinetic data for MPPT on mild steel corrosion

Conc.	E_{a}	Α	ΔH^0	ΔS^0
(ppm)	(kJ mol ⁻¹)	$(g cm^2 h^{-1})$	(kJ mol ⁻¹)	$(JK^{-1} mol^{-1})$
Blank	14.00	3.9948×10 ⁶	12.85	-193.91
10	17.94	7.6824×10 ⁷	16.79	-192.63
30	10.39	2.6742×10 ⁴	9.24	-196.09
50	8.54	1.902×10 ³	7.39	-197.23
100	7.58	1.553×10 ³	6.43	-197.32

Isotherm model:

The adsorption abilities on the metal surface of the inhibiting mechanism of the corrosion adsorption process are identified by the number of adsorption isotherm models.

In this case, the most fitted model is Langmuir isotherm and the adsorption parameters are acquired by the following isotherm eq. (11);

$$\frac{C_{\text{inh}}}{\Theta} = \frac{1}{K_{\text{ads}}} + C_{\text{inh}} \tag{11}$$

where $C_{\rm inh}$ is the concentration of the MPPT (ppm), θ is the surface coverage and $K_{\rm ads}$ is the equilibrium adsorption constant.

Table 5 and Fig. 4 reveals that the Langmuir adsorption isotherm data obtained by plotting ($C_{\rm inh}/\theta$) vs $C_{\rm inh}$ for various MPPT concentrations at different temperatures. Inspection of Table 3 demonstrates that the increasing $K_{\rm ads}$ values which

Table 5. Langmuir parameters for MPPT on mild steel corrosion at various temp.

Temp.		Langmuir parameters	
(K)	$K_{\rm ads}$ (L mol ⁻¹)	$\Delta G^0_{ m ads}$ (kJ mol ⁻¹)	R ²
305	9192.87	-33.33	0.9973
315	9129.92	-34.40	0.9982
325	9337.94	-35.55	0.9985
335	9469.7	-36.69	0.9986

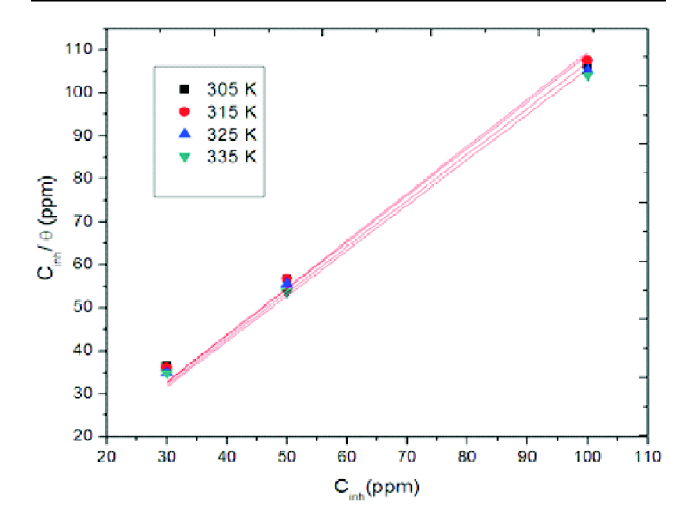


Fig. 4. Langmuir isotherm for MPPT in 1 M HCl solution.

corroborate the strong adherence performance of MPPT over the metallic surface. Furthermore, the linear regression coefficient (R^2) values at all the temperatures under investigation are closed to unity, which indicates that the adsorption mechanism is consistent with the Langmuir adsorption isotherm²⁹.

The values of standard free energy (ΔG^0) were calculated by eq. (13);

$$\Delta G_{\text{ads}} = [-RT \ln (55.5 K_{\text{ads}})] \tag{12}$$

where R is the universal gas constant, T is the thermodynamic temperature, 55.5 is the concentration of water in probed solutions and $K_{\rm ads}$ is the equilibrium adsorption constant.

Additionally, the obtained ΔG^0_{ads} values are negative suggesting the inhibition process is spontaneous and the development of protecting barrier is denser. According to the literature reports, the Gibbs free energy values around and below -20 kJ mol^{-1} describe the mechanism as physisorption whereas the values around or above -40 kJ mol^{-1} indicated a chemisorptions method³⁰. Exploration of Table 5 displays

the $\Delta G^0_{\rm ads}$ values ranged between –33.33 to –36.69 (kJ mol⁻¹) indicating the inhibition process is both the electrostatic and chemical interactions.

SEM study:

Figs. 5a-5c exhibit the SEM micrographs for polished mild steel, unprotected and protected metallic surfaces. As shown in Figs. 5a-5c, the bare steel exhibits the smoother surface while the unprotected metallic surface reflects the number of pits and cracks due to the rust formation in the corrosive medium. Moreover, the severe damages seen from the unprotected surface are almost reduced in the presence of

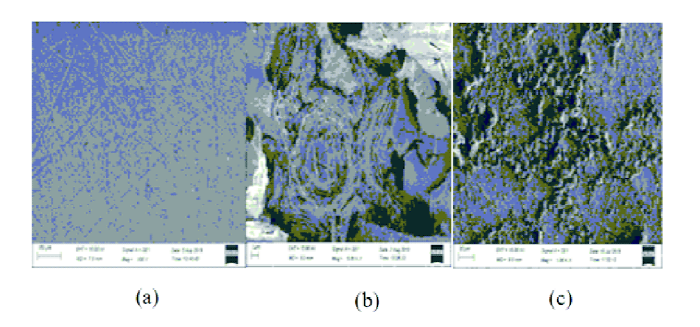


Fig. 5. SEM micrographs for (a) bare steel surface, (b) unprotected surface and (c) protected surface with MPPT in 1 *M* HCl solution

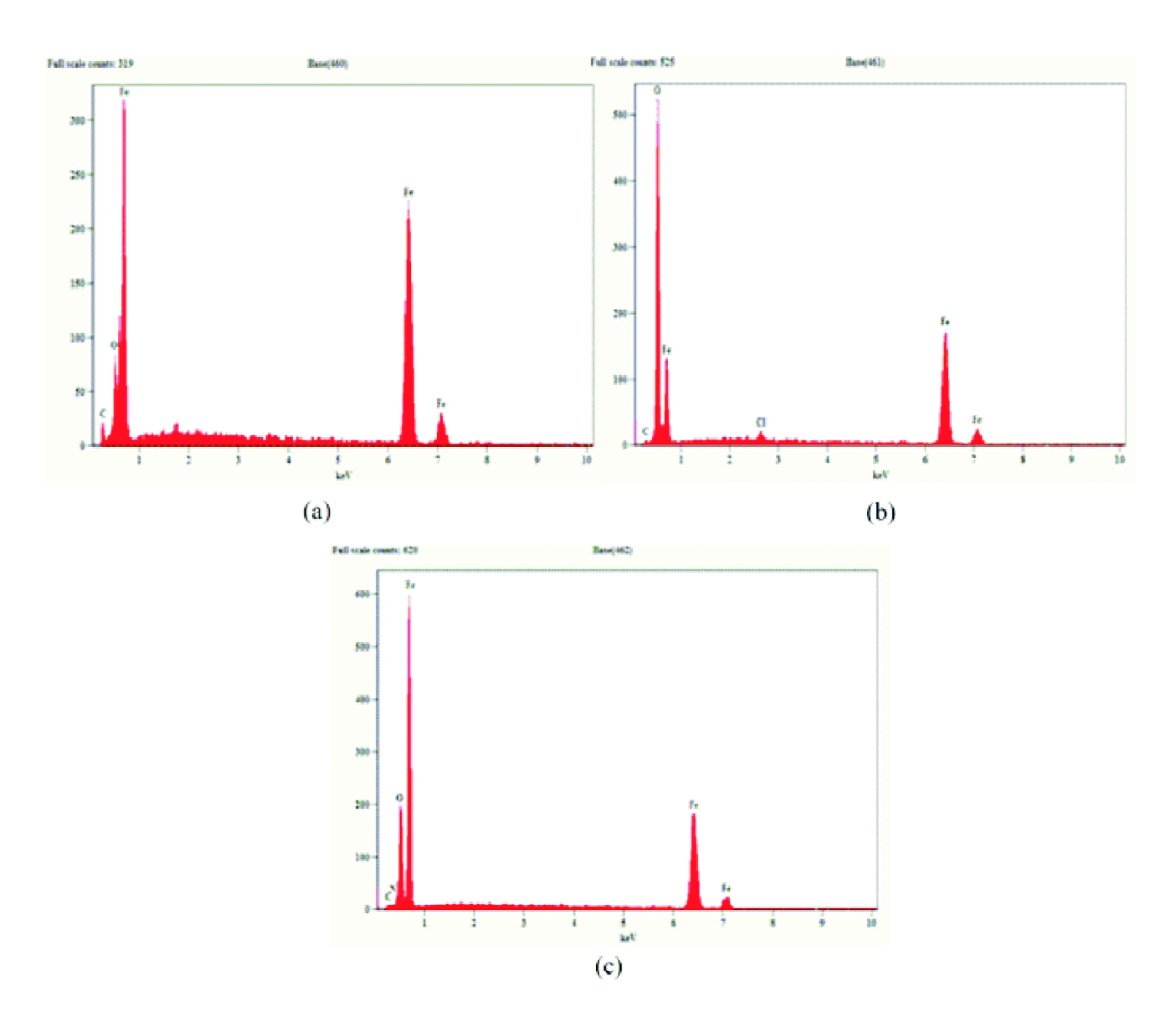


Fig. 6. EDS of (a) bare steel surface, (b) uninhibited surface and (c) inhibited surface with MPPTin 1 M HCl solution.

Vijayalakshmi et al.: 1,2,3-Triazole derivative as a potential protector for mild steel corrosion in acid media: etc.

MPPT (100 ppm) which confirms the corrosion destruction is hindered by the development of the thin film over the metallic surface¹⁸.

EDS study:

Figs. 6a-6c display the EDS interpretation for bare steel, unprotected and protected mildsteel specimens. The inspection of Figs. 10a-10c shows the appearance of chlorine peak without MPPT due to rust generation in 1 M HCl solution. The specimens examined with MPPT also demonstrate that the presence of a nitrogen peak suggests the chemical interaction of the nitrogen atom with the iron surface 19 .

Meanwhile, we notice the quantity details of EDS analysis from Table 6 that the corrosion mitigation is carried out by the coordination of O and N atoms of MPPT with the iron surface. Hence, all the EDS findings prove that the corrosion sites of the metallic surfaces are proficiently barred by heteroatoms of MPPT in the 1 *M* HCI medium³¹.

Table 6. Elemental analysis for MPPT on mild steel corrosion						
Specimens	Weight percentage					
	Fe	0	С	CI	N	
Bare mild steel	79.82	7.98	12.20	-	-	
Unprotected mild steel	49.66	43.44	5.84	1.06	_	
Protected mild steel	75.56	12.73	10.46	_	1.25	
with MPPT						

AFM study:

The AFM patterns of bare steel, uninhibited surface and inhibited surface of tested specimens with MPPT (100 ppm) are shown in Figs. 7a-7c. The bare mild steel reveals the uniform surface with small scratches while the uninhibited metallic surface demonstrates the relatively rough and po-

rous structure with large deep pores due to the corrosive environment. Meanwhile, the inhibited surface exhibits the smoother area registering the roughness decreases with the existence of the MPPT molecule.

It is also evident from the obtained values of average roughness that the mild steel specimens before immersion, unprotected immersion and protected immersion are 160.65 nm, 895.36 nm, and 188.08 nm in acidic corrosive media respectively. The similar trend that occurred to a root mean square roughness values for bare steel, unprotected, and protected mild steel specimens are 195.31 nm, 1500.1 nm, and 227.19 nm sequentially. It is clear that the closeness of the investigated roughness data between the bare steel and protected surfaces exhibiting the roughness of the metallic surface is diminished by the adsorption of the MPPT protector. Accordingly, all the AFM findings corroborate the smoother protected surface due to the development of impenetrable and ordered barrier on the surface of the mild steel 32.

Inhibition mechanism:

All the explorations referred to above showed that metallic surfaces are protected by the adsorption of inhibitor species by the development of inhibitive barriers on the steel surfaces.

Herein, the electrochemical corrosion reactions can be restricted by the adsorption of MPPT molecule either by physical and chemical interactions on the mild steel surface in the following mechanisms³³.

- (i) The electrostatic interaction takes place in 1 *M* HCl solution between the protonated nitrogen and oxygen atoms of MPPT and the chlorinated metal surface.
 - (ii) The chemical interaction exists between the vacant d

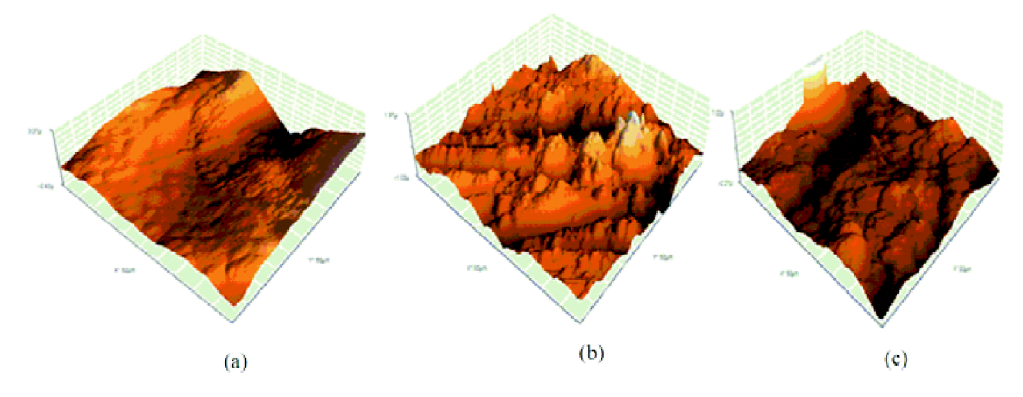


Fig. 7. 3D-AFM images of (a) polished surface, (b) unprotected surface and (c) protected surface with MPPT in 1 M HCl solution.

orbital of the iron atoms of the mild steel specimens and the unshared electron pairs of N and O atoms present in the MPPT molecule.

(iii) The donor-acceptor interaction also occurred as a result of chemisorptions via the π -electrons of MPPT species with vacant d orbital of iron atoms.

Therefore, all the conclusions interpret that the corrosion reactions are hindered by the adsorption of MPPTprotector on the metallic surface involving in both physical and chemical interaction. However, the temperature study declared that the corrosion inhibition process is more chemisorption than the physisorption.

Conclusion

The hindered efficacy of MPPT inhibitor on mild steel was determined by the gravimetric and electrochemical methods in the 1 M HCl medium. The outcomes achieved by the mass loss technique were consistent with the electrochemical approaches. Consequently, all of the above measurements showed that the defense efficiencies were enhanced in both the elevated concentrations and temperatures. Meanwhile, the electrochemical assessments pointed out that MPPT was a mixed kind protector and the adsorption isotherm interpretation exposed that the inhibition process pursued the Langmuir adsorption. The lower E_a values supported that the corrosion inhibition process was a characteristic chemical adsorption and the negative ΔG^0_{ads} values represented that the corrosion process was a spontaneous case. Here with, the positive ΔH^0 exposed that the inhibition process was an endothermic reaction and the negative values of ΔS^0 displayed the solution entropy of the adsorption system was decreased. Conclusively, SEM, EDS, and AFM examinations proved the development of inhibitive barriers on steel surfaces. All the above findings confirmed that the MPPT performed in the 1 M HCl solution as a proficient inhibitor against mild steel corrosion.

References

- S. Ramesh, S. Rajeswari and S. Maruthamuthu, Materials Letters, 2003, 57, 4547.
- R. Bhaskaran, L. Bhalla, A. Rahman, S. Juneja, U. Sonik, S. Kaur, J. Kaur and N. Rengaswamy, *Materials Performance*, 2014, 53, 56.
- S. K. Sharma, "Front Matter in Green Corrosion Chemistry and Engineering: Opportunities and Challenges", Wiley-VCH Verlag GmbH & Co., KGaA, Weinheim, Germany, 2011.

- R. G. Kelly, R. Scully, D. W. Shoesmith and R. G. Buchheit, "Electrochemical Techniques in Corrosion Science and Engineering", Marcel Dekker Press, New York, 2002.
- Guannan Mu, Xianghong Li, Qing Qu and Jun Zhou, Corros. Sci., 2006, 48, 445.
- A. E. Hughes, J. D. Gorman and P. J. K. Paterson, *Corros. Sci.*, 1976. 38. 7.
- 7. S. N. Banerjee and S. Misra, Corrosion, 1989, 45, 780.
- K. F. Khaled and N. Hackerman, Electrochimica Acta, 2004, 49, 485
- 9. Resit Yildiz, Ionics, 2019, 25, 859.
- A. Khalida, Al-Azawi, Iman Mahdi Mohammed, Shaimaa
 B. Al-Baghdadi, Taghried A. Salman, Hamsa A. Issa, Ahmed A. Al-Amiery, Tayser Sumer Gaaz and Abdul Amir H. Kadhum, Results in Physics, 2018, 9, 278.
- Ali A. Abd-Elaal, Ismail Aiad, Samy M. Shaban, Salah M.Tawfik and Atef Sayed, J. Surfact. Deterg., 2014, 17, 483.
- Dmitry Shevtsov, Oleg Kozaderov, Khidmet Shikhaliev, Ekaterina Komarova, Alexei Kruzhilin, Andrei Potapov, Chetti Prabhakar and Ilya Zartsyn, Appl. Sci., 2019, 9, 4882.
- Dakeshwar Kumar Verma, Eno E. Ebenso, M. A. Quraishi and Chandrabhan Verma, Results in Physics, 2019, 13, 102194
- John Paul Raj, Dasari Ganga Prasad, Murugesan Vajjiravel, Kesavan Karthikeyan and Jebamalai elangovan, J. Chem. Sci., 2018, 130(1-6), 44.
- Xiangyu Li, Yuwei Ye, Tong Liu, Wenru Zheng, Feng Yang, Haichao Zhao and Liping Wang, Surf. Topogr. Metrol. Prop., 2017, 5, 044001.
- Ashish Kumar Singh and M. A. Quraishi, Int. J. Electrochem. Sci., 2012, 7, 3222.
- A. Saxena, D. Prasad, R. Haldhar, G. Singh and A. Kumar, J. Environ. Chem. Eng., 2018, 6, 694.
- 18. S. K. Shetty and A. N. Shetty, J. Mol. Liq., 2017, 225, 426.
- Hassane Lgaz, Rachid Salghi, Abdelkarim Chaouiki, Shubhalaxmi, Shehdeh Jodeh and K. Subrahmanya Bhat, Cogent Engineering, 2018, 5, 1441585.
- I. B. Oboz and N. O. Obi-Egbedi, Corros. Sci., 2010, 52, 108
- H. H. Hassan, E. Abdelghani and M. A. Amin, Electrochimica Acta, 2007, 52, 6359.
- H. Ashassi-Sorkhabi, M. R. Majidi and K. Seyyedi, Applied Surface Science, 2004, 225, 176.
- M. S. Abdel-Aal and M. S. Morad, *British Journal of Corrosion*, 2001, 36, 253.
- S. E. Nataraja, T. V. Venkatesha, K. Manjunatha, Boja Poojary, M. K. Pavithra and H. C. Tandon, *Corros. Sci.*, 2011, 53, 2651.
- 25. A. Popova, Corros. Sci., 2007, 49, 2144.

Vijayalakshmi et al.: 1,2,3-Triazole derivative as a potential protector for mild steel corrosion in acid media: etc.

- L. L. Liao, S. Mo, J. Lei Lei, H. Qun Luo and N. Bing Li, J. Colloid Interface Sci., 2016, 474, 68.
- A. H. Ostovari, S. M. Hoseinieh, M. Peikari, S. R. Shadizadeh and S. J. Hashemi, Corros. Sci., 2009, 51, 1935
- 28. E. S. Ferreira, C. Giacomelli, F. C. Giacomelli and A. Spinelli, *Materials Chemistry and Physics*, 2004, **83**, 129.
- Zarrouk, B. Hammouti, H. Zarrok, R. Salghi, A. Dafali, L. Bazzi and L. Bammou, S. Al-Deyab, *Der Pharm. Chem.*, 2012, 4, 337.
- 30. W. H. Li, Q. He, S. T. Zhang, C. L. Pei and B. R. Hou, Journal of Applied Electrochemistry, 2008, 38, 289.
- M. Rabaa, M. Galai, F. Benhiba, I. B. Obot, H. Oudda, M. Ebn Touhami, B. Lakhrissi and A. Zarrouk, *Ionics*, 2019, 25, 3473.
- Shaju K. Shanmughan, Joby Thomas Kakkassery, Vinod P. Raphael and Nimmy Kuriakose, *Current Chemistry Letters*, 2015, 4, 67.
- 33. O. Benali, L. Larabi, B. Tabti and Y. Harek, *Anti-Corrosion Methods and Materials*, 2005, **52**, 280.



Effect of 1,2,3- triazole derivative on the dissolution performance of mild steel in 1M HCl medium

K Vijayalakshmi, N Punitha, R Rengamy & J Elangovan*

PG and Research Department of Chemistry, Rajah Serfoji Government College (Autonomous), Thanjavur 613 005, Tamilnadu, India. (Affiliated to Bharathidasan University, Thiruchirappalli 620 024, Tamilnadu, India.) E-mail: elangoorganic@gmail.com

Received 31 August 2020; accepted 17 June 2021

The corrosion mitigation behaviour of 1-benzyl-4-(naphthalen-2-yl)-1*H*-1,2,3-triazole (BNT) has been explored on mild steel in 1M HCl medium employing chemical and electrochemical techniques. The observed results illustrate that the hindered efficacy was increased as increasing concentration of BNT and with rising temperatures. The electrochemical studies point out that the inspected BNT is a mixed kind inhibitor and the adsorption isotherm discussions proposed the inhibition mechanism obeyed Langmuir isotherm. The kinetic and thermodynamical parameters exposed that the adsorption process is endothermic, spontaneous and the mechanism is both physical and chemical adsorption. Further, the morphological investigations have been carried out by SEM, EDS and AFM techniques. The highest efficiency perceived for BNT is found to be 91.35% and behaved as a proficient inhibitor against mild steel corrosion in the 1M HCl environment.

Keywords: Corrosion, Electrochemical, Kinetic, Langmuir isotherm, Triazole.

Mild steels are one of the most essential materials employed in human desires and they discover many applications, especially for construction, automobiles and industrial works^{1,2}. Even though mild steels encompassing a wide range of applications, they are sternly pretentious by corrosion when they are in contact with acidic atmosphere and other chemical processes^{3,4}.

Meanwhile, the environmental hazards influenced the quality of mild steels and the rusting of mild steels more easily occur in the acidic and humid atmosphere⁵. The corrosion concert of mild steel and its alloys are primarily dependent on their composition and microstructure⁶. Also, environmental factors such as temperature and degree of aeration are affected by this corrosion recital. Hence, corrosion is one of the noteworthy and costliest harms around the globe. In previous decades, many endeavors have been put into practice to resolve these problems and utilization of inhibitors is the universally accepted and widely utilized technique for curtailing the rate of corrosion. In this circumstance, organic inhibitors are employed as the foremost anti-corrosion candidates comprising heteroatoms such as nitrogen, oxygen and sulphur for mild steels in assorted corrosive environments⁷⁻¹².

In recent years, 1,2,3- triazoles derivatives have great attention to employing the mitigation of corrosion

rate in different aggressive media¹³⁻¹⁵. Moreover, the hindered efficiency chiefly depends on their molecular structure, presence of heteroatoms, substituent effect, π electron density and petite toxicity of the triazole derivatives¹⁶⁻¹⁸.

In this study, 1-benzyl-4-(naphthalen-2-yl)-1H-1,2,3-triazole (BNT) was used to evaluate the corrosion inhibition performance on mild steel in 1M HCl medium and the molecular structure of BNT is given in Fig. 1.

Experimental Section

Materials

Mild steel specimens (IRS M41/97steel) utilized in the present investigation comprising the elemental composition (wt %) were P- 0.089, Si- 0.319, Mn-0.43%, S-0.009, Al-0.028, C-0.076, Cr-0.52, Ni- 0.20, Cu-0.31 and Fe-99.69. For the mass loss method, the rectangular-shaped mild steel specimens enclosing the dimensions 5cm × 2cm × 0.2cm were employed. Mild steel specimens were prepared by different numbers (up to 1500) of SiC emery papers and the polished specimens were washed with distilled water, rinsed with ethanol and degreased with acetone¹⁹.

A corrosive solution (1M HCl) was prepared for the gravimetric experiments from 37% Analar HCl

Fig.1 — 1-benzyl-4-(naphthalen-2-yl)-1*H*-1,2,3-triazole (BNT)

with distilled water. Meanwhile, BNT was synthesized and characterized by melting point, FT-IR, ¹H NMR and ¹³C NMR analysis²⁰. The desired concentrations of BNT were prepared in ethanol for further measurements.

Gravimetric method

The gravimetric analysis was performed using accurately weighed polished mild steel specimens before and after immersion in 1M HCl solution with 10, 30, 50 and 100 ppm concentrations of BNT for six hours exposure time at room temperature. Further, all the experiments were carried out in thrice for the determination of mean mass loss values with the same conditions. From the average mass loss, the corrosion factors such as corrosion rate, inhibition efficiency and surface coverage were calculated by equations 1, 2 and 3 respectively..

$$CR = \frac{\Delta W}{At} \qquad ...(1)$$

where ΔW is the mean mass loss (mg), A is the total area (cm⁻²) and t is the immersion time (h) in the presence and absence of BNT in 1M HCl solution.

I.E(%) =
$$\left(\frac{W_o - W}{W_o}\right) \times 100$$
 ...(2)

$$\theta = \left(\frac{W_o - W}{W_o}\right) \qquad ...(3)$$

where $W_{\rm o}$ and W are the mean mass loss (mg) of mild steels in the absence and presence of BNT in 1M HCl solution respectively.

Electrochemical techniques

Polarization measurements

The potentiodynamic polarization assessments were executed by a three-electrode CH instrument (CHI-66 model). Herein, a platinum foil was used as a counter electrode and a standard calomel electrode

was employed as a reference electrode. Besides, 1cm⁻² area of the test specimen was immersed in 1M HCl in the presence and absence of the BNT performed as a working electrode and this area of the test specimens was fixed throughout the experiments. Before every measurement, the stabilization period 30 min was applied to attain the open circuit potential. After that, the polarization curves were acquired by varying the electrode potential from -500 mV to +500 mV.

From the Tafel extrapolation technique, the corrosion current density (I_{corr}) values were obtained and inhibition efficiencies for all the working concentrations were calculated using equation 4

$$IE(\%) = \left[\frac{i_{corr} - i_{corr}(inh)}{i corr}\right] \times 100 \qquad ...(4)$$

where $I_{\text{corr}\ (\text{inh})}$ and I_{corr} are the corrosion current densities in the presence and absence of BNT in 1M HCl solution.

Impedance study

The electrochemical impedance study was conducted with CH instrument and the impedance parameters were acquired from the Nyquist plots in the frequency range between 100 kHz and 10 MHz. Charge Transfer Resistance ($R_{\rm ct}$) and electrical double layer capacity ($C_{\rm dl}$) was achieved from the Nyquist plots. The inhibition efficiency (IE %) and electrical double layer capacity ($C_{\rm dl}$) values were determined from the charge transfer resistance values using equations 5 and 6 respectively.

$$I.E(\%) = \left[\frac{R_{ct}(inh) - R_{ct}}{R_{ct}(inh)}\right] \times 100 \qquad ...(5)$$

$$CdI = \frac{1}{2\pi\pi_{\text{max}}.RC_{\text{ct}}} \qquad ...(6)$$

where and $R_{\text{ct(inh)}}$ and R_{ct} are the charge transfer resistance in the presence and absence of BNT in 1M HCl solution and f_{max} is the highest peak frequency of the Nyquist plots.

Surface morphology

The morphological examinations of the tested mild steel specimens were conducted by Scanning Electron microscope (SEM), Electron dispersive spectrum (EDS), and Atomic Force Microscope (AFM) techniques. For this exploration, the mild steel specimens were immersed in 1M HCl in the absence and optimum concentration of BNT for 6 hours of exposure time.

Results and Discussion

Mass loss study

Figure 2 shows the correlation between the corrosion rates and inhibition efficiencies of various concentrations of BNT in the 1M HCl solution. As shown in Fig. 2 and Table 1, inhibition efficiencies increase with increasing concentration of BNT and the corrosion rates decrease correspondingly²¹. Inspection of Table 1 also reveals the maximum efficacy is 91.35% at 100 ppm. Meanwhile, the increasing values of surface coverage suggesting BNT species protect the large area of the metal with increasing concentration. These observations showed that the corrosion rates for mild steels are mitigated by the adsorption of BNT species in an acidic environment.

Electrochemical techniques

Polarization study

Tafel polarization curves for different concentrations of BNT in 1M HCl solution are shown in Fig. 3 and the electrochemical polarization parameters are presented in Table 2. As we can see from Fig 3 and Table 2, the values of corrosion potential (E_0) in the presence inhibitor are less than \pm 85 mV with respect to the blank solution which indicates BNT acts as a mixed type inhibitor²². It also evident from the values of Tafel slopes that the polarization occurs on both sides but cathodic polarization is more predominant than the anodic move. Besides that, the values of corrosion current density (I_0) decrease with increasing concentration of BNT which exposes the

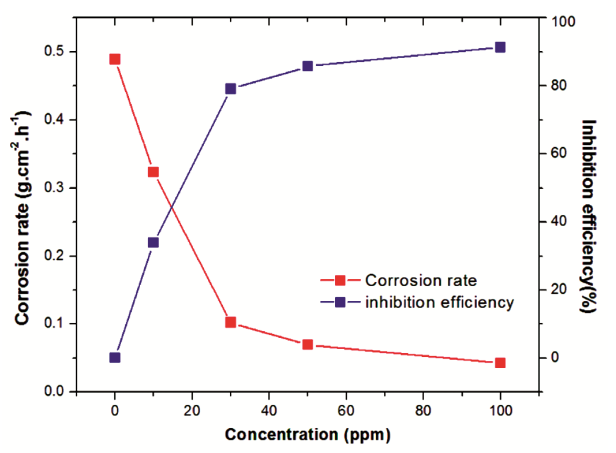


Fig. 2 — Correlation between the corrosion rates and inhibition efficiencies for BNT on mild steel specimens in 1M HCl

electrochemical corrosion reactions are hindered by the adsorption of BNT on mild steel specimens. Also, the optimum efficiency observed is 90.12% at 100 ppm. All the polarization findings conclude that BNT performed as a potential protector in the 1M HCl medium.

Impedance study

Figure 4 exhibits the Nyquist plots of different concentrations of BNT in 1M HCl solution and the diameter of the loops increases with increasing concentration of BNT which suggests that the hindrance of charge transfer in the presence of BNT. It also explains the obtained plots are not perfect circles due to the roughness of the metallic surface and uneven distribution of active centers during the corrosion process²³. Table 2 shows the decreasing values C_{dl} with increasing concentration of BNT which designates the increasing thickness of the electrical double layer at metal solution interface prevents the metallic surface from rust formation in 1M HCl solution. Further, the highest efficiency attained in this study is 90.60% which corroborates

Table 1 — Effect of BNT concentration on mild steel corrosion in 1M HCl

Conc. (ppm)	Corrosion rate (mg.cm ⁻² .h ⁻¹)	Inhibition efficiency (IE %)	Surface coverage (θ)
Blank	0.4894	-	-
10	0.3238	33.83	0.34
30	0.1022	79.12	0.79
50	0.0695	85.79	0.86
100	0.0423	91.35	0.91

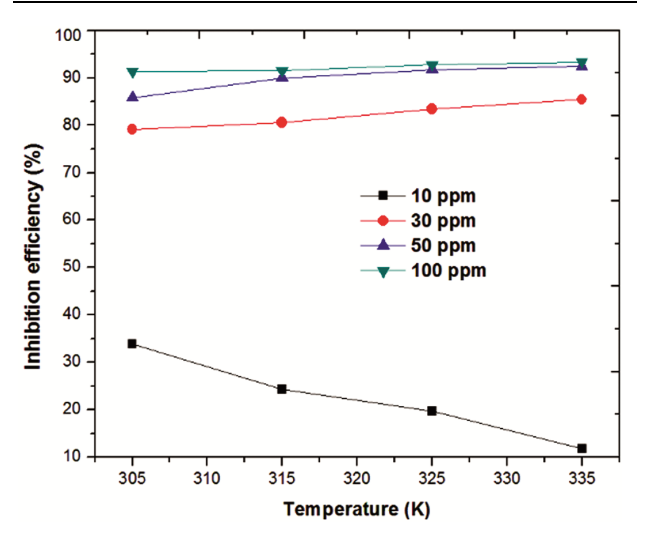


Fig. 3 — Effect of temperature on inhibition efficiencies for various concentrations of BNT on mild steel specimens in 1M HCl

Table 2	. — Electrochem	ical polarizati	on and impeda	ance parameter	s for BNT on	mild steel specin	nens in 1M HCl	
		Polar	ization parame	eters		Impe	dance parameter	rs
Conc.(ppm)	E_0 (mV)	$I_0(mA)$	$b_{c}\left(mV\right)$	$b_{a}(mV) \\$	IE (%)	$R_{ct} (\Omega.cm^2)$	C_{dl} ($\mu F.cm^{-2}$)	IE (%)
Blank	-420.613	3.46	995.82	254.55	0	9.45	3.2095	0
10	-487.864	2.05	97.82	262.02	40.90	16.61	1.2369	43.11
30	-449.694	0.63	672.88	561.31	81.68	49.26	0.1626	80.82
50	-437.671	0.56	153.55	102.96	83.96	81.77	0.0513	88.44
100	-436.141	0.34	161.80	78.76	90.12	100.55	0.0241	90.60

-1.5 -2.0 -2.5 -3.0 -3.5 -4.5 -5.0 blank

10 ppm -6.0 30 ppm -6.5 50 ppm 100 ppm -7.0 -0.50 -0.40 -0.35 E_o(mV)

Fig. 4 — Tafel polarization curves for various concentrations of BNT on mild steel samples in 1M HCl

the investigated BNT is an efficient defender against mild steel corrosion in an acidic medium.

Temperature study

Figure 5 reveals the inhibition efficiencies with various concentration of BNT in 1M HCl solution at different temperatures ranging from 305K to 335 K. It can be seen that moderate increase in hindered efficiencies from Fig. 5 for all the working concentrations (30, 50 and 100 ppm) and the inhibition efficiencies for lower concentration (10 ppm) falls in all studied temperatures. It suggests that the decreasing efficiency at elevated temperature is attributed to physical adsorption while the increasing efficiencies are associated with chemisorptions or both physical and chemical interactions²⁴. The values of corrosion rates and the inhibition efficiencies are summarized in Table 3 and the inhibition efficiencies increase with increasing BNT concentration and the maximum efficiency obtained is 93.26%. The temperature study suggests that the adsorption process of BNT on mild steels favors at elevated temperatures in the 1M HCl atmosphere.

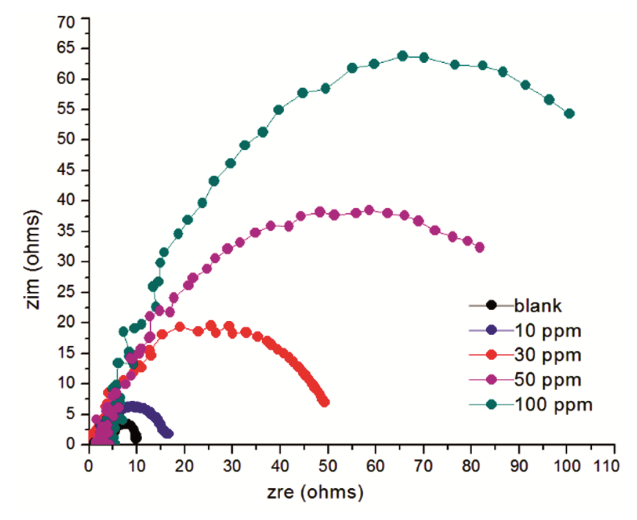


Fig. 5 — Nyquist plots for various concentrations of BNT on mild steel samples in 1M HCl

Thermodynamic activation parameters

The activation energy (Ea) and pre-exponential factor (A) were acquired by the following Arrhenius equation 7

$$\log CR = \log A - \frac{Ea}{RT} \qquad ...(7)$$

Where, R is the universal gas constant, CR is the corrosion rate (mg.cm⁻².h⁻¹) and T is the temperature (K).

Figure 6 represents the straight lines of Arrhenius plots that are attained by plotting to log CR Vs 1000/T with slope (Ea/R) and intercept (log A). Also, Ea and A values are determined from the slope and intercept respectively and listed in Table 4 As we see in Table 4, the decreasing values of activation energy as rising inhibitor concentration which stand for chemical adsorption²⁵. Moreover, we observe the decreasing values of the Arrhenius factor support the corrosion process is effectively prohibited by the adsorption of BNT onto the metal surface.

In the same way, the thermodynamic activation parameters such as entropy of activation (ΔS^*) and

Table 3 — Effect of temperature on the inhibition efficiencies for different concentrations of BNT on mild steel specimens in 1M HCl								
Conc.(ppm)	CR (mg.cm2.h-1)				I.E (%)			
	305 K	315K	325K	335K	305K	315K	325K	335K
Blank	704.70	1149.83	1636.80	2138.33	-	-	-	-
10	466.28	870.15	1314.98	1886.40	33.83	24.32	19.66	11.78
30	147.15	223.73	271.28	312.60	79.12	80.54	83.43	85.38
50	100.13	115.28	136.05	162.23	85.79	89.97	91.69	92.41
100	60.98	98.40	118.58	144.08	91.35	91.44	92.76	93.26

Table 4 — Thermodynamic activation parameters for BNT on mild steel specimens in 1M HCl

Conc.(ppm)	E_a (KJ.mol ⁻¹)	$A (g.cm^2.h^{-1})$	ΔH^* (KJ.mol ⁻¹)	$\frac{\Delta S^*}{(JK^{-1}.mol^{-1})}$	E_a - ΔH^*
Blank	31.38	1.75×10^9	28.74	111.24	2.65
10	39.23	2.59×10^{10}	36.59	135.67	2.64
30	20.98	7.33×10^6	20.98	67.72	2.66
50	23.63	6.15×10^6	18.32	66.26	2.67
100	13.69	2.17×10^{5}	11.02	38.45	2.65

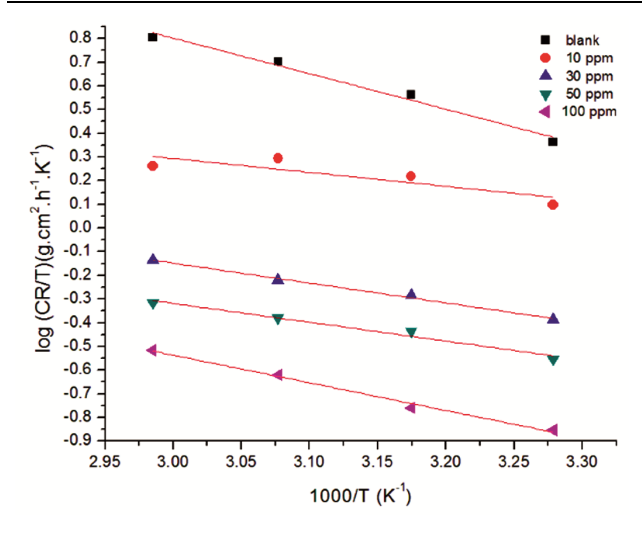


Fig. 6 — Arrhenius plots for various concentrations of BNT on mild steel samples in 1M HCl $\,$

enthalpy of activation (ΔH^*) were determined from the following transition state equation 8

$$\log\left(\frac{CR}{T}\right) = \log\left(\frac{RT}{Nh}\right) + \left(\frac{\Delta S *}{2.303R}\right) \qquad ...(8)$$

where h is Planck's constant and N is Avogadro's number.

Transition state plots are obtained by plotting log CR/T Vs 1000/T with slope (- Δ H*/2.303R) and intercept [(log (R/Nh) + Δ S*/2.303R] of the straight lines as shown in Fig. 7. The values of Δ H* and Δ S* are calculated from the slope and intercept respectively and the values for enthalpy of activation and entropy of activation are presented in Table 4.

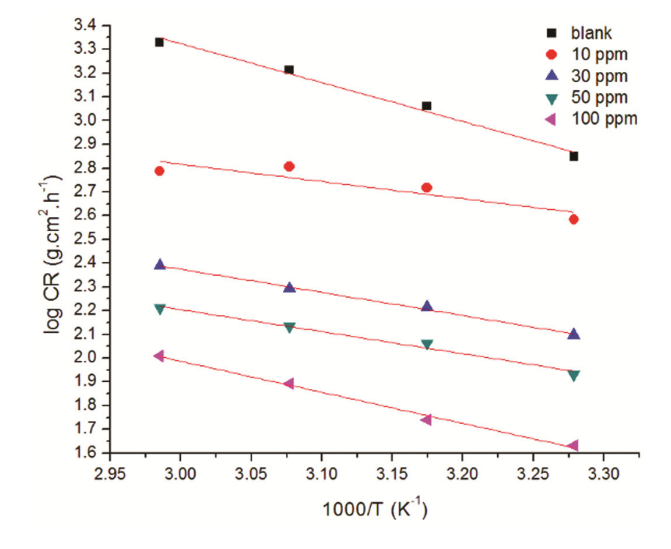


Fig. 7 — Transition state plots for various concentrations of BNT on mild steel samples in 1M HCl

It reveals the positive values of ΔH^* indicating the adsorption process is endothermic and characteristic chemisorptions²⁶. The negative values of ΔS^* suggesting the entropy decreases at metal solution interface due to the displacement of water molecules adsorbed on the metal surface by BNT species²⁷. Further, Table 4 shows the difference between the values of Ea and ΔH^* for all the concentrations are approximately equal to 2.61 KJ.mol⁻¹ (average value of RT) which gratify the equation Ea - ΔH^* = RT and it mention that the corrosion process is controlled by the thermodynamic activation parameters²⁸. Hence, the effect of temperature on the adsorption process clearly explains the adsorption mechanism involving through chemical interactions.

Langmuir adsorption isotherm

The mechanism of the corrosion inhibition process was described by many isotherm models and this adsorption process follows Langmuir isotherm. The Langmuir isotherm parameters were achieved by the following equation 9

$$\frac{C_{\text{inh}}}{\theta} = \frac{1}{K_{\text{odd}}} + C_{\text{inh}} \qquad \dots (9)$$

where C_{inh} is the concentration of BNT (ppm), θ is the Surface coverage and K_{ads} is the equilibrium adsorption constant of the adsorption process.

The equilibrium constant values (K_{ads}) are obtained from the intercept of the straight lines by plotting C_{inh}/θ Vs C_{inh} for various concentrations of BNT at different temperatures are shown in Fig. 8 and recorded in Table 5. From the tabulated results, the increasing values K_{ads} at raised temperatures suggesting the strong adsorption and we can also perceive the linear regression coefficient (R^2) values are closed to 1 which indicates the adsorption process follows Langmuir isotherm. The adsorption standard

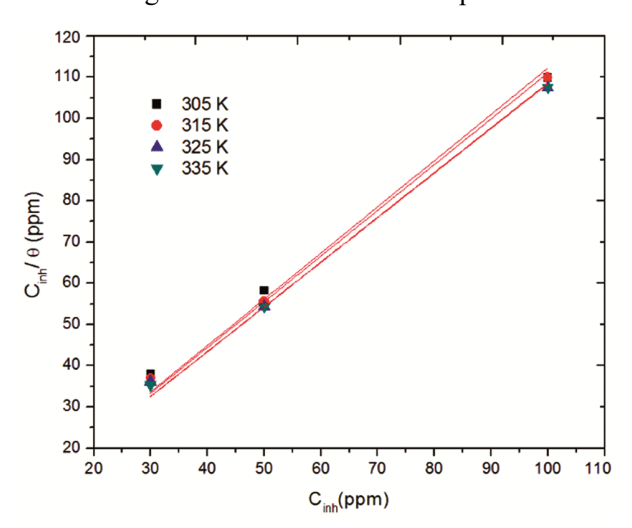


Fig. 8 — Langmuir isotherm for BNT on mild steel specimens in 1M HCl at different temperatures

Table 5 — Langmuir parameters for BNT on mild steel specimens in 1M HCl at different temperatures

Temp (K)	K_{ads} $(L.mol^{-1})$	Langmuir isotherm ΔG^{0}_{ads} (KJ.mol ⁻¹)	R^2
305	8912.42	-33.25	0.9975
315	9006.66	-34.37	0.9986
325	9206.83	-35.52	0.9987
335	9222.97	-36.61	0.9992

free energy values (ΔG^0_{ads}) were determined using the following equation 10

$$\Delta G_{ads} = \left[-RT \ln(55.5K_{ads}) \right] \qquad \dots (10)$$

where R is gas constant, T is the thermodynamic temperature (K), 55.5 is the concentration of water in tested solutions and K_{ads} is the adsorption equilibrium constant.

It can be seen from Table 5 that the ΔG^0_{ads} values ranged from -33.25 to 36.61 KJ.mol⁻¹which expose that the adsorption process involving both physical and chemical adsorptions²⁹.

Surface interpretation

SEM

Figure 9a-9c displays the SEM examination of bare steel, unprotected surface and protected surface in 1M HCl solution. The polished steel before immersion exhibits the smooth surface as shown in Fig. 9a and the mild steel after immersion in 1M HCl solution exposes severe damages as shown in Fig. 9b. Further, Fig. 9c reflects the steel surface without cracks and pits in the presence of BNT in 1M HCl solution which corroborates the thin film formation on the metallic surface against mild steel corrosion by the adsorption of BNT species in the corrosive medium³⁰.

EDS

The electron dispersive spectra of mild steel specimens before immersion, after immersion and in the presence of BNT respectively were plotted. It displays the characteristic peaks of Fe, C and O present in the bare steel and reflects the existence of chlorine peak due to rust formation. Besides that, it also shows the nitrogen peak along with the inspected elements which indicates that the corrosion damages are reduced by the adsorption of BNT molecule on the mild steel surface. The EDS data of the examined steel specimens are registered in Table.6 and the weight percentage values support that the corrosion behavior is hindered by the development of protective film via nitrogen coordination with the steel surface in 1M HCl solution³¹.

AFM

Inspection of Table 7 shows that the average roughness values for polished mild steel, specimens in the absence and presence of BNT are 160.65nm, 895.36 nm and 212.72 while the corresponding RMS values are 195.31nm, 1500.1nm and 262.45 nm respectively. The larges values of roughness noted for

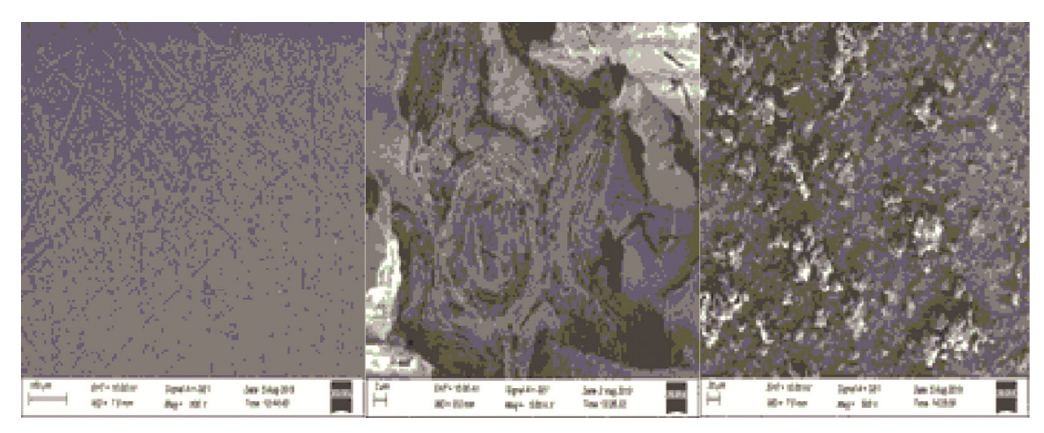


Fig. 9 — SEM images of (a) polished mild steel; (b) unhindered sample and (c) hindered sample with BNT in 1M HCl

Table 6 — Elemental analysis for polished mild steel specimen, unprotected and protected steel specimens in 1M HCl

Specimens	Weight %				
Specimens	Fe	O	C	Cl	N
Polished mild steel	79.82	7.98	12.20	-	-
Unprotected mild steel	49.66	43.44	5.84	1.06	-
Protected mild steel with BNT	75.67	9.73	13.21	-	1.39

Table 7 — AFM parameters for bare steel, unprotected and protected steel specimens in 1M HCl

Samples	Average Roughness (R_a) nm	$\begin{array}{c} RMS \\ roughness \\ (R_q) nm \end{array}$
Bare steel surface	160.65	195.31
Unprotected surface	895.36	1500.1
Protected surface with BNT inhibitor	212.72	262.45

unprotected surfaces indicating the metal surface is severely damaged by the corrosive medium. In the presence of inhibitor, the roughness values are closer to the bare steel which corroborates that the corrosion attacks are reduced by the adsorption of inhibitor.

It is also evident that the bare steel shows the smoother surface and the unprotected specimen reveals rough surface due to acid attack Further, it exhibits the roughness of the steel surface is considerably reduced by the adsorption BNT in 1M HCl solution³².

Mechanism of corrosion inhibition

The electrochemical corrosion reactions are hindered by the adsorption of BNT on to the metal surface either by physical adsorption, chemical adsorption, or both. In this study, all the verdicts explained that the inhibition process is carried out through both the physical and chemical interactions^{33,34}. Protonation happens at the heteroatom of BNT while

chloride ions adsorb on the metal surface exposed in 1M HCl solution and the surface become negatively charged. Thus, the electrostatic interaction takes place between the cationic BNT species and anionic metal surface.

Also, chemical interaction takes place in two ways; (i) the interaction between the unshared pairs of the nitrogen atom of BNT and the vacant d orbital of the Fe atoms. (ii) π electrons of the aromatic rings present in BNT molecule interact with the d orbital of the Fe atoms resulting in chemisorptions. Both kinds of mechanisms are expressed in the following equations 11 & 12

$$(FeCl^-)_{ads} + BNT^+ \longrightarrow [(FeCl^-)(BNT^+)]_{ads} \dots (11)$$

$$Fe^{2+} + BNT_{(ads)} \longrightarrow [Fe-BNT]^{2+}_{(ads)} \dots (12)$$

Moreover, the thermodynamic activation parameters suggested that the adsorption process is carried out by the displacement of water molecules ³⁵ on the mild steel surface by BNT and is given by the following equation 13

$$BNT_{(sol)} + nH_2O_{(ads)} \longrightarrow BNT_{(ads)} + nH_2O_{(sol)}$$
 ...(13)

where n is the number of water molecules replaced by BNT molecules.

Thus, all the data proposed that the corrosion process is effectively controlled by both the physical and chemical adsorption but chemical adsorption is more predominant than the electrostatic attraction.

Conclusion

The anti-corrosive effect of BNT molecule on mild steel corrosion in 1M HCl solution was investigated by mass loss, polarization and impedance techniques. All the explored methods revealed that they were in good agreement with each other and BNT act as a mixed type inhibitor with cathodic predominance according to polarization study. The thermodynamic activation parameters suggested that the adsorption process is endothermic, spontaneous and decreased the solution entropy. The adsorption process obeyed Langmuir isotherm and the mechanism involved both the physical and chemical interactions but more chemisorptions were reported. Moreover, SEM, EDS and AFM analysis corroborated the corrosion rate is hindered by the development of protective coating on the mild steel. Therefore, all the conclusions corroborated that BNT was a proficient inhibitor on mild steel surface in the 1M HCl solution.

Acknowledgement

The authors are highly thankful to PG and Research Department of Chemistry, Rajah Serfoji Government College (Autonomous), Thanjavur-613005 for providing laboratory facilities.

References

- 1 Eddy NO & Ita BI, J Mol Model, 17 (2011) 359.
- 2 Strickland D M, Ind Eng Chem, 15 (1923) 566.
- 3 Goulart C M, Esteves-Souza A, Martinez-Huitle C A, Rodrigues C J F, Maciel M A M & Echevarria A, Corros Sci, 67 (2013) 28.
- 4 Zarrok H, Saddik R, Oudda H, Hammouti B, El Midaoui A, Zarrouk A, Benchat N & Ebn Touhami M, *Der Pharm Chem*, 4 (2011) 272.
- 5 Al Hamzi A H, Zarrok H, Zarrouk A, Salghi R, Hammouti B, Al-Deyab S S, Bouachrine M, Amine A & Guenoun F, Int J Electrochem Sci, 8 (2013) 2586.
- 6 Zarrouk A, Hammouti B, Zarrok H, Salghi R, Dafali A, Bazzi Lh, Bammou L & Al-Deyab S S, *Der Pharm Chem*, 4 (2012) 337.
- 7 Abd El Rehim S S, Sayyah S M, El-Deeb M M, Kamal S M & Azooz R E, Int J Ind Chem, 7 (2016) 39.
- 8 Sudhish K S, Eno E E, Int J Electrochem Sci, 6 (2011) 3277.
- 9 Singh A K & Quraishi M A, Int J Electrochem Sci, 7 (2012) 3222.
- 10 Oyebamiji A K & Adeleke B B, Int J Corros Scale Inhib, 7 (2018) 498.
- 11 Jeeva P A, Mali G S, Dinakaran R, Mohanam K & Karthikeyan S, *Int J Corros Scale Inhib*, 8 (2019) 1.

- 12 Al-Amiery A A, Kadhum A A H, Kadihum A, Mohamad A B, Chong K, How C K & Junaedi S, *Mater*, 7 (2014) 787.
- 13 Rahmani H, Ismaily Alaoui K, Emran K M, El Hallaoui A, Taleb M, El Hajji S, Labriti B, Ech-chihbi E, Hammouti B & El-Hajjaji F, Int J Electrochem Sci, 14 (2019) 985.
- 14 Fernandes C M, Alvarez L X, Dos Santos N E, Maldonado Barrios A C & Ponzio A E, Corros Sci, 149 (2019) 185.
- 15 Desai P S & Indorwala N S, Res J Chem Sci, 5 (2015) 30.
- 16 Scendo M & Staszewska-Samson K, Int J Electrochem Sci, 12 (2017) 5668.
- 17 Kozaderov O A, Shikhaliev Kh S, Prabhakar Ch, Shevtsov D S, Kruzhilin A A, Komarova E S, Potapov A Yu & Zartsyn I D, Int J Corros Scale Inhib, 8 (2019) 422.
- 18 Gonzalez-Olvera R, Espinoza-Vazquez A, Negron-Silva G E, Palomar-Pardave M E, Romero-Romo M A & Santillan R, Molecules, 18 (2013) 15064.
- 19 Verma D K, Ebenso E E, Quraishi M A & Verma C, Results in Physics, 13 (2019) 102194.
- 20 Paulraj J, Gangaprasad D, Vajjiravel M, Karthikeyan K & Elangovan J, J Chem Sci, 130 (2018) 44.
- 21 Oboz I B & Obi-Egbedi N O, Corros Sci, 52 (2010) 198.
- 22 Ashassi-Sorkhabi H, Majidi M R & Seyyedi K, Appl Surf Sci, 225 (2004) 176.
- 23 Abdel-Aal M S & Morad M S, British J Corros, 36 (2001) 253.
- 24 Nataraja S E, Venkatesha T V, Manjunatha K, Boja Poojary, Pavithra M K & Tandon H C, Corros Sci, 53 (2011) 2651.
- 25 Al-Sabagh A M, Kandil N Gh, Ramadan O, Amer N M, Mansour R & Khamis E A, Egypt J Petrol, 20 (2011) 47.
- 26 Liao L L, Mo S, Lei Lei J, Qun Luo H & Bing Li N, J Colloid Interface Sci, 474 (2016) 68.
- 27 Yadav D K, Quraishi M A & Maiti B, Corros Sci, 55 (2012) 254.
- 28 Ostovari A H, Hoseinieh S M, Peikari M, Shadizadeh S R & Hashemi S J, Corros Sci, 51 (2009) 1935.
- 29 Hazazi O A, Fawzy A & Awad M, Int J Electrochem Sci, 9 (2014) 4086.
- 30 Tan B, Zhang S, Qiang Y, Guo L, Feng L & Liao C, J Colloid Interface Sci, 526 (2018) 268.
- 31 Van Ooij W J, Surf Technol, 6 (1977) 1.
- 32 Shanmughan S K, Kakkassery J T, Raphael V P & Kuriakose N, Current Chem Lett, 4 (2015) 67.
- 33 Bentiss F, Traisnel M & Lagrenee M, Corros Sci, 42 (2000) 127.
- 34 Benali O, Larabi L, Tabti B & Harek Y, Anti Corros Methods Mater, 52 (2005) 280.
- 35 Li L, Zhang X, Lei J, He J, Zhang S & Pan F, Corros Sci, 63 (2012) 82.